Synthesis, Pharmacological and Physicochemical Profiling of Antimalarial and Antischistosomal N-aryl 3-trifluoromethyl Pyrido [1,2-*a*] benzimidazoles.

GODFREY WABWILE MAYOKA

Supervisor: Professor Kelly Chibale

Thesis presented for the degree of

DOCTOR OF PHILOSOPHY

In the Department of Chemistry

Faculty of Science

UNIVERSITY OF CAPE TOWN

August, 2018

Declaration

I, **Godfrey Wabwile Mayoka**, do hereby declare that:

(i) I grant license to the University of Cape Town to reproduce this Thesis either in part or wholly for research purposes under the research commons agreement;

(ii) This Thesis is my original work both in the design, planning and execution with the relevant assistance from my supervisor. Where input and work from others have been included, appropriate referencing and acknowledgements have been made;

(iii) This thesis, or part thereof has not been presented nor is intended to be submitted to any University for the Award of a Degree.

Signature: Signed by candidate **Date:** 20th August 2018

Dedication

To my lovely wife Keziah Narotso Mayoka for the godly woman that you are and for the great moral support with much prayers that have lubricated my efforts in this journey. You are indeed a jewel in my crown.

Acknowledgements

My academic journey has been influenced by many people who have played indispensable roles in contributing to my career progression.

I hold deep gratitude to my parents Mr. and Mrs. Abraham and Grace Mayoka for the upbringing and tutelage in the ways of life. Their strictness, passion to see excellence in me and encouragement have been a source of great inspiration.

My teachers, lecturers and instructors in my previous academic passages at Nairobi school, University of Nairobi and University College London School of Pharmacy are warmly acknowledged for guidance in my academic endeavours. Dr. Faith Okalebo of the School of Pharmacy, University of Nairobi deserves special mention for being the bridge that conveyed me to my PhD supervisor. Owing to her good reputation during her PhD studentship, her recommendation of my PhD candidature was considered despite severe space constraints in my prospective supervisor's lab facilities at the time.

To Prof. Kelly Chibale, I owe my deepest gratitude, respect and admiration for an exemplary supervisor and mentor. Thank you for daring not only to dream but also to pursue fervently the dream to a tangible realisation. Your pioneering efforts in drug discovery and development on the African continent has availed an open door for the training of young researchers and academics among whom I am honoured to be numbered. Your unique approach to supervision greatly encouraged my metamorphosis into curving and developing independent judgements, enabling me to find a niche in the complex drug discovery and development field. The opportunity to pursue my PhD in your lab under your guidance with generous financial support from your funding sources is beyond a privilege; it is a blessing.

Given the multidisciplinary nature of the research undertaken in this thesis, contributions by other departments and institutions were crucial. I thank the UCT Department of Medicine, Division of Clinical Pharmacology for the assistance with antiplasmodial assays, drug metabolism and pharmacokinetics studies. Prof. Lynn-marie Birkholtz and her team at University of Pretoria, Department of Biochemistry and Institute of sustainable Malaria control was instrumental in performing the gametocyte assays as was Prof. Theresa Coetzer of the Wits Research Institute for Malaria, University of the Witswatersrand.

I am grateful to Dr. Miguel Prudencio in whose lab the liver stage activity was carried out at the Instituto de Medicina Molecular, Universidae de Lisboa, Portugal. All the antischistosomal tests were graciously performed by the Swiss TPH Parasitology group under Prof. Jennifer Keiser while Dr. Sergio Wittlin's lab tested for antiplasmodial activities on selected compounds against both the drug sensitive and multidrug resistant strains and *in vivo* efficacy studies.

This journey was made lighter and enjoyable by the cohort-both past and present-of the Kelly Chibale medicinal chemistry Research Group. Our mutual exchanges, critique and feedback especially during our vibrant academic research group meetings and lab sessions were impactful. My special thanks go to members of the pyrido [1,2-*a*] benzimidazole team: Kawaljit Singh, John Okombo, Ferdinand Ndubi, Linley Barnard, Consolata Nsanzubuhoro and Kelly Chisanga, with whom we have worked, at different stages, to understand the medicinal chemistry profile of this chemotype. I would like to further appreciate my peer Peter Cheuka with whom I have journeyed in this PhD undertaking and often held useful discussions. Special thanks are due to my long-time friend and colleague Dr. Mathew Njoroge for the exceptional sacrifices to aid especially with pharmacological aspects of this work and for the insightful discourses and engagements throughout my PhD studentship.

Much gratitude goes to the UCT Drug Discovery and Development Centre, H3D that offered invaluable technical expertise and infrastructure throughout my studentship. Administrative input from the UCT Department of Chemistry staff and H3D staff especially Elaine Jones-Rutherford, Saroj Naicker, Deidre Brooks, Ayesha Bandeker and Deirdre van Rooyen are deeply acknowledged. I thank Peter Roberts for kindly attending to requests regarding NMR analyses.

Thanks are due to The UCT Postgraduate Centre and Funding office for financial support through the Jagger Scholarship for International Students and for supplementing my Travel and Conference expenses during my PhD studies. I am also thankful to the Keystone Symposia Funding Future of Science Travel Scholarship granted through the National Institute of Allergy and Infectious Diseases to attend the Conference in 2017. Further gratitude goes to the Bill and Melinda Gates Foundation for contributing towards a Travel Award administered through the American Society for Tropical Medicine and Hygiene (ASTMH) Travel Award Committee to attend the ASTMH 67th Annual General Meeting in New Orleans, Louisiana, 2018.

Ultimately, to God be the glory, great things He has done! The sublime opportunity to pursue this PhD, the health, strength, focus and inspiration are, doubtless, to me, the work of divine orchestration.

Abstract

Malaria and schistosomiasis represent the two most prevalent parasitic infections with grievous repercussions on the socio-economic development of affected countries, mainly in sub-Saharan Africa and South-East Asia. Despite their ravaging effects, the treatments of these two diseases have been committed to a limited arsenal of drugs that are threatened by resistance. This scenario, therefore, calls for decisive steps being taken towards the discovery and development of novel drugs with the ability to target multiple parasite stages and be efficacious against resistant parasite strains to achieve effective control and treatment of malaria and schistosomiasis.

Originating from a World Health Organisation-Tropical Disease Research initiative, a phenotypic whole cell screening was conducted on a commercial library against *Plasmodium falciparum* whereupon novel hits exemplified by compound **1**, embodying a pyridobenzimidazole (PBI) scaffold, were found to portray *in vitro* potency against both chloroquine sensitive and resistant parasites. Initial medicinal chemistry iterations generated analogues including **2** from which improved *in vitro* potency and demonstrable *in vivo* efficacy in a mouse model were observed.

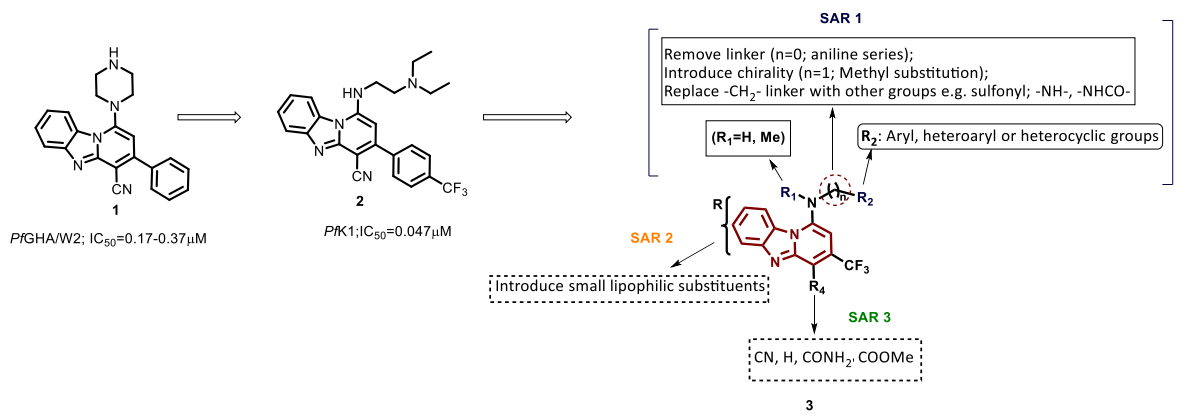

***Figure 1**: Phenotypic whole cell screening hit **1**, initial lead **2** and medicinal chemistry plan **3** followed in this thesis.*

In this thesis, further structural diversity around the PBI motif **3** (**Figure 1**) was pursued with the aim of generating analogues for structure-activity and structure-property relationship studies. Beyond the asexual blood stage activity, the library of compounds generated was also evaluated for activity against the liver and gametocyte stages of *Plasmodium*.

In exploring the probable mechanism of antimalarial action based on their planar morphology and existence of basic centres, the compounds were evaluated for their capacity to disrupt the heme detoxification process, a recognised druggable target in antimalarial drug discovery. Prioritised compounds, based on *in vitro* potency, were progressed for *in vitro* drug metabolism and pharmacokinetics assessment, including metabolic stability and cytotoxicity against Chinese hamster ovarian cell lines. Representative compounds were evaluated for their interaction potential with the human ether-a-go-go-related gene (hERG), a potassium ion channel whose inhibition can cause potentially fatal irregular heartbeats due to perturbed repolarisation of the myocardial action potential. *In vivo* proof-of-concept efficacy and pharmacokinetics studies were carried out on the most promising leads according to a predetermined screening cascade.

Arising from this work, structure-activity relationship (SAR) trends were discernible with electron withdrawing substituents on the aromatic side appendage providing active analogues compared to compounds comprising hydrophilic electron-releasing or donating substituents. Following *in vitro* microsomal metabolic stability analysis, the series displayed moderate to good metabolic stability with compounds incorporating heteroaromatic side groups showing increased susceptibility to biotransformation usually arising from the aromatic ring. In a *P. berghei* mouse model at an oral dose of 50mg/kg over four consecutive days, two compounds **1j/GMP-19** and **4i/GMP-75** achieved 98% and 99.9% reduction in parasitaemia and led to mean survival days of 12 and 14, respectively, compared to the untreated infected mice which survived for only 6 days.

A drug repositioning approach was pursued, exploiting the cellular and biological similarities in the haemoglobin degradation pathways existent in both *Plasmodium* parasites and schistosomes. Out of the 57 analogues tested, 12 were found to be potent inhibitors of the adult worms ($IC_{50} \leq 2$ μM), with several compounds also displaying potency against the newly transformed schistosomula.

Structural features consistent with good antischistosomal potency, interestingly, overlapped with those present in some compounds that also showed good antiplasmodial activity. Prioritised compounds subjected to *in vivo* efficacy studies in mice infected with schistosomes identified **1b/GMP-09**, **1j**/**GMP-19** and **4i**/**GMP-75** with modest antischistosomal activity (55-70% total worm reduction).

Metabolic stability and physicochemical properties correlated with observed *in vivo* efficacy and solubility- limited absorption was implicated to contribute to low *in vivo* exposure of the compounds. Further profiling of physicochemical parameters revealed the interdependence of the properties and that crystallinity, as measured by the melting point, influenced compound solubility.

In summary, the work pursued in this thesis has unravelled the structural features compatible with potent antimalarial and antischistosomal activities of N-aryl substituted 3-trifluoromethyl PBI derivatives. Additionally, structure-property trends of generated analogues have been delineated. The evolvable nature of the structure-activity and structure-property relationship trends make these compounds appealing as candidates for further optimisation campaigns to impart improvements in physicochemical properties and drug metabolism and pharmacokinetics attributes without abrogating activity. Moreover, having identified the overlap as well as divergence in chemical spaces relating to antimalarial and antischistosomal potencies of these series inspire further investigations into the mechanisms of observed antiparasitic actions. Finally, that this work has identified targets which are pan-active across multiple stages of both *Plasmodium* and schistosomes, and possessing favourable safety profiles, provide an exciting opportunity for pursuing these analogues as antimalarial and antischistosomal leads with the potential for malaria chemoprevention and transmission blocking.

Conferences, Seminars and Publications

Conferences and Seminars

1. Keystone Symposia, 24-28 January 2016, Drug Discovery for Parasitic Diseases. Venue: Granlibakken Resort, Tahoe City, California, USA. Poster Title: *Synthesis and Structure- Activity Relationship Studies of Antiplasmodial 3-Trifluoromethyl [1, 2-a] Pyridobenzimidazoles*.
2. H3D Symposium, 15-19 November 2016, Malaria, Tuberculosis and Neglected Tropical Diseases: Progress in Drug Discovery and Development. Venue: Goudini Spa, Western Cape, Republic of South Africa. Poster Title: *Repositioning of Antimalarial Pyridobenzimidazoles as Antischistosomal Agents*.
3. Keystone Symposia, 19-23 February 2017, Malaria: From Innovation to Eradication. Venue: Speke Conference Centre, Kampala, Uganda. Poster Title: *Potential Antiplasmodial Leads from Pyrido (1,2-a) benzimidazoles: Synthesis and Structure-Activity Relationship Studies*.
4. American Society for Tropical Medicine and Hygiene, 66th Annual General Meeting November 5-9, 2017; Baltimore Maryland, USA. Abstract Title: *Antischistosomal Activity of Pyridobenzimidazole Derivatives*.
5. Gordon Research Seminar and Conference, Salve Regina University, New Port, Rhode Island, USA; Biology of Host-Parasite Interactions. June 9-10, 2018, Gordon Research Seminar followed by the Gordon Research Conference, June 10-15, 2018. Poster Title: *Identification of Pyrido[1,2-a] benzimidazole Derivatives with In vivo Antimalarial and Antischistosomal Efficacy*.
6. American Society for Tropical Medicine and Hygiene, 67th Annual General Meeting October 28 - 1 November 2018; New Orleans, Louisiana, USA. Abstract Title: *Antimalarial and Antischistosomal Efficacy of Pyridobenzimidazole Derivatives*.

Publications

1. The Role of Natural Products in Drug Discovery and Development against Neglected Tropical Diseases. Molecules 2017, 22, 58; doi:10.3390/molecules22010058. Peter Mubanga Cheuka, **Godfrey Mayoka**, Peggoty Mutai and Kelly Chibale.

2. Antischistosomal Activity of Pyrido[1,2-*a*] benzimidazole Derivatives and Correlation with Inhibition of β-Hematin Formation. ACS Infect. Dis. 2017, 3 (6) 411-420; DOI: 10.1021/acsinfecdis.6b00205. John Okombo, Kawaljit Singh, **Godfrey Mayoka**, Ferdinand Ndubi, Linley Barnard, Peter M. Njogu, Mathew Njoroge, Liezl Gibhard, Christel Brunschwig, Mireille Vargas, Jennifer Keiser, Timothy J. Egan, and Kelly Chibale.

List of abbreviations, symbols and units

WHO	World Health Organisation
ITNs	Insecticide-treated mosquito nets
IRS	Indoors residual spraying
CQ	Chloroquine
DHFR	Dihydrofolate reductase
DHPTS	Dihydropteroate synthase
DHODH	Dihydroorotate dehydrogenase
G6PD	Glucose-6-phosphate dehydrogenase
SP	Sulfadoxine-pyrimethamine
ACT	Artemisinin combination therapy
FDCs	Fixed dose combinations
MMV	Medicines for malaria venture
DNDi	Drugs for neglected diseases initiative
HIV/AIDs	Human immuno-deficiency virus/ Acquired immune deficiency syndrome
DMPK	Drug metabolism and pharmacokinetics
SAR	Structure-activity relationship
ADMET	Absorption, distribution, metabolism, excretion and toxicity
PKPD	Pharmacokinetics and pharmacodynamics
PBPK	Physiological-based pharmacokinetics
PK	Pharmacokinetics
NTDs	Neglected tropical diseases
US FDA	United States Food and Drug Administration
PCPs	Physicochemical properties
BCS	Biopharmaceutical Classification System
BDDS	Biopharmaceutical Drug Disposition and Classification System
GIT	Gastro-intestinal tract
CYP450	Cytochrome P450
PBI	Pyrido [1,2-*a*] benzimidazole

WHO-TDR	World Health Organisation-Tropical Disease Research
NTS	Newly Transformed Schistosomula
Log P	Logarithm of the partition co-efficient between n-octanol and an aqueous phase
Log S	Logarithm of the solubility
hERG	Human ether-a-go-go-related gene
SI	Selectivity index
HPLC	High performance liquid chromatography
MS	Mass spectrometry
LC-MS	Liquid chromatograph coupled to mass spectrometer
TLC	Thin layer chromatography
NMR	Nuclear magnetic resonance
LHS	Left hand side
Rf	Retardation factor
tR	Retention time
UCT	University of Cape Town
Swiss TPH	Swiss Tropical and Public Health Institute
pLDH	Parasite lactate dehydrogenase
DNA	Deoxy-ribonucleic acid
BHI	Beta hematin inhibition
CQS	Chloroquine-sensitive
CQR	Chloroquine-resistant
***Pf*CRT**	*Plasmodium falciparum* chloroquine resistance transporter
DMSO	Dimethyl sulfoxide
GFP	Green-fluorescent protein
CHO	Chinese hamster ovarian cells
MLM	Mouse liver microsomes
HLM	Human liver microsomes
NADH	Nicotinamide adenine dinucleotide (reduced form)
NADPH	Nicotinamide adenine dinucleotide phosphate (reduced form)
IC_{50}	Concentration resulting in 50% activity

tPSA	Topological polar surface area
HBD	Hydrogen bond donor
HBA	Hydrogen bond acceptor
LLE	Ligand lipophilicity efficiency
ESI	Electron spray ionisation
APCI	Atmospheric pressure chemical ionisation
m/z	Mass-to-charge ratio
UV	Ultra-violet
NH_4OAc	Ammonium acetate
MeoH	Methanol
EtoAc	Ethylacetate
DCM	Dichloromethane
Hex	Hexane
THF	Tetrahydrofuran
MP	Melting point
ATP	Adenosine-5-triphosphate
°C	Degrees Celsius
Da	Dalton
µL	Microliter
M	Molar
mM	Millimolar
µM	Micromolar
µg	Microgram
mg	Milligram
Kg	Kilogram
mL	Millilitre
nm	Nanometre
J	NMR coupling constant
Hz	Hertz
MHZ	Megahertz
$Å^2$	Square Ångström

Overview of Thesis Chapters

Table of Contents

List of Figures

List of Schemes

List of Tables

Chapter 1

Introduction and Literature Review

1.1 Chapter overview

This chapter will provide a background to malaria and schistosomiasis. The epidemiology, life cycles and an account of the control and treatment of these parasitic diseases will be covered together with the challenges and opportunities for drug discovery and development of newer therapies. To follow is a discussion on some of the methods used in drug discovery to identify leads for further development. The physicochemical parameters crucial to drug-likeness will be described, as will their interrelationships and impact on drug efficacy. Some of the strategies to modify physicochemical characteristics towards improving their suitability for development will also be presented. The chapter will conclude with a description of pharmacokinetic parameters and their influence on *in vivo* studies and how they are used to drive drug discovery and development projects.

1.2 Malaria

1.2.1 Epidemiology

Malaria is caused by parasites of the plasmodia genus of which four major species are implicated: *P. falciparum, P. malaria, P. ovale and P. vivax*.[1–3] A plasmodium species of simian origin *P. knowlesi*, has also been reported to be infectious to humans albeit with milder virulence.[4,5] *Plasmodium* species differ in their geographical distribution and hence the global variations in the type of malaria. However, it is *P. falciparum* and *P. vivax* that are mostly responsible for infections in Africa and South-East Asia, respectively, with *falciparum* infections being the leading cause of malaria fatalities world-wide.[1,6,7]

Recent statistics by the World Health Organisation (WHO) concede that there were 216 million cases and close to half a million fatalities due to malaria.[8] Consistently, most cases of morbidity and mortality occur not only in Africa but also among the most vulnerable populations comprising children below five years and pregnant women.[9,10]

The negative impact that malaria exerts on productivity, human resource capital and expenditure on treatment further strains the already fragile economies of the poor countries, leading to an endless cycle of poverty.[11–13]

1.2.2 Life cycle and pathophysiology

Malaria transmission relies on both the non-vertebrate mosquito vector and the definite vertebrate human host.[14] A bite, during a blood meal, from a female Anopheles mosquito deposits the plasmodium sporozoites in a human host (**Figure 1.1**).[7] The sporozoites are subsequently translocated from the site of injection to the liver, via the blood stream, where they mature into schizonts. After several multiplication cycles in the liver, the schizonts produce merozoites which are released into systemic circulation where they infect the red blood cells and hence initiate the erythrocytic phase of plasmodium infection. Asexual division continues within the erythrocytes, where the merozoites transform into trophozoites and blood schizonts, which proliferate and rupture, releasing more merozoites to infect even more red blood cells.[15,16] If untreated, this cycle of bursting of red blood cells and re-infection continues unabated. Some of the merozoites differentiate into male and female gametes, the sexual forms of the parasite.[3,17] The gametocytes are taken up by a mosquito during a blood-meal and mature within the gut. In a subsequent encounter with a human host, the infected mosquito injects the mature sporozoites thus completing the life cycle of the parasite.[18]

While some of the sporozoites move to the blood stream resulting in the erythrocytic stage of infection, some dormant forms, referred to as hypnozoites, may lodge in the liver, as occurs with infections mediated by *P. ovale* and *P. vivax*. Once activated by various stimuli such as infections, these otherwise dormant forms can initiate a new infection. [19,20]

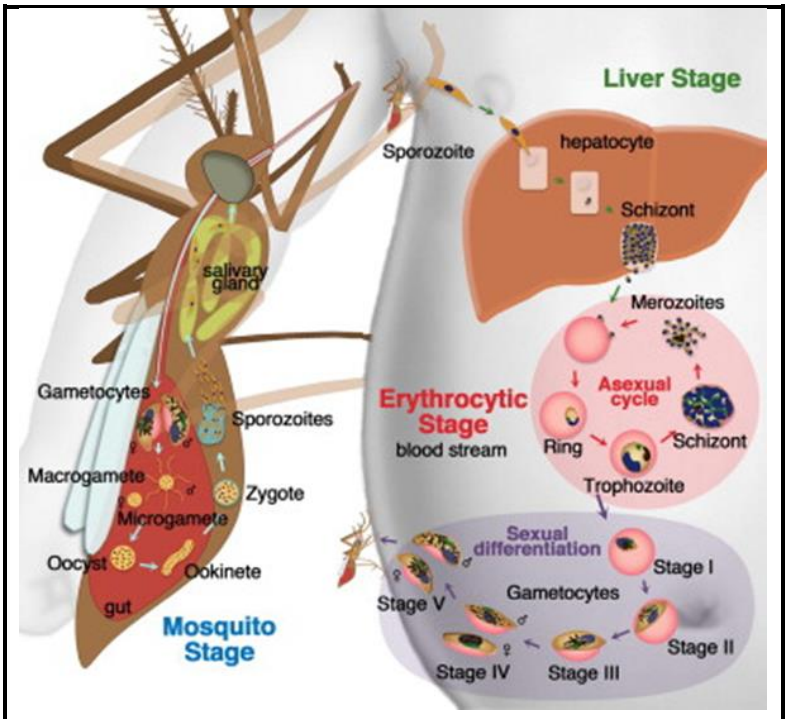

Figure 1.1: *Plasmodium life cycle.*[7]

Rupture of red blood cells is a typical sequela of malaria infections often accompanied by a cassette of symptoms such as fever, headaches, chills, vomiting, anaemia, joint pains and coloured urine.[5,21,22] If not treated promptly, the disease can affect other organs beyond the circulatory system. Cerebral malaria is a severe form of the disease wherein the parasites lodge in the brain leading to impairments in neural and cognitive functions and is frequently fatal in the absence of speedy treatment.[23,24] Other organs and tissues that may be compromised in untreated malaria include kidneys, liver and spleen whose diminished functions can deteriorate to life-threatening conditions including hypoglycaemia, metabolic acidosis with consequent respiratory distress, hypotension and cardiovascular collapse.[5,25,26]

1.2.3 Treatment and prevention

Malaria control aims to provide relief of the clinical symptoms inflicted by the asexual erythrocytic stage of the disease[14] and to prevent vector-to-host transmission propagated through the bite by an infected female Anopheles mosquito. A further goal is to clear the dormant liver forms that are candidates for future activation and harbour the potential to initiate new infections.[27,28]

Non-therapeutic approaches, targeting vector control, complement chemotherapy in the management of malaria. Insecticide treated mosquito nets (ITNs), Indoor Residual Spraying (IRS) with insecticides and mosquito repellents have been employed to prevent vector-host interactions thereby reducing malaria transmission. Commonly used insecticides for ITNs and IRS are those based on pyrethroids due to their environmental and human safety profiles. Other approaches have encompassed the clearing of or disinfecting stagnant water to destroy the breeding grounds for the mosquitoes to disrupt the parasite life cycle.[29–31]

Finding a vaccine against malaria has been elusive and efforts are yet to bear fruit owing to challenges associated with the heterogeneity of surface proteins expressed by the parasite. The *Plasmodium* parasite has a complicated life cycle and a similarly complex genetic make-up. For this reason it has been difficult to come up with a product that can induce antibody production to curtail the reproduction and proliferation of the parasite *in vivo*.[28–30] Even for the most promising malaria vaccine under clinical investigation, affordability and accessibility by the target population are a concern due to the likelihood that it will, of necessity, require additional caution regarding storage facilities to maintain the cold chain besides the more costly intravenous mode of administration.[32] These are unfavourable profiles for an intervention intended to alleviate the suffering of a poor population for which costs of production and treatment should be kept low.

Chemotherapy remains, largely, the mainstay of malaria control and has witnessed interesting evolution since the first antimalarial drug, quinine, an alkaloid from the bark of the cinchona tree *Cinchona officinalis*, Rubiciae that grows wildly in South America.[15,35] Quinine was used to treat fevers from as far back as the 16th century even before proper understanding of the pathogenesis of malaria. It was, however, not until the 19th century that chemical isolation of quinine was attained.[35,36]

Events surrounding the two major World Wars necessitated greater supplies of quinine which natural sources could not satiate. Pressed by the need to protect the military against the ravages of malaria, investments were made towards the discovery of antimalarial drugs.[35,37] The initial approach was to explore chemical synthesis as an alternative to the botanical source of quinine. Despite being unsuccessful, the scaffold present in quinine provided an important starting point for the synthesis of active antimalarial analogues.[36,38,39]

Chloroquine (CQ), a 4-aminoquinoline, is the most well-known and, arguably, the most successful quinine-like antimalarial drug of the 20th century. Used clinically since the 1930s, CQ was the backbone of malaria treatment till. resistant parasites emerged and spread, prompting the relegation in use of what was a promising drug in the fight against malaria. By the 1970s, CQ had been discontinued in many countries[40–43]. Nonetheless, CQ still finds use, in combination with other standard antimalarial drugs, in areas where there is no widespread resistance to CQ.

Prior to the discovery of chloroquine, other quinoline agents employed as antimalarials, although to a limited extent, included pamaquine and mepacrine (quinacrine)[35,44]. Subsequent research identified primaquine, an 8-amino quinoline, which displayed remarkable activity against malaria caused by *P. vivax* and *P. ovale* species and had superior safety profiles compared to pamaquine. Primaquine quickly found use as a prophylactic and radical cure drug[20]. The quinoline methanol mefloquine was discovered by the American-based Walter Reed Army Institute of Research in the late 1960s and it demonstrates superior activity to chloroquine including potency against CQR strains of the parasite.[45–47]

Besides the quinoline antimalarials, other drugs were discovered that target previously unexplored biosynthetic pathways in the plasmodium parasite such as folic acid biosynthesis. For instance, proguanil is an inhibitor of the dihydrofolate reductase (DHFR) enzyme which is essential in the conversion of dihydrofolate to tetrahydrofolate, a key step in the synthesis of parasite DNA (**Figure 1.2**).[48,49] Chlorproguanil, a chlorinated analogue of proguanil was discovered in subsequent studies and has been used in combination with dapsone, a sulphonamide, for the treatment of uncomplicated malaria but haemolysis in glucose-6-phosphate dehydrogenase (G6PD)- deficient patients led to its withdrawal from clinical use.[50] Pyrimethamine, a 2,4-diaminopyrimidine, with structural congruence to proguanil also inhibits the dihydrofolate reductase enzyme and is an important antimalarial drug when used in combination with others.[49,51–53]

In the 1970s, the sulphonamides were characterised to have antimalarial activity in addition to the previously documented antibacterial effects. This class of drugs was found to interfere with synthesis of DNA albeit at a different target from DHFR inhibiting drugs: they inhibit the enzyme dihydropteroate synthase (DHPTS) that catalyses the first step in the pathway involving synthesis of dihydrofolate from para-amino benzoic acid (**Figure 1.2**). Due to structural similarities, sulphonamides act as competitive inhibitors, blocking the uptake of para-amino benzoic acid, which is the substrate for this process. Exploiting synergy, antimalarial therapies were employed using the antifolate drugs such as pyrimethamine and trimethoprim in combination with the sulphonamides, sulfadoxine and sulfamethoxazole respectively.[54,55]

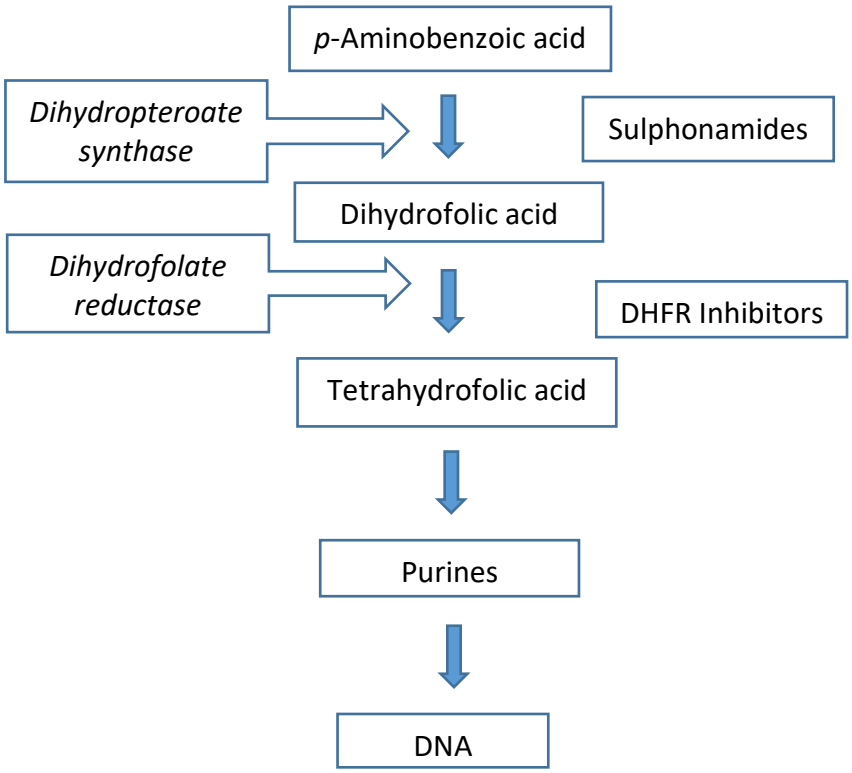

Figure 1.2: *Diagrammatic depiction of the steps in folic acid synthesis in plasmodium and targets of action of antifolate drugs.*

Unfortunately, resistance to sulphonamides quickly developed causing a decline in the use of this class of agents.[41,56,57] There is renewed interest in the use of antifolates in the context of combinational therapy with other standard antimalarial drugs. Typically, sulfadoxine-pyrimethamine combination is the preferred option for prevention of malaria among pregnant women and is widely used in intermittent preventive therapy due to its safety profile while trimethoprim-sulfamethoxazole (co-trimoxazole®) has been widely used in treatment of childhood fevers, bacterial infections and traveller's diarrhoea. [54,58–61]

In the decades between 1960 and 1980, the other new chemical entities discovered and employed in the treatment of malaria include atovaquone, piperaquine, pyronaridine, lumefantrine and naphthoquine (**Figure 1.3**), which portray a prolonged duration of action. Notably, lumefantrine, piperaquine and pyronaridine have since found utility as partner drugs with shorter-acting antimalarial drugs to enhance efficacy and discourage development of resistance.[37,62–65]

Other agents discovered to have antimalarial activity are the tetracycline antibiotics such as tetracycline, doxycycline and minocycline (**Figure 1.3**), which remain recommended in the management of some cases of malaria in combination with suitable standard drugs.[62,66,67]

It is perhaps the introduction of the artemisinin-derived drugs in the 21st century that has resuscitated hopes of conquering malaria. Artemisinin is obtained from the Chinese herb *Qinhao* (Sweet wormwood) *Artemisia annua* L., Compositae whose traditional use in treatment of fevers in China for over 2000 years sparked interest in the research into its antimalarial properties.[37,68] Although evidence existed as far back as the 1970s of their antimalarial potential, the artemisinins were not widely used until in the early 2000 when they received WHO approval as the drugs of choice for uncomplicated malaria.[56,69] In their work, Chinese researchers unravelled the structure of the active antimalarial component where they demonstrated a unique endoperoxide functionality, which is critical to their antimalarial action.[34,61,68]

Clinically, artemisinin is not administered but rather its derivatives, chiefly: artesunate, artemether and the active metabolite dihydroartemisinin, which have superior efficacy and physicochemical qualities compared to the precursor artemisinin.[70] A significant advantage of the artemisinins is their ability to quickly clear blood parasites to below detectable levels.[20] These drugs also have a short elimination half-life and therefore do not encourage selection pressure for development of resistance. A set-back, however, with the artemisinins when used alone is recrudescence, the re-appearing of plasmodium parasites after initial apparent cure due to their short *in vivo* half-life.[21]

To curb resistance and to achieve high efficacy, the artemisinin drugs are therefore used in combination with other standard anti-malarial drugs like lumefantrine, mefloquine, amodiaquine, sulfadoxine plus pyrimethamine (SP) and piperaquine. It is recommended that the drugs used in combination with the artemisinins act via a different mechanism and have a slower *in vivo* elimination to achieve synergy and reduce the chances of development of resistance in addition to minimizing side effects.[43,71–73]

The current artemisinin combination therapy (ACT) regimen include: artemether plus lumefantrine; artesunate plus chloroquine, amodiaquine or mefloquine; artesunate plus sulfadoxine-pyrimethamine and dihydroartemisinin plus piperaquine and are the recommended first-line treatment in falciparum malaria endemic regions.[1,34,74,75] Formulation of these drugs as fixed dose combinations (FDCs) has improved drug dosing regimen and encouraged patient adherence.[21,23] Second-line antimalarial drugs are used in the event of treatment failure or resistance to the first line regimen. Usually, the recommendation is to use an alternative ACT expected to be effective based on resistance data in the respective region. Artesunate or quinine may also be used in combination with a tetracycline antibiotic such as tetracycline, doxycycline or clindamycin.[21,36,67,76] In the case of severe complicated malaria, limited options exist involving the use of either quinine, artesunate or artemether administered intravenously or intramuscularly[25,74] On the other hand, primaquine is currently the only available drug for radical cure while investigations with tafenoquine are at advanced stages.[29,77,78]

Malaria prophylaxis is a particularly important malaria control strategy especially in people traveling to endemic areas from otherwise malaria-free regions.[26] In this case, the individuals receive prescribed doses of drugs before, during and after the visit. Ideal features of drugs used in prophylaxis include a long half-life to ensure adequate drug levels are maintained for sufficient periods to prevent infections and to maintain low parasite count in the blood. Drugs used presently for prophylaxis against malaria include an ACT or quinine together with SP, proguanil plus atovaquone and mefloquine.[15] Primaquine has also been used for malaria prophylaxis with the necessary precaution[47] as have been antibiotics like azithromycin in combination with a standard antimalarial drug such as CQ.[79,80]

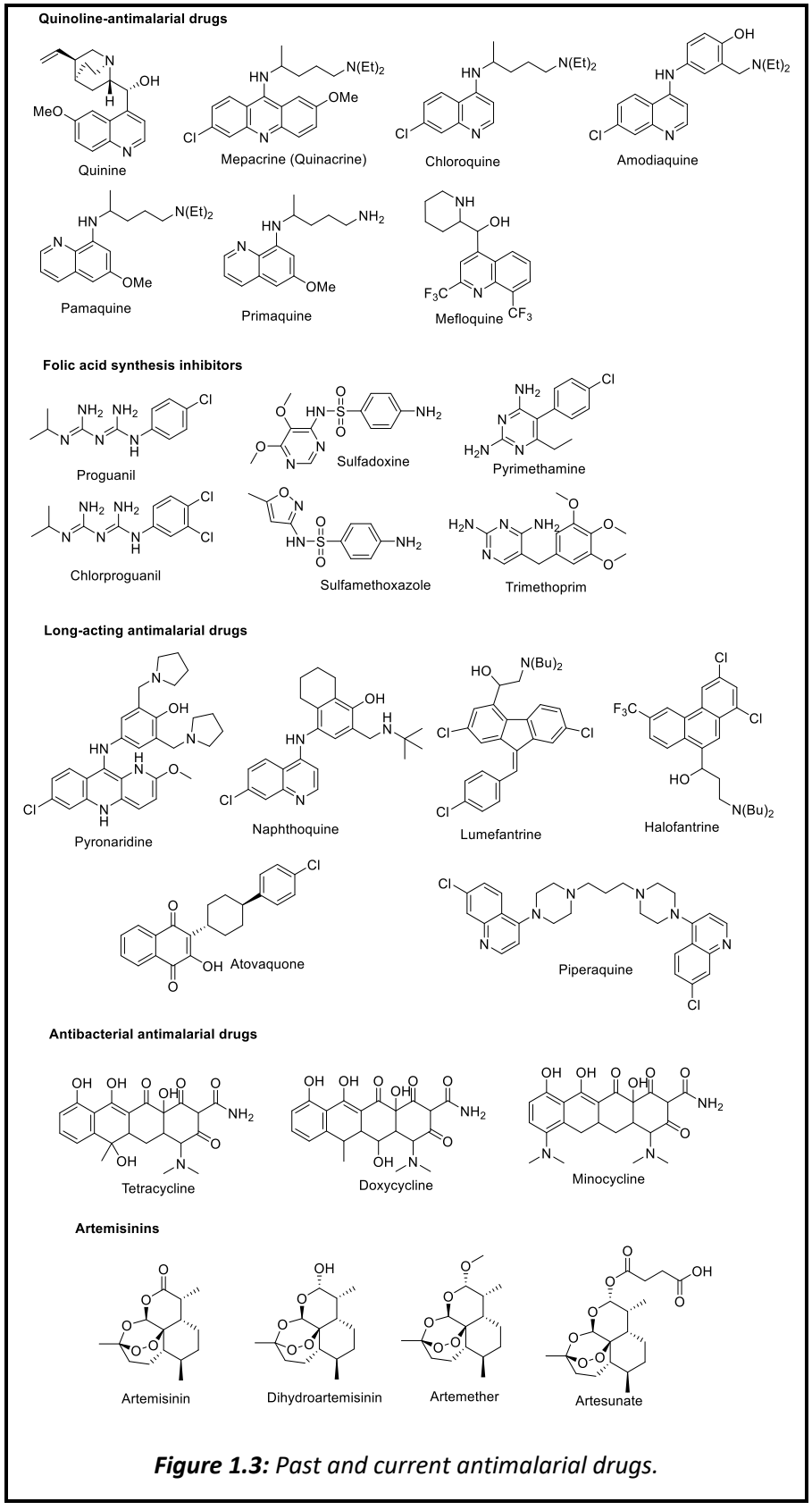

Figure 1.3: *Past and current antimalarial drugs.*

1.2.4 Challenges in malaria chemotherapy

Despite impressive strides taken towards malaria eradication, challenges still abound with the most formidable being the emergence and spread of drug-resistant parasites that threaten the longevity of current therapies.[83–86] This situation is further spurred, in part, by irrational drug use of the limited treatment options.[85,86] Travelling and interactions among people from malaria endemic and non-endemic regions also contribute to the obstacles in malaria eradication as transmission remains an undeniable reality.[57,87,88] Unfortunately, not all malaria-infected people have access to treatment, a scenario that perpetuates the pool of infected hosts who then serve as reservoirs for future infections. On the other hand, reports abound of mosquitoes developing resistance to some of the insecticides used in IRS, thereby reducing the effectiveness of this critical complementary approach to malaria control.[31,89,90]

The unsatisfactory safety profiles of some of the present antimalarial drugs warrants the search for better alternatives. Primaquine, the sole agent in clinical use with activity against the hepatic forms of *P. vivax*, causes fatal haemolysis among patients lacking glucose-6-phosphate dehydrogenase (G6PD), an enzyme involved in regulating cellular oxidative stress.[20,91] Amodiaquine, on the other hand, is associated with hepatotoxicity and blood toxicities, including agranulocytosis and aplastic anaemia, thought to result from its metabolism to the quinone imine and aldehyde reactive metabolites, respectively.[92–95] Skin reactions have been reported with quinine ascribed to its ability to induce photosensitivity.[96,97] Some partner drugs like the sulphonamides may cause severe hypersensitivity reactions like the Stevens-John's syndrome[98,99] while neurological repercussions have been described in the use mefloquine amongst some patients.[100–102]

Most of the current drugs are active at only one of the *Plasmodium* life cycle stages, chiefly the erythrocytic phase associated with clinical symptoms of malaria. Drugs capable of targeting all the life cycle stages of the plasmodia parasite are required if malaria transmission is to be blocked and radical cure achieved, in addition to the relief of clinical symptoms.[1,18]

Newer drugs acting by novel mechanisms and with the capacity to interrupt the parasite life cycle at multiple stages are therefore a dire need. Furthermore, for a long time, there have been no formulations convenient for the paediatric populations who are disproportionately affected by the malaria scourge. Only recently have dispersible ACT formulations[103,104] as well as rectal artesunate[105,106] been made available for use in this crucial population segment.

1.2.5 Antimalarial drug development pipeline

The vibrant antimalarial drug discovery and development efforts witnessed in the past century gradually waned off and, by the last quarter of the century, there was virtually a paucity in research in this therapeutic area with no new antimalarial chemotypes discovered. Since malaria, as with other numerous tropical diseases, afflicts mainly the world's poorest, there is projected meagre returns on investments in this disease despite the significant public health impact it poses.[36,75]

Despite the prolonged dearth, there has been a laudable renaissance towards antimalarial drug discovery arising from a greater sense of responsibility amongst the scientific community that has prompted joint efforts in tackling diseases like malaria that have received limited focus yet. This positive development has been spearheaded by the budding of product development partnerships like Medicines for Malaria Venture (MMV) and Drugs for Neglected Diseases initiative (DNDi) and fanned by the benevolence of funding agencies such as the Bill and Melinda Gates Foundation. Consequently, the recent decade has seen a flourishing of partnerships and collaborations featuring academic institutions, pharmaceutical companies, sponsors and non-governmental organisations geared towards drug discovery for diseases of the poor.[3,14,61]

In this private-public partnership, the aim is to inspire and encourage greater commitment to finding new drugs for diseases which would otherwise remain neglected due to the prospects of low financial returns on investment.[107] As a result, there has been impressive progress in the translation of basic research and the advancement of hit molecules to pre-clinical studies. Several molecules are in preclinical stages of development because of these efforts and others have been investigated in the clinic **(Figure 1.4**).

Moreover, owing to the support in basic research into understanding parasite biochemistry, physiology and disease pathophysiology, additional diverse targets upon which potential antimalarial drug discovery programmes can be based, have been unravelled.

The current antimalarial drug pipeline is robust in terms of the number, and diversity of chemical structure as well as putative mechanisms of action of the investigational agents. The potential drugs range from modifications of previously documented antimalarial scaffolds as in AQ-13, a chloroquine analogue[61], the pre-clinical candidate dihydrofolate reductase inhibitor P218,[108] drug hybrids exemplified by trioxaquines that combine features of the artemisinins and quinoline antimalarial drugs,[17] artemisinin-mimics containing a peroxide moiety such as 1,2,4-trioxolanes typified by OZ439 (artefenomel) in advanced clinical trials.[7,17,109] Others are novel chemical scaffolds with hitherto unexplored biochemical pathways in malaria chemotherapy such as the Phase II candidate MMV390048 which targets the parasite's phosphatidylinositol 4-kinase (*Pf*PI4K),[110,111]the triazolopyrimidine dihydroorotate dehydrogenase (DHODH) inhibitor DSM265,[112,113] the spiroindolone cipargamin (NITD609)[1,114] and the imidazolopiperazine KAF156[113,115] which are all in Phase II clinical trials.[29] The prevailing commitment towards enriching the drug development pipeline should be sustained especially since we are confronted perennially with the challenge of drug resistance.

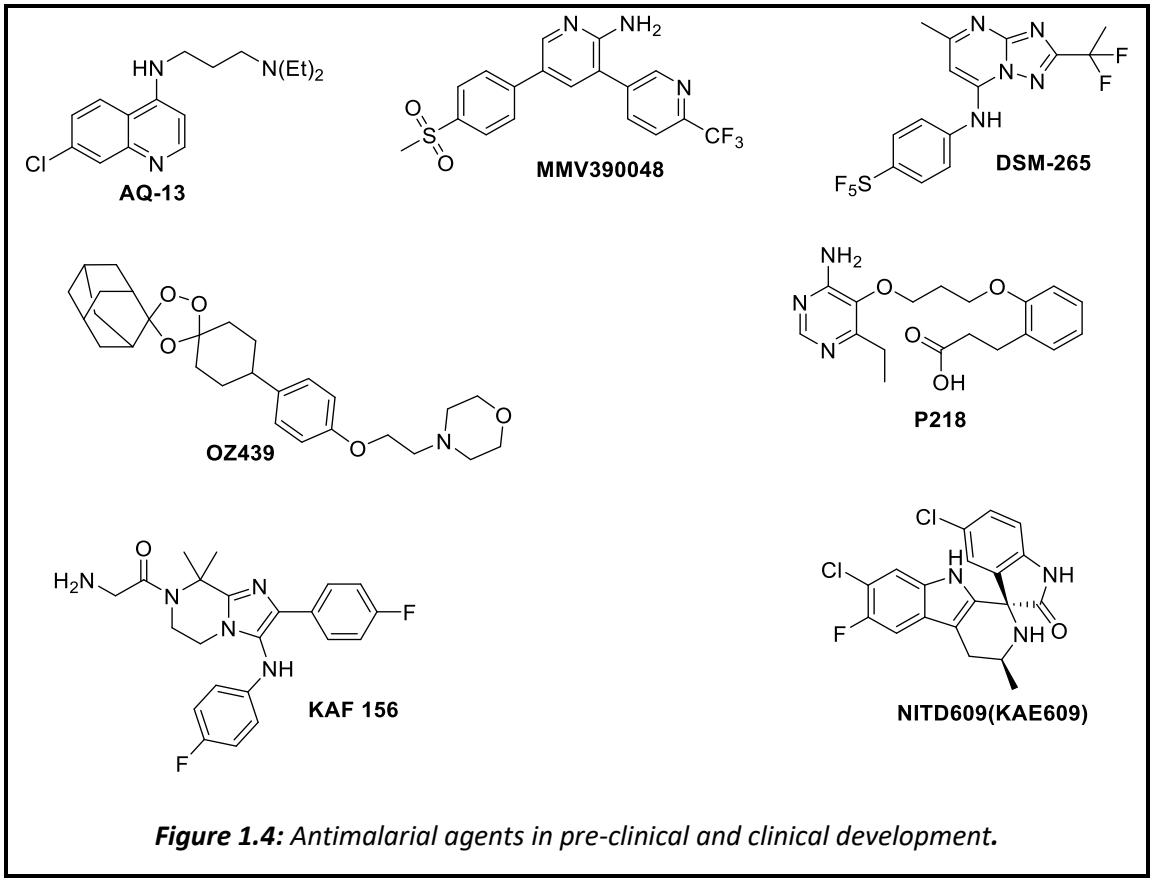

Figure 1.4: *Antimalarial agents in pre-clinical and clinical development.*

1.3 Schistosomiasis

1.3.1 Epidemiology, transmission and life cycle

The public health importance of schistosomiasis is attested to by statistics revealing that there are over 200 million people infected, 700 million at risk of infection and that the disease is endemic in 78 countries.[116–118] This profile makes schistosomiasis rank only second to malaria in terms of prevalence among parasitic infections.[116,119] Close to 250,000 deaths were reported in 2016 due to schistosome-related infections, a figure that is disputed by others, citing underestimation.[120] As with malaria, schistosomiasis is rife in regions experiencing tropical and sub-tropical climates, chiefly sub-Saharan Africa, Middle East, Caribbean and South America, where over 90% of the global incidences and mortalities are recorded.[121–124]

Schistosomiasis, also known as bilharzia or bilharziosis, is caused by trematodes of the *Schistosoma* genus with the most prevalent species being *mansoni*, *japonicum* and *haematobium*.[125] Other implicated species, albeit to a rather local extent, include *S. intercalatum*, *S. guineensis* (West and Central Africa) and *S. mekongii* (Laos and Cambodia).[17,126] There is geographical variation in the global distribution of the major schistosoma species and hence prevalence in the different forms of schistosomiasis: *S. mansoni* is predominant in Africa, the Middle East, Caribbean and South America, whereas *S. haematobium* is reported mainly in Africa with *S. japonicum* being prevalent in Asia, particularly in China and the Philippines.[125,127] The differences in the geographical distribution of the schistosome species emanates from the optimum habitats for the types of the snails, which are intermediate hosts, critical in the completion of their respective life cycles. Thus, *S. mansoni* replicate in certain species of *Biomphalaria* snails, *S. haematobium* utilises *Bulinus spp* while *S. japonicum* depend on the Oncomelania *spp*.[127]

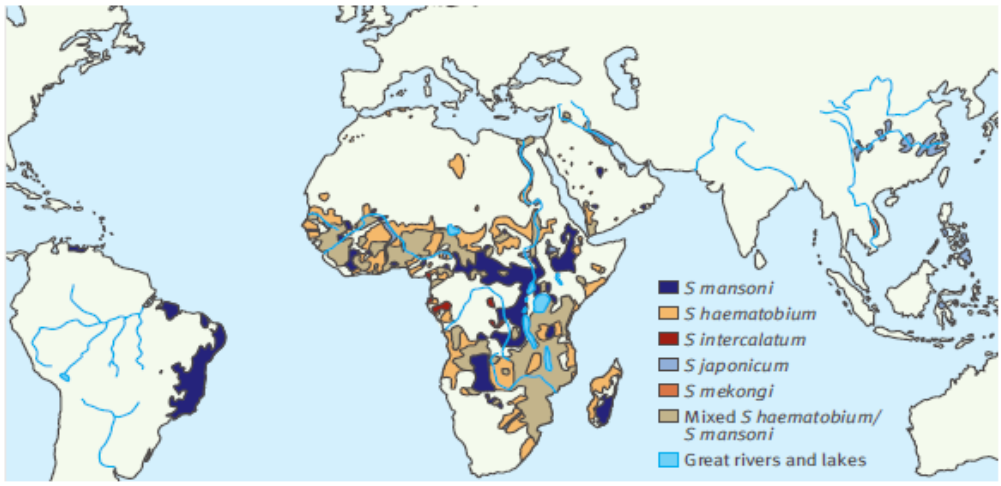

Figure 1.5: *Global distribution of schistosomiasis.*[126]

The life cycle of schistosomes depends on the human definitive host and an intermediate snail vector situated in fresh water environments.[128] Infection to humans occurs when they interact with fresh water infested with the appropriate snail vector whereupon the larval form, cercaria, penetrates the skin. The cercaria sheds off its tail during this invasion, transforming into a schistosomula, and migrates to the lungs via the venous arm of the circulatory system.[17] Subsequently, the juvenile worms move to the hepatic portal system after entering the arterial circulation through the pulmonary capillaries, where they mature into adult worms. Mature male and female worms pair up inseparably, with the female embedded in the gynaecophoric groove of the male, and, depending on the species, migrate to either the mesenteric vessels-in the case of *S. mansoni* and *S. japonicum*-or to the urinary bladder vessels, in infections caused by *S. haematobium*.[129] At these sites, the adult worms reproduce sexually, with the female laying eggs, some of which are shed in faeces or urine. The eggs, in fresh water, hatch into ciliated forms called miracidia which encounter and infect aquatic snails of the appropriate species. While in the intermediate snail vector, the miracidium transforms by asexual reproduction to a cercaria, before infecting the next human host, thus completing the cycle.[17,130,131]

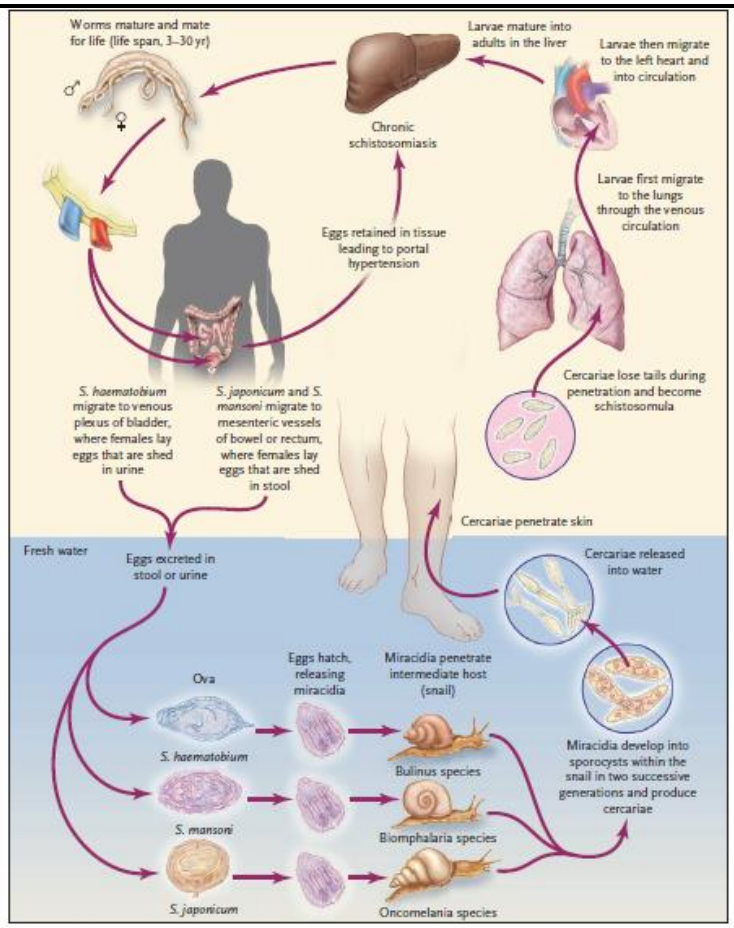

Figure 1.6: *Transmission of schistosomiasis*.[129]

1.3.2 Pathophysiology and complications of schistosomiasis

The presentation of schistosomiasis is inextricably connected to the events characterising the invasion and migration phases, response of the host immune system to the eggs and the presence of the adult worms in the sites of lodging.[126,129] Cercarial dermatitis, also referred to as "swimmer's itch", is an allergic reaction of the skin in response to the penetration of cercaria of schistosomes for which the human host is unsuitable for their further development.[130] Katayama fever, a syndrome of acute schistosomiasis, presents with a host of generalised non-specific symptoms comprising, headache, cough, diarrhoea, malaise, myalgia and poor appetite.[126,129,130]

Immune-induced hypersensitivity reactions against the eggs are largely responsible for the manifestations of schistosomiasis.[116] When the paired adult worms lodge in the mesenteric venules of the gastrointestinal tract, they may cause an array of symptoms ranging from abdominal discomfort, bleeding, to intestinal obstruction in case of heavy worm burden. Malnutrition due to impaired food absorption is commonly reported in countries with high endemicity.[125] Chronic inflammation, propagated in part by the evasion of immune response by the eggs, result in formation of granulomatous lesions and fibrosis in affected organs with consequent compromise of organ function in advanced disease. Some of the complications of chronic schistosomiasis include portal hypertension,[132–134] liver scarring and fibrosis and gastro-intestinal ulceration and anaemia. Other complications secondary to hepatic involvement include ascites and oesophageal varices which can be potentially fatal.[128,130]

In schistosomiasis induced by *haematobium* species, immune reactions to the eggs laid by the adult worms residing in the renal venules may cause ulceration of the epithelia of the urinary lining causing blood to appear in the urine, a condition termed haematuria.[125,135] Sustained inflammation of the renal apparatus predisposes patients to cancer of the urinary bladder, and increased risk of acquiring urinary tract infections caused by urinary retention.[128,130] Female genital schistosomiasis attracts special attention due to its implication as an exacerbating factor for the transmission of HIV/AIDs infection due to the compromised mucosal barrier secondary to urogenital schistosomiasis[136].

Besides, the female reproductive system can be severely damaged leading to miscarriages, barrenness and ectopic pregnancies which have poor prognosis in advanced schistosomiasis.[137]

Embolism of adult worms and concomitant laying of eggs in ectopic sites such as in the brain and spinal cord, can present with debilitating pathologies relating to impaired cognitive, neural and motor functions.[138,117] Due to the insidious nature of the disease, many of the symptoms and complications of schistosomiasis are usually only detected in advanced stages. This is further confounded by the fact that most of the symptoms are non-specific and present in myriad other diseases, leading to frequent misdiagnosis of schistosomiasis.[125,127]

1.3.3 Treatment, control and prevention

The control and elimination of schistosomiasis depends on treatment of infected persons and blocking transmission of the parasites from the intermediate snail host to humans.[134,139] Consequently, multipronged approaches comprising chemotherapy, snail vector control and public health campaigns relating to improvements in hygiene and sanitation have been employed.[127] Snail control has entailed use of natural and chemical molluscides with significant contribution to the schistosomiasis control agenda although, is some instances, at the expense of interference with other aquatic life forms.[137] Despite enduring efforts, public health education on hygiene and sanitation especially with regards to proper disposal of human waste and human-snail habitat contact remain underachieved due to the poor living conditions and economic activities of most of the communities where the disease is endemic.[127]

In the absence of a vaccine against infections by schistosomes, chemotherapy, therefore, remains the backbone of schistosomiasis control.[140] Praziquantel (**Figure 1.7**), a pyrazinoisoquinoline analogue, is the drug of choice for the treatment of all types of human schistosomiasis.[141,142] The drug, introduced in the 1980s, changed the landscape of schistosomiasis treatment which was until then, managed by a limited range of drugs with unfavourable toxicological profiles besides being costly.[143]

Praziquantel is active against the adult worms with little activity towards the juvenile worms, a factor that necessitates repeated administration to ensure effective control.[116,121,144] The safety, affordability (largely due to generous donations and sponsorship) and ease of administration (single oral dose) of praziquantel has endeared it as a tool for mass drug administration especially among school-going children who are vastly affected by schistosomiasis.[145,146] Other important drugs deployed in treatment to schistosomiasis, albeit to a lesser extent, are metrifonate and oxamniquine (**Figure 1.7**) which are singly active against infections caused by haematobium and *mansoni* species.[126,130] Oxamniquine has particularly been extensively used in Brazil but has since been replaced by praziquantel whereas metrifonate has been withdrawn from many markets and is no longer commercially available.[125,129,145]

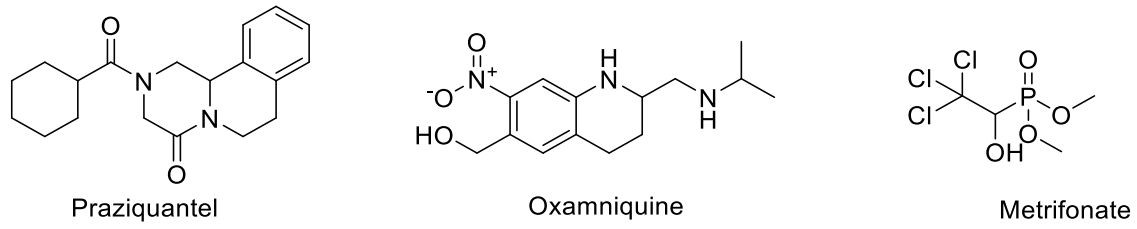

Figure 1.7: *Drugs used in the treatment of schistosomiasis.*

1.3.4 Challenges and opportunities in antischistosomal chemotherapy and drug discovery

The treatment of schistosomiasis remains inadequate especially with the dependence upon only one drug which, although induces activity in all the adult worms causing human schistosomiasis, has no activity against the immature stages.[17,140,147] As such, transmission of the disease and re-infection are bound to persist. Besides, the complete reliance on a single therapeutic agent for a disease with such high morbidity and mortality is deeply unsafe and is potentially catastrophic should resistance emerge in the absence of an effective alternative.[142,148]

Praziquantel, the sole drug employed in the treatment of schistosomiasis, is associated with a bitter taste making it unappealing to children who are the most infected individuals. Additionally, the drug is sold as a racemic mixture although it is established that only one isomer is responsible for its schistosomicidal activity.[127,145] In view of these challenges, there is a compelling need to find alternative active agents as antischistosomal drugs that can backup praziquantel in the possible setting of resistance and importantly, that will display potency against the newly transformed schistosomula in addition to being active against adult worms.[149]

Schistosomiasis has remained, largely, a neglected tropical disease with little investments in drug discovery and development. Among others, two factors seem to be contributing to this fate: the disease course subsequent to infection with schistosomiasis is insidious with generalised non-specific symptoms mirrored by other ailments with only serious effects observable in overly progressed cases.[125,140,150] The second, and perhaps more important, reason is that there is no motivation for investments in a disease that affects mostly the impoverished populations who may not afford the cost of treatment to return the heavy investments in research and development.[151,152] Consequently, there are few agents in the discovery phase for antischistosomal efficacy and the drug development pipeline has been, virtually, empty. The landscape is, however, gently changing with improved commitment to drug discovery for schistosomiasis, fuelled by concerted efforts and collaborations between academic research institutions and the pharmaceutical industry.[148]

There is some progress towards populating the drug discovery pipeline which is currently replete mostly with drugs that have been extensively studied for other disease conditions. Some of these drugs are detailed in the context of drug repurposing and repositioning, discussed later.[120]

1.4 Approaches to drug discovery and development

1.4.1 Whole cell screening and target-based strategies

Advances in technology and the advent of combinatorial chemistry has accelerated the pace at which compounds are tested for biological activity and thus, the progress of medicinal chemistry programs.[153] The large compound libraries and the improved infrastructure that allows for automation has made it possible to screen large volumes of compounds within a relatively short time.[17] This high throughput screening has increasingly been utilised and continues to provide new starting points for several medicinal chemistry optimisation campaigns[16,78,140] and the thriving private-public partnership ventures have created platforms for sharing chemical and biological resources thus enhancing tropical and neglected tropical diseases drug discovery efforts.[7,140,148,154]

Compounds can either be tested against whole parasitic cells or, if characterised, the isolated, purified target to which ligands bind to induce pharmacological outcomes.[155] Each of the two approaches have attendant benefits and pitfalls; whole cell screening, however, has proven to be more successful in providing new clinical candidates than other approaches.[17] Some molecules in preclinical and clinical development whose frontrunner leads were identified via this approach include the antimalarial candidates: triazolopyrimidine (DSM265), spiroindolone NTD609 and imidazolopiperazine KAF156 (**Figure 1.4**).

Chemical matter identified to be potent in a whole cell screening assay have inherent physicochemical properties that allow for traversing biological membranes of the parasite and subsequent interaction with the target that result in the observed activity.[17] Inversely, in target-based screening, the drug molecule is tested for its ability to bind to the target in isolation, without the milieu characterising the whole cell or parasite. This inadequate recapitulation of biological systems is deemed to be among the chief reasons for the failure of many target-based hits to induce *in vivo* efficacy.[148,157] The fact that activity is observed in whole cell screens regardless of the knowledge of the target protein is of benefit in the search for novel sites and modes of action; thus, making whole cell screening an appealing technique in exploring hitherto unidentified drug targets.[17]

Moreover, it is not uncommon for a drug to produce a pharmacological effect by interacting or interfering with multiple physiological or biochemical pathways which would be unrecognised in the classical target-based screening approach.[17,140] Besides, a target may be discovered not to be critical in the survival of the parasite or that its inhibition is insufficient to bring about the desired outcome. A prevailing downside of whole cell screening, however, is the need for subsequent target deconvolution, which can be laborious and lengthy, delaying lead development, a fact that has made others to prefer target-based screening.[17]

Proponents of the target-based screening strategy argue that knowledge of the target protein to which investigational agents bind to produce the desired effect would facilitate quicker medicinal chemistry iterations leading to the identification of more potent analogues.[17,155] This has been greatly augmented by the application of *in silico* tools and availability of X-ray crystallographic structures of numerous protein targets leading to the burgeoning field of computer-aided drug discovery. Testament to the utility of the target-based approach is the identification of the preclinical antimalarial candidate P218, a dihydrofolate reductase inhibitor.[17]

1.4.2 *In silico* and computer-aided drug discovery

As intimated previously, drug efficacy is driven by various factors including those relating to the drug, biological and physiological environment of the parasite and host**.** The understanding and adequate documentation of these variables can allow for rationale execution of medicinal chemistry plans and inform decisions at the various stages of early drug discovery, preclinical assessments and even *in vivo* experimentation. *In silico* and computational tools have progressively become integrated in drug discovery platforms where they have contributed to the expedited progress and cost reduction towards development of clinical candidates.[156,158,159]

Simple yet powerful tools and guidelines such as the Lipinski rule of 5 (**Figure 1.8**) continue to direct medicinal chemistry programmes in the selection, design and synthesis of molecules with appropriate characteristics to enhance their *in vivo* efficacy. The properties described by Lipinski such as molecular weight, number of hydrogen bond donor and acceptor groups and lipophilicity influence physicochemical traits and therefore drug metabolism and pharmacokinetics (DMPK).[160] Careful control of these parameters within acceptable limits is crucial. There are however notable exceptions to this rule for which rationale reference is to be observed depending on the series and projects.[161,162]

a. Lipinski criteria for good oral absorption

- Molecular weight ≤ 500 Da
- No. of hydrogen bond acceptors ≤10
- No. of hydrogen bond donors ≤5
- cLogP≤5

b. Craig plot

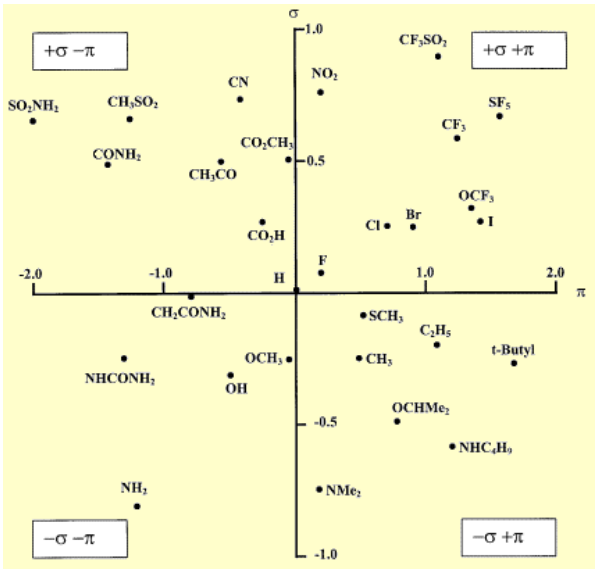

c. Topliss tree

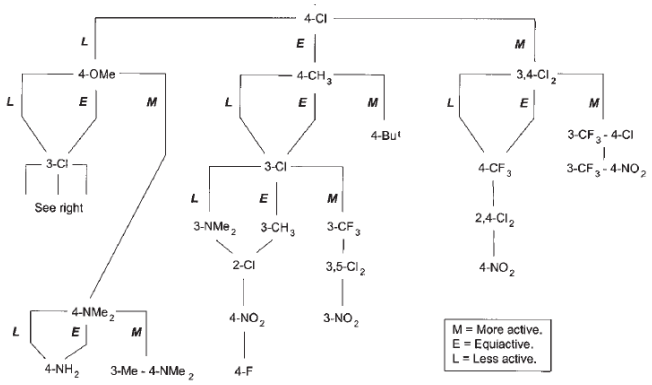

Figure 1.8: *Lipinski rule of five (a), Craig plot (b) and the Topliss decision tree (c).*

The Craig plot (**Figure 1.8**)[163] forms another pertinent reference resource for medicinal chemistry teams. In elucidating structure-activity and structure-property relationships, various groups differing in electronic and lipophilic characters are explored. A scaffold with an evolvable structure-activity relationship (SAR) profile will then point to the favoured quadrant within the Craig plot from which several analogues may be pursued to drive the medicinal chemistry plan. Physicochemical data generated *in silico* can be used for prioritising synthesis of analogues predicted to bear more drug-like attributes. The rational synthesis of such selected target compounds redeems time and resources.[164]

A complementary medicinal chemistry tool is the Topliss decision tree[165,166] (**Figure 1.8**) that gives guidance on how initial assay results with forerunner analogues can direct choice of subsequent alterations. For example, a lipophilic group associated with improved potency may trigger synthesis of second generation analogues with an additional lipophilic group or with greater lipophilicity. If, however, the lipophilic group results in abrogation of activity, a more hydrophilic group may be selected, and should this analogue be more active than its precursor, an additional hydrophilic or a more hydrophilic moiety may be considered.

The chemical structures of compounds can be used to generate their physicochemical and in *in silico* absorption, distribution, metabolism and excretion (ADME) attributes readily by use of several software such as Chemdraw®[167] and Stardrop®,[168–171] respectively. Together with the medicinal chemistry tools discussed above, a limited number of analogues can be rationally synthesized to gain understanding of the SAR of a given series and evaluate its developability, based on predicted physicochemical properties, without excessive indulgence of the expensive organic synthesis resources and time.[172,173]

Technological advancements and improved understanding of biochemical and physiological mechanisms and pathways has also paved way for the development of physiological-based pharmacokinetic (PBPK) and pharmacokinetic-pharmacodynamic (PKPD) simulation software such as SIMCYP®[174–177] and Gastroplus®[178–180] that can assist with predicting drug exposure in different scenarios. Such platforms can estimate DMPK profiles and provide useful insights to drug discovery project teams.[181,182]

Molecular docking and modelling studies have become synchronised in many Pharma set-ups and play a vital role from the inception of medicinal chemistry projects.[167,183–185]This field has been buoyed by the greater understanding and maturation of the areas of molecular biology, genomics, proteomics and X-ray crystallography.[186] With more protein targets being identified and isolated in purified form, and their X-ray structures being unravelled, target-based drug discovery, discussed earlier, has become popular. The X-ray structures reveal the architecture of the putative binding sites with regards to nature and arrangement of amino acid residues involved in interactions with the ligand. This information facilitates the design and synthesis of analogues predicted to possess greater and better binding affinity and, hence, potency.[155,187–189]

1.4.3 Drug repurposing and repositioning

The escalating costs of *de novo* drug discovery has inspired other alternatives with the prospects of shortening the time and reduce financial investments in this already expensive venture. This is particularly appropriate for diseases of the poor such as malaria and schistosomiasis for which returns on investments are expected to be dismal.[151,190] One way of finding new drugs is by exploring new therapeutic indications for already existing drugs utilised in different disease conditions; a concept referred to as drug repurposing.[17] Otherwise, if the reference drugs are used as templates to guide further medicinal chemistry optimisation to generate analogues for new therapeutic uses, the approach is termed drug repositioning. Drug rescue is another closely related term which applies when a lead compound, previously terminated from development, or a drug withdrawn from clinical use, due to a liability like toxicity, undergoes structural alterations to circumvent the shortcomings prior to being investigated in a disease of interest.[17,191]

A common starting point for drug repositioning is biochemical or pharmacological similarities between the targets in the diseases of interest. Additionally, retrospective analysis of the clinical effect of a drug may reveal an unexpected or unintended outcome that may form the basis for future investigations into the new use of the drug.[17,125,190] For instance, during co-infections, the treatment of one of the diseases may result in the remission of the other disease thereby arousing interest in the potential use of the drug in the other disease.

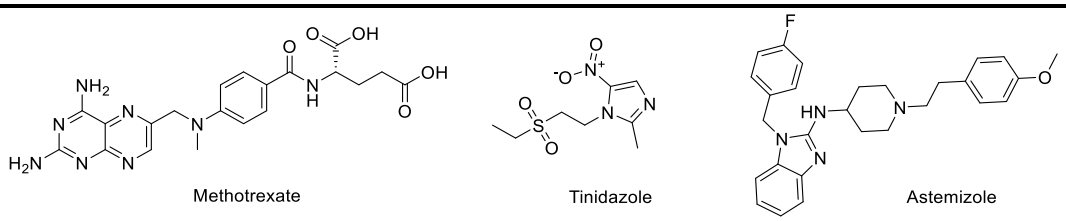

Figure 1.9: *Examples of repurposed and repositioned drugs for malaria.*

These similarities in molecular and cell biology or unexpected clinical observations may then be exploited to furnish new analogues for evaluation as potential drugs.[192] These methods have been used in drug discovery and development in several therapeutic areas including malaria and schistosomiasis.[67,78,193]

Methotrexate, an antifolate anticancer agent attracted interest for testing as an antimalarial agent based on the premise that both cancer cells and malaria parasites require folic acid for their survival and are rapidly multiplying cells in comparison to normal cells. In the use of methotrexate as an anticancer drug, high doses are used which induce toxicity in patients. However, at low doses, methotrexate can clear the malaria parasites without adverse toxicity.[74]

The antihistaminic drug astemizole, was identified in a high throughput screen against *P. falciparum* and shown to be active against multiple plasmodia strains.[194,195] Astemizole was previously withdrawn from clinical use due to severe cardiotoxicity believed to arise from disruptions in the functions of potassium ion channels that control myocardial contractions.[196–198] Chemical evolution based on astemizole structure have been pursued to generate active analogues with potentially safer profiles.[199]

Tinidazole is a nitroimidazole drug and an analogue of metronidazole which is used in the treatment of amoebic dysentery. In the treatment of a patient established to be co-infected with malaria, tinidazole was found to cause remission of malaria symptoms and parasitological cure with activity against the hepatic forms of the parasite. This has led to the investigation into the potential therapeutic application of tinidazole in *P. vivax* malaria.[107,199]

Evaluation of the antischistosomal effects of the anticancer drugs miltefosine[200] and chlorambucil[201] in animal models revealed interesting *in vivo* efficacy, with the latter leading to over 85% total worm reduction, with greater activity being against the juvenile worms.[120] In another study on an oncology drug library at the National Cancer Institute, the kinase inhibitors trametinib and vandetanib were identified with good efficacy in a murine model of schistosomiasis (**Figure 1.10**).[202]

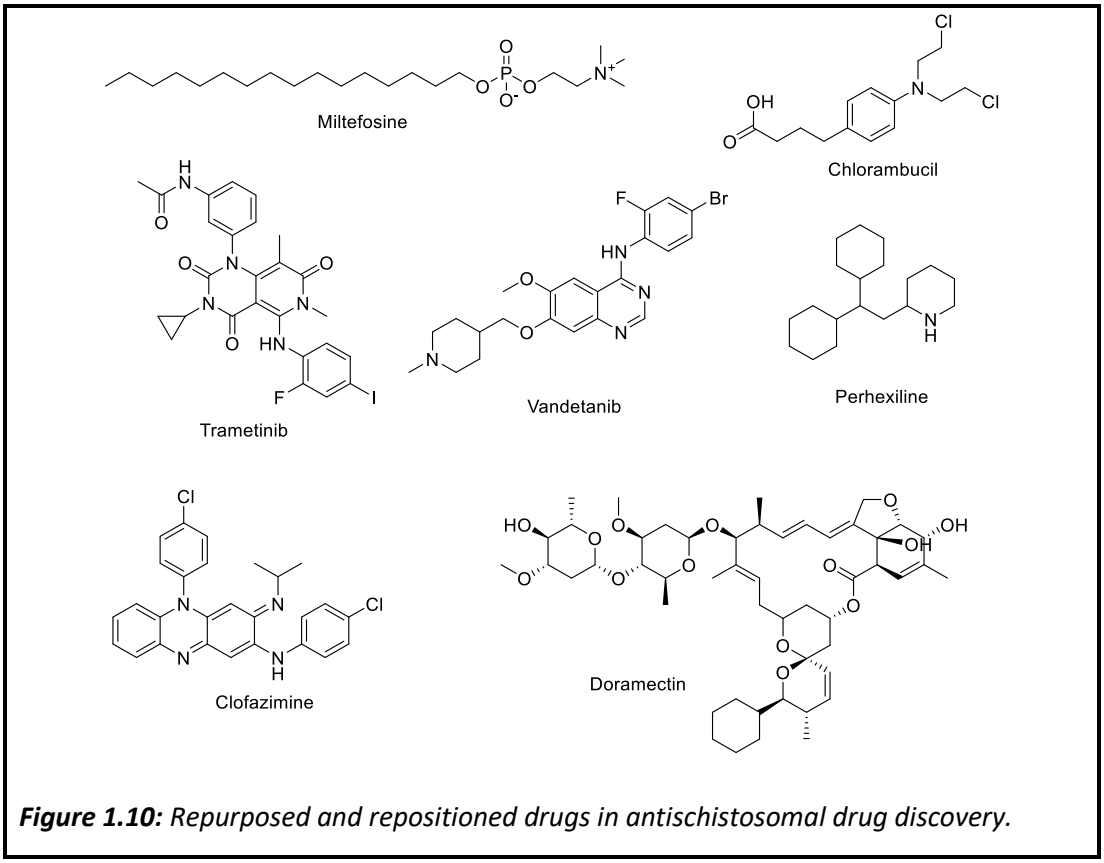

Figure 1.10: *Repurposed and repositioned drugs in antischistosomal drug discovery.*

This work prompts further investigation of kinases as druggable targets in antischistosomal drug discovery. Other approved drugs such as perhexiline (angina),[203] clofazimine (antibiotic) and doramectin (antihelminthic)[204] have also demonstrated promising *in vivo* antischistosomal activity and can serve as important leads (**Figure 1.10**).

Regarding drug repositioning and repurposing in the discovery of new antischistosomal agents from antimalarial drugs and leads, similarities in the haemoglobin catabolism between plasmodia and schistosomes have been cited **(Figure 1.11)**. Haemoglobin is the oxygen-carrying protein in the blood of mammals. Blood-feeding parasites such as *Plasmodium* and the schistosomes depend on haemoglobin for their nutritional requirements.[149,205] These parasites degrade haemoglobin, the process in which amino acids are liberated and utilised for nourishment while the non-globin part, heme, is released as waste product **(Figure 1.11)**. However, free heme is toxic to the parasite which has developed a mechanism to convert it to the inert hemozoin.[206] This heme detoxification pathway is a druggable target and is certainly one of the contributing mechanisms of action of notable antimalarial agents such as the quinine-based compounds like chloroquine, mentioned earlier.[149,207]

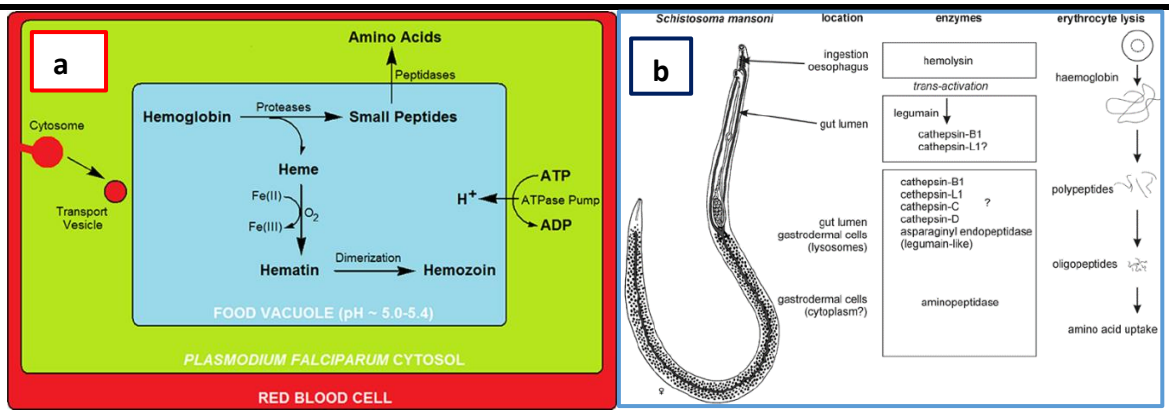

Figure 1.11: *Haemoglobin-degradation pathways in Plasmodium (a) and Schistosoma (b) parasites.*[208]

Several drugs used in the treatment of malaria have exhibited antischistosomal properties.[120,190] This observation has sparked interest in the testing of antimalarial lead compounds in antischistosomal assays as a way of identifying potential starting points for drug discovery towards schistosomiasis. To this end, an open resource referred to as the "Malaria Box" has been availed by the Medicines for Malaria Venture (MMV) for screening against neglected tropical diseases (NTDs) including schistosomiasis.[209–211]

Derivatives featuring the N,N'-diarylurea (MMV665852) and 2,3-dianilinoquinoxaline (MMV007224) scaffolds (**Figure 1.12**) are two examples of active antischistosomal hits arising from the utilisation of this resource in a repositioning approach and are promising lead candidates for further development.[120,212]

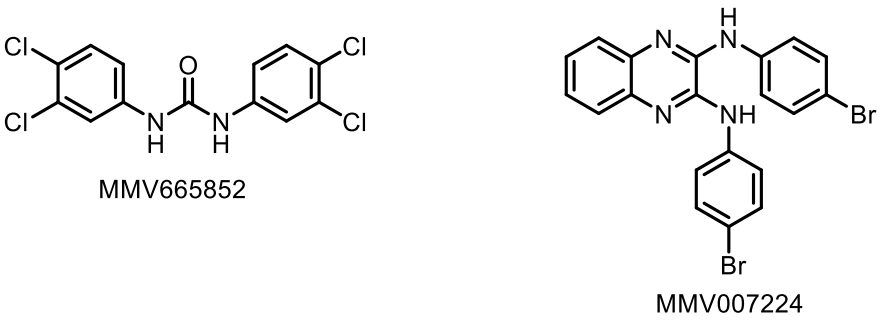

Figure 1.12: *Antischistosomal drug leads from MMV Malaria Box.*

There is a general overlap in the global epidemiological profiles of malaria and schistosomiasis making co-infections with the two diseases a frequent occurrence.[154] Some researchers have exploited this co-incidence to assess the antischistosomal impact of clinically approved antimalarial drugs.[206] In West Africa, Keiser and co-workers observed the antischistosomal efficacy of mefloquine when used in intermittent preventive therapy against malaria among expectant mothers. A similar observation was registered in the use of ACTs containing artesunate and artemether among school going children with greater efficacy noted when administered together with the standard antischistosomal drug, praziquantel.[154,206,213]

Artemisinins have been shown to be particularly active against the immature worms, a profile lacking with praziquantel. There is therefore pleasant synergy when the two drugs are used together. Having an antimalarial agent that contains antischistosomal activity is an advantage on many fronts: It will be cheaper to treat two diseases with one drug, reducing both the costs and pill burden hence improving patient compliance. There is also the advantage of reducing potential for drug-drug interactions since fewer medications would be required. There is, however, concern over the potential for selection of drug-resistant plasmodia parasites if antimalarial drugs are to be used as antischistosomal agents, indiscriminately in malaria endemic regions.[125]

These examples provide credit to the deployment of drug repurposing and repositioning approaches as cheaper and quicker alternatives to drug discovery and development. Indeed, a previous analysis showed that, in 2004, close to 40% of the registered drugs by the US FDA were investigated for other indications other than those for which they were originally discovered and registered.[74]

1.5 Physicochemical properties in drug discovery and development

Physical and chemical characteristics like molecular weight, lipophilicity, number of hydrogen bond donors and acceptors, the total polar surface area, number of rotatable bonds and dihedral angles influence the overall properties of a compound and have a bearing on such important properties as solubility and permeability. These molecular properties have been used to prioritise compounds for their drug-likeness due to their influence on DMPK properties upon which *in vivo* efficacy depends. [159,162,186,214]

1.5.1 Solubility

Solubility, the maximum concentration of a dissolved substance under specific solvent conditions, is among the essential physicochemical properties (PCPs) that impact greatly on the probability of a drug lead to be developed further.[215] For orally administered solid drugs, disintegration into smaller particles precedes dissolution and absorption processes. Therefore, bioavailability, the fraction of administered dose that reaches systemic circulation, is directly linked to the solubility of the drug. Poorly soluble drugs risk precipitating in biological fluids and thereby compromising drug absorption. Besides causing inadequate drug exposure, precipitation may lead to organ damage such as formation of renal crystals in the kidneys or gastrointestinal (GIT) discormfort.[216] For injectable medications, low solubility would necessitate the use of large infusion volumes or frequent dosing that may increase the costs of the medication.

In the early drug discovery and development phases, knowledge of the solubility profiles of compounds is vital for several reasons. The bioassays performed to guide project decisions can only produce reliable results if the compounds analysed have acceptable solubility. Poor solubility may lead to skewed judgements and decisions owing to inaccurate biological activity results.[217] For instance, a highly insoluble compound may register artificially low potency since insufficient concentrations of the compound are attained in the assay conditions. Moreover, the poorly soluble compound is also likely to show exaggeratedly high metabolic stability since, due to precipitation, not all the compound is exposed to the drug metabolising enzymes during the assay.[164,217]

During lead optimization and pre-clinical evaluation, reproducible results are more likely with compounds having good solubility. This also allows for *in vitro* to *in vivo* correlations and dose projections. The solubility profiles of candidate compounds would guide formulation strategies for animal dosing experiments and, if advanced further, clinical trials.[160] Compounds with a combination of good potency, adequate permeability and solubility are predicted to require lower doses to achieve the desired therapeutic outcomes.

During clinical trials, poorly soluble drugs are associated with erratic absorption and inconsistent exposures in test subjects. The inter-individual variability in the pharmacokinetics of a drug candidate can derail its development and may necessitate further investigations to meet recommendations and restrictions set by drug regulatory authorities. This can significantly increase the overall costs and time taken in drug development.[215]

1.5.2 Lipophilicity and permeability

Frequently, drugs must traverse biological membranes such as those of the gastrointestinal system and blood vessels to reach their sites of action. Thus, lead compounds require not only good solubility but also the right lipophilicity. Lipophilicity (LogP) is defined as the ratio of the concentration of a drug when partitioned between a lipid layer (usually n-octanol) and an aqueous layer (water). Substances with high logP values have the propensity to distribute into the octanol layer more than the aqueous layer whereas low logP signifies the ease of association of a compound with the aqueous layer over the organic phase. Whereas solubility is requisite for a compound to dissolve, lipophilicity allows it to traverse the phospholipid membranes. Solubility and lipophilicity are thus contrasting yet inseparable parameters that collectively drive bioavailability.[218–221]

Besides influencing drug absorption, lipophilicity affects other PK parameters and its optimisation can improve the drug-likeness of early drug discovery leads.[220] For instance, highly lipophilic molecules are associated with increased capacity for interaction with biomolecules such as proteins leading to high plasma protein binding which reduces the free fraction of drug available to interact with receptors. It is the unbound drug concentration that determines *in vivo* activity.

This tissue-binding propensity causes high volumes of distribution, decreased clearance and prolongation of elimination half-life.[222] Whereas this might be desirable in certain cases, it can potentially be a source of toxicity especially through drug-drug interactions when another high protein-binding drug is co-administered and compete for binding to the same proteins or in disease conditions where binding profiles may be altered due to decreased levels of proteins. In both these instances, the concentration of free drug may be elevated above the therapeutic range leading to toxicity.[223]

Toxicity, due to off-target interactions, seems to increase with an increase in lipophilicity as does the susceptibility to drug metabolism.[224] The cytochrome P450 drug metabolizing enzymes, which are responsible for the biotransformation of most marketed drugs contain a hydrophobic pocket which makes highly lipophilic drugs good substrates, a property that renders them metabolically labile and can compromise their suitability as leads. Interestingly, hydrophobic interactions, and hence high lipophilicity, are often key mediators of drug-target binding that precede a pharmacological outcome. It is therefore of paramount importance to ensure a proper balance between the solubility and lipophilicity of a lead compound to boost its chances of eliciting the intended clinical outcome with good potency, efficacy and safety profiles.

The speed at which molecules cross the semipermeable membranes is a measure of their permeability. As with other physicochemical attributes, the permeability of a compound depends on multiple factors including size, polarity and lipophilicity.[225] Smaller molecules can travel faster across the membrane while the correct balance of polarity is required for association with the phospholipid bi-layers that are made up of inner hydrophobic and outer hydrophilic centres. Lipophilicity will mediate the interactions of the compound with the hydrophobic interiors while polar groups ensure that the drug can associate with the hydrophilic surfaces on the epithelial cells of the gastrointestinal membranes, crucial for absorption of orally administered drugs. Jointly, solubility, permeability and metabolic stability are key in determining the eventual drug concentration in the systemic circulation, hence, the bioavailability.[226]

1.5.3 Biopharmaceutical Classification System

The relevance of determining physicochemical profiles of leads upstream in the drug development continuum is exemplified by the Biopharmaceutical Classification System (BCS); a system developed to predict oral bioavailability based on *in vitro* parameters chiefly solubility and permeability.[160,216] A closely related Biopharmaceutical Drug Disposition and Classification System (BDDS) factors in the disposition of a drug and the potentials for drug-drug interactions based on its physicochemical attributes.[227] Based on the BCS, drugs are classified into any of the four quadrants according to their solubility and permeability profiles (**Figure 1.13**).

Compounds that are both highly soluble and permeable **I**, are predicted to be easily absorbed and have high bioavailability. Some compounds may be highly soluble but poorly permeable (**II**) for example highly polar molecules (antibiotics, peptides). These drugs would require modifying their polarity by introducing lipophilic groups as in pro-drugs. The increased lipophilicity is expected to enhance permeability. In some cases, the drug leads may be sufficiently lipophilic with good permeation ability but with low soluble (**III**). In such cases, formulation strategies would be required to influence the dissolution profile.

The least favourable category comprises leads or drugs that have both low solubility and poor permeability (**IV**) and for which *in vitro*-to- *in vivo* correlation is impossible. This category is associated with high drug development costs as investments in formulation strategies to improve absorption are often necessary.[216,228,229]

Class I	Class II
High solubility	Low solubility
High permeability	High permeability
Class III	**Class IV**
High solubility	Low solubility
Low permeability	Low permeability

Figure 1.13: *The Biopharmaceutics Classification System.*

Many drug discovery projects use information on the solubility, permeability and metabolic stability of series to prioritise compounds for further development as these have better potentials of translating into clinical candidates. Moreover, based on the logical prediction that compounds with good solubility and permeability profiles are more likely to achieve high exposures *in vivo*, pharmaceutical companies have used the BCS in conjunction with other tests such as *in vitro* and *in vivo* animal ADME studies, to seek and obtain biowaivers from drug regulatory authorities such as the FDA. This approach has been instrumental in expediting the progress to registration of new drugs that would have otherwise required extended and costly bioequivalence studies.[216,230–232]

1.5.4 Strategies to improve physicochemical characteristics

The hits and initial leads of drug discovery projects are often characterised by inadequate PCPs that require optimisation and one of the key properties targeted is solubility.[217,233] Approaches to improve solubility include physical methods, chemical modification and supramolecular-derivation. Formulation strategies may also be employed in the later stages, usually as a last resort, when structure-based modification is unsuccessful.[216] Physical methods of improving solubility entail approaches such as reducing particle size to increase the surface area of particles that are in contact with the solvent system to maximise solute-solvent interactions. As a result, the dissolution and absorption of the active pharmaceutical ingredient is enhanced. Other physical approaches include use of dispersion systems and co-formulations.[234–236]

Chemical structure modification, a commonly used technique in medicinal chemistry, has been successful in elucidating the structure-solubility relationship profiles of many compound series.[216] In this method, changes to the lead compound are executed by, for example, introducing groups that improve polar interactions (OH, NH, SH). The ensuing hydrogen-bond polar interactions between the compound and the solvent increase the solubility of the analogues. Introducing polar groups in the pro-drug strategy has been critical in improving solubility of several drugs.[237]

Aromaticity is a feature associated with high lipophilicity which as mentioned earlier, has reciprocal relationship to solubility.[238] The dense electron character and flat architecture in various aromatic compounds encourage pi-pi stacking resulting in low energy forms with high melting points and increased solvation energy. Improvements in solubility can, therefore, be achieved by de-aromatisation of molecules.[239] As such, cyclic saturated systems have been used in SAR optimisation programs aimed at improving solubility. Planarity and molecular symmetry are features that favour crystal packing and low energy conformations associated with decreased solubility; when disrupted, molecules with higher energy states and better solubility can be realised.[239] This can be achieved via substitutions at appropriate sites on a given scaffold such as at benzylic positions or in di-aryl systems.

Reduction in molecular size is another avenue for the generation of more soluble analogues. For compounds containing cyclic aliphatic or aromatic rings, a SAR campaign using smaller rings or lipophilic groups can be explored and if these alternatives result in similarly active compounds, these are preferred as they will possess better solubility.

Medicinal chemistry changes to improve permeability are those that will increase lipophilicity and are often opposite to those that favour solubility. The changes include reducing polarity by transforming polar functional groups to non-polar ones for example, converting carboxylic acid group to an ester and hydroxyl group to an ether. These added moieties are usually cleaved after absorption to unmask the previously covered functional group to accomplish the pharmacological action; this is the pro-drug concept.[162,186] Moreover, reducing molecular size has the potential to improve permeability as it does for solubility.[218]

1.6 Pharmacokinetic principles in drug discovery and development

The changes that occur on a drug following its administration into a living system define its pharmacokinetic profile. In the case of an orally administered drug, the events occurring include the ADME processes. As safety is paramount in drug discovery projects, the study of the toxicological profile is increasingly being front-loaded in which case the acronym ADMET is used.[240–243]

Absorption of a drug describes the phase where the drug crosses the biological membranes of the gastrointestinal tract before entering the systemic circulation. Since dissolution of the solid drug into aqueous biological media must take place followed by penetration of the drug molecules across the GIT membranes, both solubility and permeability are pre-requisites for absorption. Once absorbed into the mesenteric vessels of the GIT, the drug is transported to the liver via the hepatic portal circulation which conveys nutrient-rich blood from the GIT to the liver. During this first passage through the liver, significant drug metabolism may occur, hence first pass metabolism, before the drug finally enters the general systemic circulation.[242] This phenomenon can influence the amount of drug that eventually reaches target sites of action. Bioavailability is the fraction of the administered oral dose that eventually reaches the systemic circulation and is thus a function of both the solubility, permeability and metabolic stability of a drug.

The body recognises drugs as being foreign substances and endeavours to eliminate them, usually after bio-transformations. Drug metabolism occurs principally in the liver as it has high concentrations of drug-metabolising enzymes and is highly perfused.[244] Other sites such as the kidney, gastro-intestinal tract, blood plasma and lungs may also participate in drug metabolism albeit, to a lesser extent. Metabolism may be classified largely as either phase I or Phase II. In phase I, the drug is modified mainly to increase its polarity to enhance its removal from the body. Phase I reactions include oxidation, reduction and hydrolysis and take place mainly in the microsomes of the smooth endoplasmic reticulum where Cytochrome P450 (CYP450) superfamily of enzymes are located. Phase II reactions occur mainly in the cytosol and involve the attachment of a polar group, such as glucuronide or sulphate via conjugation reactions mediated by the soluble transferase enzymes.[242,245–247]

Over 90% of marketed drugs undergo metabolism mediated by the CYP450 enzymes making *in vitro* drug metabolism profiling therefore using these enzymes a compelling practice in many drug discovery programs.[248,249] The ability of a new chemical entity to withstand metabolism to an acceptable degree is an important parameter as it impacts on the bioavailability and hence pharmacological outcome, in combination with the potency.[241,242,250,251] Thus, metabolic stability assays are important components of early drug discovery screening cascades for their role not only is choosing analogues with suitable metabolic stability but also providing insights critical in identifying metabolic hotspots in a molecule. The information can assist medicinal chemistry teams in executing chemical modifications to address this liability.[155,252]

In many cases, metabolism produces inactive metabolites. However, active metabolites can be formed following biotransformation with the potential to prolong the pharmacological action of the parent compound. Such an observation may prompt research teams to synthesize the active metabolite and study its biological activity, *in vitro* drug metabolism and pharmacokinetics. In the case of pro-drugs, metabolism usually serves to cleave off the protecting group to reveal the active pharmacological entity. On the other hand, toxic metabolites have been characterised for some compounds and have resulted in discontinuation from development or withdrawal from the market of previously approved drugs. Metabolite identification studies, especially for compounds with structural alerts are, therefore, recommended in drug discovery.[240,252,253] Medicinal chemistry optimization of metabolic stability is usually viable with the replacement of the labile functionalities with alternative groups that are more resistant to metabolism but that preserve the ability of the molecule to interact with its biological target hence maintaining biological activity.[254,255]

Since drugs are xenobiotics, they should be removed from the body after achieving their pharmacological activities. The process of excretion occurs mainly in the kidney although other organs such as the liver, skin, lungs, tears and even breast milk, may play a role.[256]

A rapidly cleared drug may have a short-lived pharmacological effect whereas overly prolonged drug concentrations may be a cause for the toxicity of some drugs. In the case of rapidly cleared drugs, combination with other agents that reduce their clearance to improve their half-life can be explored as seen in the co-administration of the antibiotic penicillin with the renal re-uptake inhibitor probenecid in the treatment of certain bacterial infections.[257,258] Prolonged drug exposure long after completing desired pharmacological actions raises propensity for toxicity and drug-drug interactions during co-treatment with other drugs. Chemical modifications may also be applied to optimise the excretion profile of a compound.

Drug safety is fundamental and delineating this property via toxicity assessments as early as possible is crucial in identifying compounds with greater chances of advancing to the clinic.[155,242] The ideal compound should be potent with minimal toxicity observed as a higher selectivity index during *in vitro* assays and wider therapeutic window in clinical evaluations. The selectivity is determined by establishing the concentration of compound required to produce a desired effect in the target in comparison to the concentration at which inhibition of normal cells is achieved: the higher the ratio, the better the selectivity and, hence, safety of the drug.[242,245]

In addition to the tests in mammalian cell lines, interactions with other specific targets such as the human ether-a-go-go-related (hERG) gene have become crucial. This gene controls the expression of potassium ion channels that regulate ion flux during myocardial activity.[259–261] Disruptions in the function of these ion channels have been reported with drugs like astemizole leading to fatal heart attacks and is the reason for the withdrawal of the drug from the market.[262] Additionally, during pre-clinical animal studies, acute and chronic effects of the selected leads are investigated on major systems including the heart, kidneys, liver, lungs and nervous system. Other studies include effects on the reproductive system, mutagenicity and carcinogenicity.[263]

1.7 Chapter Summary

This chapter has provided a background to malaria and schistosomiasis that are the focus of the research work upon which this thesis is based. Insights into the prevalence, current treatment options and challenges as well as the current state of discovery and development of new interventions, were discussed. The chapter further described the opportunities and compelling need for discovering newer therapeutic agents against these diseases and the various approaches to drug discovery and development including the application of whole cell screening and drug repositioning which are of special interest in this thesis. Finally, the physical and chemical characteristics of drugs as well as *in vitro* ADME properties have been discussed in relation to how they influence *in vivo* studies and pharmacological outcomes.

1.8 References

(1) Burrows, J. N.; Hooft van Huijsduijnen, R.; Möhrle, J. J.; Oeuvray, C.; Wells, T. N. Designing the next Generation of Medicines for Malaria Control and Eradication. *Malar. J.* **2013**, *12* (1), 187.

(2) Tangpukdee, N.; Duangdee, C.; Wilairatana, P.; Krudsood, S. Malaria Diagnosis: A Brief Review. *Korean J. Parasitol.* **2009**, *47* (2), 93–102.

(3) Flannery, E. L.; Chatterjee, A. K.; Winzeler, E. A. Antimalarial Drug Discovery — Approaches and Progress towards New Medicines. *Nat. Rev. Microbiol.* **2013**, *11* (12), 849–862.

(4) Carter, R.; Mendis, K. N. Evolutionary and Historical Aspects of the Burden of Malaria. *Clin. Microbiol. Rev.* **2002**, *15* (4), 564–594.

(5) Murphy, S. C.; Shott, J. P.; Parikh, S.; Etter, P.; Prescott, W. R.; Stewart, V. A. Review Article: Malaria Diagnostics in Clinical Trials. *Am. J. Trop. Med. Hyg.* **2013**, *89* (5), 824–839.

(6) Keurulainen, L.; Vahermo, M.; Puente-Felipe, M.; Sandoval-Izquierdo, E.; Crespo-Fernández, B.; Guijarro-López, L.; Huertas-Valentín, L.; de las Heras-Dueña, L.; Leino, T. O.; Siiskonen, A.; Ballell-Pages, L.; Sanz, L. M.; Castañeda-Casado, P.; Jiménez-Díaz, M. B.; Martínez-Martínez, M. S.; Viera, S.; Kiuru, P.; Calderón, F.; Yli-Kauhaluoma, J. A Developability-Focused Optimization Approach Allows Identification of *in vivo* Fast-Acting Antimalarials: N -[3-[(Benzimidazol-2-Yl)amino]propyl]amides. *J. Med. Chem.* **2015**, *58* (11), 4573–4580.

(7) Biamonte, M. A.; Wanner, J.; Le Roch, K. G. Recent Advances in Malaria Drug Discovery. *Bioorg. Med. Chem. Lett.* **2013**, *23* (10), 2829–2843.

(8) World Health Organisation (WHO). *World Malaria Report*; Geneva, 2017.

(9) Radloff, P.; Philips, J.; Nkeyi, M.; Kremsner, P.; Radloff, P.; Hutchinson, D.; Kremsner, P. Atovaquone and Proguanil for *Plasmodium falciparum* Malaria. *Lancet* **1996**, *347* (9014), 1511–1514.

(10) Desai, M.; ter Kuile, F. O.; Nosten, F.; McGready, R.; Asamoa, K.; Brabin, B.; Newman, R. D. Epidemiology and Burden of Malaria in Pregnancy. *Lancet Infect. Dis.* **2007**, *7* (2), 93–104.

(11) Shepard, D. S.; Ettling, M. B.; Brinkmann, U.; Sauerborn, R. The Economic Cost of Malaria in Africa. *Trop. Med. Parasitol.* **1991**, *42* (3), 199–203.

(12) Sachs, J.; Malaney, P. The Economic and Social Burden of Malaria. *Nature* **2002**, *415* (6872), 680–685.

(13) Chima, R. I.; Goodman, C. A.; Mills, A. The Economic Impact of Malaria in Africa: A Critical Review of the Evidence. *Health Policy (New. York).* **2003**, *63* (1), 17–36.

(14) Barnett, D. S.; Guy, R. K. Antimalarials in Development in 2014. *Chem. Rev.* **2014**, *114*, 11221–11241.

(15) Cox, F. E. History of the Discovery of the Malaria Parasites and Their Vectors. *Parasit. Vectors* **2010**, *3* (Figure 1), 5.

(16) Bhagavathula, A. S.; Elnour, A. A.; Shehab, A. Alternatives to Currently Used Antimalarial Drugs: In Search of a Magic Bullet. *Infect. Dis. Poverty* **2016**, *5* (1), 103.

(17) Njoroge, M.; Njuguna, N. M.; Mutai, P.; Ongarora, D. S. B.; Smith, P. W.; Chibale, K. Recent Approaches to Chemical Discovery and Development Against Malaria and the Neglected Tropical Diseases Human African Trypanosomiasis and Schistosomiasis. *Chem. Rev.* **2014**, *114* (22), 11138–11163.

(18) Wells, T. N. C.; Alonso, P. L.; Gutteridge, W. E. New Medicines to Improve Control and Contribute to the Eradication of Malaria. *Nat. Rev. Drug Discov.* **2009**, *8* (11), 879–891.

(19) Mendis, K.; Sina, B. J.; Marchesini, P.; Carter, R. The Neglected Burden of Plasmodium Vivax Malaria. *Am. J. Trop. Med. Hyg.* **2001**, *64* (1–2 Suppl), 97–106.

(20) Burgoine, K. L.; Bancone, G.; Nosten, F. The Reality of Using Primaquine. *Malar. J.* **2010**, *9* (1), 376.

(21) Banek, K.; Lalani, M.; Staedke, S. G.; Chandramohan, D. Adherence to Artemisinin-Based Combination Therapy for the Treatment of Malaria: A Systematic Review of the Evidence. *Malar. J.* **2014**, *13*, 7.

(22) Freedman, D. O. Malaria Prevention in Short-Term Travelers. *N. Engl. J. Med.* **2008**, *359* (6), 603–612.

(23) Lödige, M.; Hiersch, L. Design and Synthesis of Novel Hybrid Molecules against Malaria. *Int. J. Med. Chem.* **2015**, *2015*, 1–23.

(24) Garcia, C. R.; Markus, R. P.; Madeira, L. Tertian and Quartan Fevers: Temporal Regulation in Malarial Infection. *J. Biol. Rhythms* **2001**, *16* (321), 436–443.

(25) Olliaro, P. L.; Taylor, W. R. J. Antimalarial Compounds: From Bench to Bedside. *J. Exp. Biol.* **2003**, *206*, 3753–3759.

(26) Sheehy, T. W.; Reba, R. C. Complications of Falciparum Malaria and Their Treatment. *Ann. Intern. Med.* **1967**, *66* (4), 807–809.

(27) Hulden, L.; Hulden, L. Activation of the Hypnozoite: A Part of Plasmodium Vivax Life Cycle and Survival. *Malar. J.* **2011**, *10* (1), 90.

(28) Fernando, D.; Rodrigo, C.; Rajapakse, S. Primaquine in Vivax Malaria: An Update and Review on Management Issues. *Malar. J.* **2011**, *10* (1), 351.

(29) White, N. J. Can New Treatment Developments Combat Resistance in Malaria? *Expert Opin. Pharmacother.* **2016**, *17* (10), 1303–1307.

(30) World Health Organization. The Use of DDT in Malaria Vector Control. *WHO position statement* **2007**.

(31) Ranson, H.; N'Guessan, R.; Lines, J.; Moiroux, N.; Nkuni, Z.; Corbel, V. Pyrethroid Resistance in African Anopheline Mosquitoes: What Are the Implications for Malaria Control? *Trends Parasitol.* **2011**, *27* (2), 91–98.

(32) Targett, G. A. T.; Moorthy, V. S.; Brown, G. V. Malaria Vaccine Research and Development: The Role of the WHO MALVAC Committee. *Malar. J.* **2013**, *12* (1), 362.

(33) Winzeler, E. A. Malaria Research in the Post-Geno Era. *Nat. Rev.* **2008**, *455* (October), 751–756.

(34) Na-Bangchang, K.; Karbwang, J. Current Status of Malaria Chemotherapy and the Role of Pharmacology in Antimalarial Drug Research and Development. *Fundam. Clin. Pharmacol.* **2009**, *23*, 387–409.

(35) Meshnick, S. R.; Dobson, M. J. The History of Anti-Malarial Drugs. *Antimalar. Chemother. Mech. Action, Resist. New Dir. Drug Discov.* **1948**, *14*, 14–16.

(36) Achan, J.; Talisuna, A. O.; Erhart, A.; Yeka, A.; Tibenderana, J. K.; Baliraine, F. N.; Rosenthal, P. J.; D'Alessandro, U. Quinine, an Old Anti-Malarial Drug in a Modern World: Role in the Treatment of Malaria. *Malar. J.* **2011**, *10* (1), 144.

(37) Chen, C. Development of Antimalarial Drugs and Their Application in China: A Historical Review. *Infect. Dis. poverty* **2014**, *3* (1), 9.

(38) Kaur, K.; Jain, M.; Reddy, R. P.; Jain, R. Quinolines and Structurally Related Heterocycles as Antimalarials. *Eur. J. Med. Chem.* **2010**, *45*, 3245–3264.

(39) Foley, M.; Tilley, L. Quinoline Antimalarials: Mechanisms of Action and Resistance. *Int. J. Parasitol.* **1997**, *27* (2), 231–240.

(40) Farooq, U.; Mahajan, R. C. Drug Resistance in Malaria. *J. Vector Borne Dis.* **2004**, *41* (3–4), 45–53.

(41) Klein, E. Y. Antimalarial Drug Resistance: A Review of the Biology and Strategies to Delay Emergence and Spread. *Int. J. Antimicrob. Agents* **2013**, *41* (4), 311–317.

(42) Packard, R. M. The Origins of Antimalarial-Drug Resistance. *N. Engl. J. Med.* **2014**, *371* (5), 397–399.

(43) Antony, H. A.; Parija, S. C. Antimalarial Drug Resistance: An Overview. *Trop. Parasitol.* **2016**, *6* (1), 30–41.

(44) Vennerstrom, J. L.; Makler, M. T.; Angerhofer, C. K.; Williams, J. A. Antimalarial Dyes Revisited: Xanthenes, Azines, Oxazines, and Thiazines. *Antimicrob. Agents Chemother.* **1995**, *39* (12), 2671–2677.

(45) Maguire, J. D.; Krisin; Marwoto, H.; Richie, T. L.; Fryauff, D. J.; Baird, J. K. Mefloquine Is Highly Efficacious against Chloroquine-Resistant Plasmodium Vivax Malaria and *Plasmodium falciparum* Malaria in Papua, Indonesia. *Clin. Infect. Dis.* **2006**, *42* (8), 1067–1072.

(46) Sowunmi, A.; Oduola, A. M. J. Open Comparison of Mefloquine, Mefloquine/sulfadoxine/pyrimethamine and Chloroquine in Acute Uncomplicated Falciparum Malaria in Children. *Trans. R. Soc. Trop. Med. Hyg.* **1995**, *89* (3), 303–305.

(47) Weiss, W. R.; Oloo, A. J.; Johnson, A.; Koech, D.; Hoffman, S. L. Daily Primaquine Is Effective for Prophylaxis against Falciparum Malaria in Kenya: Comparison with Mefloquine, Doxycycline, and Chloroquine plus Proguanil. *J. Infect. Dis.* **1995**, *171* (6), 1569–1575.

(48) Fidock, D. A.; Wellems, T. E. Transformation with Human Dihydrofolate Reductase Renders Malaria Parasites Insensitive to WR99210 but Does Not Affect the Intrinsic Activity of Proguanil. *Proc. Natl. Acad. Sci.* **1997**, *94* (20), 10931–10936.

(49) Plowe, C. V.; Djimde, A.; Bouare, M.; Doumbo, O.; Wellems, T. E. Pyrimethamine and Proguanil Resistance-Conferring Mutations in *Plasmodium falciparum* Dihydrofolate Reductase: Polymerase Chain Reaction Methods for Surveillance in Africa. *Am. J. Trop. Med. Hyg.* **1995**, *52* (6), 565–568.

(50) Van Malderen, C.; Van Geertruyden, J.-P.; Machevo, S.; González, R.; Bassat, Q.; Talisuna, A.; Yeka, A.; Nabasumba, C.; Piola, P.; Daniel, A.; Turyakira, E.; Forret, P.; Van Overmeir, C.; Van Loen, H.; Robert, A.; D' Alessandro, U. Glucose-6-Phosphate Dehydrogenase Deficiency, Chlorproguanil-Dapsone with Artesunate and Post-Treatment Haemolysis in African Children Treated for Uncomplicated Malaria. *Malar. J.* **2012**, *11* (1), 139.

(51) Triglia, T.; Cowman, A. F. Primary Structure and Expression of the Dihydropteroate Synthetase Gene of *Plasmodium falciparum*. *Proc. Natl. Acad. Sci.* **1994**, *91* (15), 7149–7153.

(52) Brooks, D. R.; Wang, P.; Read, M.; Watkins, W. M.; Sims, P. F. G.; Hyde, J. E. Sequence Variation of the Hydroxymethyldihydropterin Pyrophosphokinase: Dihydropteroate Synthase Gene in Lines of the Human Malaria Parasite, *Plasmodium falciparum*, with Differing Resistance to Sulfadoxine. *Eur. J. Biochem.* **1994**, *224* (2), 397–405.

(53) Bzik, D. J.; Li, W. B.; Horii, T.; Inselburg, J. Molecular Cloning and Sequence Analysis of the *Plasmodium falciparum* Dihydrofolate Reductase-Thymidylate Synthase Gene. *Proc. Natl. Acad. Sci.* **1987**, *84* (23), 8360–8364.

(54) Fasan, P. O. Trimethoprim plus Sulphamethoxazole Compared with Chloroquine in the Treatment and Suppression of Malaria in African Schoolchildren. *Ann. Trop. Med. Parasitol.* **1971**, *65* (1), 117–121.

(55) Bushby, S. R. M.; Hitchings, G. H. Trimethoprim, a Sulphonamide Potentiator. *Br. J. Pharmacol. Chemother.* **1968**, *33* (1), 72–90.

(56) White, N. Antimalarial Drug Resistance and Combination Chemotherapy. *Philos. Trans. R. Soc. B Biol. Sci.* **1999**, *354* (1384), 739–749.

(57) Schlagenhauf, P. Malaria: From Prehistory to Present. *Infect. Dis. Clin. North Am.* **2004**, *18* (2), 189–205.

(58) Aviado, D. M.; Singh, G.; Berkley, R. Pharmacology of New Antimalarial Drugs Sulfonamides and Trimethoprim. *Chemotherapy* **1969**, *14* (1), 37–53.

(59) Gutman, J.; Mwandama, D.; Wiegand, R. E.; Ali, D.; Mathanga, D. P.; Skarbinski, J. Effectiveness of Intermittent Preventive Treatment With Sulfadoxine-Pyrimethamine During Pregnancy on Maternal and Birth Outcomes in Machinga District, Malawi. *J. Infect. Dis.* **2013**, *208* (6), 907–916.

(60) Rogerson, S. J.; Chaluluka, E.; Kanjala, M.; Mkundika, P.; Mhango, C.; Molyneux, M. E. Intermittent Sulfadoxine-Pyrimethamine in Pregnancy: Effectiveness against Malaria Morbidity in Blantyre, Malawi, in 1997–1999. *Trans. R. Soc. Trop. Med. Hyg.* **2000**, *94* (5), 549–553.

(61) Burrows, J. N.; Chibale, K.; Wells, T. N. C. The State of the Art in Anti-Malarial Drug Discovery and Development. *Curr. Top. Med. Chem.* **2011**, *11*, 1226–1254.

(62) Hutchinson, D. B.; Chulay, J. D.; Canfield, C. J.; Looareesuwan, S. Malarone (Atovaquone and Proguanil Hydrochloride): A Review of Its Clinical Development for

Treatment of Malaria. Malarone Clinical Trials Study Group. *Am. J. Trop. Med. Hyg.* **1999**, *60* (4), 533–541.

(63) Rueangweerayut, R.; Phyo, A. P.; Uthaisin, C.; Poravuth, Y.; Binh, T. Q.; Tinto, H.; Pénali, L. K.; Valecha, N.; Tien, N. T.; Abdulla, S.; Borghini-Fuhrer, I.; Duparc, S.; Shin, Chang-Sik.; Fleckenstein, L. Pyronaridine–Artesunate versus Mefloquine plus Artesunate for Malaria. *N. Engl. J. Med.* **2012**, *366* (14), 1298–1309.

(64) Kurth, F.; Bélard, S.; Basra, A.; Ramharter, M. Pyronaridine–artesunate Combination Therapy for the Treatment of Malaria. *Curr. Opin. Infect. Dis.* **2011**, *24* (6), 564–569.

(65) Ramharter, M.; Kurth, F.; Schreier, A. C.; Nemeth, J.; Glasenapp, I. von; Bélard, S.; Schlie, M.; Kammer, J.; Koumba, P. K.; Cisse, B.; Mordmüller, B.; Lell, B.; Issifou, S.; Oeuvray, C.; Fleckenstein, L.; Kremsner, P. G. Fixed-Dose Pyronaridine-Artesunate Combination for Treatment of Uncomplicated Falciparum Malaria in Pediatric Patients in Gabon. *J. Infect. Dis.* **2008**, *198* (6), 911–919.

(66) Gaillard, T.; Madamet, M.; Pradines, B. Tetracyclines in Malaria. *Malar. J.* **2015**, *14* (1), 445.

(67) Gaillard, T.; Madamet, M.; Tsombeng, F. F.; Dormoi, J.; Pradines, B. Antibiotics in Malaria Therapy: Which Antibiotics except Tetracyclines and Macrolides May Be Used against Malaria? *Malar. J.* **2016**, *15* (1), 556.

(68) Vangapandu, S.; Jain, M.; Kaur, K.; Patil, P.; Patel, S. R.; Jain, R. Recent Advances in Antimalarial Drug Development. *Med. Res. Rev.* **2007**, *27* (1), 65–107.

(69) Price, R. N.; Douglas, N. M. Artemisinin Combination Therapy for Malaria: Beyond Good Efficacy. *Clin. Infect. Dis.* **2009**, *49* (11), 1638–1640.

(70) Klayman, D. Qinghaosu (Artemisinin): An Antimalarial Drug from China. *Science (80-.).* **1985**, *228* (4703), 1049–1055.

(71) Majori, G. Combined Antimalarial Therapy Using Artemisinin. *Parassitologia* **2004**, *46* (1–2), 85–87.

(72) Aweeka, F. T.; German, P. I. Clinical Pharmacology of Artemisinin-Based Combination Therapies. *Clin. Pharmacokinet.* **2008**, *47* (2), 91–102.

(73) Fidock, D. A.; Rosenthal, P. J.; Croft, S. L.; Brun, R.; Nwaka, S. Antimalarial Drug Discovery: Efficacy Models for Compound Screening. *Nat. Rev. Drug Discov.* **2004**, *3* (6), 509–520.

(74) Nzila, A.; Ma, Z.; Chibale, K. Drug Repositioning in the Treatment of Malaria and TB. *Future Med. Chem.* **2011**, *3* (11), 1413–1426.

(75) Cui, L.; Su, X. Discovery, Mechanisms of Action and Combination Therapy of Artemisinin. *Expert review of anti-infective therapy*. October 2009, pp 999–1013.

(76) Bakshi, R.; Hermeling-Fritz, I.; Gathmann, I.; Alteri, E. An Integrated Assessment of the Clinical Safety of Artemether-Lumefantrine: A New Oral Fixed-Dose Combination Antimalarial Drug. *Trans. R. Soc. Trop. Med. Hyg.* **2000**, *94* (4), 419–424.

(77) John, G. K.; Douglas, N. M.; von Seidlein, L.; Nosten, F.; Baird, K. J.; White, N. J.; Price, R. N. Primaquine Radical Cure of Plasmodium Vivax: A Critical Review of the Literature. *Malar. J.* **2012**, *11* (1), 280.

(78) Andrews, K. T.; Fisher, G.; Skinner-Adams, T. S. Drug Repurposing and Human Parasitic Protozoan Diseases. *Int. J. Parasitol. Drugs Drug Resist.* **2014**, *4* (2), 95–111.

(79) Dunne, M. W.; Singh, N.; Shukla, M.; Valecha, N.; Bhattacharyya, P. C.; Dev, V.; Patel, K.; Mohapatra, M. K.; Lakhani, J.; Benner, R.; Lele, C.; Patki, K. A Multicenter Study of Azithromycin, Alone and in Combination with Chloroquine, for the Treatment of Acute Uncomplicated *Plasmodium falciparum* Malaria in India. *J. Infect. Dis.* **2005**, *191* (10), 1582–1588.

(80) Chico, R. M.; Pittrof, R.; Greenwood, B.; Chandramohan, D. Azithromycin-Chloroquine and the Intermittent Preventive Treatment of Malaria in Pregnancy. *Malar. J.* **2008**, *7* (1), 255.

(81) Meshnick, S. R. Artemisinin: Mechanisms of Action, Resistance and Toxicity. *Int. J. Parasitol.* **2002**, *32* (13), 1655–1660.

(82) White, N. J. Antimalarial Drug Resistance. *J Clin Invest* **2004**, *113* (8), 1084–1092.

(83) Cui, L.; Mharakurwa, S.; Ndiaye, D.; Rathod, P. K.; Rosenthal, P. J. Antimalarial Drug Resistance: Literature Review and Activities and Findings of the ICEMR Network. *American Journal of Tropical Medicine and Hygiene*. 2015, pp 57–68.

(84) Hewitt, S.; Delacollette, C.; Chavez, I. Malaria Situation in the Greater Mekong Subregion. *Southeast Asian J. Trop. Med. Public Health* **2013**, *44 Suppl 1*, 46-72-7.

(85) Khan, S. Y.; Khan, A.; Arshad, M.; Tahir, H. M.; Mukhtar, M. K.; Ahmad, K. R.; Arshad, N. Irrational Use of Antimalarial Drugs in Rural Areas of Eastern Pakistan: A Random Field Study. *BMC Public Health* **2012**, *12* (1), 941.

(86) Nsimba, S. E. D.; Massele, A. Y.; Eriksen, J.; Gustafsson, L. L.; Tomson, G.; Warsame, M. Case Management of Malaria in under-Fives at Primary Health Care Facilities in a Tanzanian District. *Trop. Med. Int. Heal.* **2002**, *7* (3), 201–209.

(87) Franco-Paredes, C.; Santos-Preciado, J. I. Problem Pathogens: Prevention of Malaria in Travellers. *Lancet Infect. Dis.* **2006**, *6* (3), 139–149.

(88) Steffen, R.; Behrens, R. H. Travellers' Malaria. *Parasitol. Today* **1992**, *8* (2), 61–66.

(89) Hargreaves, K.; Koekemoer, L. L.; Brooke, B. D.; Hunt, R. H.; Mthembu, J.; Coetzee, M. Anopheles Funestus Resistant to Pyrethroid Insecticides in South Africa. *Med. Vet. Entomol.* **2000**, *14* (2), 181–189.

(90) N'Guessan, R.; Corbel, V.; Akogbéto, M.; Rowland, M. Reduced Efficacy of Insecticide-Treated Nets and Indoor Residual Spraying for Malaria Control in Pyrethroid Resistance Area, Benin. *Emerg. Infect. Dis.* **2007**, *13* (2), 199–206.

(91) Beutler, E. G6PD Deficiency. *Blood* **1994**, *84* (11), 3613–3636.

(92) Olliaro, P.; Nevill, C.; LeBras, J.; Ringwald, P.; Mussano, P.; Garner, P.; Brasseur, P. Systematic Review of Amodiaquine Treatment in Uncomplicated Malaria. *Lancet* **1996**, *348* (9036), 1196–1201.

(93) Lind, D. E.; Levi, J. A.; Vincent, P. C. Amodiaquine-Induced Agranulocytosis: Toxic Effect of Amodiaquine in Bone Marrow Cultures *In vitro*. *BMJ* **1973**, *1* (5851), 458–460.

(94) Hatton, C. Frequency of Severe Neutropenia Associated with Amodiaquine Prophylaxis against Malaria. *Lancet* **1986**, *327* (8478), 411–414.

(95) Larrey, D. Amodiaquine-Induced Hepatitis. *Ann. Intern. Med.* **1986**, *104* (6), 801.

(96) Ferguson, J.; Addo, H. A.; Johnson, B. E.; Frain-Bell, W. Quinine Induced Photosensitivity: Clinical and Experimental Studies. *Br. J. Dermatol.* **1987**, *117* (5), 631–640.

(97) Ljunggren, B. Systemic Quinine Photosensitivity. *Arch. Dermatol.* **1986**, *122* (8), 909.

(98) Kuritsky, J. N.; Lobel, H. O.; Stern, R.; Miller, K. D.; Satriale, R. F.; Campbell, C. C. Severe Cutaneous Reactions among American Travelers Using Pyrimethamine-Sulfadoxine (Fansidar®) for Malaria Prophylaxis. *Am. J. Trop. Med. Hyg.* **1986**, *35* (3), 451–458.

(99) Hellgren, U.; Rombo, L.; Berg, B.; Carlson, J.; Wiholm, B. E. Adverse Reactions to Sulphadoxine-Pyrimethamine in Swedish Travellers: Implications for Prophylaxis. *BMJ* **1987**, *295* (6594), 365–366.

(100) Hood, J. E.; Jenkins, J. W.; Milatovic, D.; Rongzhu, L.; Aschner, M. Mefloquine Induces Oxidative Stress and Neurodegeneration in Primary Rat Cortical Neurons. *Neurotoxicology* **2010**, *31* (5), 518–523.

(101) Ringqvist, Å.; Bech, P.; Glenthøj, B.; Petersen, E. Acute and Long-Term Psychiatric Side Effects of Mefloquine: A Follow-up on Danish Adverse Event Reports. *Travel Med. Infect. Dis.* **2015**, *13* (1), 80–88.

(102) Nevin, R. L. Limbic Encephalopathy and Central Vestibulopathy Caused by Mefloquine: A Case Report. *Travel Med. Infect. Dis.* **2012**, *10* (3), 144–151.

(103) Abdulla, S.; Sagara, I.; Borrmann, S.; D'Alessandro, U.; González, R.; Hamel, M.; Ogutu, B.; Mårtensson, A.; Lyimo, J.; Maiga, H.; Sasi, P.; Nahum, A.; Bassat, Q.; Juma, E.; Otieno, L.; Björkman, A.; Beck, H. P.; Andriano, K.; Cousin, M.; Lefèvre, G.; Ubben, D.; Premji, Z. Efficacy and Safety of Artemether-Lumefantrine Dispersible Tablets Compared with Crushed Commercial Tablets in African Infants and Children with Uncomplicated Malaria: A Randomised, Single-Blind, Multicentre Trial. *Lancet* **2008**, *372* (9652), 1819–1827.

(104) Kurth, F.; Bélard, S.; Adegnika, A. A.; Gaye, O.; Kremsner, P. G.; Ramharter, M. Do Paediatric Drug Formulations of Artemisinin Combination Therapies Improve the Treatment of Children with Malaria? A Systematic Review and Meta-Analysis. *Lancet Infect. Dis.* **2010**, *10* (2), 125–132.

(105) Tozan, Y.; Klein, E. Y.; Darley, S.; Panicker, R.; Laxminarayan, R.; Breman, J. G. Prereferral Rectal Artesunate for Treatment of Severe Childhood Malaria: A Cost-Effectiveness Analysis. *Lancet* **2010**, *376* (9756), 1910–1915.

(106) Barnes, K.; Mwenechanya, J.; Tembo, M.; Mcllleron, H.; Folb, P.; Ribeiro, I.; Little, F.; Gomes, M.; Molyneux, M. Efficacy of Rectal Artesunate Compared with Parenteral Quinine in Initial Treatment of Moderately Severe Malaria in African Children and Adults: A Randomised Study. *Lancet* **2004**, *363* (9421), 1598–1605.

(107) Granizo, J. J.; Pía Rodicio, M.; Manso, F. J.; Giménez, M. J. Tinidazole: A Classical Anaerobical Drug with Multiple Potential Uses Nowadays]. *Rev. Esp. Quimioter.* **2009**, *22* (2), 106–114.

(108) Yuthavong, Y.; Tarnchompoo, B.; Vilaivan, T.; Chitnumsub, P.; Kamchonwongpaisan, S.; Charman, S. A.; McLennan, D. N.; White, K. L.; Vivas, L.; Bongard, E.; Thongphanchang, C.; Taweechai, S.; Vanichtanankul, J.; Rattanajak, R.; Arwon, U.; Fantauzzi, P.; Yuvaniyama, J. Charman, W. N.; Matthews, D. Malarial Dihydrofolate Reductase as a Paradigm for Drug Development against a Resistance-Compromised Target. *Proc. Natl. Acad. Sci.* **2012**, *109* (42), 16823–16828.

(109) Charman, S. A.; Arbe-Barnes, S.; Bathurst, I. C.; Brun, R.; Campbell, M.; Charman, W. N.; Chiu, F. C. K.; Chollet, J.; Craft, J. C.; Creek, D. J.;Dong, Y.; Matile, H.; Maurer, M.; Morizzi, J.; Nguyen, T.; Papastogiannidis, P.; Scheurer, C.; Shackleford, D. M.; Sriraghavan, K.; Stingelin, L.; Tang, Y.; Urwyler, H.; Wang, X.; White, K. L.; Wittlin, S.; Zhou, L.; Vennerstrom, J. L. Synthetic Ozonide Drug Candidate OZ439 Offers New Hope for a Single-Dose Cure of Uncomplicated Malaria. *Proc. Natl. Acad. Sci.* **2011**, *108* (11), 4400–4405.

(110) Paquet, T.; Le Manach, C.; Cabrera, D. G.; Younis, Y.; Henrich, P. P.; Abraham, T. S.; Lee, M. C. S.; Basak, R.; Ghidelli-Disse, S.; Lafuente-Monasterio, M. J.; Bantscheff, M.; Ruecker,

A.; Blagborough, A. M.; Zakutansky, S. E.; Zeeman, A-M.; White, K. L.; Shackleford, D. M.; Mannila, J.; Morizzi, J.; Scheurer, C.; Angulo-Barturen, I.; Martínez, M. S.; Ferrer, S.; Sanz, L. M.; Gamo, F. J.; Reader, J.; Botha, M.; Dechering, K. J.; Sauerwein, R. W.; Tungtaeng, A.; Vanachayangkul, P.; Lim, C. S.; Burrows, J.; Witty, M. J.; Marsh, K. C.; Bodenreider, C.; Rochford, R.; Solapure, S. M.; Jiménez-Díaz, M. B.; Wittlin, S.; Charman, S. A.; Donini, C.; Campo, B.; Birkholtz, L-M.; Hanson, K. K.; Drewes, G.; Kocken, C. H. M.; Delves, M. J.; Leroy, D.; Fidock, D. A.; Waterson, D.; Street, L. J.; Chibale, K. Antimalarial Efficacy of MMV390048, an Inhibitor of Plasmodium Phosphatidylinositol 4-Kinase. *Sci. Transl. Med.* **2017**, *9* (387), eaad9735.

(111) Ghidelli-Disse, S.; Lafuente-Monasterio, M. J.; Waterson, D.; Witty, M.; Younis, Y.; Paquet, T.; Street, L. J.; Chibale, K.; Gamo-Benito, F. J.; Bantscheff, M.; Drewes, G. Identification of Plasmodium PI4 Kinase as Target of MMV390048 by Chemoproteomics. *Malar. J.* **2014**, *13* (1), P38.

(112) Sulyok, M.; Rückle, T.; Roth, A.; Mürbeth, R. E.; Chalon, S.; Kerr, N.; Samec, S. S.; Gobeau, N.; Calle, C. L.; Ibáñez, J.; Sulyok, Z.; Held, J.; Gebru, T.; Granados, P.; Brückner, S.; Nguetse, C.; Mengue, J.; Lalremruata, A.; Sim, B. K. L.; Hoffman, S. L.; Möhrle, J. J.; Kremsner, P. G.; Mordmüller, B. DSM265 for *Plasmodium falciparum* Chemoprophylaxis: A Randomised, Double Blinded, Phase 1 Trial with Controlled Human Malaria Infection. *Lancet Infect. Dis.* **2017**, *17* (6), 636–644.

(113) Ashley, E. Investment in Antimalarial Drug Development Is Bearing Fruit. *Lancet Infect. Dis.* **2017**, *17* (6), 568–570.

(114) Rottmann, M.; McNamara, C.; Yeung, B. K. S.; Lee, M. C. S.; Zou, B.; Russell, B.; Seitz, P.; Plouffe, D. M.; Dharia, N. V.; Tan, J.; Cohen, S. B.; Spencer, K. R.; Gonzalez-Paez, G. E.; Lakshminarayana, S. B.; Goh, A.; Suwanarusk, R.; Jegla, T.; Schmitt, E. K.; Beck, H.-P.; Brun, R.; Nosten, F.; Renia, L.; Dartois, V.; Keller, T. H.; Fidock, D. A.; Winzeler, E. A.; Diagana, T. T. Spiroindolones, a Potent Compound Class for the Treatment of Malaria. *Science.* **2010**, *329* (5996), 1175–1180.

(115) Kuhen, K. L.; Chatterjee, A. K.; Rottmann, M.; Gagaring, K.; Borboa, R.; Buenviaje, J.; Chen, Z.; Francek, C.; Wu, T.; Nagle, A.; Barnes, S. W.; Plouffe, D.; Lee, M. C. S.; Fidock, D. A.;

Graumans, W.; van de Vegte-Bolmer, M.; van Gemert, G. J.; Wirjanata, G.; Sebayang, B.; Marfurt, J.; Russell, B.; Suwanarusk, R.; Price, R. N.; Nosten, F.; Tungtaeng, A.; Gettayacamin, M.; Sattabongkot, J.; Taylor, J.; Walker, J. R.; Tully, D.; Patra, K. P.;Flannery, E. L.; Vinetz, J. M.; Renia, L.; Sauerwein, R. W.; Winzeler, E. A.; Glynne, Richard J.; Diagana, T. T. KAF156 Is an Antimalarial Clinical Candidate with Potential for Use in Prophylaxis, Treatment, and Prevention of Disease Transmission. *Antimicrob. Agents Chemother.* **2014**, *58* (9), 5060–5067.

(116) Siqueira, L. da P.; Fontes, D. A. F.; Aguilera, C. S. B.; Timóteo, T. R. R.; Ângelos, M. A.; Silva, L. C. P. B. B.; de Melo, C. G.; Rolim, L. A.; da Silva, R. M. F.; Neto, P. J. R. Schistosomiasis: Drugs Used and Treatment Strategies. *Acta Trop.* **2017**, *176*, 179–187.

(117) Colley, D. G.; Bustinduy, A. L.; Secor, W. E.; King, C. H. Human Schistosomiasis. In *The Lancet*; 2014; Vol. 383, pp 2253–2264.

(118) Lamberton, P. H. L.; Faust, C. L.; Webster, J. P. Praziquantel Decreases Fecundity in *Schistosoma mansoni* Adult Worms That Survive Treatment: Evidence from a Laboratory Life-History Trade-Offs Selection Study. *Infect. Dis. Poverty* **2017**, *6* (1), 110.

(119) Utzinger, J.; Shuhua, X.; N'Goran, E. K.; Bergquist, R.; Tanner, M. The Potential of Artemether for the Control of Schistosomiasis. *International Journal for Parasitology*. 2001, pp 1549–1562.

(120) Bergquist, R.; Utzinger, J.; Keiser, J. Controlling Schistosomiasis with Praziquantel: How Much Longer without a Viable Alternative? *Infect. Dis. Poverty* **2017**, *6* (1), 74.

(121) King, C. H. Toward the Elimination of Schistosomiasis. *N. Engl. J. Med.* **2009**, *360* (2), 106–109.

(122) King, C. H.; Dickman, K.; Tisch, D. J. Reassessment of the Cost of Chronic Helmintic Infection: A Meta-Analysis of Disability-Related Outcomes in Endemic Schistosomiasis. *Lancet (London, England)* **2005**, *365* (9470), 1561–1569.

(123) Mathers, C. D.; Ezzati, M.; Lopez, A. D. Measuring the Burden of Neglected Tropical Diseases: The Global Burden of Disease Framework. *PLoS Negl. Trop. Dis.* **2007**, *1* (2), e114.

(124) Chitsulo, L.; Engels, D.; Montresor, A.; Savioli, L. The Global Status of Schistosomiasis and Its Control. *Acta Trop.* **2000**, *77* (1), 41–51.

(125) Keiser, J. Antimalarials in the Treatment of Schistosomiasis. *Curr. Pharm. Des.* **2012**, *18*, 3531–3538.

(126) Gray, D. J.; Ross, A. G.; Li, Y.-S.; McManus, D. P. Diagnosis and Management of Schistosomiasis. *BMJ* **2011**, *342* (may17 1), d2651–d2651.

(127) da Silva, V. B. R.; Campos, B. R. K. L.; de Oliveira, J. F.; Decout, J.-L.; do Carmo Alves de Lima, M. Medicinal Chemistry of Antischistosomal Drugs: Praziquantel and Oxamniquine. *Bioorg. Med. Chem.* **2017**, *25* (13), 3259–3277.

(128) Fenwick, A. Waterborne Infectious Diseases--Could They Be Consigned to History? *Science (80-.).* **2006**, *313* (5790), 1077–1081.

(129) Ross, A. G. P.; Bartley, P. B.; Sleigh, A. C.; Olds, G. R.; Li, Y.; Williams, G. M.; McManus, D. P. Schistosomiasis. *N. Engl. J. Med.* **2002**, *346* (16), 1212–1220.

(130) Gryseels, B.; Polman, K.; Clerinx, J.; Kestens, L. Human Schistosomiasis. *Lancet* **2006**, *368* (9541), 1106–1118.

(131) Gray, D. J.; McManus, D. P.; Li, Y.; Williams, G. M.; Bergquist, R.; Ross, A. G. Schistosomiasis Elimination: Lessons from the Past Guide the Future. *Lancet Infect. Dis.* **2010**, *10* (10), 733–736.

(132) Miranda, M. A. C.; Ferraz, Á. A. B.; Domingues, A. L. C.; Chaves, R. C. M.; Jucá, N.; Mota, D. L. da. Improvement of Schistosomal Portal Hypertensive Colopathy after Surgical Treatment. *Arq. Gastroenterol.* **2013**, *50* (2), 153–156.

(133) Leite, L. A. C.; Pimenta Filho, A. A.; Ferreira, R. de C. dos S.; da Fonseca, C. S. M.; dos Santos, B. S.; Montenegro, S. M. L.; Lopes, E. P. de A.; Domingues, A. L. C.; Owen, J. S.; Lima, V. L. de M. Splenectomy Improves Hemostatic and Liver Functions in Hepatosplenic Schistosomiasis Mansoni. *PLoS One* **2015**, *10* (8), e0135370.

(134) Weerakoon, K. G. A. D.; Gobert, G. N.; Cai, P.; McManus, D. P. Advances in the Diagnosis of Human Schistosomiasis. *Clin. Microbiol. Rev.* **2015**, *28* (4), 939–967.

(135) King, C. H. Parasites and Poverty: The Case of Schistosomiasis. *Acta Trop.* **2010**, *113* (2), 95–104.

(136) Mbabazi, P. S.; Andan, O.; Fitzgerald, D. W.; Chitsulo, L.; Engels, D.; Downs, J. A. Examining the Relationship between Urogenital Schistosomiasis and HIV Infection. *PLoS Negl. Trop. Dis.* **2011**, *5* (12), e1396.

(137) Lardans, V.; Dissous, C. Snail Control Strategies for Reduction of Schistosomiasis Transmission. *Parasitol. Today* **1998**, *14* (10), 413–417.

(138) Marcial-Rojas, R. A. Neurologic Complications of Schistosomiasis. *Ann. Intern. Med.* **1963**, *59* (2), 215.

(139) Savioli, L.; Fenwick, A.; Rollinson, D.; Albonico, M.; Ame, S. M. An Achievable Goal: Control and Elimination of Schistosomiasis. *Lancet* **2015**, *386* (9995), 739.

(140) Neves, B. J.; Dantas, R. F.; Senger, M. R.; Melo-Filho, C. C.; Valente, W. C. G.; de Almeida, A. C. M.; Rezende-Neto, J. M.; Lima, E. F. C.; Paveley, R.; Furnham, N.; Muratov, E.; Kamentsky, L.; Carpenter, A. E.; Braga, R. C.; Silva-Junior, F. P.; Andrade, C. H. Discovery of New Anti-Schistosomal Hits by Integration of QSAR-Based Virtual Screening and High Content Screening. *J. Med. Chem.* **2016**, *59* (15), 7075–7088.

(141) Utzinger, J.; Chollet, J.; Tu, Z.; Shuhua, X.; Tanner, M. Comparative Study of the Effects of Artemether and Artesunate on Juvenile and Adult *Schistosoma mansoni* in Experimentally Infected Mice. *Trans. R. Soc. Trop. Med. Hyg.* **2002**, *96*, 318–323.

(142) Cioli, D.; Valle, C.; Angelucci, F.; Miele, A. E. Will New Antischistosomal Drugs Finally Emerge? *Trends in Parasitology*. 2008, pp 379–382.

(143) Cioli, D.; Pica-Mattoccia, L.; Archer, S. Antischistosomal Drugs: Past, Present … and Future? *Pharmacol. Ther.* **1995**, *68*, 35–85.

(144) Doenhoff, M. J.; Pica-Mattoccia, L. Praziquantel for the Treatment of Schistosomiasis: Its Use for Control in Areas with Endemic Disease and Prospects for Drug Resistance. *Expert Rev. Anti. Infect. Ther.* **2006**, *4* (2), 199–210.

(145) Pica-mattoccia, D. C. L.; Archer, S. Antischistosomal Drugs : *Pharmacol. Ther.* **1995**, *68*, 35–85.

(146) Colley, D. G. Morbidity Control of Schistosomiasis by Mass Drug Administration: How Can We Do It Best and What Will It Take to Move on to Elimination? *Trop. Med. Health* **2014**, *42* (2 Suppl), 25–32.

(147) Utzinger, J.; Chollet, J.; Jiqing, Y.; Jinyan, M.; Tanner, M.; Shuhua, X. Effect of Combined Treatment with Praziquantel and Artemether on Schistosoma Japonicum and *Schistosoma mansoni* in Experimentally Infected Animals. *Acta Trop.* **2001**, *80*, 9–18.

(148) Neves, B. J.; Muratov, E.; Machado, R. B.; Andrade, C. H.; Cravo, P. V. L. Modern Approaches to Accelerate Discovery of New Antischistosomal Drugs. *Expert Opinion on Drug Discovery*. **2016**, 11 (6), 557–567.

(149) Okombo, J.; Singh, K.; Mayoka, G.; Ndubi, F.; Barnard, L.; Njogu, P. M.; Njoroge, M.; Gibhard, L.; Brunschwig, C.; Vargas, M.; Keiser, J.; Egan, T. J.; Chibale, K. Antischistosomal Activity of Pyrido[1,2- a]Benzimidazole Derivatives and Correlation with Inhibition of β-Hematin Formation. *ACS Infect. Dis.* **2017**, *3* (6), 411–420.

(150) Neves, B. J.; Braga, R. C.; Bezerra, J. C. B.; Cravo, P. V. L.; Andrade, C. H. *In silico* Repositioning-Chemogenomics Strategy Identifies New Drugs with Potential Activity against Multiple Life Stages of *Schistosoma mansoni*. *PLoS Negl. Trop. Dis.* **2015**, *9* (1), e3435.

(151) Klug, D. M.; Gelb, M. H.; Pollastri, M. P. Repurposing Strategies for Tropical Disease Drug Discovery. *Bioorg. Med. Chem. Lett.* **2016**, *26* (11), 2569–2576.

(152) Khan, M. O. F.; Keiser, J.; Amoyaw, P. N. A.; Hossain, M. F.; Vargas, M.; Le, J. G.; Simpson, N. C.; Roewe, K. D.; Freeman, T. N. C.; Hasley, T. R.; Maples, R. D.; Archibald, S. J.; Hubin, T. Discovery of Antischistosomal Drug Leads Based on Tetraazamacrocyclic Derivatives and Their Metal Complexes. *Antimicrob. Agents Chemother.* **2016**, *60* (9), 5331–5336.

(153) Kennedy, J. P.; Williams, L.; Bridges, T. M.; Daniels, R. N.; Weaver, D.; Lindsley, C. W. Application of Combinatorial Chemistry Science on Modern Drug Discovery. *J. Comb. Chem.* **2008**, *10*(3), 345–354.

(154) Panic, G.; Duthaler, U.; Speich, B.; Keiser, J. Repurposing Drugs for the Treatment and Control of Helminth Infections. *Int. J. Parasitol. Drugs Drug Resist.* **2014**, *4* (3), 185–200.

(155) Hughes, J.; Rees, S.; Kalindjian, S.; Philpott, K. Principles of Early Drug Discovery. *Br. J. Pharmacol.* **2011**, *162* (6), 1239–1249.

(156) Lipinski, C. A.; Lombardo, F.; Dominy, B. W.; Feeney, P. J. Experimental and Computational Approaches to Estimate Solubility and Permeability in Drug Discovery and Development Settings. *Adv. Drug Deliv. Rev.* **2012**, *64*, 4–17.

(157) Dar, O.; Khan, M. S.; Adagu, I. The Potential Use of Methotrexate in the Treatment of Falciparum Malaria: *In vitro* Assays against Sensitive and Multidrug-Resistant Falciparum Strains. *Jpn. J. Infect. Dis.* **2008**, *61* (3), 210–211.

(158) Yu, H.; Adedoyin, A. ADME–Tox in Drug Discovery: Integration of Experimental and Computational Technologies. *Drug Discov. Today* **2003**, *8* (18), 852–861.

(159) Leeson, P. D. Molecular Inflation, Attrition and the Rule of Five. *Adv. Drug Deliv. Rev.* **2016**, *101*, 22–33.

(160) Elder, D.; Holm, R. Aqueous Solubility: Simple Predictive Methods (*in silico*, *in vitro* and Bio-Relevant Approaches). *Int. J. Pharm.* **2013**, *453* (1), 3–11.

(161) Lipinski, C. A.; Lombardo, F.; Dominy, B. W.; Feeney, P. J. Experimental and Computational Approaches to Estimate Solubility and Permeability in Drug Discovery and Development. The Article Was Originally Published in Advanced Drug Delivery Reviews 23 (1997) 3. *Adv. Drug Deliv. Rev.* **2001**, *46* (1–3), 3–26.

(162) Krämer, S. D.; Aschmann, H. E.; Hatibovic, M.; Hermann, K. F.; Neuhaus, C. S.; Brunner, C.; Belli, S. When Barriers Ignore the “rule-of-Five.” *Adv. Drug Deliv. Rev.* **2016**, *101*, 62–74.

(163) Ritchie, T. J.; Ertl, P.; Lewis, R. The Graphical Representation of ADME-Related Molecule Properties for Medicinal Chemists. *Drug Discov. Today* **2011**, *16* (1–2), 65–72.

(164) Kerns, E. H. High Throughput Physicochemical Profiling for Drug Discovery. *J. Pharm. Sci.* **2001**, *90* (11), 1838–1858.

(165) Rando, D. G.; Sato, D. N.; Siqueira, L.; Malvezzi, A.; Leite, C. Q. F.; Do_Amaral, A. T.; Ferreira, E. I.; Tavares, L. C. Potential Tuberculostatic Agents. Topliss Application on Benzoic Acid [(5-Nitro-Thiophen-2-Yl)-Methylene]-Hydrazide Series. *Bioorg. Med. Chem.* **2002**, *10* (3), 557–560.

(166) Jorge, S. D.; Palace-Berl, F.; Masunari, A.; Cechinel, C. A.; Ishii, M.; Pasqualoto, K. F. M.; Tavares, L. C. Novel Benzofuroxan Derivatives against Multidrug-Resistant Staphylococcus Aureus Strains: Design Using Topliss' Decision Tree, Synthesis and Biological Assay. *Bioorg. Med. Chem.* **2011**, *19* (16), 5031–5038.

(167) Jorgensen, W. L. The Many Roles of Computation in Drug Discovery. *Science (80-.).* **2004**, *303* (5665), 1813–1818.

(168) T'jollyn, H.; Boussery, K.; Mortishire-Smith, R. J.; Coe, K.; De Boeck, B.; Van Bocxlaer, J. F.; Mannens, G. Evaluation of Three State-of-the-Art Metabolite Prediction Software Packages (Meteor, MetaSite, and StarDrop) through Independent and Synergistic Use. *Drug Metab. Dispos.* **2011**, *39* (11), 2066–2075.

(169) Rydberg, P.; Olsen, L. Predicting Drug Metabolism by Cytochrome P450 2C9: Comparison with the 2D6 and 3A4 Isoforms. *ChemMedChem* **2012**, *7* (7), 1202–1209.

(170) Pähler, A.; Brink, A. Software Aided Approaches to Structure-Based Metabolite Identification in Drug Discovery and Development. *Drug Discov. Today Technol.* **2013**, *10* (1), e207–e217.

(171) G. Shin, Y.; Le, H.; Khojasteh, C.; E.C.A. Hop, C. Comparison of Metabolic Soft Spot Predictions of CYP3A4, CYP2C9 and CYP2D6 Substrates Using MetaSite and StarDrop. *Comb. Chem. High Throughput Screen.* **2011**, *14* (9), 811–823.

(172) Basanta K. R. B.; Karunakar, A. Biopharmaceutics Classification System: A Regulatory Approach. *Dissolution Technol.* **2011**, *18* (February), 31–37.

(173) Blake, J. Chemoinformatics – Predicting the Physicochemical Properties of "Drug-Like" Molecules. *Curr. Opin. Biotechnol.* **2000**, *11* (1), 104–107.

(174) Shaffer, C. L.; Scialis, R. J.; Rong, H.; Obach, R. S. Using SimCYP® to Project Human Oral Pharmacokinetic Variability in Early Drug Research to Mitigate Mechanism-Based Adverse Events. *Biopharm. Drug Dispos.* **2012**, *33* (2), 72–84.

(175) Jamei, M.; Marciniak, S.; Feng, K.; Barnett, A.; Tucker, G.; Rostami-Hodjegan, A. The SimCYP® Population-Based ADME Simulator. *Expert Opin. Drug Metab. Toxicol.* **2009**, *5* (2), 211–223.

(176) Rakhit, A.; Pantze, M. P.; Fettner, S.; Jones, H. M.; Charoin, J.-E.; Riek, M.; Lum, B. L.; Hamilton, M. The Effects of CYP3A4 Inhibition on Erlotinib Pharmacokinetics: Computer-Based Simulation (SimCYP®) Predicts *in vivo* Metabolic Inhibition. *Eur. J. Clin. Pharmacol.* **2008**, *64* (1), 31–41.

(177) Dumont, C.; Mentré, F.; Gaynor, C.; Brendel, K.; Gesson, C.; Chenel, M. Optimal Sampling Times for a Drug and Its Metabolite Using SimCYP® Simulations as Prior Information. *Clin. Pharmacokinet.* **2013**, *52* (1), 43–57.

(178) Heikkinen, A. T.; Baneyx, G.; Caruso, A.; Parrott, N. Application of PBPK Modeling to Predict Human Intestinal Metabolism of CYP3A Substrates – An Evaluation and Case Study Using GastroPlus™. *Eur. J. Pharm. Sci.* **2012**, *47* (2), 375–386.

(179) Bolger, M. B.; Lukacova, V.; Woltosz, W. S. Simulations of the Nonlinear Dose Dependence for Substrates of Influx and Efflux Transporters in the Human Intestine. *AAPS J.* **2009**, *11* (2), 353–363.

(180) Okumu, A.; DiMaso, M.; Löbenberg, R. Computer Simulations Using GastroPlus™ to Justify a Biowaiver for Etoricoxib Solid Oral Drug Products. *Eur. J. Pharm. Biopharm.* **2009**, *72* (1), 91–98.

(181) Lavé, T.; Parrott, N.; Grimm, H. P.; Fleury, A.; Reddy, M. Challenges and Opportunities with Modelling and Simulation in Drug Discovery and Drug Development. *Xenobiotica* **2007**, *37* (10–11), 1295–1310.

(182) Chien, J. Y.; Friedrich, S.; Heathman, M. A.; de Alwis, D. P.; Sinha, V. Pharmacokinetics/pharmacodynamics and the Stages of Drug Development: Role of Modeling and Simulation. *AAPS J.* **2005**, *7* (3), E544--E559.

(183) Gschwend, D. A.; Good, A. C.; Kuntz, I. D. Molecular Docking towards Drug Discovery. *J. Mol. Recognit.* **1996**, *9* (2), 175–186.

(184) Yang, S.-Y. Pharmacophore Modeling and Applications in Drug Discovery: Challenges and Recent Advances. *Drug Discov. Today* **2010**, *15* (11–12), 444–450.

(185) Meng, X.-Y.; Zhang, H.-X.; Mezei, M.; Cui, M. Molecular Docking: A Powerful Approach for Structure-Based Drug Discovery. *Curr. Comput. Aided-Drug Des.* **2011**, *7* (2), 146–157.

(186) Matsson, P.; Doak, B. C.; Over, B.; Kihlberg, J. Cell Permeability beyond the Rule of 5. *Adv. Drug Deliv. Rev.* **2016**, *101*, 42–61.

(187) Ambre, P. K.; Wavhale, R. D.; Coutinho, E. C. New Horizons in Antimalarial Drug Discovery in the Last Decade by Chemoinformatic Approaches. *Comb. Chem. High Throughput Screen.* **2015**, *18* (2), 129–150.

(188) Frecer, V.; Megnassan, E.; Miertus, S. Design and *in silico* Screening of Combinatorial Library of Antimalarial Analogs of Triclosan Inhibiting *Plasmodium falciparum* Enoyl-Acyl Carrier Protein Reductase. *Eur. J. Med. Chem.* **2009**, *44* (7), 3009–3019.

(189) Kitchen, D. B.; Decornez, H.; Furr, J. R.; Bajorath, J. Docking and Scoring in Virtual Screening for Drug Discovery: Methods and Applications. *Nat. Rev. Drug Discov.* **2004**, *3*, 935.

(190) Keiser, J.; Utzinger, J. Antimalarials in the Treatment of Schistosomiasis. *Curr. Pharm. Des.* **2012**, *18* (24), 3531–3538.

(191) Aubé, J. Drug Repurposing and the Medicinal Chemist. *ACS Med. Chem. Lett.* **2012**, *3* (6), 442–444.

(192) Bellera, C. L.; Balcazar, D. E.; Vanrell, M. C.; Casassa, A. F.; Palestro, P. H.; Gavernet, L.; Labriola, C. A.; Gálvez, J.; Bruno-Blanch, L. E.; Romano, P. S.; Carrillo, C.; Talevi, A. Computer-Guided Drug Repurposing: Identification of Trypanocidal Activity of Clofazimine, Benidipine and Saquinavir. *Eur. J. Med. Chem.* **2015**, *93*, 338–348.

(193) De Clercq, D.; Vercruysse, J.; Verlé, P.; Niasse, F.; Kongs, A.; Diop, M. Efficacy of Artesunate against *Schistosoma mansoni* Infections in Richard Toll, Senegal. *Trans. R. Soc. Trop. Med. Hyg.* **2000**, *94*, 90–91.

(194) Chong, C. R.; Chen, X.; Shi, L.; Liu, J. O.; Sullivan, D. J. A Clinical Drug Library Screen Identifies Astemizole as an Antimalarial Agent. *Nat. Chem. Biol.* **2006**, *2* (8), 415–416.

(195) Musonda, C. C.; Whitlock, G. A.; Witty, M. J.; Brun, R.; Kaiser, M. Chloroquine–astemizole Hybrids with Potent *in vitro* and *in vivo* Antiplasmodial Activity. *Bioorg. Med. Chem. Lett.* **2009**, *19* (2), 481–484.

(196) Yap, Y. G.; Camm, A. J. Potential Cardiac Toxicity of H1-Antihistamines. *Clin. Allergy Immunol.* **2002**, *17*, 389–419.

(197) Rao, K. A.; Adlakha, A.; Verma-Ansil, B.; Meloy, T. D.; Stanton, M. S. Torsades de Pointes Ventricular Tachycardia Associated With Overdose of Astemizole. *Mayo Clin. Proc.* **1994**, *69* (6), 589–593.

(198) Smith, S. J. Cardiovascular Toxicity of Antihistamines. *Otolaryngol. Neck Surg.* **1994**, *111* (3P2), 348–354.

(199) Roman, G.; Crandall, I. E.; Szarek, W. A. Synthesis and Anti- Plasmodium Activity of Benzimidazole Analogues Structurally Related to Astemizole. *ChemMedChem* **2013**, *8* (11), 1795–1804.

(200) Eissa, M. M.; El-Azzouni, M. Z.; Amer, E. I.; Baddour, N. M. Miltefosine, a Promising Novel Agent for Schistosomiasis Mansoni. *Int. J. Parasitol.* **2011**, *41* (2), 235–242.

(201) Eissa, M. M.; Mossallam, S. F.; Amer, E. I.; Younis, L. K.; Rashed, H. A. Repositioning of Chlorambucil as a Potential Anti-Schistosomal Agent. *Acta Trop.* **2017**, *166*, 58–66.

(202) Cowan, N.; Keiser, J. Repurposing of Anticancer Drugs: *In vitro* and *in vivo* Activities against *Schistosoma mansoni*. *Parasit. Vectors* **2015**, *8* (1), 417.

(203) Guidi, A.; Lalli, C.; Perlas, E.; Bolasco, G.; Nibbio, M.; Monteagudo, E.; Bresciani, A.; Ruberti, G. Discovery and Characterization of Novel Anti-Schistosomal Properties of the Anti-Anginal Drug, Perhexiline and Its Impact on *Schistosoma mansoni* Male and Female Reproductive Systems. *PLoS Negl. Trop. Dis.* **2016**, *10* (8), e0004928.

(204) Panic, G.; Vargas, M.; Scandale, I.; Keiser, J. Activity Profile of an FDA-Approved Compound Library against *Schistosoma mansoni*. *PLoS Negl. Trop. Dis.* **2015**, *9* (7), e0003962.

(205) Lawrence, J. D. The Ingestion of Red Blood Cells by *Schistosoma mansoni*. *J. Parasitol.* **1973**, *59* (1), 60–63.

(206) Keiser, J.; N'Guessan, N. A.; Adoubryn, K. D.; Silué, K. D.; Vounatsou, P.; Hatz, C.; Utzinger, J.; N'Goran, E. K. Efficacy and Safety of Mefloquine, Artesunate, Mefloquine-Artesunate, and Praziquantel against Schistosoma Haematobium: Randomized, Exploratory Open-Label Trial. *Clin. Infect. Dis.* **2010**, *50* (9), 1205–1213.

(207) Kumar, S.; Guha, M.; Choubey, V.; Maity, P.; Bandyopadhyay, U. Antimalarial Drugs Inhibiting Hemozoin (Beta-Hematin) Formation: A Mechanistic Update. *Life Sci.* **2007**, *80* (9), 813–828.

(208) Sajid, M.; McKerrow, J. H. Cysteine Proteases of Parasitic Organisms. *Mol. Biochem. Parasitol.* **2002**, *120* (1), 1–21.

(209) Ingram-Sieber, K.; Cowan, N.; Panic, G.; Vargas, M.; Mansour, N. R.; Bickle, Q. D.; Wells, T. N. C.; Spangenberg, T.; Keiser, J. Orally Active Antischistosomal Early Leads Identified from the Open Access Malaria Box. *PLoS Negl. Trop. Dis.* **2014**, *8* (1), e2610.

(210) Van Voorhis, W. C.; Adams, J. H.; Adelfio, R.; Ahyong, V.; Akabas, M. H.; Alano, P.; Alday, A.; Alemán Resto, Y.; Alsibaee, A.; Alzualde, A.; Andrews, K. T.; Avery, S. V.; Avery, V. M.; Ayong, L.; Baker, M.; Baker, S.; Ben Mamoun, C.; Bhatia, S.; Bickle, Q.; Bounaadja, L.; Bowling, T.; Bosch, J.; Boucher, L. E.; Boyom, F. F.; Brea, J.; Brennan, M.; Burton, A.; Caffrey, C. R.; Camarda, G.; Carrasquilla, M.; Carter, D.; Belen Cassera, M.; Chih-Chien Cheng, K.; Chindaudomsate, W.; Chubb, A.; Colon, B. L.; Colón-López, D. D.; Corbett, Y.; Crowther, G. J.; Cowan, N.; D'Alessandro, S.; Le Dang, N.; Delves, M.; De Risi, J. L.; Du, A. Y.; Duffy, S.; Abd El-Salam El-Sayed, S.; Ferdig, M. T.; Fernández Robledo, J. A.; Fidock, D. A.; Florent, I.; Fokou, P. V. T.; Galstian, A.; Gamo, F. J.; Gokool, S.; Gold, B.; Golub, T.; Goldgof, G. M.; Guha, R.; Guiguemde, W. A.; Gural, N.; Guy, R. K.; Hansen, Michael A. E.; Hanson, K. K.; Hemphill, A.; Hooft van Huijsduijnen, R.; Horii, T.; Horrocks, P.; Hughes, T. B.; Huston, C.; Igarashi, I.; Ingram-Sieber, K.; Itoe, M. A.; Jadhav, A.; Naranuntarat Jensen, A.; Jensen, L. T.; Jiang, R.H. Y.; Kaiser, A.; Keiser, J.; Ketas, T.; Kicka, S.; Kim, S.; Kirk, K.; Kumar, V. P.; Kyle, D. E.; Lafuente, M. J.; Landfear, S.; Lee, N.; Lee, S.; Lehane, A. M.; Li, F.; Little, D.; Liu, L.; Llinás, M.; Loza, M. I.; Lubar, A.; Lucantoni, L.; Lucet, I.; Maes, L.; Mancama, D.; Mansour, N. R.; March, S.; McGowan, S.;

Medina Vera, I.; Meister, S.; Mercer, L.; Mestres, J.; Mfopa, A. N.; Misra, R. N.; Moon, S.; Moore, J. P.; Morais Rodrigues da Costa, F.; Müller, J.; Muriana, A.; Nakazawa Hewitt, S.; Nare, B.; Nathan, C.; Narraidoo, N.; Nawaratna, S.; Ojo, K. K.; Ortiz, D.; Panic, G.; Papadatos, G.; Parapini, S.; Patra, K.; Pham, N.; Prats, S.; Plouffe, D. M.; Poulsen, S. -A.; Pradhan, A.; Quevedo, C.; Quinn, R. J.; Rice, C. A.; Abdo Rizk, M.; Ruecker, A.; St. Onge, R.; Salgado F.; Rafaela Samra, J.; Robinett, N. G.; Schlecht, U.; Schmitt, M.; Silva Villela, F.; Silvestrini, F.; Sinden, R.; Smith, D. A.; Soldati, T.; Spitzmüller, A.; Stamm, S. M.; Sullivan, D. J.; Sullivan, W.; Suresh, S.; Suzuki, B. M.; Suzuki, Y.; Swamidass, S. J.; Taramelli, D.; Tchokouaha, L. R. Y.; Theron, A.; Thomas, D.; Tonissen, K. F.; Townson, S.; Tripathi, A. K.; Trofimov, V.; Udenze, K. O.; Ullah, I.; Vallieres, C.; Vigil, E.; Vinetz, J. M.; Voong Vinh, P.; Vu, H.; Watanabe, Nao-aki.; Weatherby, K.; White, P. M.; Wilks, A. F.; Winzeler, E. A.; Wojcik, E.; Wree, M.; Wu, W.; Yokoyama, N.; Zollo, P. H. A.; Abla, N.; Blasco, B.; Burrows, J.; Laleu, B.; Leroy, D.; Spangenberg, T.; Wells, T. Willis, P. A. Open Source Drug Discovery with the Malaria Box Compound Collection for Neglected Diseases and Beyond. *PLOS Pathog.* **2016**, *12* (7), e1005763.

(211) Spangenberg, T.; Burrows, J. N.; Kowalczyk, P.; McDonald, S.; Wells, T. N. C.; Willis, P. The Open Access Malaria Box: A Drug Discovery Catalyst for Neglected Diseases. *PLoS One* **2013**, *8* (6), e62906.

(212) Ingram-Sieber, K.; Cowan, N.; Panic, G.; Vargas, M.; Mansour, N. R.; Bickle, Q. D.; Wells, T. N. C.; Spangenberg, T.; Keiser, J. Orally Active Antischistosomal Early Leads Identified from the Open Access Malaria Box. *PLoS Negl. Trop. Dis.* **2014**, *8*, 30.

(213) Basra, A.; Mombo-Ngoma, G.; Capan Melser, M.; Akerey Diop, D.; Würbel, H.; Mackanga, J.-R.; Fürstenau, M.; Manego Zoleko, R.; Adegnika, A. A.; Gonzalez, R.; Menendez, C.; Kremsner, P. G.; Ramharter, M. Efficacy of Mefloquine Intermittent Preventive Treatment in Pregnancy Against Schistosoma Haematobium Infection in Gabon: A Nested Randomized Controlled Assessor-Blinded Clinical Trial. *Clin. Infect. Dis.* **2013**, *56* (6), e68–e75.

(214) Lipinski, C. A. Lead- and Drug-like Compounds: The Rule-of-Five Revolution. *Drug Discov. Today Technol.* **2004**, *1* (4), 337–341.

(215) Di, L.; Fish, P. V.; Mano, T. Bridging Solubility between Drug Discovery and Development. *Drug Discov. Today* **2012**, *17* (9–10), 486–495.

(216) Kawabata, Y.; Wada, K.; Nakatani, M.; Yamada, S.; Onoue, S. Formulation Design for Poorly Water-Soluble Drugs Based on Biopharmaceutics Classification System: Basic Approaches and Practical Applications. *Int. J. Pharm.* **2011**, *420* (1), 1–10.

(217) Alsenz, J.; Kansy, M. High Throughput Solubility Measurement in Drug Discovery and Development. *Adv. Drug Deliv. Rev.* **2007**, *59* (7), 546–567.

(218) Doak, B. C.; Over, B.; Giordanetto, F.; Kihlberg, J. Oral Druggable Space beyond the Rule of 5: Insights from Drugs and Clinical Candidates. *Chem. Biol.* **2014**, *21* (9), 1115–1142.

(219) Arnott, J. A.; Planey, S. L. The Influence of Lipophilicity in Drug Discovery and Design. *Expert Opin. Drug Discov.* **2012**, *7* (10), 863–875.

(220) Waring, M. J. Lipophilicity in Drug Discovery. *Expert Opin. Drug Discov.* **2010**, *5* (3), 235–248.

(221) Lombardo, F.; Shalaeva, M. Y.; Tupper, K. A.; Gao, F.; Abraham, M. H. ElogP Oct : A Tool for Lipophilicity Determination in Drug Discovery. *J. Med. Chem.* **2000**, *43* (15), 2922–2928.

(222) Lombardo, F.; Shalaeva, M. Y.; Tupper, K. A.; Gao, F. ElogD OCt : A Tool for Lipophilicity Determination in Drug Discovery. 2. Basic and Neutral Compounds. *J. Med. Chem.* **2001**, *44* (15), 2490–2497.

(223) Abramson, F. P. Methadone Plasma Protein Binding: Alterations in Cancer and Displacement from α1-Acid Glycoprotein. *Clin. Pharmacol. Ther.* **1982**, *32* (5), 652–658.

(224) Leeson, P. D.; Springthorpe, B. The Influence of Drug-like Concepts on Decision-Making in Medicinal Chemistry. *Nat. Rev. Drug Discov.* **2007**, *6* (11), 881–890.

(225) Hou, T.; Wang, J.; Zhang, W.; Wang, W.; Xu, X. Recent Advances in Computational Prediction of Drug Absorption and Permeability in Drug Discovery. *Curr. Med. Chem.* **2006**, *13* (22), 2653–2667.

(226) Veber, D. F.; Johnson, S. R.; Cheng, H.-Y.; Smith, B. R.; Ward, K. W.; Kopple, K. D. Molecular Properties That Influence the Oral Bioavailability of Drug Candidates. *J. Med. Chem.* **2002**, *45* (12), 2615–2623.

(227) Benet, L. Z. The Role of BCS (Biopharmaceutics Classification System) and BDDCS (Biopharmaceutics Drug Disposition Classification System) in Drug Development. *J. Pharm. Sci.* **2013**, *102* (1), 34–42.

(228) Lãbenberg, R. Modern Bioavailability, Bioequivalence and Biopharmaceutics Classification System. New Scientific Approaches to International Regulatory Standards. *Eur. J. Pharm. Biopharm.* **2000**, *50* (1), 3–12.

(229) Daousani, C.; Macheras, P. Biopharmaceutic Classification of Drugs Revisited. *Eur. J. Pharm. Sci.* **2016**, *95*, 82–87.

(230) Cook, J.; Addicks, W.; Wu, Y. H. Application of the Biopharmaceutical Classification System in Clinical Drug Development—An Industrial View. *AAPS J.* **2008**, *10* (2), 306–310.

(231) Daousani, C.; Macheras, P. Scientific Considerations Concerning the EMA Change in the Definition of “dose” of the BCS-Based Biowaiver Guideline and Implications for Bioequivalence. *Int. J. Pharm.* **2015**, *478* (2), 606–609.

(232) Ku, M. S. Use of the Biopharmaceutical Classification System in Early Drug Development. *AAPS J.* **2008**, *10* (1), 208–212.

(233) Ishikawa, M.; Hashimoto, Y. Improvement in Aqueous Solubility in Small Molecule Drug Discovery Programs by Disruption of Molecular Planarity and Symmetry. *J. Med. Chem.* **2011**, *54* (M), 1539–1554.

(234) Leuner, C. Improving Drug Solubility for Oral Delivery Using Solid Dispersions. *Eur. J. Pharm. Biopharm.* **2000**, *50* (1), 47–60.

(235) Huang, Y.; Dai, W.-G. Fundamental Aspects of Solid Dispersion Technology for Poorly Soluble Drugs. *Acta Pharm. Sin. B* **2014**, *4* (1), 18–25.

(236) Vo, C. L.-N.; Park, C.; Lee, B.-J. Current Trends and Future Perspectives of Solid Dispersions Containing Poorly Water-Soluble Drugs. *Eur. J. Pharm. Biopharm.* **2013**, *85* (3), 799–813.

(237) Stella, V. J.; Nti-Addae, K. W. Prodrug Strategies to Overcome Poor Water Solubility. *Adv. Drug Deliv. Rev.* **2007**, *59* (7), 677–694.

(238) Lipinski, C. A. Drug-like Properties and the Causes of Poor Solubility and Poor Permeability. *J. Pharmacol. Toxicol. Methods* **2000**, *44* (1), 235–249.

(239) Ishikawa, M.; Hashimoto, Y. Improvement in Aqueous Solubility in Small Molecule Drug Discovery Programs by Disruption of Molecular Planarity and Symmetry. *J. Med. Chem.* **2011**, *54* (6), 1539–1554.

(240) Lin, J. H.; Lu, A. Y. H. Role of Pharmacokinetics and Metabolism in Drug Discovery and Development. *Pharmacol. Rev.* **1997**, *49* (4), 403 LP-449.

(241) Eddershaw, P. J.; Beresford, A. P.; Bayliss, M. K. ADME/PK as Part of a Rational Approach to Drug Discovery. *Drug Discov. Today* **2000**, *5* (9), 409–414.

(242) Li, A. P. Screening for Human ADME/Tox Drug Properties in Drug Discovery. *Drug Discov. Today* **2001**, *6* (7), 357–366.

(243) Ursu, O.; Rayan, A.; Goldblum, A.; Oprea, T. I. Understanding Drug-Likeness. *Wiley Interdiscip. Rev. Comput. Mol. Sci.* **2011**, *1* (5), 760–781.

(244) Xu, C.; Li, C. Y.-T.; Kong, A.-N. T. Induction of Phase I, II and III Drug Metabolism/transport by Xenobiotics. *Arch. Pharm. Res.* **2005**, *28* (3), 249.

(245) Vrbanac, J.; Slauter, R. ADME in Drug Discovery. In *A Comprehensive Guide to Toxicology in Preclinical Drug Development*; Elsevier, 2013; pp 3–30.

(246) David Josephy, P.; Peter Guengerich, F.; Miners, J. O. "Phase I and Phase II" Drug Metabolism: Terminology That We Should Phase Out? *Drug Metab. Rev.* **2005**, *37* (4), 575–580.

(247) Jancova, P.; Anzenbacher, P.; Anzenbacherova, E. Phase II Drug Metabolizing Enzymes. *Biomed. Pap.* **2010**, *154* (2), 103–116.

(248) Frank, A.; Unger, M. Analysis of Frankincense from Various Boswellia Species with Inhibitory Activity on Human Drug Metabolising Cytochrome P450 Enzymes Using Liquid Chromatography Mass Spectrometry after Automated on-Line Extraction. *J. Chromatogr. A* **2006**, *1112* (1–2), 255–262.

(249) Guengerich, F. P. Cytochromes P450, Drugs, and Diseases. *Mol. Interv.* **2003**, *3* (4), 194–204.

(250) Morgan, P.; Van Der Graaf, P. H.; Arrowsmith, J.; Feltner, D. E.; Drummond, K. S.; Wegner, C. D.; Street, S. D. A. Can the Flow of Medicines Be Improved? Fundamental Pharmacokinetic and Pharmacological Principles toward Improving Phase II Survival. *Drug Discov. Today* **2012**, *17* (9–10), 419–424.

(251) Wienkers, L. C.; Heath, T. G. Predicting *in vivo* Drug Interactions from *in vitro* Drug Discovery Data. *Nat. Rev. Drug Discov.* **2005**, *4*, 825.

(252) Kumar, G. N.; Surapaneni, S. Role of Drug Metabolism in Drug Discovery and Development. *Med. Res. Rev.* **2001**, *21* (5), 397–411.

(253) Segall, M. D.; Barber, C. Addressing Toxicity Risk When Designing and Selecting Compounds in Early Drug Discovery. *Drug Discov. Today* **2014**, *19* (5), 688–693.

(254) Kim, S.; Cho, M.; Lee, T.; Lee, S.; Min, H.-Y.; Lee, S. K. Design, Synthesis, and Preliminary Biological Evaluation of a Novel Triazole Analogue of Ceramide. *Bioorg. Med. Chem. Lett.* **2007**, *17* (16), 4584–4587.

(255) Biot, C.; Bauer, H.; Schirmer, R. H.; Davioud-Charvet, E. 5-Substituted Tetrazoles as Bioisosteres of Carboxylic Acids. Bioisosterism and Mechanistic Studies on Glutathione Reductase Inhibitors as Antimalarials. *J. Med. Chem.* **2004**, *47* (24), 5972–5983.

(256) Gardiner, S. J. Pharmacogenetics, Drug-Metabolizing Enzymes, and Clinical Practice. *Pharmacol. Rev.* **2006**, *58* (3), 521–590.

(257) Cunningham, R. F.; Israili, Z. H.; Dayton, P. G. Clinical Pharmacokinetics of Probenecid. *Clin. Pharmacokinet.* **1981**, *6* (2), 135–151.

(258) Dacey, R. G.; Sande, M. A. Effect of Probenecid on Cerebrospinal Fluid Concentrations of Penicillin and Cephalosporin Derivatives. *Antimicrob. Agents Chemother.* **1974**, *6* (4), 437–441.

(259) Aronov, A. M. Common Pharmacophores for Uncharged Human Ether-a-Go-Go-Related Gene (hERG) Blockers. *J. Med. Chem.* **2006**, *49* (23), 6917–6921.

(260) Fermini, B.; Fossa, A. A. The Impact of Drug-Induced QT Interval Prolongation on Drug Discovery and Development. *Nat. Rev. Drug Discov.* **2003**, *2* (6), 439–447.

(261) Raschi, E.; Ceccarini, L.; De Ponti, F.; Recanatini, M. hERG-Related Drug Toxicity and Models for Predicting hERG Liability and QT Prolongation. *Expert Opin. Drug Metab. Toxicol.* **2009**, *5* (9), 1005–1021.

(262) Aronov, A. Predictive *in silico* Modeling for hERG Channel Blockers. *Drug Discov. Today* **2005**, *10* (2), 149–155.

(263) Yu, H.; Adedoyin, A. ADME–Tox in Drug Discovery: Integration of Experimental and Computational Technologies. *Drug Discov. Today* **2003**, *8* (18), 852–861.

Chapter 2

Pyrido [1,2-*a*] benzimidazoles

2.1 Chapter overview

This chapter will provide a brief account of the chemistry and pharmacological spectrum of pyridobenzimidazoles and describe their activity with respect to their potential as antimalarial and antischistosomal drug development leads. A recap of the unmet medical need and, thus, a statement of justification for the current research will be expressed, including the aims, objectives and hypothesis underpinning this study. The medicinal chemistry plans leading to the synthesis of target compounds and a description of the subsequent work flow will be provided. Lastly, using representative compounds, the synthesis and characterization undertaken to realise and confirm structures of the target compounds, will be discussed.

2.2 General chemistry and pharmacology

The pyridobenzimidazole (PBI) nucleus consists of benzene, imidazole and pyridine motifs fused into a single tricyclic scaffold (**b**, **Figure 2.1**).[1] On the other hand, the structurally related benzimidazole chemotype is a bicyclic structure in which the benzene and imidazole moieties have been fused together **(a**, **Figure 2.1**). Therefore, the PBI nucleus may be considered as a derivative or extension of the benzimidazole core, both of which are pivotal in drug discovery.[2,3]

Figure 2.1: *Chemical structures of benzimidazole (a) and pyrido [1, 2-a] benzimidazole (b) scaffolds.*

Benzimidazole is a privileged structure in medicinal chemistry and has been implicated not only in natural biomolecules such as vitamin B_{12} but also in several drugs with a large spectrum of biological and pharmacological activities including as anti-ulcer, antiparasitic, antipsychotic, anticancer and antitubercular. Other indications include as antifungal, antihypertensive and antiviral (**Figure 2.2**).[4–7]

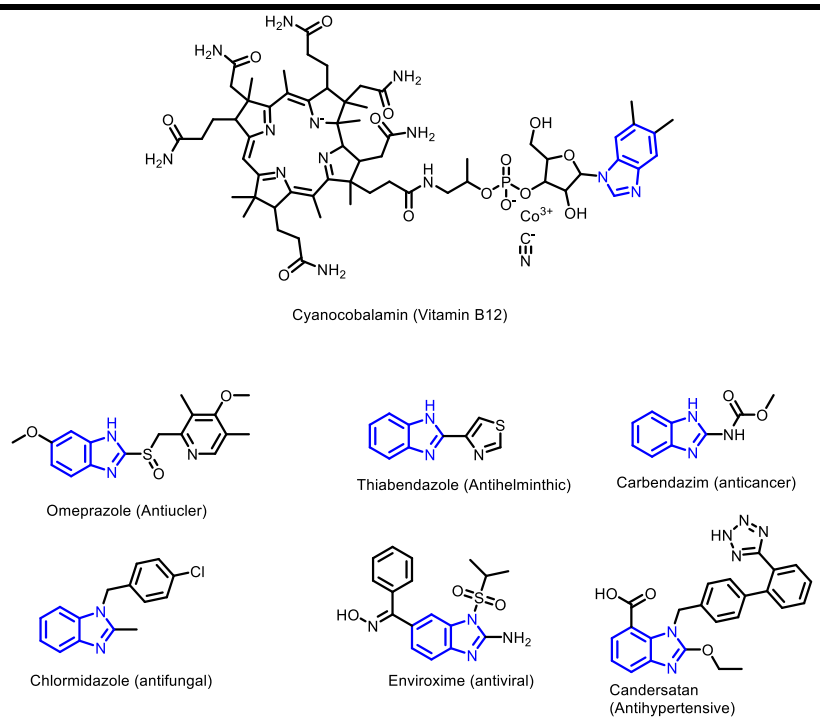

Figure 2.2: *Chemical structures of vitamin B_{12} and drugs incorporating a benzimidazole moiety.*

The PBI nucleus has continued to inspire interest in medicinal chemistry towards drug discovery. The flourishing of synthesis methods and the amenability of the PBI scaffold to chemical modifications has enabled generation of a large range of analogues with diverse pharmacological and biological effects.[1,8–12] The PBI system is an appealing scaffold in medicinal chemistry, lending itself to chemical evolution, allowing for transformation into diverse structural derivatives for structure-activity and structure-property relationships studies.

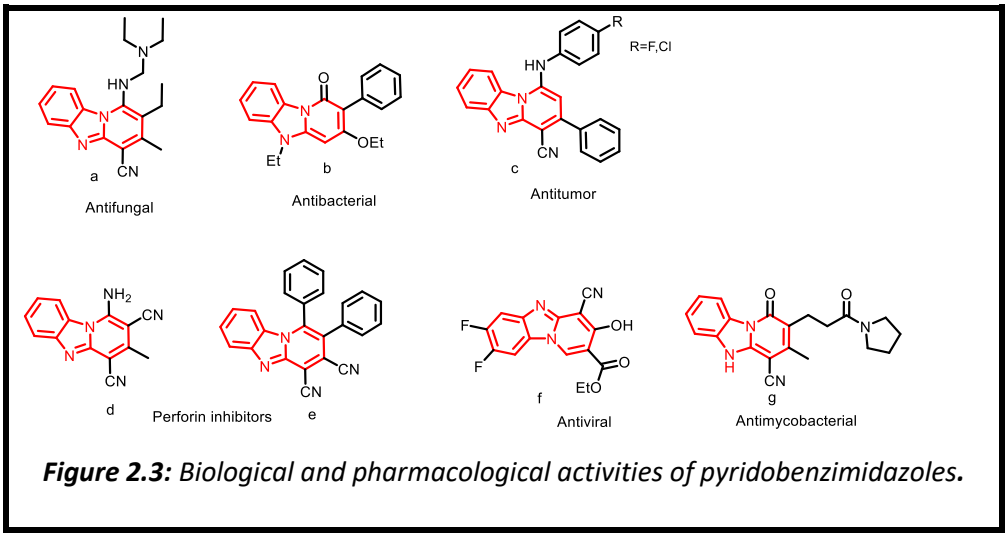

Figure 2.3: *Biological and pharmacological activities of pyridobenzimidazoles.*

2.3 Pyrido [1,2-*a*] benzimidazoles as antimalarial agents

As part of the initiative to promote tropical disease research, a commercial compound library of 1440 non-propriety compounds with diverse chemical structures was screened *in vitro* against the human malaria parasite *Plasmodium falciparum*. As a result of this work carried out jointly by the WHO-TDR and the Belgian company Tibotec®, hit **1** (**Figure 2.4**) was identified as having moderate activity against *P. falciparum* GHA and W2 strains (0-17-0.37 µM).[13] A subsequent screening of 535 other compounds that incorporate the PBI core in their structures identified compounds **2** and **3** which were more potent and had better selectivity indices compared to the hit **1 (Figure 2.4**).

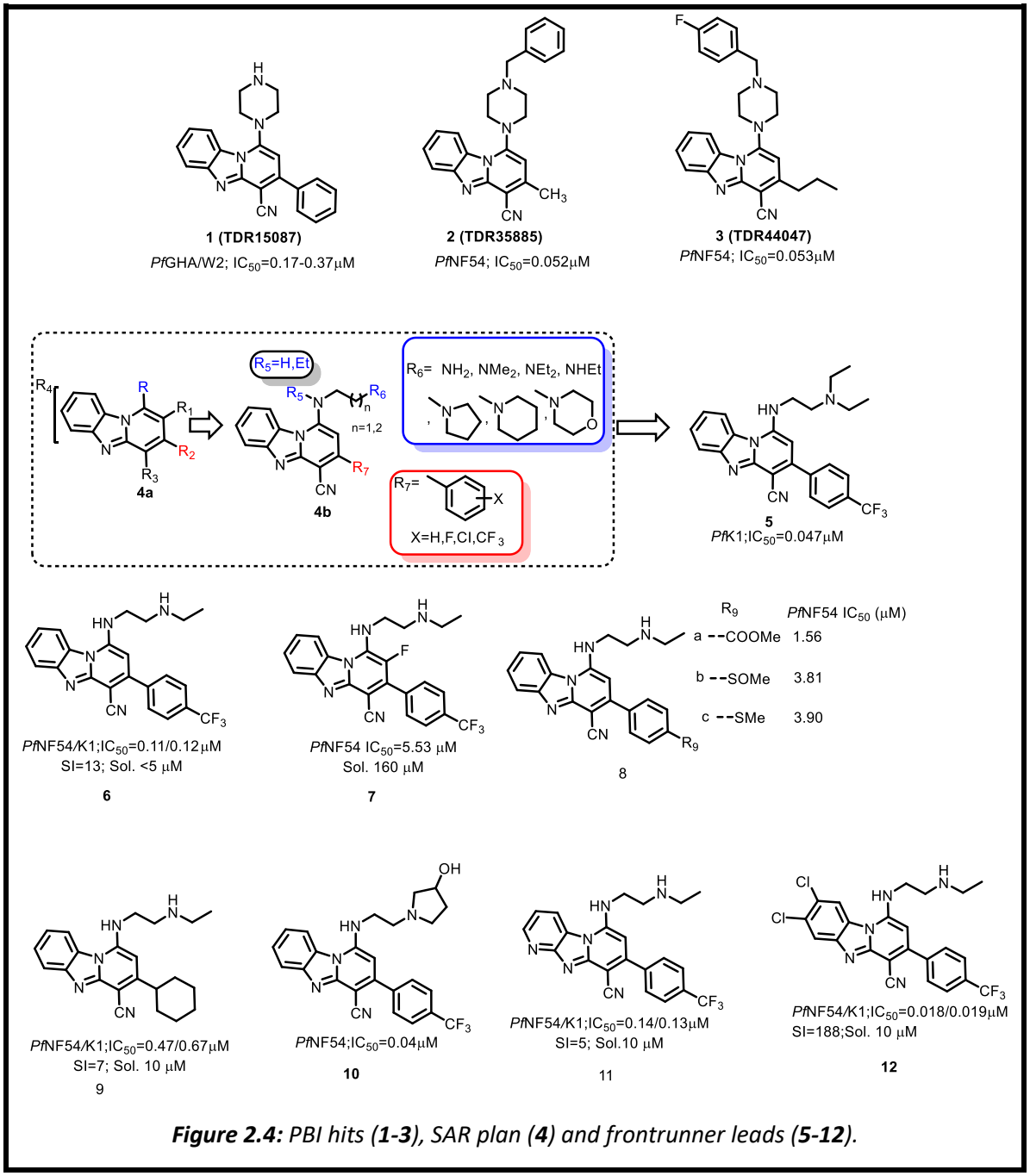

Figure 2.4: *PBI hits (**1-3**), SAR plan (**4**) and frontrunner leads (**5-12**).*

Unfortunately, neither the hit **1** nor the surrogates **2** and **3** demonstrated any *in vivo* efficacy when tested in a murine model of malaria even to doses up to 4x100mg/kg; a fate attributed to poor solubility and metabolic stability. This observation prompted for a SAR campaign **4a** focussing on introducing diversity around the PBI core with the aim of finding analogues with *in vivo* antimalarial activity. Accordingly, targets with aryl groups at $\mathbf{R_2}$ and alkyl amine side chains at **R** were synthesised (**Figure 2.4**).

The most active compound in the series **5** (**Figure 2.4**), displayed improved *in vitro* activity (IC_{50}=0.047µM) in comparison to both the hit compound **1** and the standard drug used in the assay, chloroquine (IC_{50}=0.17 µM), against the K1 drug resistant strain of *P. falciparum* and had negligible cytotoxicity to mammalian (L-6) cell lines as indicated by a high selectivity index (SI>600) towards *Plasmodium* parasites.

Distinct SAR trends were unravelled from this initial medicinal chemistry campaign. It was observed that the *in vitro* activity was driven by the lipophilicity of the compounds. Generally, the compounds with a secondary or tertiary terminal nitrogen in the side chain ($\mathbf{R_6}$, **4b**, **Figure 2.4**) were more active than those with a primary nitrogen and activity was retained when the terminal nitrogen atom was incorporated in cyclic rings ($\mathbf{R_6}$, **4b**, **Figure 2.4**). Furthermore, the antiplasmodial activity was comparable in compounds with either ethylene (n=0) or propylene (n=1) chain linkers between the nitrogen atoms on the alkyl side chain (between $\mathbf{R_5}$ and $\mathbf{R_6}$; **4b**, **Figure 2.4**). Additionally, it was noted that phenyl or aryl substitutions resulted in compounds with greater potency than simple alkyl or haloalkyl groups at $\mathbf{R_7}$ (**4b**, **Figure 2.4**) with substitution at the para position being the most ideal.

Additional SAR findings from our research group have been reported.[14] Based on metabolism studies carried out on the earlier analogue **5 (Figure 2.4)**, the des-ethyl analogue **6** was found to retain potency and have better DMPK properties compared to the parent compound **5** (**Figure 2.4**). Compound **6** was therefore used to guide future optimization campaigns. Consequently, the SAR strategy involved modifying the appendages at **R** and $\mathbf{R_2}$, introducing small lipophilic groups at $\mathbf{R_1}$ with the aim of potentially minimizing crystal packing of the molecules, and attempting changes on the benzenoid portion of the motif, $\mathbf{R_4}$ (**4a**, **Figure 2.4**). Regarding changes at **R**, the alkyl side chain could be replaced with cyclic amines with

retention of activity, the best of which was the introduction of 3-hydroxy pyrrolidine, compound **10 (Figure 2.4)**. Introducing fluorine at $\mathbf{R_1}$ (as in compound **7**), although leading to improvement in solubility, was unfortunately detrimental to activity. Groups on the aromatic appendage at $\mathbf{R_7}$ (**4b, Figure 2.4**) could be moved around the ring or be replaced with other lipophilic groups while maintaining antiplasmodial activity.

However, polar substituents such as methylester (**8a**), sulfoxide (**8b**) and thiomethyl (**8c**) were not tolerated although they had been envisaged to improve solubility. Saturation of the aromatic system, consistent with introducing cycloalkyl systems at this site, could be carried out but not without the loss of selective antiplasmodial activity as in **9** (**Figure 2.4**). The decreased lipophilicity was also beneficial to increasing solubility but resulted in the decrease in microsomal metabolic stability. SAR alterations at $\mathbf{R_4}$ (**4a, Figure 2.4**) aimed at decreasing lipophilicity and improving solubility, by incorporating a pyridyl functionality (**11**), produced analogues with good activity but at the expense of selectivity. It was, however, the introduction of lipophilic substituents, using halogens, on this portion of the initial lead compound that generated analogues, exemplified by compound **12**, with not only enhanced *in vitro* activity and metabolic stability but also improved *in vivo* efficacy.

Building upon the findings of these earlier works, we devised other SAR approaches to explore newer chemical spaces, by introducing other structural variations, with the hope of identifying potent antimalarial leads with suitable physicochemical and drug metabolism and pharmacokinetic properties.

2.4 Antischistosomal activity of pyrido [1,2-*a*] benzimidazoles

In the context of drug repositioning, the set of PBI analogues synthesized in the antimalarial program described earlier, were screened for activity against schistosome parasites. From this work, compounds with modest antischistosomal activity were identified (**Figure 2.5**).[15]

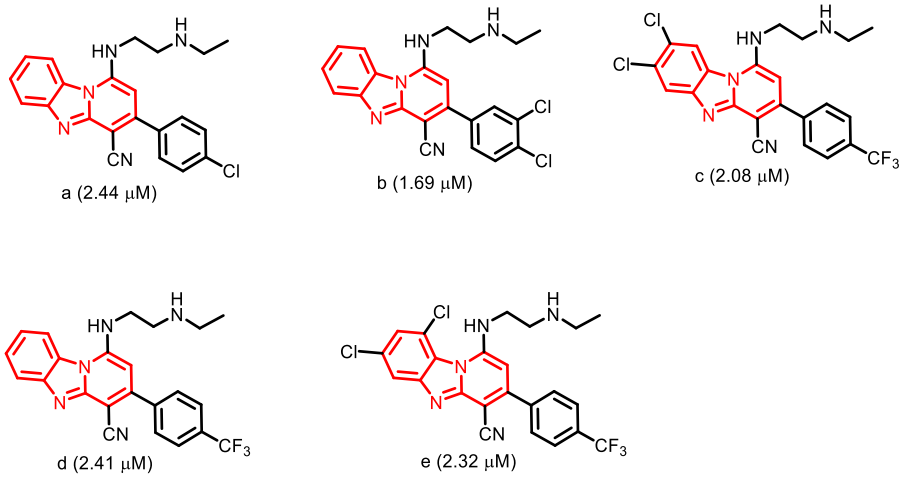

Figure 2.5: *Examples of PBI derivatives with in vitro potency (IC_{50}) against adult S. mansoni.*

As with the antimalarial program discussed previously, subsequent medicinal chemistry studies improved the *in vitro* activity of second generation analogues but insufficient *in vivo* exposure, perceived to arise from low solubility and metabolic instability, remained a challenge.[15] These initial results provided a basis for further investigations into new PBIs as potential antischistosomal leads.

2.5 Hypothesis and Justification

2.5.1 Hypothesis

The pyridobenzimidazole scaffold can be utilized to generate small molecule drug leads with good *in vitro* and *in vivo* antimalarial and antischistosomal activities having favourable physicochemical, drug metabolism and pharmacokinetic profiles.

2.5.2 Justification

Malaria and schistosomiasis are the two most prevalent parasitic diseases in the tropical and subtropical regions of the world. Mortality and morbidity due to malaria have been on a steady decline in the last two decades but the emergence and spread of parasites resistant to the front-line regimes comprising the artemisinins present a formidable hurdle in sustaining the gains made in malaria control. On the other hand, praziquantel remains, for over three decades, the only available pan-active antischistosomal drug against the major species of schistosomes associated with human schistosomiasis. Concerns of resistance to praziquantel have been on the rise, especially with the use of the drug in mass drug administration for preventive chemotherapy in endemic countries. The search for novel antimalarial and antischistosomal drugs is therefore warranted. Safe and effective alternatives should be made available, as a necessary precaution, should current therapies become compromised. Furthermore, antimalarial treatment with the ability to interrupt other stages of the life cycle of the parasite in addition to the asexual blood stage are required to enhance blocking transmission and achieving chemoprevention which are additional desirable target product profiles within the context of malaria eradication. Similarly, active agents against the larval stages of *Schistosoma* parasites, in addition to the mature forms, are also required since the current drug of choice, praziquantel, is only active against the adult worms, making repeated dosing necessary.

As already alluded to, biological profiling of pyridobenzimidazoles has unravelled vast and diverse pharmacological activities including antiplasmodial and antischistosomal effects. The initial SAR plan carried out by our group generated compounds with unsatisfactory physicochemical attributes such as low solubility. The chemical tractability of the scaffold coupled with discernible SAR trends, inspired the prosecution of the current research plan with the hope of finding improved antimalarial and antischistosomal leads.

2.6 Aims and Objectives

2.6.1 Main Objective

The overall objective for this project was to optimise 3-trifluoromethyl pyrido [1, 2-*a*] benzimidazole-based compounds as potential antimalarial and antischistosomal agents.

2.6.2 Specific Aims

In tandem with the overall objective for this project, we envisaged the following specific aims which are expounded in greater detail in subsequent chapters:

i. Perform the synthesis, antiplasmodial and antischistosomal structure-activity relationship (SAR) studies of N-aryl 3-trifluromethyl pyrido [1,2-*a*] benzimidazole derivatives;

ii. Profile target compounds for physicochemical properties including melting point, solubility, lipophilicity, and discern structure-property trends;

iii. Undertake metabolic stability, metabolite identification and cytotoxicity studies of prioritised compounds;

iv. Evaluate prioritised leads for *in vivo* efficacy in relevant disease models and conduct their pharmacokinetic studies.

2.7 Design

2.7.1 Medicinal chemistry plan

In the current design, the sites targeted for alteration are as depicted in **Figure 2.6** wherein we sought to introduce further structural diversity around the PBI core by executing modifications at the highlighted positions.

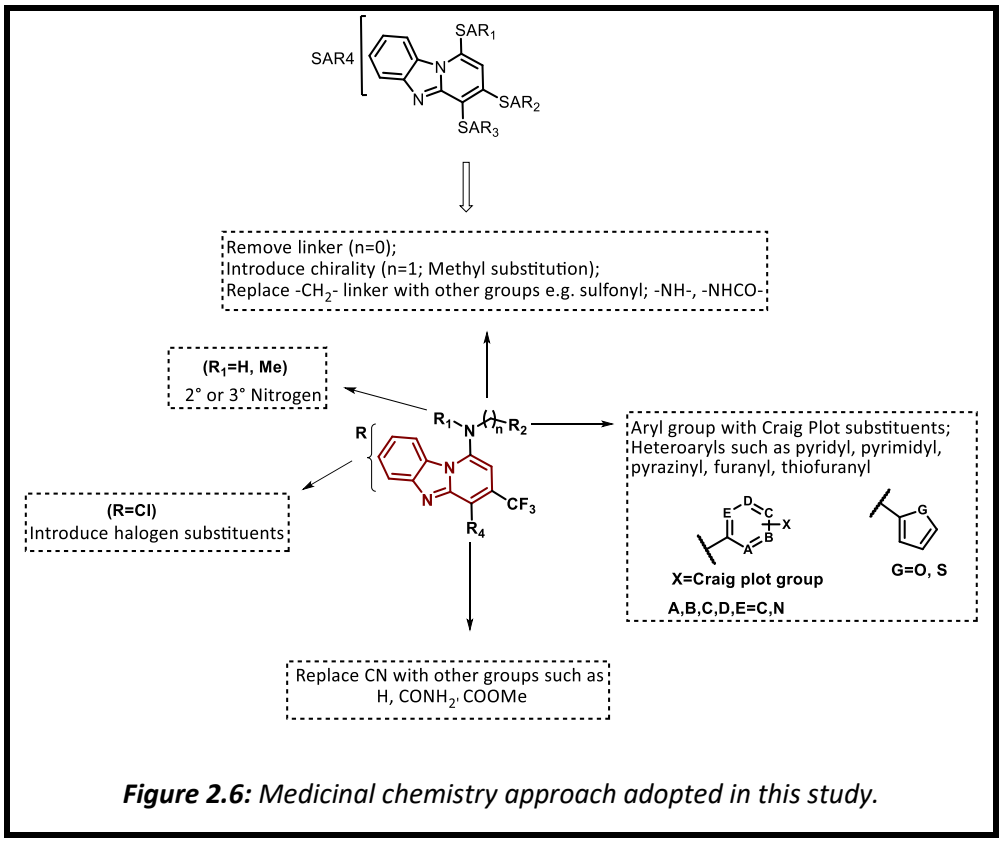

Figure 2.6: *Medicinal chemistry approach adopted in this study.*

At position **SAR$_1$**, instead of using aliphatic amines as explored earlier (**Figure 2.4**), aromatic side groups in the form of aniline- and benzylamine-type moieties were employed. In the aniline-type series, the PBI core is linked directly to the aromatic appendage by means of a nitrogen linkage (n=0; **Figure 2.6**). Conversely, in the analogues with benzylamine-type side groups, a methylene linker connects the nitrogen attached to the PBI core with the aromatic side portion (n=1; **Figure 2.6**).

In exploring this SAR wherein, a methylene linker is incorporated as opposed to directly attaching the side group to the PBI core, we presumed the introduction of some degree of flexibility in the analogues with the projected benefit of improving solubility, by potentially reducing π-π stacking interactions in the molecules. The substitutions on the aromatic side groups in **SAR$_1$** were performed in line with medicinal chemistry practices using the Craig plot to ensure diversity in the lipophilic and electronic characteristics in target compounds.

In some analogues, a methyl substitution was introduced on the methylene linker to introduce chirality at this position which was envisaged to not only potentially reduce crystal packing further but also to explore new chemical space in the series. Such analogues would also facilitate the interrogation of the effect of chirality on both biological activity and physicochemical properties. Towards improving the solubility attributes of the target compounds, analogues in which the methylene linker was replaced with hydrogen bonding moieties such as amine (-NH-), sulfone (-SO_2-) and amide (-NHCO-) groups were pursued. Modification of the linker nitrogen in the side group (**R$_1$**, **Figure 2.6**) was proposed for some analogues to facilitate the evaluation of steric and electronic factors as well as the influence of the presence of a hydrogen-bonding centre around this region of the molecule.

Furthermore, towards expanding the SAR around position **SAR$_1$**, and with the aim of introducing solubility-enhancing features, heteroaromatic amines were also used (**R$_2$**, **Figure 2.6**). Moreover, other heteroaromatic amines such as the pyridyl group have protonatable sites to facilitate salt formation in the context of improving aqueous solubility for oral drug administration.

With the use of aromatic side chains as opposed to the earlier explored aliphatic ones at **SAR$_1$**, significant increases in the molecular weight of the target compounds beyond the Lipinski's-recommended 500 Da for good oral absorption were anticipated in case of the 3-trifluorophenyl (3-Ph-CF_3) moiety at position **SAR$_2$**. For this reason, the smaller trifluoromethyl (CF_3) group, which from previous studies was tolerated for antiplasmodial activity, was used at position **SAR$_2$**.

Since the PBI core is an electron dense system, challenges related to metabolic instability for target compounds were anticipated. To forestall this liability, small lipophilic groups that could impart metabolic stability by blocking some of the putative metabolic hotspots were introduced at **SAR_4**. Halogen substituents were accordingly introduced on this phenyl portion of the PBI scaffold (**R**, **Figure 2.6**).

Based on the X-ray crystallographic structure of an analogous PBI (**Figure 2.7**), the nitrile group at **SAR_3** was depicted to be coplanar to the PBI core, a feature that is likely to encourage crystal packing in the compounds, a possible contributor to their low solubility. To thus attempt to potentially disrupt this planarity, replacement of this nitrile group with other groups hypothesized to result in non-co-planarity with the PBI core was undertaken on some analogues (**R_4**, **Figure 2.6**). Some of the proposed moieties, such as the amide group, were expected to help address the solubility shortcoming of this series by facilitating hydrogen-bond interactions, reducing lipophilicity and increasing polarity.

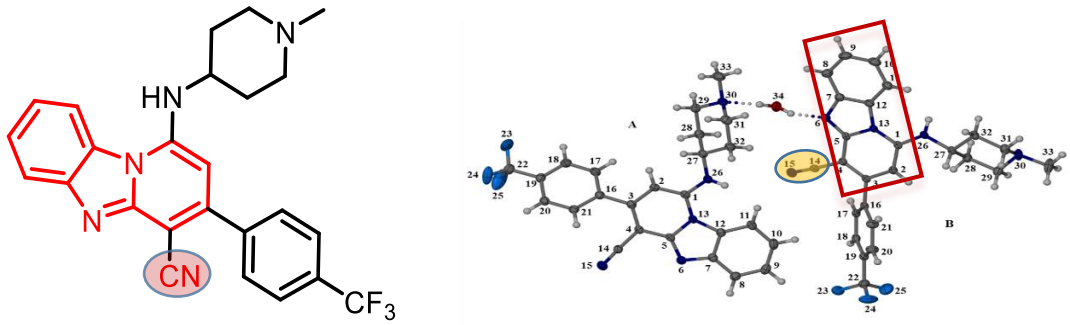

Figure 2.7: *Chemical (left) and X-ray (right) structures of a PBI derivative. Coplanarity is exhibited between the nitrile group (highlighted in oval) and the PBI core (shown with a rectangle).*[16]

2.7.2 Research program

The work flow adopted in this research is depicted in **Figure 2.8**. Target compounds were synthesized and sufficiently characterised as described in **section 2.8** of this chapter. All target molecules were profiled with respect to their *in vitro* antiplasmodial and antischistosomal activities and structure-activity relationship trends analysed as detailed in **Chapters 3** and **4**, respectively. Initially, antiplasmodial assays were carried out in the chloroquine sensitive (NF54) strain of *Plasmodium falciparum* focussing on the asexual blood stage parasites. Selected compounds, based on potency, were then evaluated for activity against the gametocyte and liver stages of the parasite as well against the chloroquine resistant (K1) strain of *Plasmodium falciparum*. On the other hand, the antischistosomal tests were performed on both the adult worms and the larval stages referred to as newly transformed schistosomula (NTS). Concurrently, the physicochemical profile of the analogues (melting points, solubility and cLogP) was determined experimentally and by use of *in silico* tools to delineate structure-property relationships as discussed in **Chapter 5**. The cytotoxicity profile of compounds with promising *in vitro* activity was evaluated by testing their inhibition of the growth of Chinese hamster ovarian cells and the selectivity index (SI) determined. Moreover, selected analogues were also tested for their ability to interact with the human ether-a-go-go related gene (hERG) implicated in the functioning of potassium ion channels that controls the contractile activity of heart muscles. Inhibition of the hERG channel can cause fatal heart arrhythmias called torsade de pointes.

Analogues that displayed satisfactory cytotoxicity profiles were progressed to *in vitro* metabolic stability evaluation in human and mouse liver microsomes. Those compounds that satisfied the *in vitro* microsomal metabolic stability criteria, possessed a good SI profile with acceptable solubility were then investigated for efficacy in appropriate animal models to provide *in vivo* proof-of-concept. Moreover, to understand the predisposition of the series, representative compounds were selected for pharmacokinetic studies. Additionally, compounds that were active *in vitro* but portrayed poor metabolic stability in human and mouse liver microsomes were proposed for metabolite identification studies.

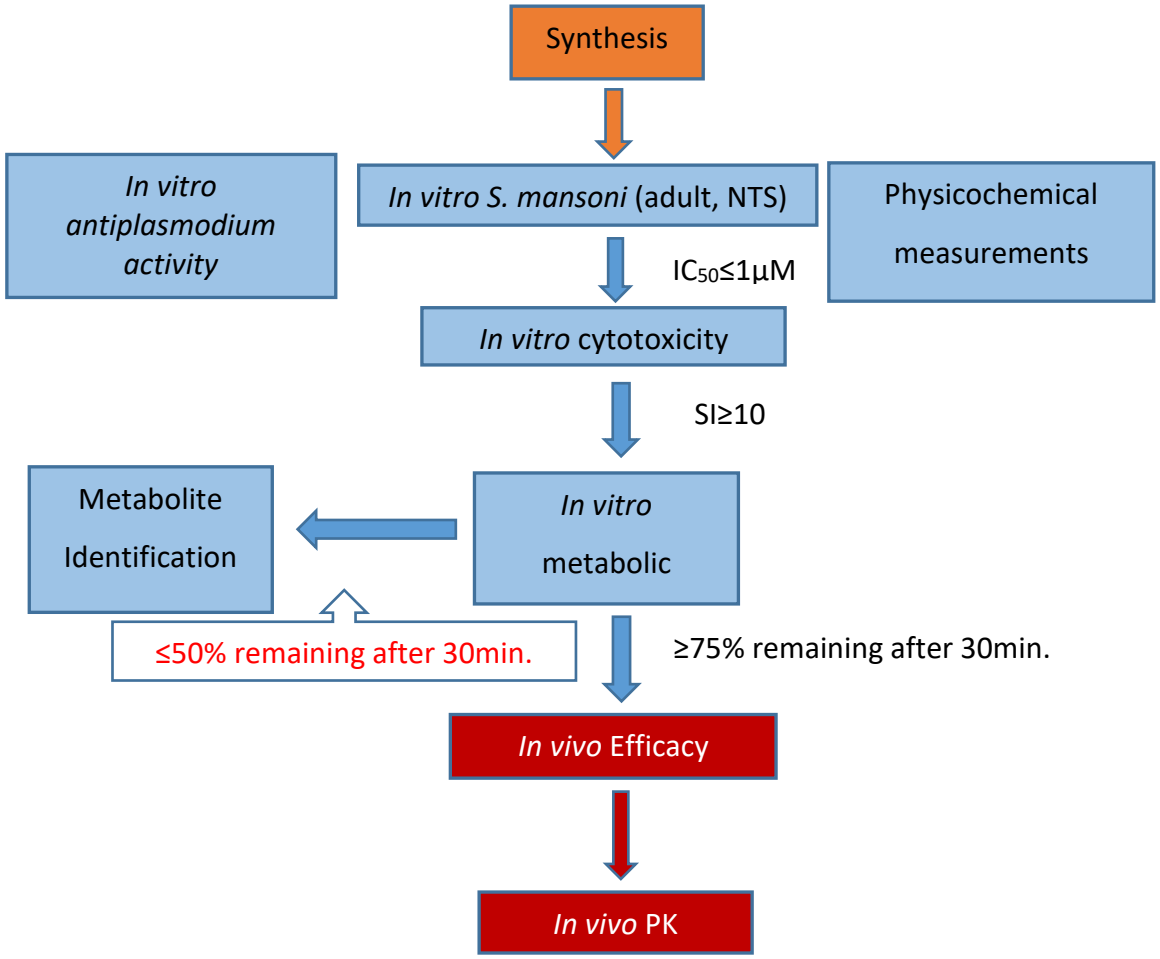

Pf: *Plasmodium falciparum*; ***S.mansoni***: *Schistosoma mansoni*; **NTS**: Newly transformed schistosomula

CHO: Chinese Hamster Ovarian cell line; **SI**: Selectivity Index; **HLM/MLM**: Human/Mouse liver microsomes

PK: Pharmacokinetics; **F**: Bioavailability; $t_{1/2}$: half-life.

Figure 2.8: *Workflow followed in this research.*

2.8 Synthesis and characterization

2.8.1 Synthesis

2.8.1.1 General overview of the synthesis

With the increasing exploitation of the PBI nucleus in medicinal chemistry, the synthesis of pyridobenzimidazoles has been reported in the literature. In the present work, reference is made mainly to the work reported by researchers from our lab.[13–15] Consequently, most of the target compounds **Va** were synthesised using a straightforward three-step approach from commercially available benzimidazole acetonitrile **IIa**. Other targets (**Vb** and **Vc**), with alterations on the benzenoid portion of the PBI core, required an extra initial step **i** to generate the appropriately substituted benzimidazole acetonitrile intermediates **IIb** and **IIc**. Regarding changes at **SAR$_3$** (**Scheme 2.1**) wherein the cyano group was replaced with other groups, different approaches were employed, including varying the starting material from benzimidazole acetonitrile **IIa** to a benzimidazole methyl ester **IId** and transformation of the nitrile group of the chloro intermediate **IVa** to the amide **VI**, to furnish the target compounds **Vd** and **Vf**, respectively (**Scheme 2.1**).

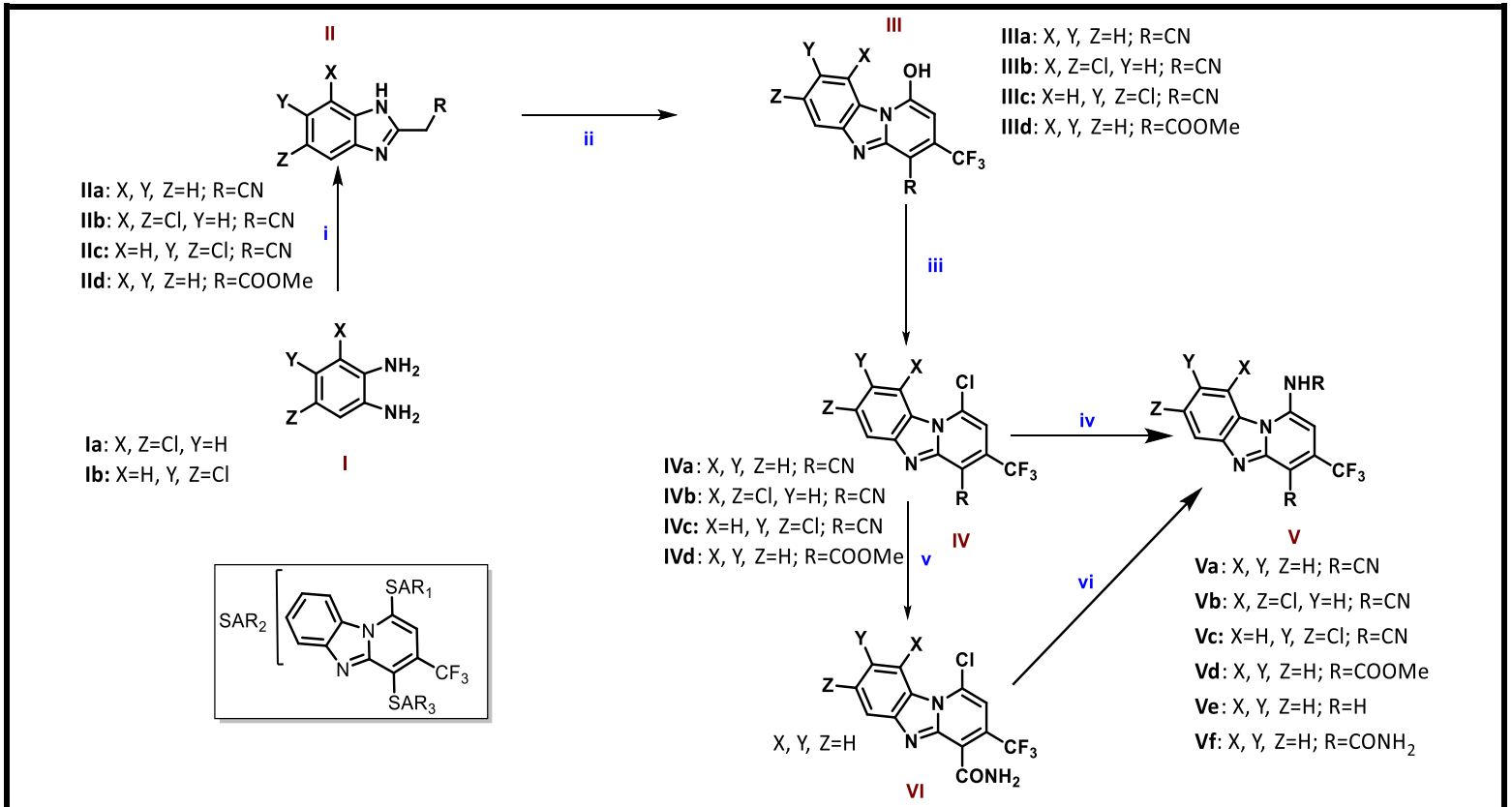

Scheme 2.1: *SAR modification sites and general scheme for the synthesis of target compounds. Reagents and conditions: (i) Ethyl cyanoacetate, DMF, 160˚C, 2 h; (ii) Ethyl 4,4,4-trifluoro-3-oxobutanoate, NH_4OAc, 145˚C, 2h; (iii) $POCl_3$, (20eq), 130˚C, 3 h; (iv) Relevant amine (RNH_2), Et_3N, microwave, 80˚C, 150 W, 20-60 min or the appropriate amine, $Pd_2(dba)_3$, BINAP or Brettphos, K_2CO_3 or Cs_2CO_3, toluene or 1,4-dioxane or tert-butanol, 100-120˚C, 12-16 h; (v) conc. Sulphuric acid, 2h.*

2.8.1.2 Synthesis of unsubstituted SAR_2 analogues

In the case of analogues with no substitution of the benzene portion of the scaffold, benzimidazole acetonitrile **IIa** was condensed with the beta keto ester ethyl-4,4,4-trifluoroethylester, in the presence of ammonium acetate, under reflux (**ii**, **Scheme 2.1**), to afford the tricyclic hydroxyl intermediate **IIIa**. In this reaction, the ammonium acetate abstracts a proton from the methylene carbon, sandwiched between the benzimidazole ring and the nitrile group, generating a resonance-stabilized carbanion (**i**, **Scheme 2.2**). This carbanion then attacks the more electrophilic carbonyl on the beta keto ester (**ii**, **Scheme 2.2**). Subsequent sequential proton abstraction from ammonium ion and acetic acid forms the intermediate **v**, (**Scheme 2.2**). The acetate ion picks up the hydrogen on the alpha carbon, next to the nitrile, leading to the loss of a water molecule with formation of intermediate **vi** (**Scheme 2.2)**. Next, cyclisation triggered by the more nucleophilic benzimidazole nitrogen, which attacks the ester carbonyl group of the beta keto ester, leads to the tricyclic intermediate **vii (Scheme 2.2)**. Proton transfer and expulsion of the ethoxy group driven by the formation of a keto functionality gives intermediate **ix**. Finally, the abstraction of the acidic proton in **ix** by the ethoxy anion gives the intermediate product **IIIa** with ethanol as a by-product (**Scheme 2.2**).

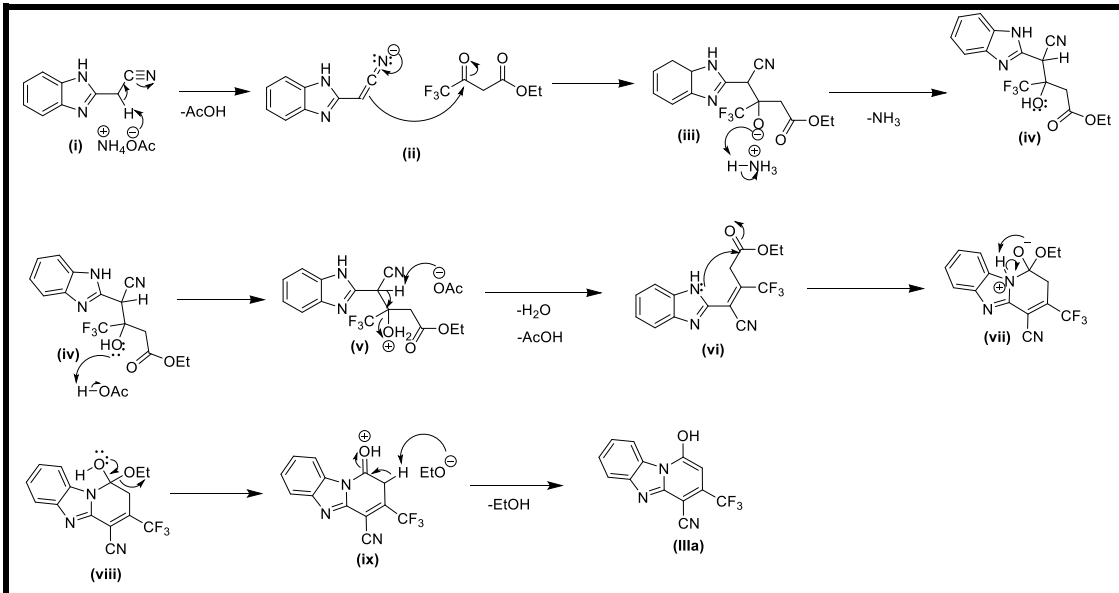

Scheme 2.2: *Proposed mechanism leading to intermediate* ***IIIa.***

In the next reaction (**iii, scheme 2.1**), the hydroxyl group in intermediate **III** is converted to the chloro group, which is a better leaving group in nucleophilic substitution reactions, compared to the hydroxyl. This reaction was readily mediated by phosphoryl oxychloride under reflux conditions. The reaction proceeds, as illustrated in **i**, **Scheme 2.3**, by the attack on the electron-deficient phosphorus by one of the lone pairs of electrons on the hydroxyl oxygen. The electron withdrawing nature of the chloro and oxygen atoms attached to the phosphorus atom makes the phosphorus readily susceptible to this nucleophilic attack. Subsequent steps in this reaction involve reforming the oxygen-phosphorus double bond accompanied by the expulsion of a chloride ion. Next, the ejected chloride ion serves as a nucleophile (**ii**, **Scheme 2.3**), attacking the carbon on the PBI core which now has enhanced electrophilicity due to the positive charge on the oxygen to which it is attached, resulting in the breaking of the carbon-oxygen bond and formation of the new carbon-chloro bond. Thus, the intermediate **IVa** is formed with the generation of phosphenic chloride and hydrochloride gas as by-products.

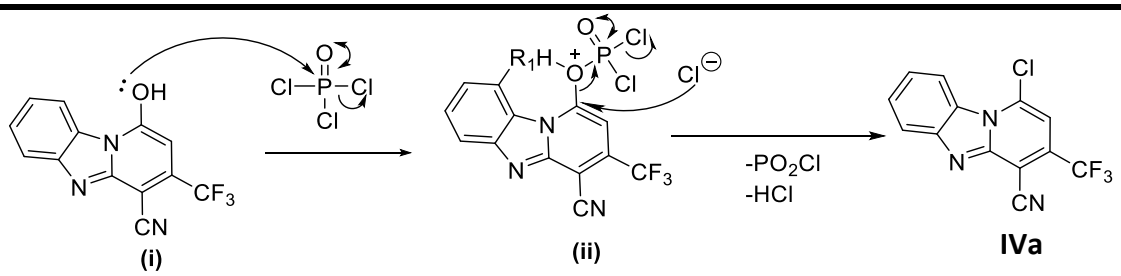

Scheme 2.3: *Proposed chlorination mechanism leading to intermediate* ***IVa*****.**

The chloro penultimate intermediate **IVa** was then transformed in the final step **iv** (**Scheme 2.1**) that entailed appending the predetermined amine either via nucleophilic aromatic substitution or by employing the palladium-catalysed Buchwald-Hartwig reaction conditions in the case of unreactive or poorly nucleophilic amines. Where nucleophilic aromatic substitution was elected for the synthesis of target compounds, triethylamine was included as the base and an appropriate solvent used. This reaction was completed in a microwave reactor in a sealed tube.

This reaction is proposed to proceed as depicted in **Scheme 2.4** where the lone pair of electrons on the amine nitrogen attack the electron-deficient carbon to which the chlorine atom is attached (**i**). Due to conjugation in the PBI system and ensuing resonance effects, there is a shift in the pyridyl double bonds leading to a negative charge residing on the nitrile nitrogen (**ii**). Consequently, the nitrile triple bond and the double bonds in the pyridyl reform, kicking out the chloro group. As a result, the intermediate **iii** is formed. In the final step, triethylamine abstracts a proton from the amino group thus neutralising the positive charge and forming the target amine compound **Va** together with triethylamine hydrochloride salt as by-product.

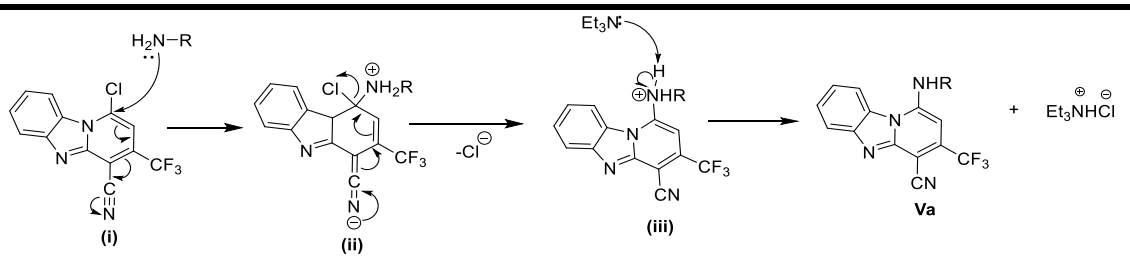

Scheme 2.4: *Proposed mechanism for the nucleophilic substitution reaction leading to final targets* ***Va*****.**

Notably, and expectedly so, this reaction generally resulted in the synthesis of analogues from the benzylamine-type series in better yields than those of the aniline-type series (**Table 2.1**). Moreover, the Craig plot substituent on the phenyl ring influenced the reactivity of the amine in the nucleophilic substitution reaction: electron withdrawing groups such as cyano and amide reduced the nucleophilicity of the amino nitrogen whereas electron-donating or releasing groups improved the nucleophilicity of respective amines. These features influenced the yields of respective analogues (**Table 2.1**). As already alluded to above, targets that could not be obtained through the conventional nucleophilic substitutions reactions or whose yields were expected to be too low, an alternative synthesis protocol involving the palladium-catalysed Buchwald-Hartwig amination reaction was utilised.[17–20]

In the use of the Buchwald-Hartwig amination reaction, whose general catalytic cycle is depicted in **Scheme 2.5**, various catalyst-ligand combinations were explored. The cycle starts with an oxidative addition process in which the palladium inserts between the carbon and chloro atom of the chloro intermediate **IVa** (**Scheme2.5**) after which the amine coordinates with the palladium. Proton abstraction by the base followed by attack on the palladium results in expulsion of the chloro leaving group. The target aryl amine product is generated in a reductive elimination step accompanied by the regeneration of the catalyst.

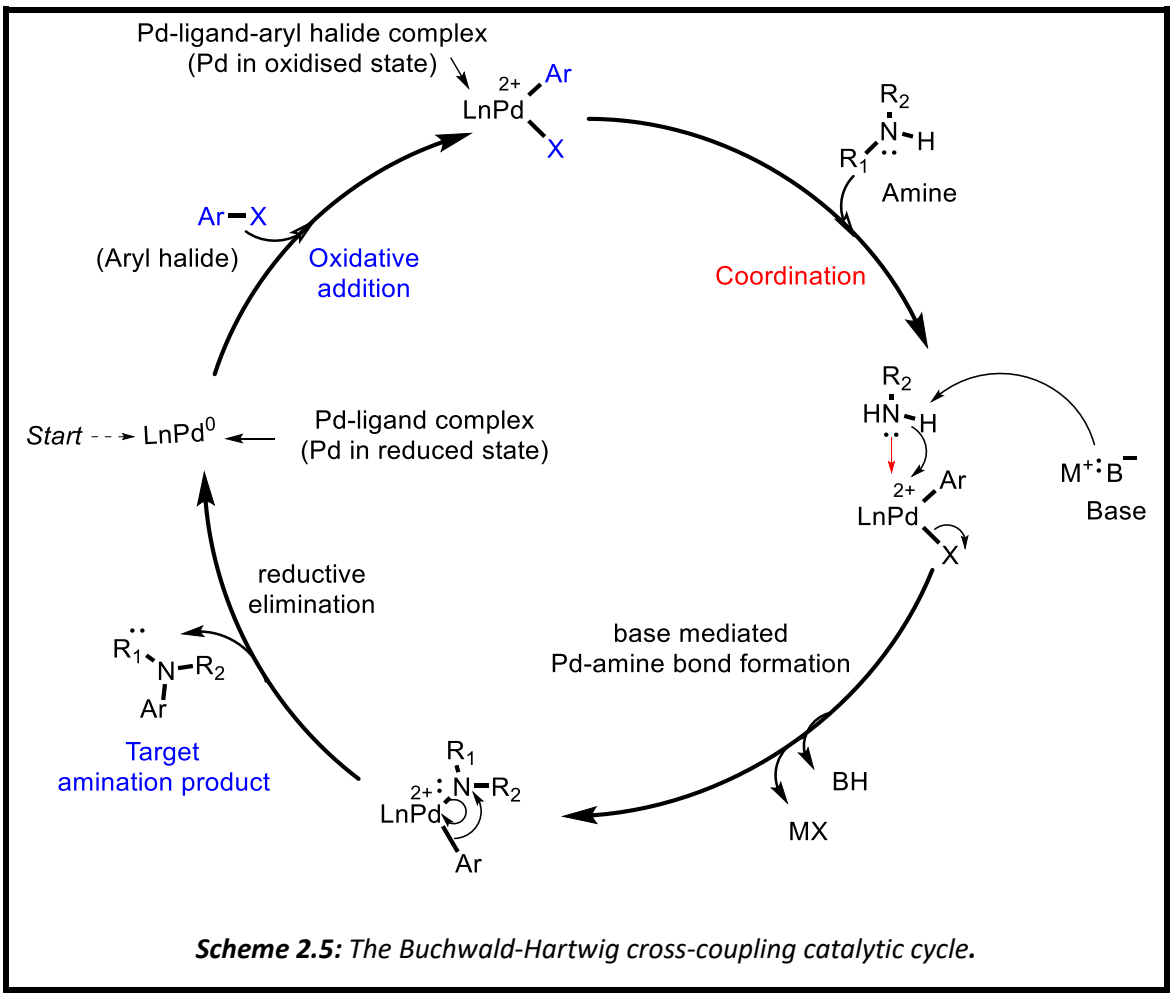

Scheme 2.5: *The Buchwald-Hartwig cross-coupling catalytic cycle.*

2.8.1.3 Synthesis of SAR_2 analogues

As highlighted earlier, analogues with substitutions on the phenyl portion were derived from appropriately substituted diaminobenzenes **I** (**scheme 2.1**). In the case of **SAR_2** analogues, the benzimidazole nitrile starting material was synthesized as mechanistically depicted in **Scheme 2.6**. The substituted benzimidazole nitriles **II** were subsequently used as described in section **2.8.1.2**.to furnish targets **Vb** and **Vc**.

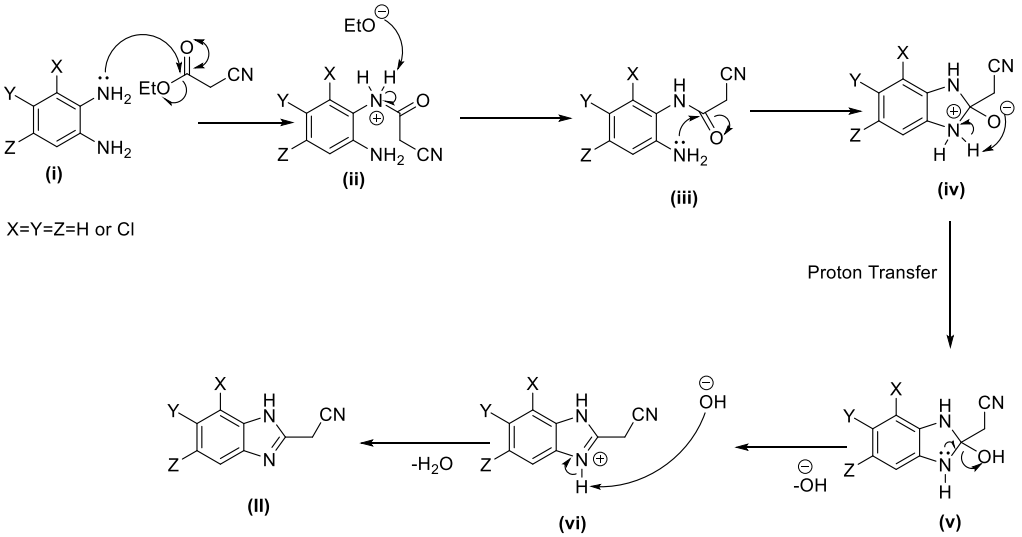

Scheme 2.6: *Proposed mechanism for the condensation reaction leading to intermediates* ***IIb*** *and* ***IIc*****.**

2.8.1.4 Synthesis of SAR_3 analogues

To replace the cyano functionality attached to the pyridyl portion of the PBI motif, different approaches were explored including varying the benzimidazole starting material. In this case, the methyl ester surrogate **IId** of benzimidazole acetonitrile **IIa** was used as a starting reagent. In exploring this alternative, it was hypothesized that, in line with the proposed mechanism for the formation of the hydroxyl intermediate (**Scheme 2.2**), the ester group would impart the necessary electron-withdrawing character as with the cyano group, to render the methylene protons acidic enough to be abstracted by the ammonium acetate base. The subsequent reaction steps would then proceed as discussed earlier (**Scheme 2.2**).

The above mentioned synthetic strategy was successful, albeit it resulted in lower yields of intermediate **IIId** compared to that achieved for **IIIa** when benzimidazole acetonitrile **IIa** was used as the starting material. An analysis on the other components of the reaction mixture revealed the presence of compounds whose identity could be rationalised. Among the major peaks observed was that of a protonated molecular ion mass of [M-58] corresponding to the decarboxylated product. Given the thermal conditions under which the reaction was carried out, it was reasoned that sufficient energy must have been generated to induce the decarboxylation reaction. Improved yields, albeit slightly, were achieved when the reaction was carried out at lower temperatures. Intermediate **IVd** and the final target **Vd** were synthesized subsequently from **IIId** as per the previously described protocol (**Scheme 2.1**).

Serendipitously, the chloro intermediate bearing the ester moiety (**IVd**, **Scheme 2.1**) resulted in the amination product, which had a mass and spectral profile matching the decarboxylated analogue, with a m/z of [M-58]. This observation paralleled that of the decarboxylation observed during the formation of the hydroxyl intermediate **IIId**. The microwave conditions applied appear sufficiently forceful to bring about sequential ester hydrolysis and decarboxylation (**Scheme 2.7**). Nonetheless, this unexpected reaction afforded us a useful target compound, **Ve** (**Scheme 2.1**) that would enable us to interrogate the role of the nitrile group in the antimalarial and antischistosomal activities of the PBIs.

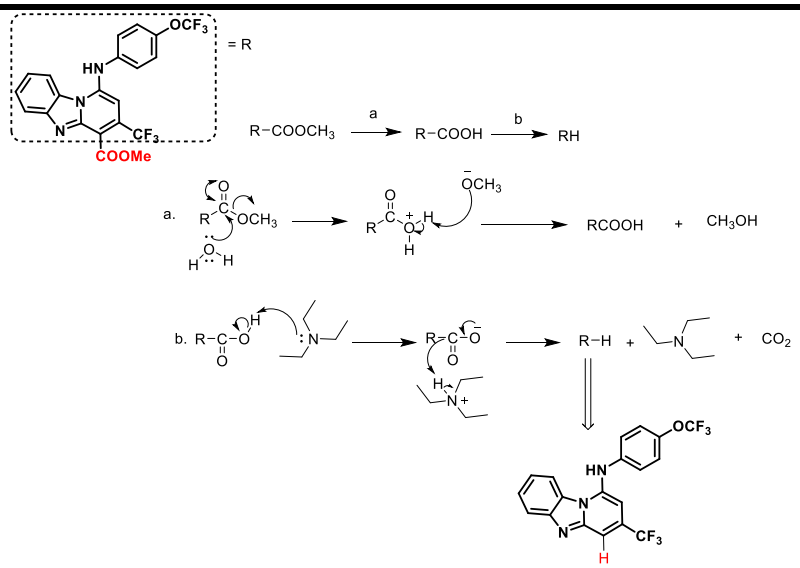

Scheme 2.7: *Mechanism for the ester hydrolysis and decarboxylation reactions leading to target* ***Ve*****.**

We explored other cyano-replacement strategies including the conversion of the cyano to an amide at the hydroxyl stage using concentrated sulphuric acid (**Scheme 2.8**). The mechanism of this functional group interconversion, that entails hydration, is proposed to proceed via an initial protonation of the nitrile nitrogen which increases the susceptibility of the nitrile carbon to an electrophilic attack carried out by water (**b**, **Scheme 2.8**). Subsequent proton transfer (**c**) from the oxygen to nitrogen facilitates formation of the amide carbonyl (**d**). Subsequently, the sulphate anion picks up the proton on the positively charged oxygen (**e**) to regenerate the acid and give the desired amide target. This reaction proceeded readily giving quantitative yields.

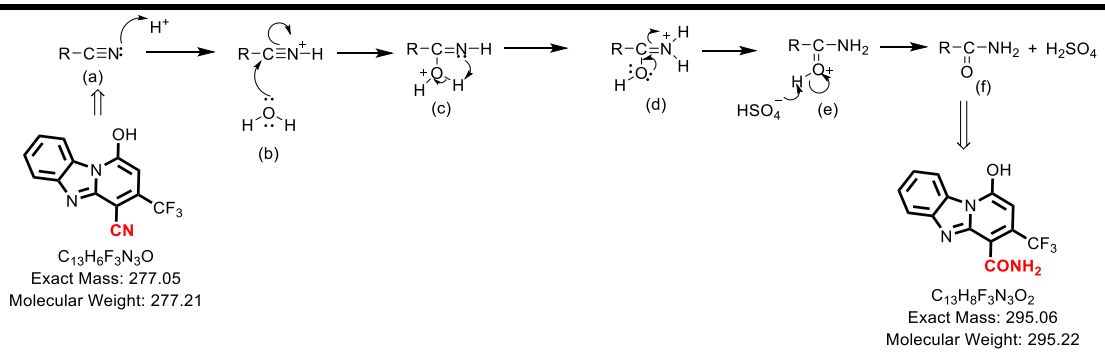

Scheme 2.8: *Proposed reaction mechanism for nitrile oxidation using conc. Sulphuric acid.*

Chlorination of the now derived hydroxyl intermediate (**f**, **Scheme 2.8**) was then carried out using $POCl_3$ as described with the other targets (**iii**, **Scheme 2.1**). Surprisingly, the expected product **vi** (Scheme **2.9**) was not obtained. Instead, on the LCMS, the compound produced a peak with a different retention time but the same protonated molecular ion mass $[M+H]^+$ as the hydroxyl precursor **f**, **Scheme 2.8**. This MS profile was consistent with that of the chloro intermediate **IVa** which has a nitrile group instead of an amide at **SAR$_3$**, **Scheme 2.1**. Following literature investigations, it was established that $POCl_3$ had converted not only the hydroxyl group of **ii** to the chloro, but also the amide back to the nitrile as illustrated in **Scheme 2.9**.[21]

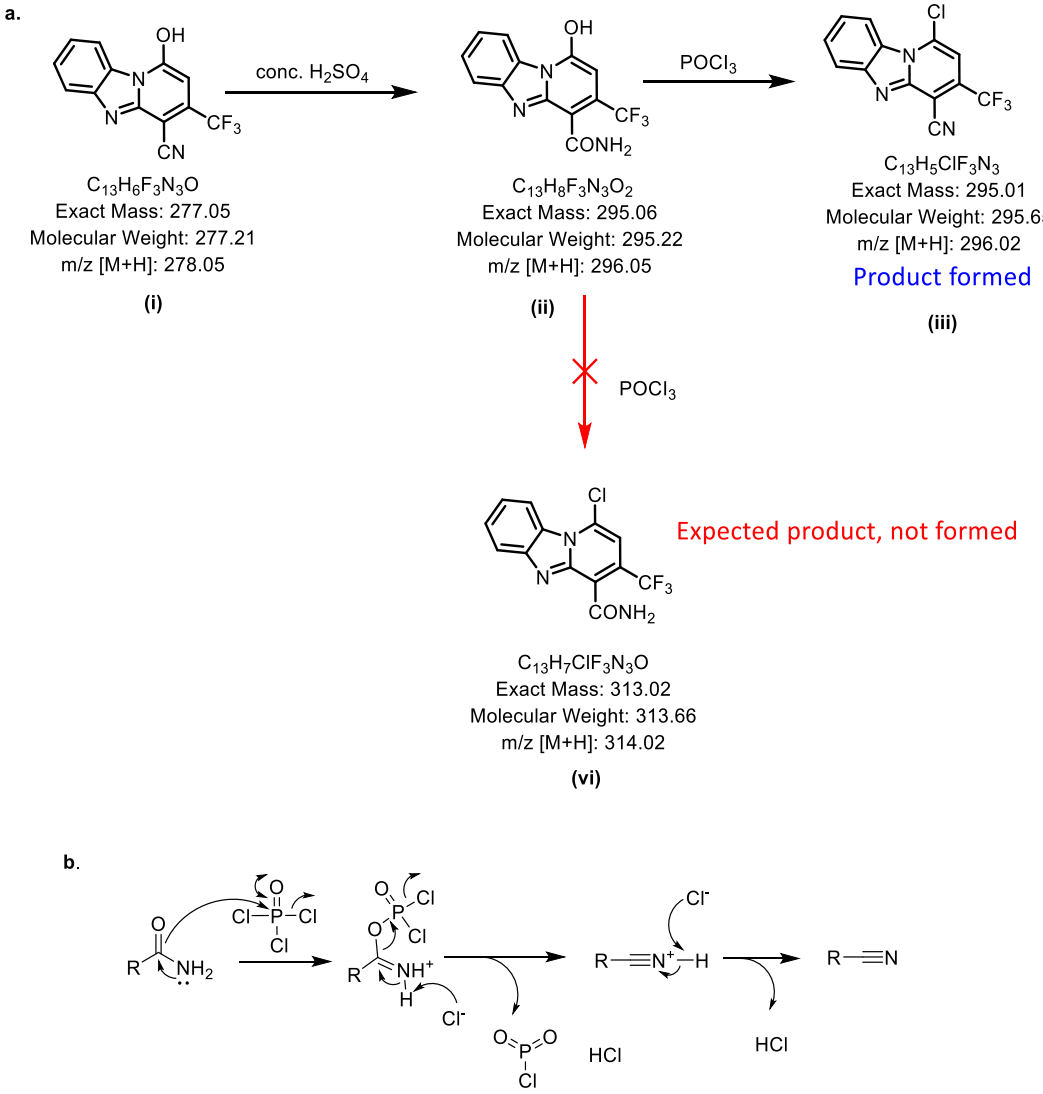

Scheme 2.9: *(a) Reaction path for the unsuccessful synthesis of **vi** and (b) the proposed mechanism of the $POCl_3$-mediated amide dehydration reaction contributing to formation of **iii**.*

Thus, realising that the hydroxyl intermediate was unsuitable for transforming the nitrile to the amide under the proposed reaction conditions, this change was attempted at the chloro intermediate stage. Gladly, this reaction proceeded unhindered and gave good yields. Using the now synthesized chloro intermediate having an amide functionality (**VI**, **Scheme 2.1**), the final amination step could be carried out as in step **iv** to furnish analogues **Vf** (**Scheme 2.1**).

Numerous attempts to introduce more diversity at the nitrile site were unsuccessful. For example, the well reported cyano to carboxylic acid conversion using base or acid catalysis were unfruitful under different conditions of bases, acids, temperatures and solvents. Instead, in some cases, molecular ions observed on MS analysis pointed to possible fragmentation of the PBI scaffold under some extreme conditions attempted. Similarly, attempts to generate the primary amine, carboxylic acid and tetrazole analogues at this position failed, despite their wide applications in organic chemistry.[22] These syntheses failures prompted the hypothesis that the rich electron density and continuous electron flow in the PBI scaffold, coupled with conjugation and resonance involving the nitrile group (**Scheme 2.10**) are likely features rendering this group inert to the attempted transformations. Changes at this SAR site were thus limited by the synthetic challenges experienced.

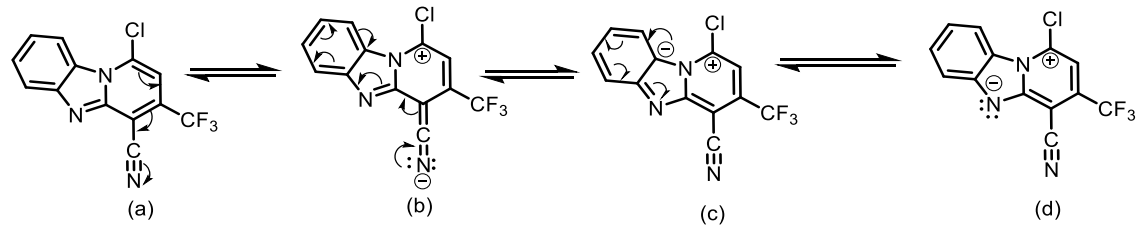

Scheme 2.10: *Resonance and conjugation in the PBI system illustrating involvement of the nitrile in maintaining the aromaticity.*

2.8.2 Characterisation

2.8.2.1 Overview of characterisation techniques

To establish the identity of intermediates and target compounds, analytical and spectroscopic techniques were used, in a complementary manner. Thin layer chromatography (TLC) on silica adsorbed on alumina with the corresponding optimised mobile phase enabled monitoring of reaction progress. High performance liquid chromatography coupled to a mass spectrometer (HPLC-MS) further aided in monitoring progress of reactions through identification of the molecular ion of the formed product in the reaction mixture. Following purification and isolation of target compounds using an array of methods including trituration, precipitation, preparative TLC and column chromatography, purity was determined using HPLC with UV detection, given the aromatic nature of the compounds which endows them with UV absorption capacity. Nuclear magnetic resonance (NMR) involving both proton (^{1}H) and carbon (^{13}C) nuclei further supplemented the compound identification process by generating peaks whose chemical shifts (^{1}H and ^{13}C) and coupling patterns (^{1}H) directed the structure assignment. In the succeeding section, representative intermediates and target compounds from each of the SAR positions are described to illustrate how these techniques were used to characterise the compounds.

2.8.2.2 Hydroxyl Intermediate IIIa with no modification on SAR_2

In the case of compounds where there are no changes made at **SAR_2**, and **SAR_3** is fixed as a nitrile, transformation of the benzimidazole acetonitrile **IIa** to the tricyclic hydroxyl intermediate **IIIa** was detected by a decrease in polarity based on analytical TLC analysis. The corresponding mass peak m/z [M+H] of 278.1 on the LC-MS together with the increase in retention time, reflective of increased lipophilicity, provided more evidence for the formation of this initial intermediate (**Figure 2.9**).

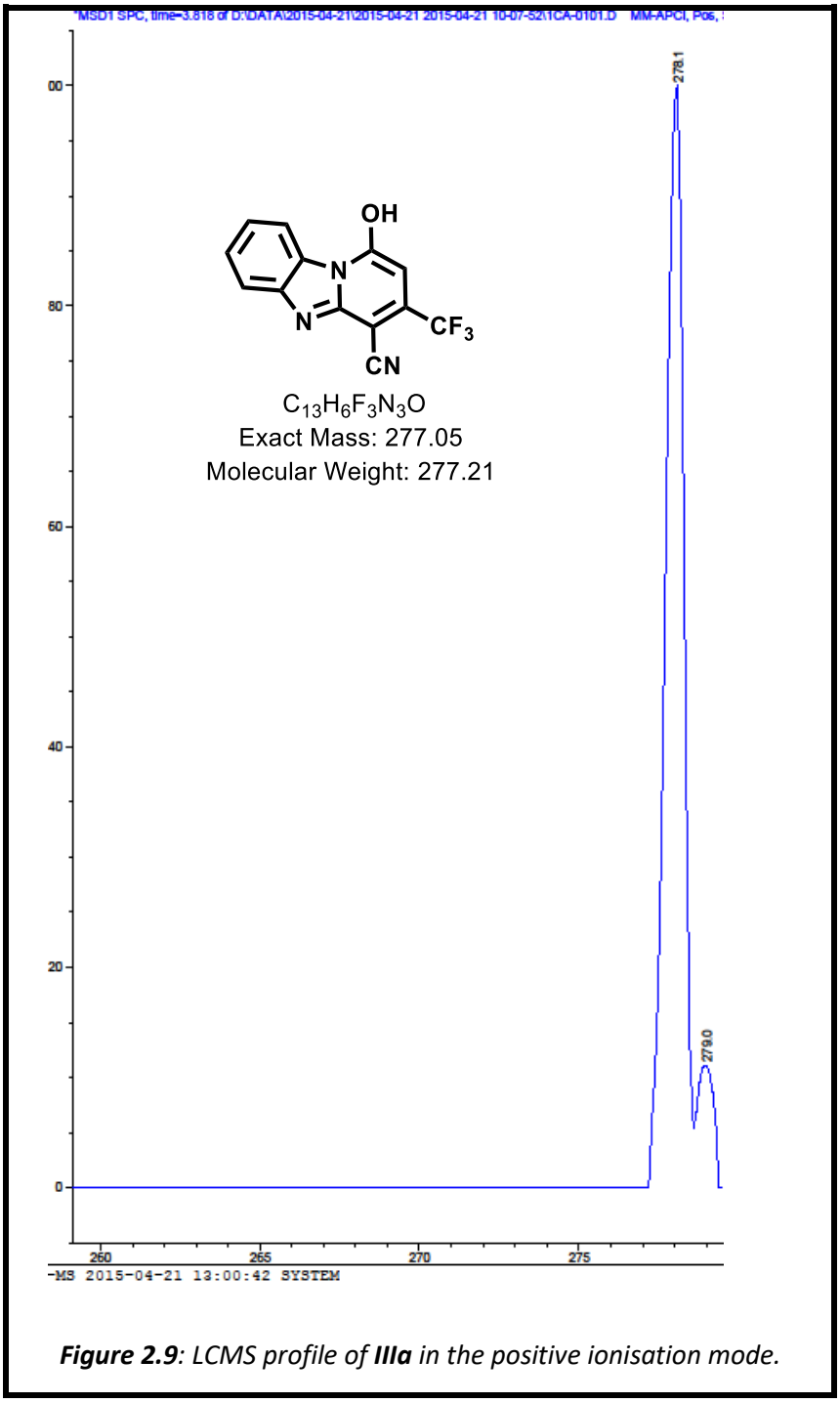

***Figure 2.9**: LCMS profile of **IIIa** in the positive ionisation mode.*

Analyses of ^{1}H NMR spectra (**Figure 2.10**) corroborated with the structure for intermediate **IIIa** wherein peaks that integrated for five protons were observed downfield (6-9 ppm), representing the 5 aromatic protons present on the PBI core. Four of these protons are the protons in the phenyl region (LHS) of the PBI scaffold displaying chemical shifts between 7.46 and 8.60 ppm. In addition to the position of the NMR peaks, which reflects the chemical environment with respect to shielding and deshielding effects, in which the protons are located, the coupling constants directed the assignment of peaks to the respective protons. Consequently, proton **H1** resonates furthest downfield at 8.60 ppm and appears as a doublet of triplet arising from J_{ortho} coupling to **H2** (J= 8.16 Hz) and J_{meta} coupling to **H3** (J=0.91 Hz). Signals due to protons **H2** and **H4** appear in close proximity between 7.70-7.57 ppm with their peaks superimposing, resulting in a multiplet which integrates for two protons. The **H3** proton, appearing as a doublet of doublets of doublets at 7.46 ppm, experiences J_{ortho} coupling with both **H4** (J=8.6 Hz) and **H2** (J=6.8 Hz) with an additional J_{meta} coupling with **H1** (J=1.8 Hz). The signal at 6.43 ppm, which was diagnostic for this intermediate and integrates for one proton, represents the **H5** proton present next to the carbon bearing the hydroxyl group on the pyridyl portion of the PBI core while the signal due to the hydroxyl proton (**H6**) usually appeared downfield as a broad singlet.

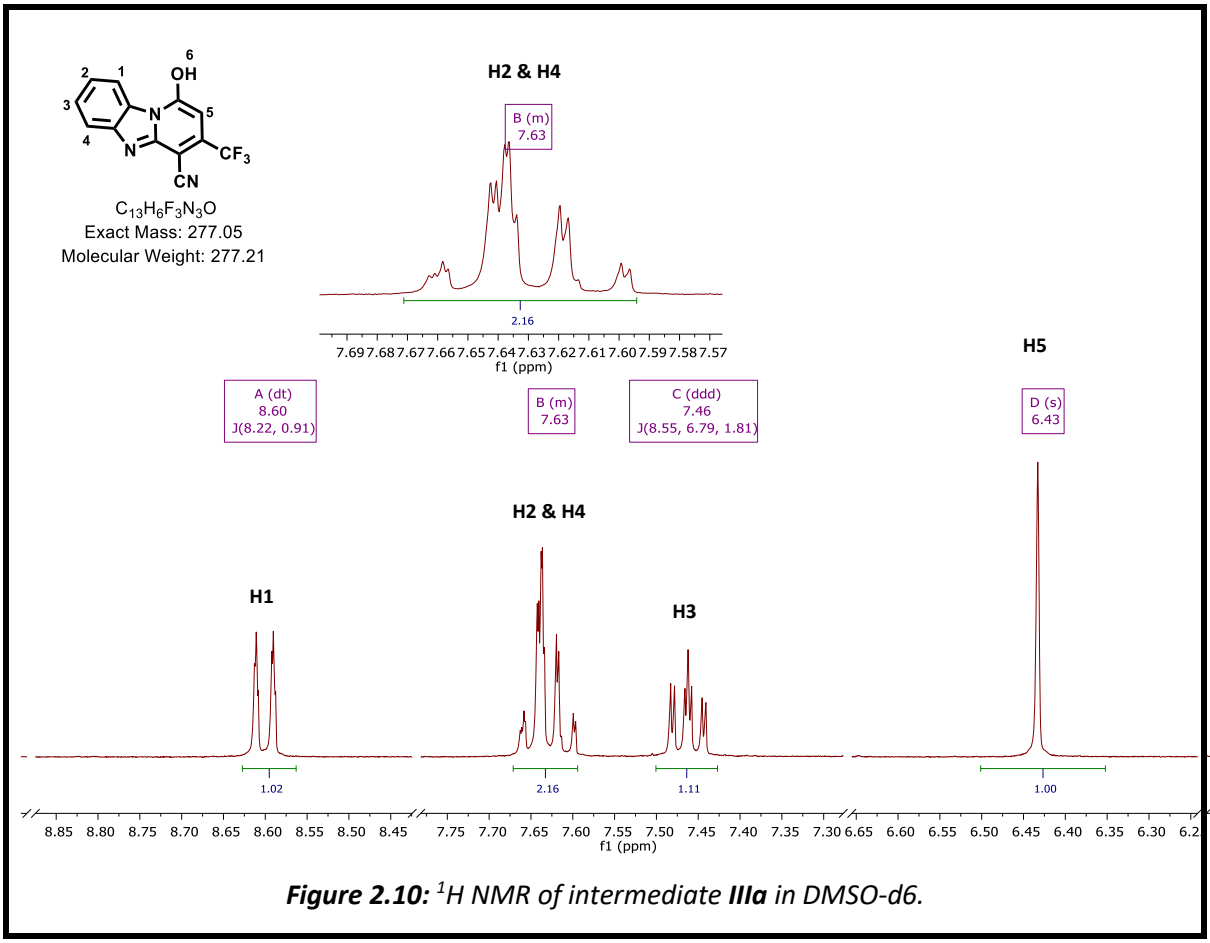

Figure 2.10: *^{1}H NMR of intermediate **IIIa** in DMSO-d6.*

Similarly, ^{13}C NMR analysis aided the confirmation of the structure based on the positions of the carbon signals which largely paralleled that of the protons. Thirteen (13) carbon signals were identifiable with chemical shifts between ca. 100-160ppm due to the aromatic and deshielding electronic environment within the PBI nucleus and the attached substituents.

2.8.2.3. Chloro Intermediate IVa

Formation of the chloro intermediate **IVa** after the reaction between the hydroxyl intermediate **IIIa** and $POCl_3$ was discernible by changes in appearance, molecular mass and polarity. In addition to the disappearance of grey colour of **IIIa** and emergence of a yellow one, a molecular ion of m/z $[M+H]^+$ of 296.0/298.0 which gave the classical chlorine splitting pattern in the ratio of 3:1, consistent with the ratio of abundance of ^{35}Cl to ^{37}Cl, was apparent (**Figure 2.11**).

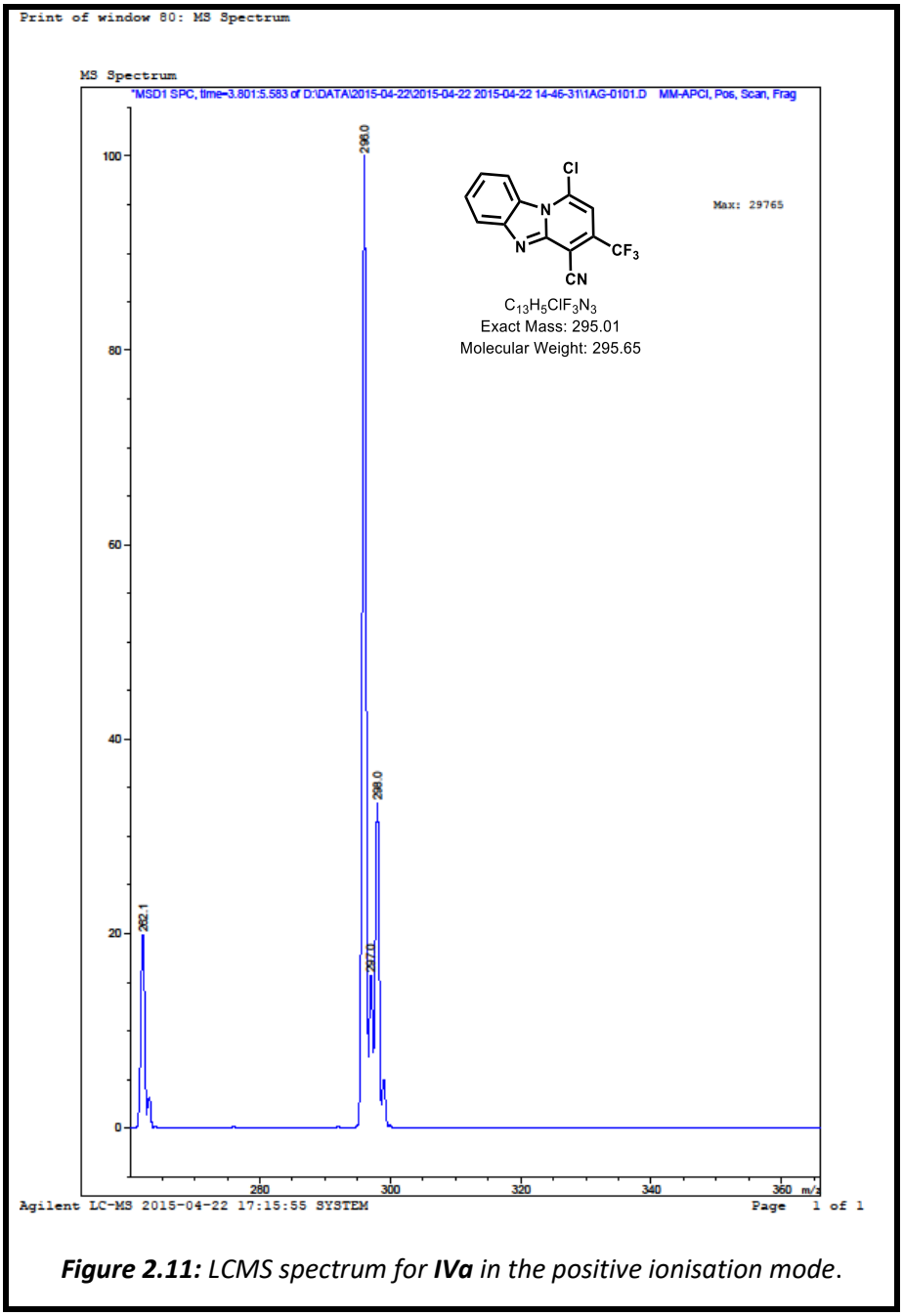

Figure 2.11: *LCMS spectrum for **IVa** in the positive ionisation mode.*

The NMR spectra (**Figure 2.12**), expectedly, resembled that of the hydroxyl intermediate **IIIa**, with 5 aromatic protons discerned between 6-9 ppm. As such, the peak due to **H1** resonates downfield at 8.57 ppm and appears as a doublet of triplet resulting from J_{ortho} coupling to **H2** and J_{meta} coupling to **H3**. Signals due to protons **H2**, **H3** and **H4** adopted a doublet of doublet of doublets splitting pattern occasioned by coupling to immediate neighbouring protons and to protons farther away. Effectively, proton **H4** couples to **H3** (J=8.10 Hz) and **H2** (J=1.33 Hz) while **H2** clearly couples with **H1** (J=8.36 Hz) and **H3** (J=7.14 Hz) via J_{ortho} coupling and with **H4** (J=1.40 Hz) via J_{meta} coupling. The protons **H3** and **H1** both couple to **H2** and to each other while **H3** has additional coupling to **H4**. Consistently, the ^{13}C NMR resembled that of intermediate **IIIa** with regards to chemical shift position of the respective carbons. In this case, it is the carbon attached to the chloro group that resonated most downfield.

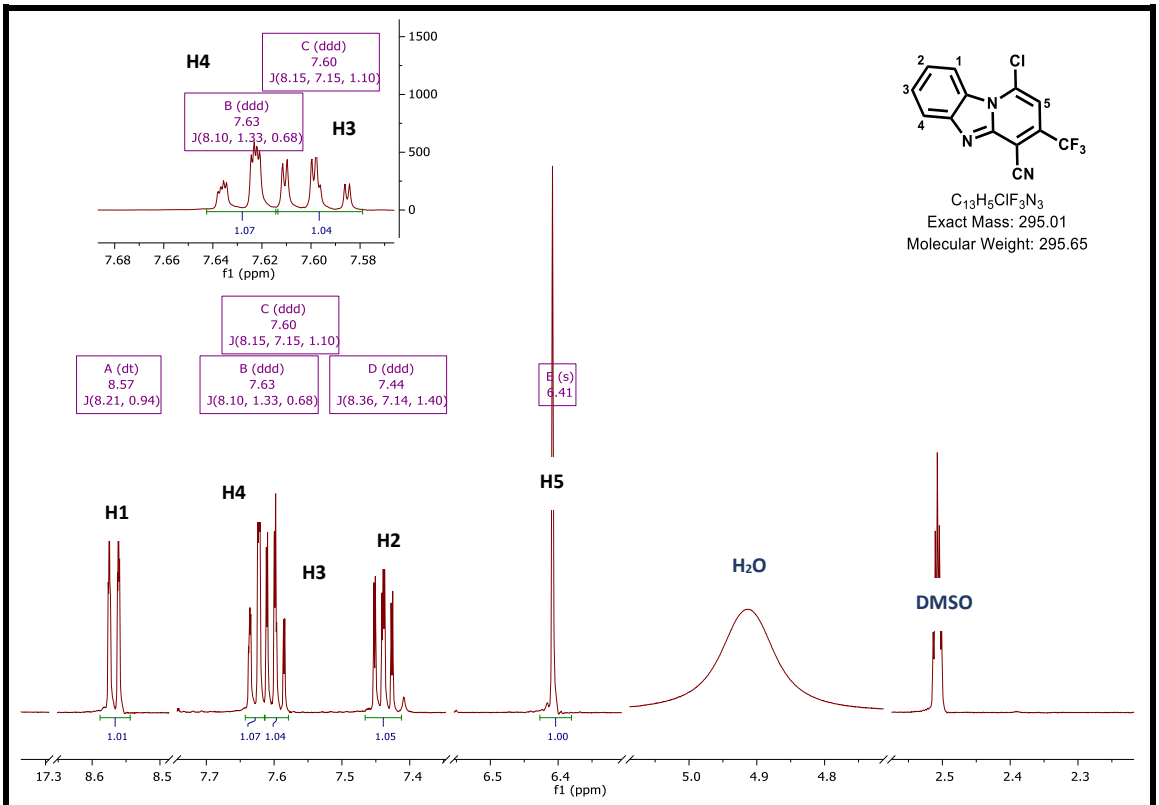

***Figure 2.12**: [1]H NMR of intermediate **IVa** in DMSO-d6.*

2.8.2.4 Final compounds Va without SAR_2 changes

The final amination targets were, as with the intermediates, confirmed by making observations on the colour, mass spectrometry molecular ion and evaluating the respective ^{1}H and ^{13}C NMR spectra. Since the side groups introduced were mostly aromatic in nature, we anticipated additional proton signals, to what was observed for the prior intermediates **IIIa** and **IVa**, in the aromatic region. Indeed, for the para-substituted aniline-type series analogues, signals corresponding to four additional aromatic protons were observed, frequently appearing as two separate coupling (doublets) signals, with occasional deviations depending on the nature of substituents borne on the aromatic ring. If the side group substituent contained aliphatic protons, these emerged, as expected, in the upfield region. The corresponding ^{13}C NMR spectra compared with the ^{1}H NMR one with regards to the chemical shift positions whereby additional carbon signals in the aromatic regions, arising from the carbons on the attached aromatic side group, were evident.

For equivalent carbons, the signals appeared as taller peaks, consistent with the number of equivalent carbons. Where applicable, carbon signal(s) corresponding to the substituent(s) on the side group were also identifiable. For example, with **1j/GMP-19**, the ^{1}H NMR spectrum has four additional protons (**H7** and **H8**; **Figure 2.13**), to those present in the preceding intermediates **IIIa** and **IVa** (**Figures 2.10 and 2.12**), in the aromatic region (6-9 ppm). These are the protons present in the trifluoromethoxy aniline appendage and appear as two doublets. Protons **H8**, experiencing shielding effects from the electron-rich trifluoromethoxy group, resonate slightly upfield of **H7** protons, which are deshielded by the nitrogen linker between the PBI nucleus and the aromatic side group. Congruently, the ^{13}C NMR reflects the additional carbon signals due to the aromatic and the trifluoromethyl carbons. The proposed structure was further supported by the MS profile, which yielded a protonated molecular ion of 437.1 in the positive ionisation mode (**Figure 2.14**).

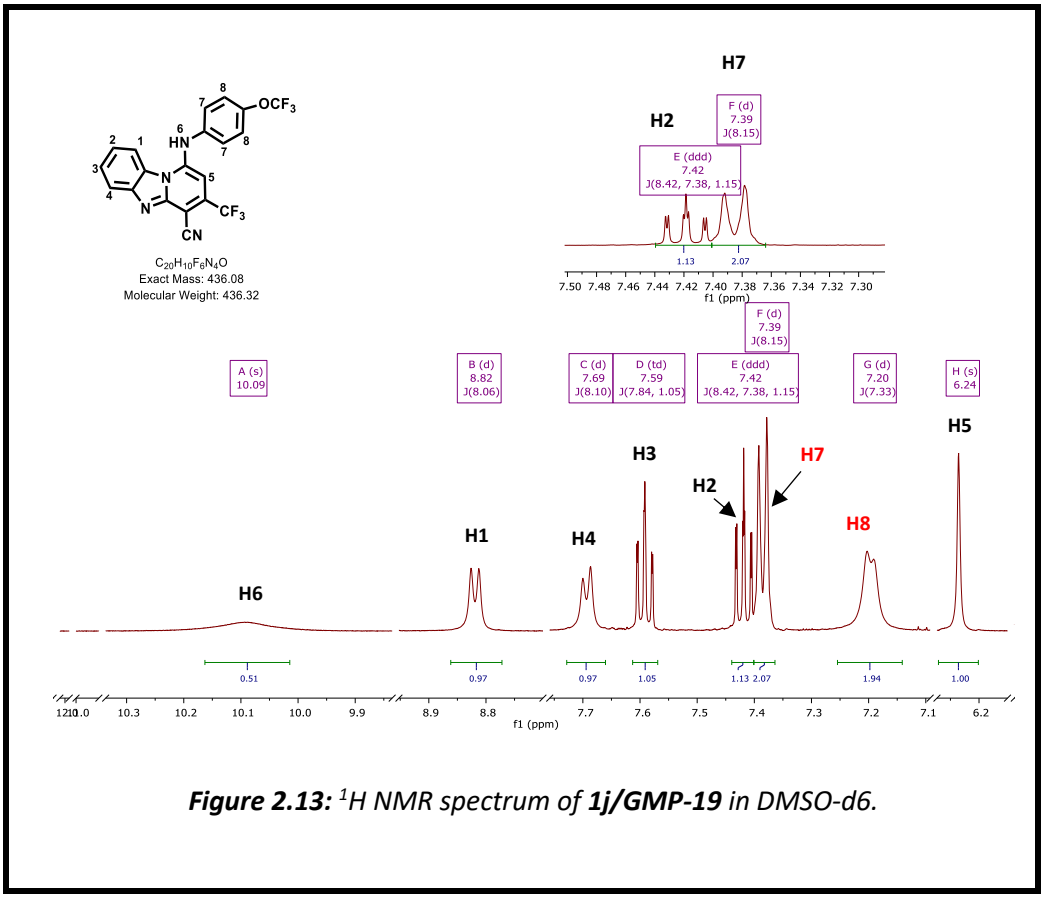

Figure 2.13: *^{1}H NMR spectrum of **1j/GMP-19** in DMSO-d6.*

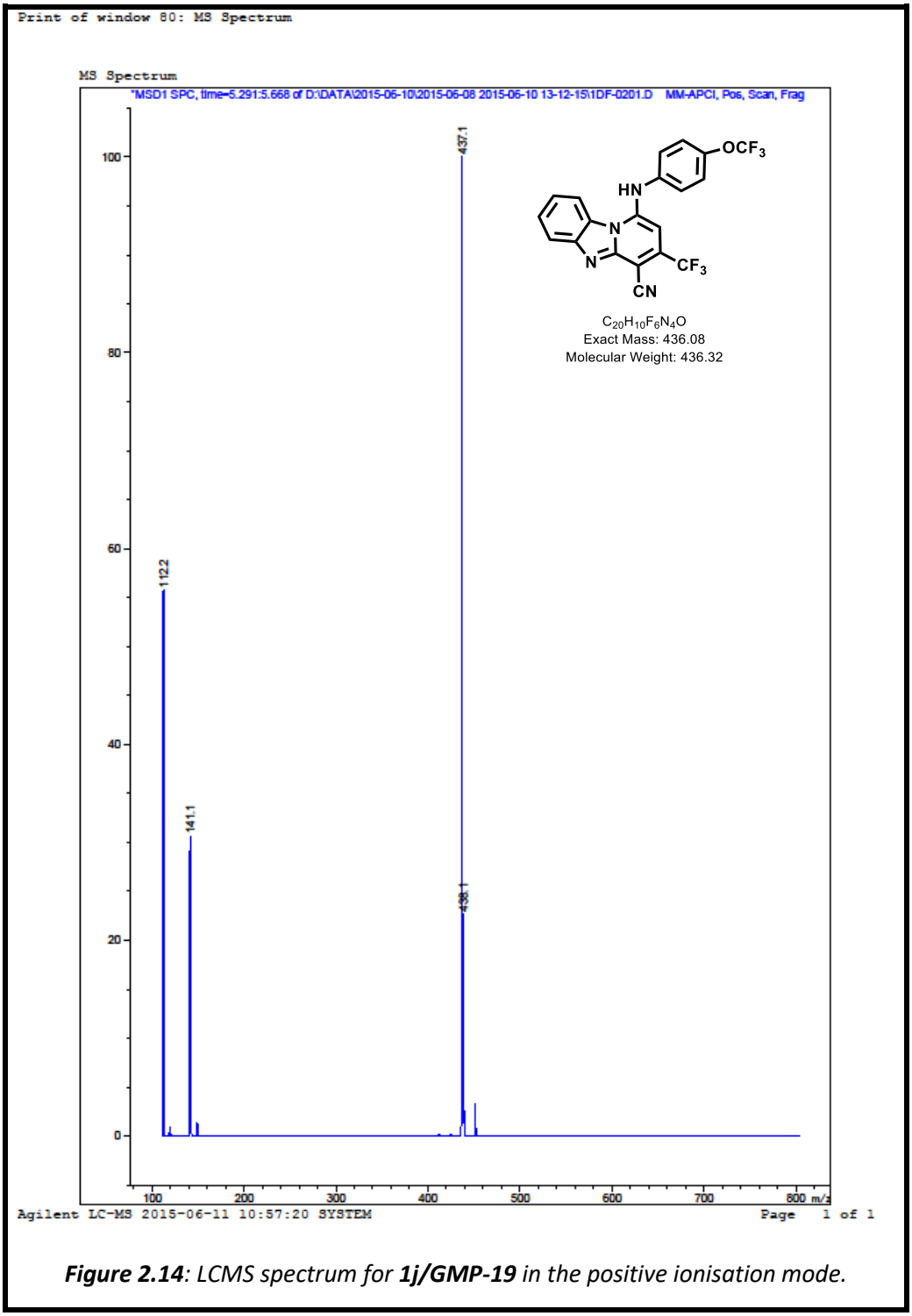

***Figure 2.14**: LCMS spectrum for **1j/GMP-19** in the positive ionisation mode.*

In the case of benzylamine series analogues, in addition to tracing the changes in NMR spectra described for the aniline series, there emerged an aliphatic signal upfield integrating for two protons, corresponding to the methylene protons linking the aromatic portion of the side group to the nitrogen attached to the PBI core. Using **3o/GMP-50** as an example, the proton (**H6**) on the nitrogen linking the aromatic side group and the PBI core is noticeable as a broad singlet at 8.64 ppm while the two methylene protons (**H7**), also appearing as a singlet, resonate at 4.86 ppm, rather downfield for aliphatic protons, due to the deshielding effect of the nearby phenyl and amine groups. The methyl protons (**H10**) resonate at 2.29 ppm, appearing as a singlet that integrates for three protons, due to shielding effects by the phenyl ring to which the carbon bearing them is attached (**Figure 2.15**). Diagnostic peaks in the ^{13}C NMR spectrum comprised of the additional aromatic carbon peaks between 127-130 ppm; the methylene carbon peak **C14** at 46.57 ppm and the methyl carbon **C19** at 21.14 ppm (**Figure 2.15**). These features were consistent with the proposed structure of the molecule that produced a MS spectrum with m/z, in the positive ionisation mode, of 381.1 (**Figure 2.16**).

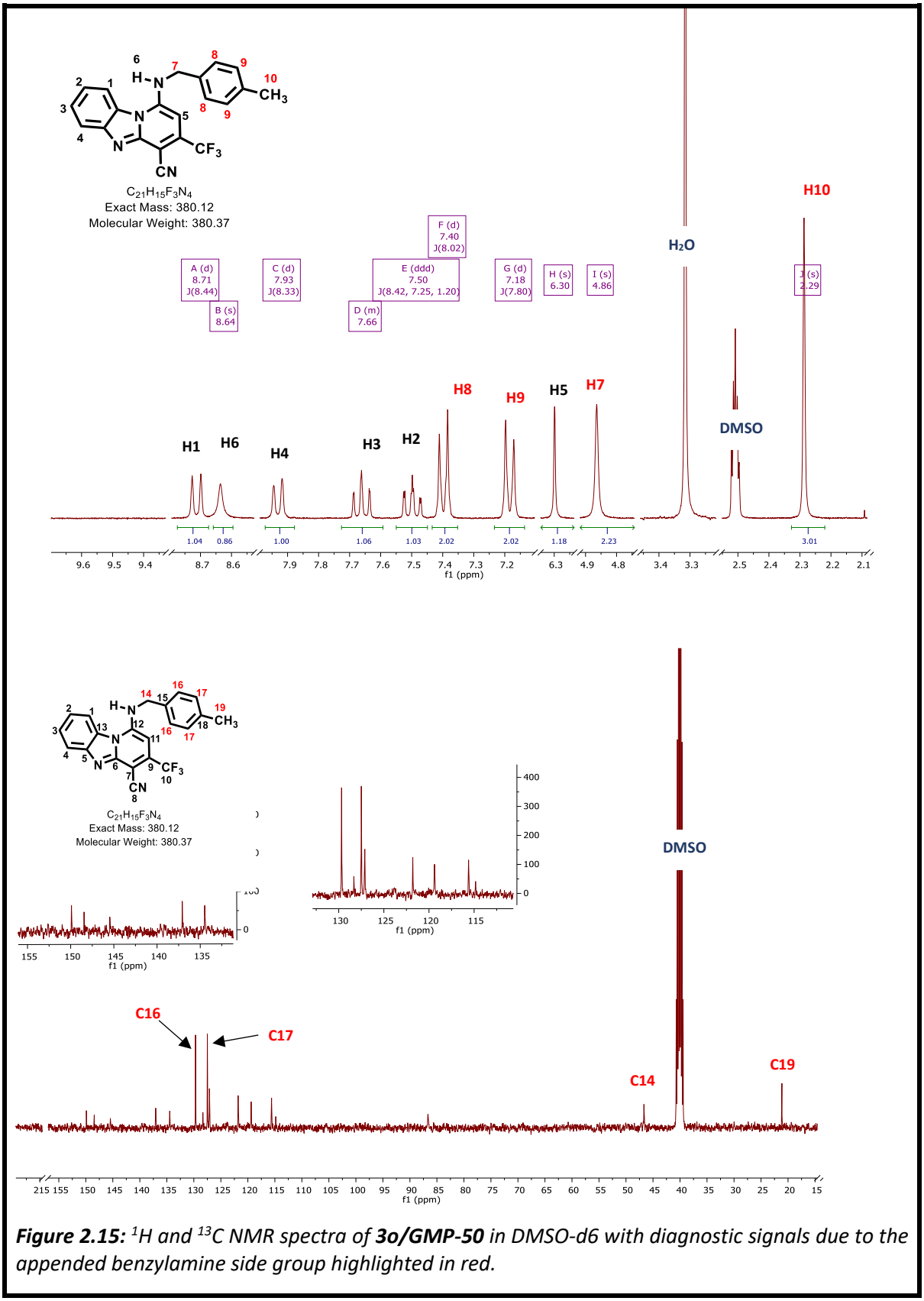

Figure 2.15: *^{1}H and ^{13}C NMR spectra of **3o/GMP-50** in DMSO-d6 with diagnostic signals due to the appended benzylamine side group highlighted in red.*

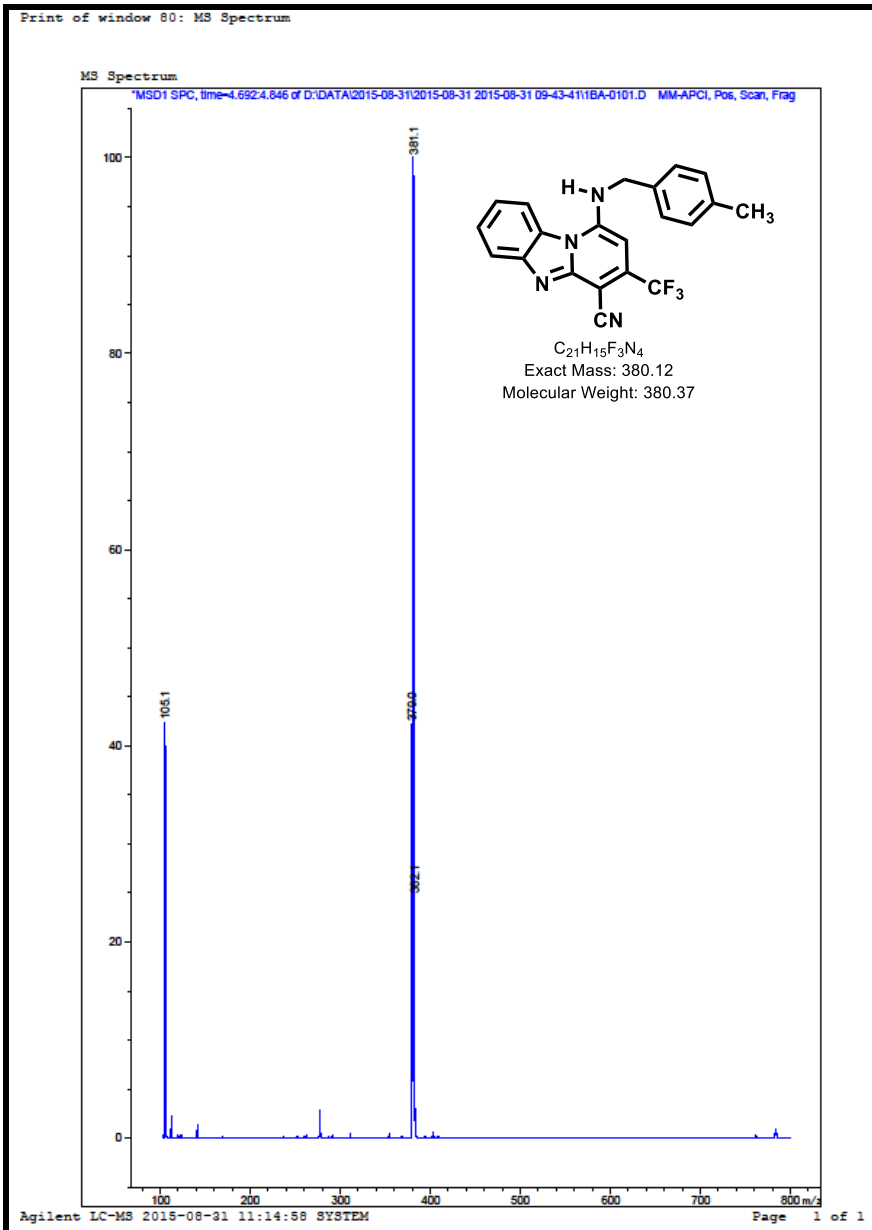

Figure 2.16: *LCMS spectrum for* ***3o/GMP-50*** *in the positive ionisation mode.*

2.8.2.5 SAR2- modified analogues

The appropriately substituted benzimidazole acetonitrile was synthesised as the first intermediate in the case of those analogues having modifications on the LHS of the PBI core (**SAR_2**). Subsequent hydroxyl (**IIIb** and **IIIc**) and chloro (**IVb** and **IVc**) intermediates were synthesized using the same protocol as those without **SAR_2** changes (**IIIa** and **IVa**; steps **ii** and **iii**, **Scheme 2.1**) and their structures, together with final targets **Vb** and **Vc** were ascertained as described before, using a combination of colour changes, TLC R_f value, HPLC-MS and NMR techniques. As an example, the structures of intermediates **IIc**, **IIIc**, **IVc** and the final target **4i/GMP-75**, bearing 4, 5- dichloro substitutions were rationalised as described hereafter.

Successful conversion of the substituted di-amino benzene starting material **Ib** to the corresponding intermediate **IIc** was ascertained by observing a MS peak with m/z of 226.0/228.0 consistent with the expected pseudomolecular ion $[M+H]^+$ which adopted the classical chloro splitting pattern (3:1). Features of the ^1H NMR (**Figure 2.17**) included the appearance of proton signals in the aromatic region, integrating for two protons, representing the aromatic hydrogens (**H1** and **H2**) on the benzene portion of the benzimidazole core. These peaks, due to their comparable electronic environments, appear together at 7.75-7.94 ppm and appear as a poorly split doublet which, on manual integration, suggest closely positioned singlet peaks, integrating for one proton each at 7.80 (**H2**) and 7.89 ppm (**H1**). Moreover, a deshielded aliphatic signal integrating for two protons due to the methylene protons (**H3**) on the carbon connected to benzimidazole and the nitrile groups, was evident. On the other hand, the proton **H4** on one of the imidazole nitrogen atoms could be discerned at 12.90 ppm, consistent with a highly deshielded proton. Additionally, the position of signals on the ^{13}C NMR spectrum reinforced the structure assignment for this intermediate whereby, besides the downfield location of benzimidazole and the nitrile carbons, there was an upfield signal due to the aliphatic methylene carbon **C8** at 18.90 ppm (**Figure 2.17**).

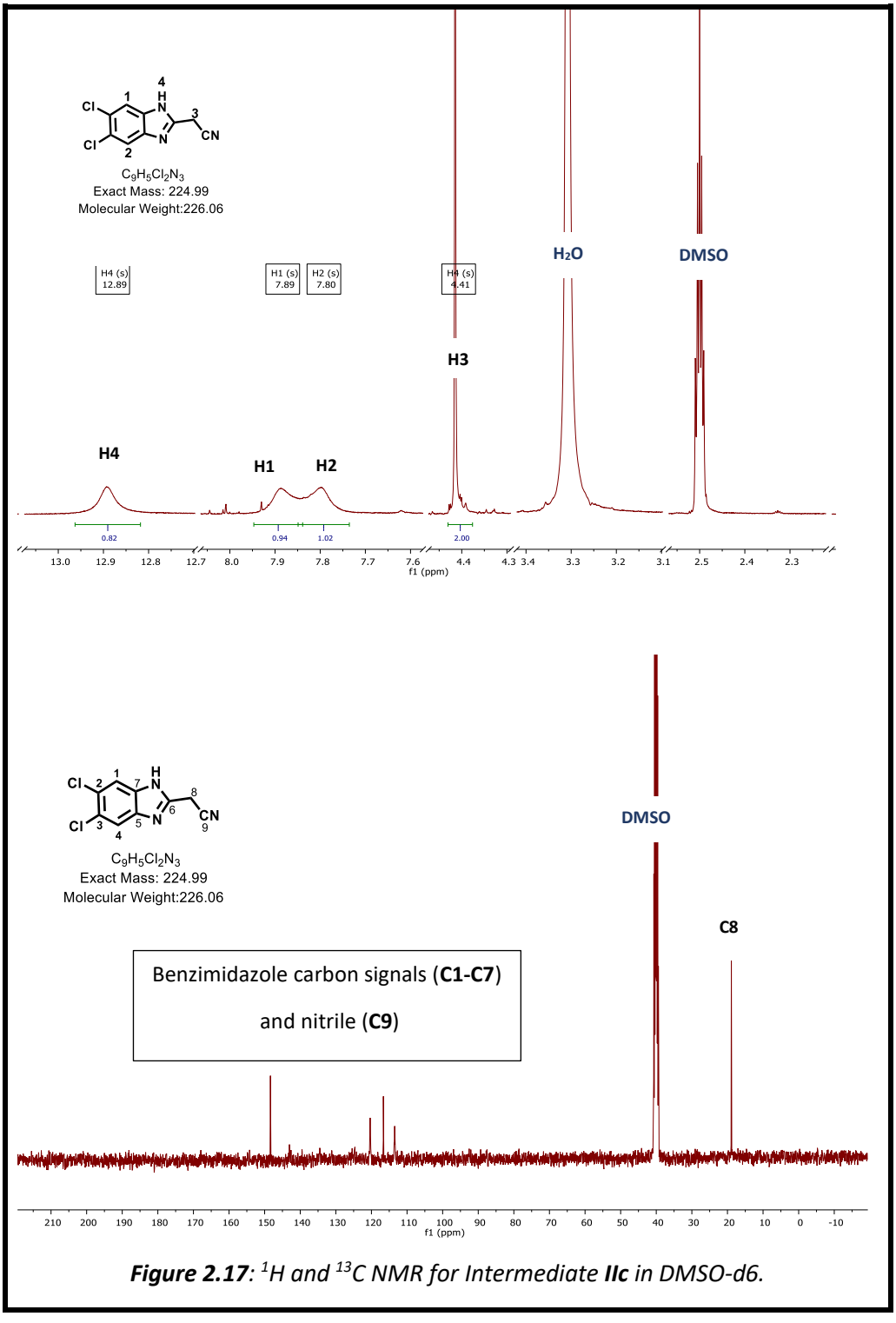

***Figure 2.17**: ^{1}H and ^{13}C NMR for Intermediate **IIc** in DMSO-d6.*

Subsequent hydroxyl (**IIIc**) and chloro (**IVc**) intermediates were confirmed by examining their LCMS profile whereby m/z profiles matched the expected pseudomolecular ions $[M-H]^-$ =344.0/345.0; 346.0/347.0 (**IIIc**) and $[M+H]^+$= 364.0/366.0 (**IVc**) displaying the standard chloro pattern. ^1H NMR spectra further supported the successful synthesis of these intermediates whereby the two methylene protons in the previous benzimidazole derivative **IIc** disappeared and in its stead, a singlet peak integrating for one proton (**H3**) emerged further downfield at 5.87 and 6.45ppm in **IIIc** and **IVc**, respectively (**Figure 2.18**). As expected, the ^{13}C NMR of **IIIc** and **IVc** reflected the increase in the number of carbon atoms to thirteen from nine and the disappearance of the methylene carbon, previously observed at 18.90 ppm in **IIc (Figure 2.17)**. Like intermediates **IIIa** and **IVa**, the chemical shifts of the signals paralleled the electronic environment of the carbons, with deshielded atoms resonating further downfield.

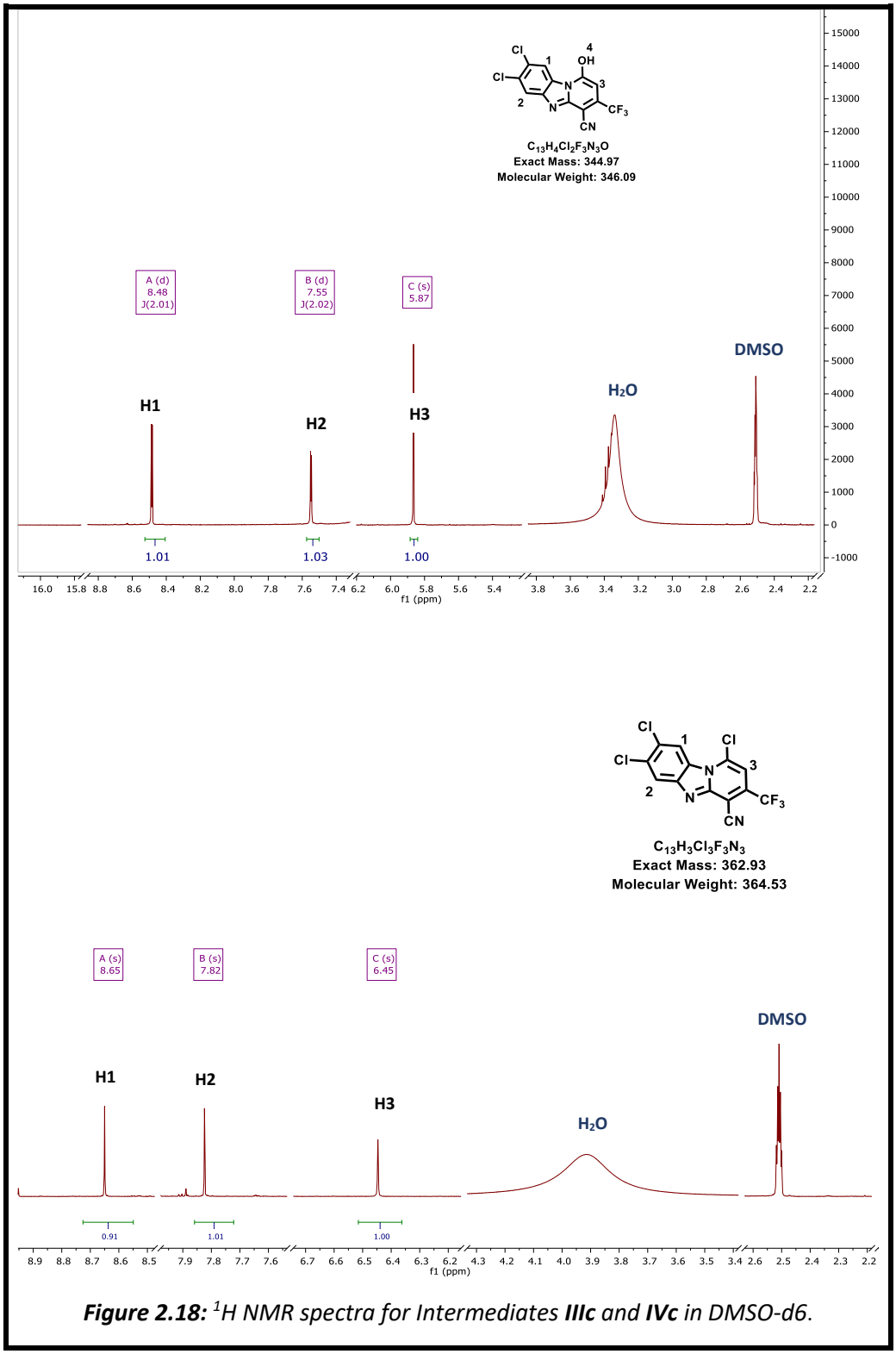

Figure 2.18: *^{1}H NMR spectra for Intermediates **IIIc** and **IVc** in DMSO-d6.*

In addition to detecting the anticipated molecular ion using LCMS (**Figure 2.19**), NMR spectral changes for final targets bearing the **SAR$_2$** manipulations comprised the presence of additional peaks downfield representing the aromatic protons on the appended amine side group as exemplified by **4i/GMP-75** in **Figure 2.20**. Corresponding changes were manifested in the ^{13}C NMR spectrum whereby extra carbon peaks due to the benzyl side group appeared in the aromatic downfield and aliphatic upfield regions as previously described for **3o/GMP-50**.

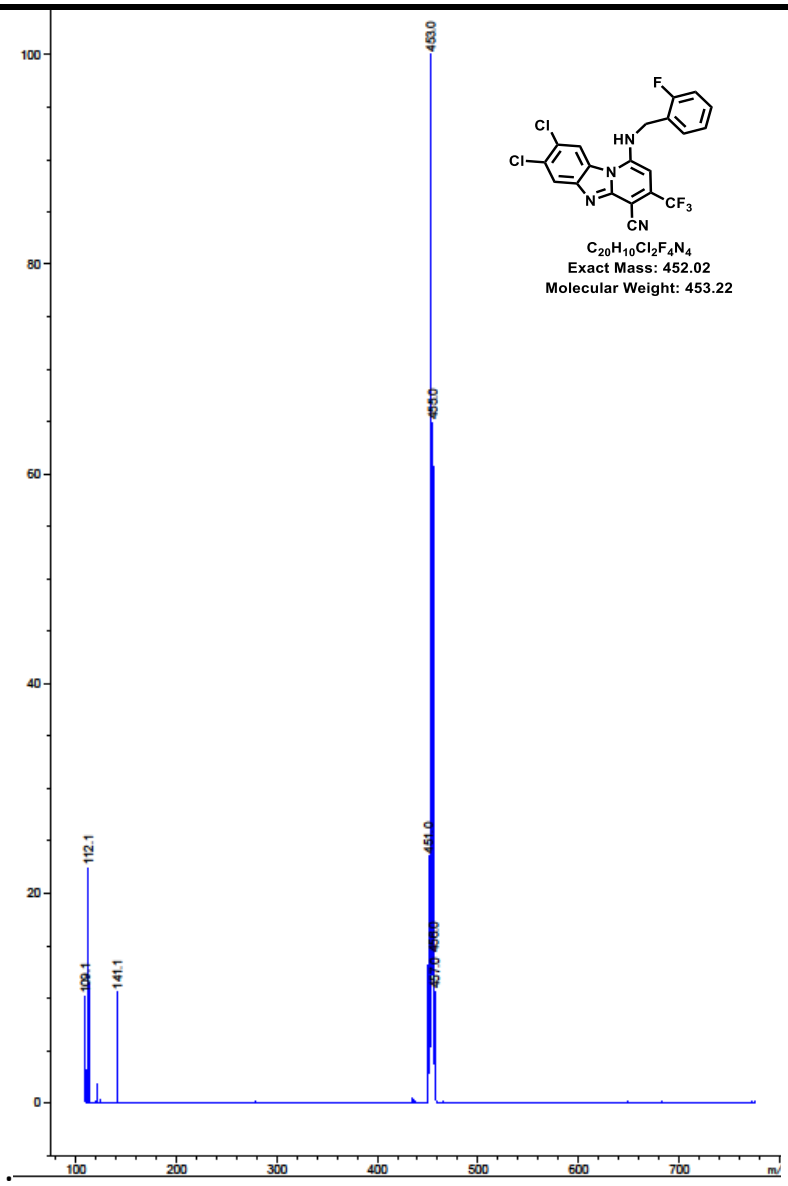

Figure 2.19: *LCMS profile for* ***4i/GMP-75*** *in the positive ionisation mode.*

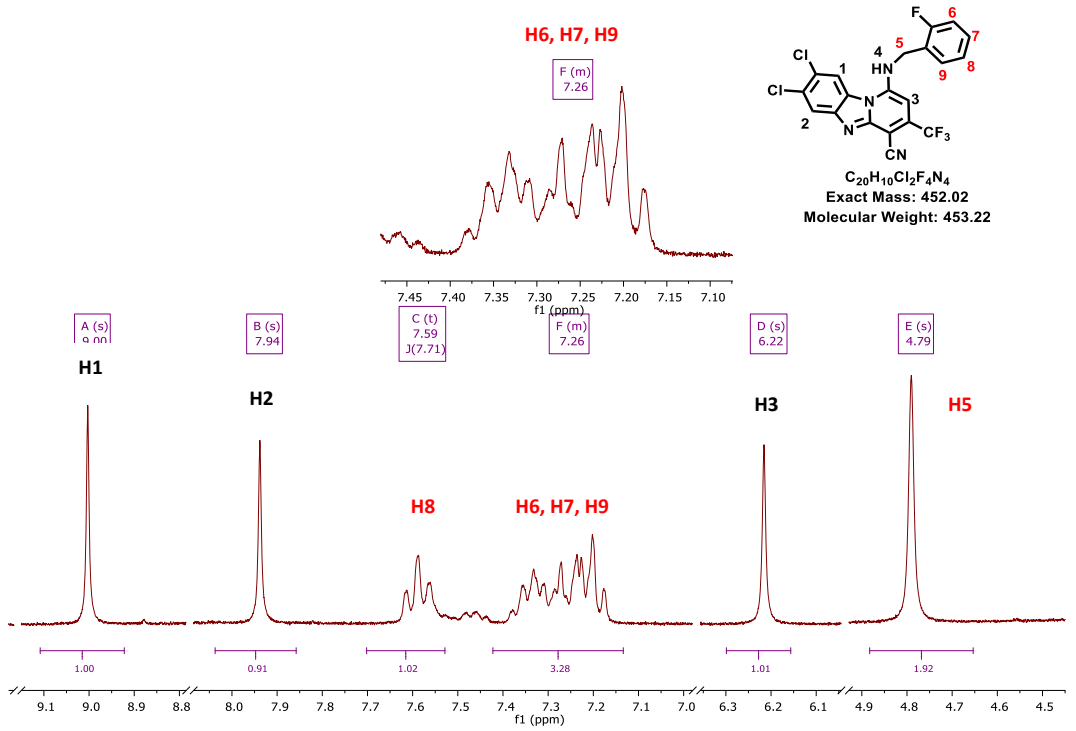

Figure 2.20: *^{1}H NMR spectrum for **4i/GMP-75** in DMSO-d6 with the signals due to the benzylamine side group shown in red.*

2.8.2.6 Cyano-replacement (SAR_3) analogues

The replacement of the nitrile at **SAR_3** with other groups was confirmed as with the other intermediates and targets. In the case where the nitrile was replaced by a hydrogen (**Ve**; **5a/GMP-120**), there was a distinct singlet peak at 7.95 ppm in the proton NMR spectrum, integrating for one proton (**H5**), a feature missing in **1j/GMP-19**, the analogous target with a nitrile at this position (**Figure 2.21**). This ^1H NMR picture corroborated the MS profile for a molecule with the formula $C_{19}H_{11}F_6N_30$ that produced a pseudo molecular ion with the expected m/z of 412.1 in the positive ionisation mode (**Figure 2.21**).

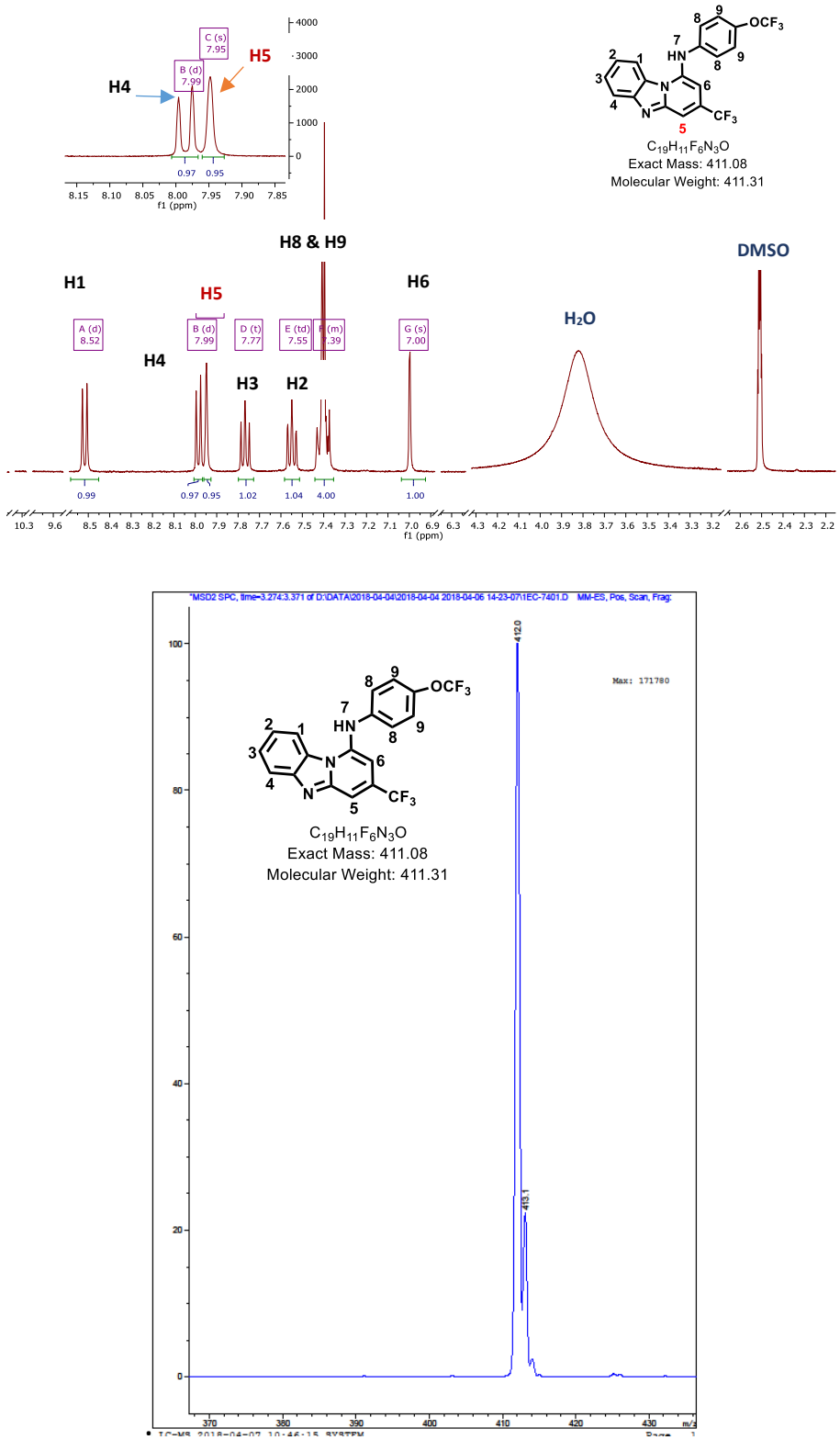

Figure 2.21: *^{1}H NMR (in DMSO-d6) and LCMS spectra (in positive ionisation mode) for* ***5a/GMP-120.***

The conversion of the nitrile in **IVa** to the amide analogue **VI** (step **v**, **Scheme 2.1**) was detected on the LCMS by observing the molecular ion, in the positive ionisation mode, of $[M+H]^+$=314.0. Subsequent amination reactions to give targets in the **Vf** series were judged successful because of both the LCMS and NMR profiles. Using **5b/GMP-128** as an example, the ^1H NMR spectra was characterised by the presence of two singlet peaks that integrated for one proton each at 7.81 and 8.02 ppm, due to the amide hydrogens (**H5**) (**Figure 2.22**). Resonance in the amide group results in the hydrogens attached to the amide nitrogen being magnetically non-equivalent and, therefore, resonate at slightly different frequencies resulting in the disparate chemical shifts. In the ^{13}C NMR, the amide carbon signal, being the most deshielded, is located further downfield at 165 ppm.

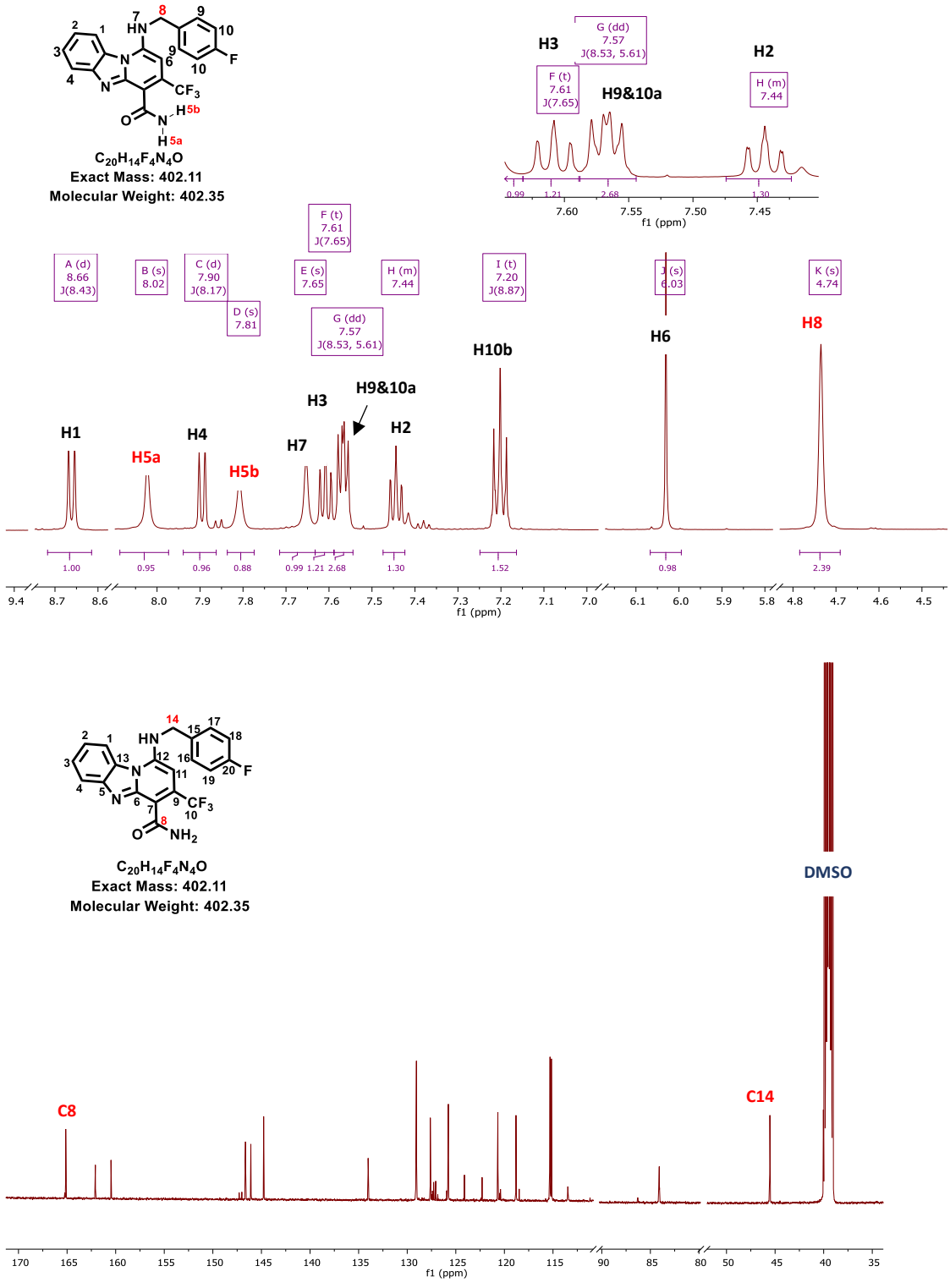

Figure 2.22: *^{1}H and ^{13}C NMR for **5b/GMP-128** in DMSO-d6. Diagnostic peaks are labelled in red with the amide protons assigned arbitrarily as **H5a and H5b.***

In the synthesis of intermediates leading to the target compound with an ester at **SAR_3**, the conspicuous feature on the ^{1}H NMR spectra comprised of an aliphatic singlet signal integrating for three protons due to the ester methyl protons **H5** (**Figure 2.23** and **Figure 2.24**). These protons resonated at ca. 3.9 ppm due to the de-shielding effect of the ester carbonyl group. The accompanying ^{13}C NMR revealed a diagnostic deshielded methyl carbon signal **C9** at ca. 52 ppm and a carbonyl signal **C8** located downfield at ca. 163 ppm because of the ester carbonyl (**Figure 2.23 and Figure 2.24**). Additional proton and carbon peaks, as explained before, were discerned after the reaction between **IVd** and trifluoromethoxy aniline to give the target compound **5e/GMP-120E** (**Figure 2.25**).

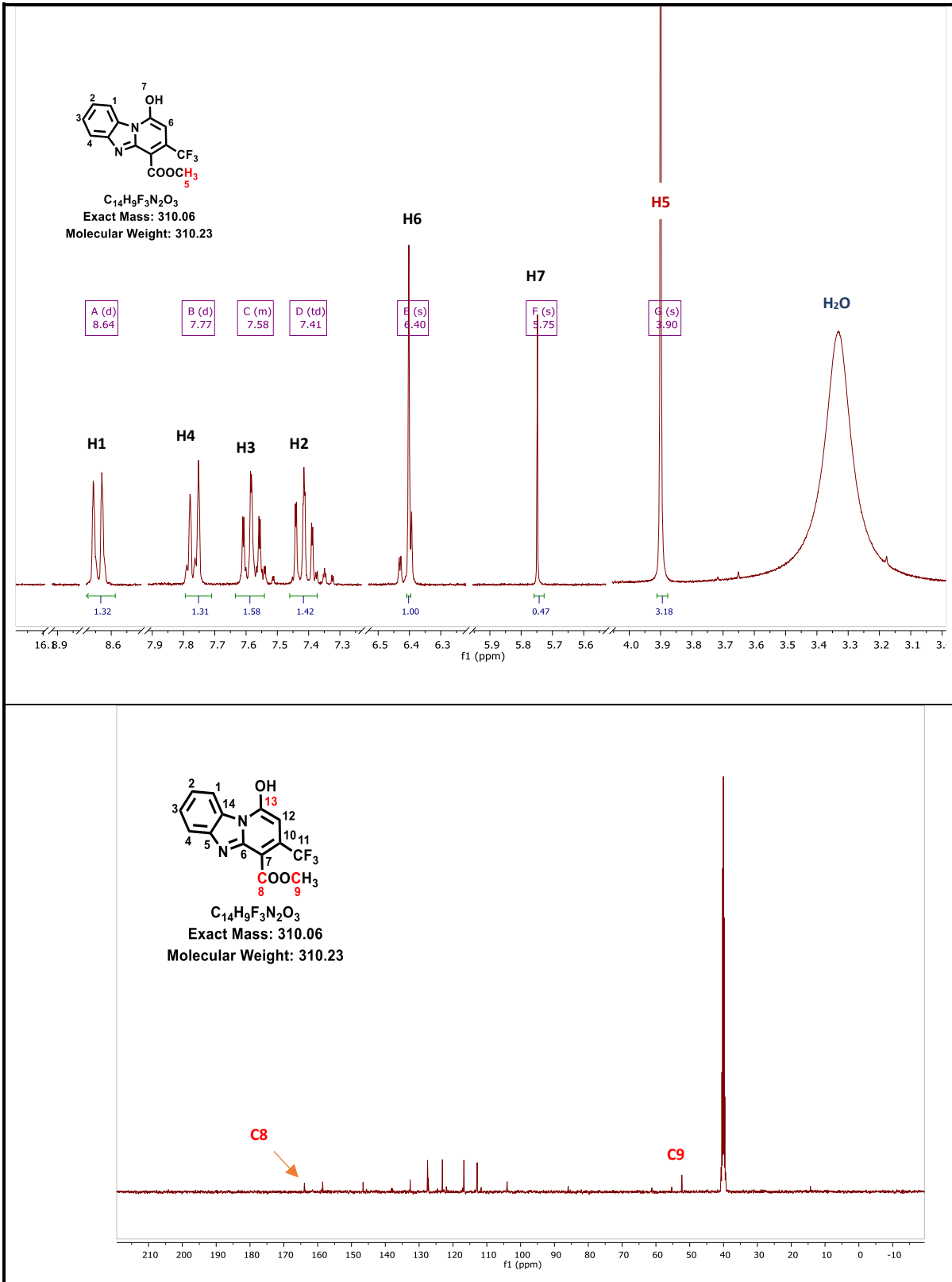

***Figure 2.23**: ^{1}H and ^{13}C NMR spectra for **IIId (GMP-118)** in DMSO-d6 with diagnostic peaks highlighted in red.*

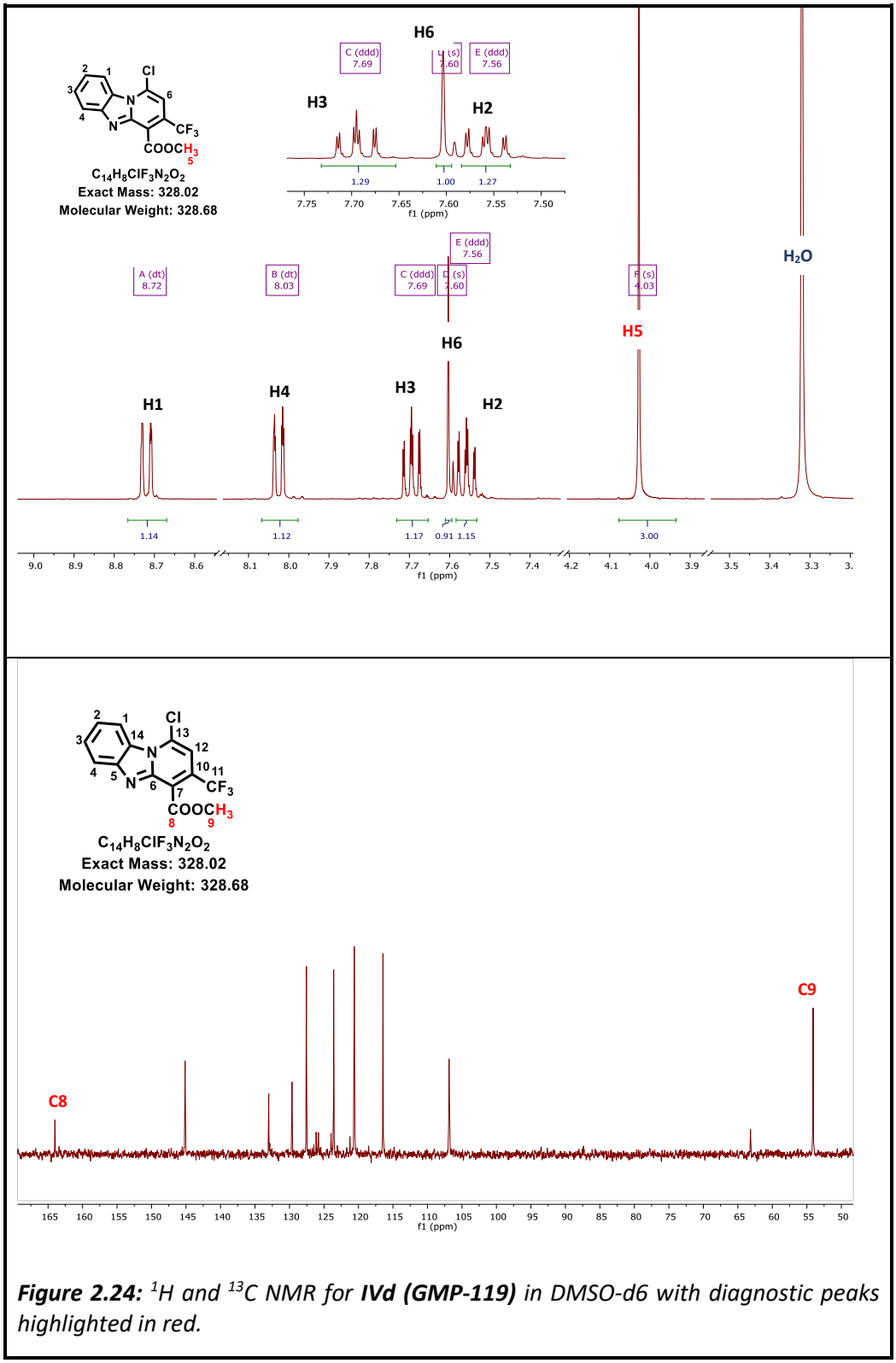

Figure 2.24: *^{1}H and ^{13}C NMR for **IVd (GMP-119)** in DMSO-d6 with diagnostic peaks highlighted in red.*

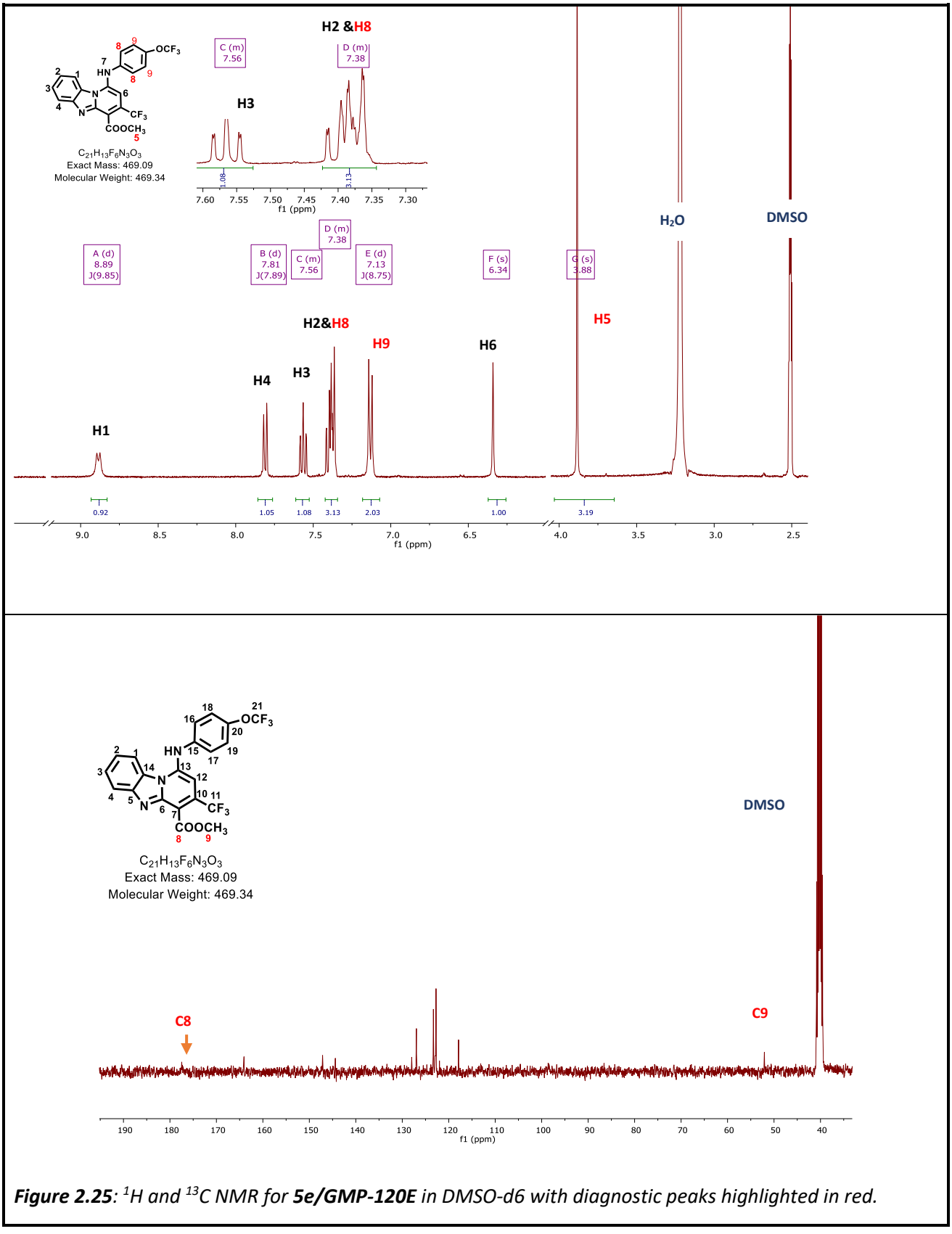

***Figure 2.25**: ^{1}H and ^{13}C NMR for **5e/GMP-120E** in DMSO-d6 with diagnostic peaks highlighted in red.*

2.8.3 Chemical structures and yields of target compounds

Table 2.1: *Compound Number/Codes, chemical structures and yields.*

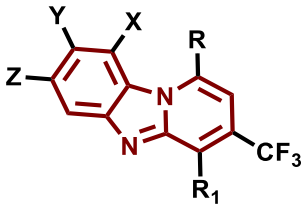

Compound Number/Code		X	Y	Z	R	R_1	[a]Yield (%)
1.	**1a/GMP-06**	H	H	H	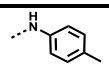	CN	38
2.	**1b/GMP-09**	H	H	H	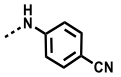	CN	27
3.	**1c/GMP-10**	H	H	H	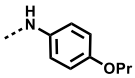	CN	56
4.	**1d/GMP-11**	H	H	H	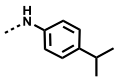	CN	23
5.	**1e/GMP-12**	H	H	H	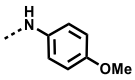	CN	51
6.	**1f/GMP-13**	H	H	H	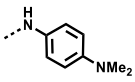	CN	51
7.	**1g/GMP-15**	H	H	H	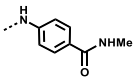	CN	13
8.	**1h/GMP-17**	H	H	H	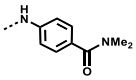	CN	18
9.	**1i/GMP-18**	H	H	H	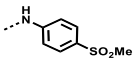	CN	40
10.	**1j/GMP-19**	H	H	H	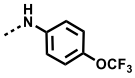	CN	19
11.	**1m/GMP-20**	H	H	H	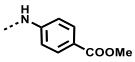	CN	19
12.	**1n/GMP-32**	H	H	H	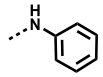	CN	23
13.	**1p/GMP-46**	H	H	H	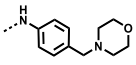	CN	25
14.	**1o/GMP-37**	H	H	H	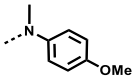	CN	17
15.	**2b/GMP-30**	H	H	H	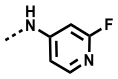	CN	6

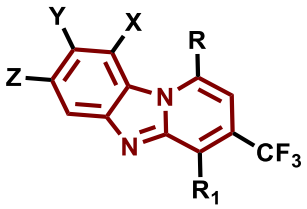

Compound Number/Code		X	Y	Z	R	R_1	[a]Yield (%)
16.	**2d/GMP-57**	H	H	H	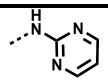	CN	25
17.	**2a/GMP-23**	H	H	H	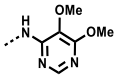	CN	54
18.	**2e/GMP-58**	H	H	H	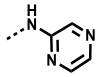	CN	23
19.	**2c/GMP-31**	H	H	H	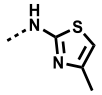	CN	37
20.	**3d/GMP-33**	H	H	H	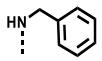	CN	50
21.	**3o/GMP-50**	H	H	H	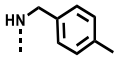	CN	35
22.	**3e/GMP-34**	H	H	H	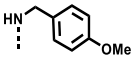	CN	43
23.	**3n/GMP-48**	H	H	H	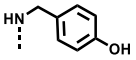	CN	70
24.	**3f/GMP-35**	H	H	H	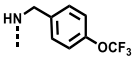	CN	49
25.	**3a/GMP-24**	H	H	H	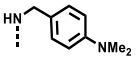	CN	56
26.	**3b/GMP-28**	H	H	H	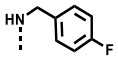	CN	59
27.	**3g/GMP-36**	H	H	H	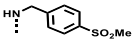	CN	56
28.	**3s/GMP-55**	H	H	H	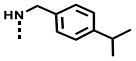	CN	65
29.	**3p/GMP-52**	H	H	H	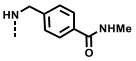	CN	30
30.	**3q/GMP-53**	H	H	H	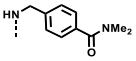	CN	67
31.	**3r/GMP-54**	H	H	H	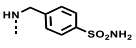	CN	52
32.	**3m/GMP-47**	H	H	H	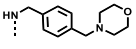	CN	48
33.	**3h/GMP-38**	H	H	H	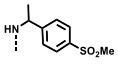	CN	38
34.	**3j/GMP-25**	H	H	H	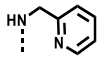	CN	63

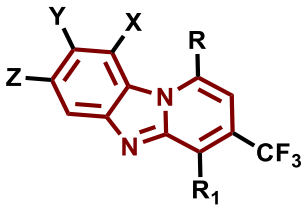

	Compound Number/Code	X	Y	Z	R	R_1	[a]Yield (%)
35.	**3l/GMP-44**	H	H	H	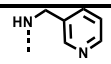	CN	62
36.	**3k/GMP-43**	H	H	H	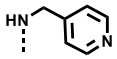	CN	20
37.	**3c/GMP-29**	H	H	H	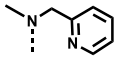	CN	63
38.	**3i/GMP-45**	H	H	H	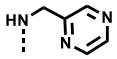	CN	53
39.	**3t/GMP-56**	H	H	H	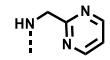	CN	6
40.	**3v/GMP-87**	H	H	H	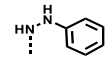	CN	32
41.	**3w/GMP-88**	H	H	H	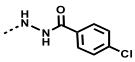	CN	52
42.	**3u/GMP-77**	H	H	H		CN	38
43.	**4k/GMP-81**	H	Cl	Cl		CN	53
44.	**4f/GMP-70**	H	Cl	Cl	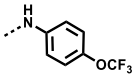	CN	9
45.	**4b/GMP-66**	H	Cl	Cl	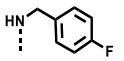	CN	22
46.	**4j/GMP-76**	H	Cl	Cl	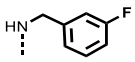	CN	37
47.	**4i/GMP-75**	H	Cl	Cl	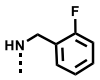	CN	58
48.	**4c/GMP-67**	H	Cl	Cl	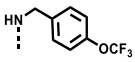	CN	25
49.	**4e/GMP-69**	H	Cl	Cl	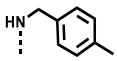	CN	50
50.	**4a/GMP-62**	Cl	H	Cl	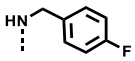	CN	86
51.	**4d/GMP-68**	H	Cl	Cl	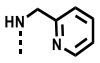	CN	39
52.	**4g/GMP-71**	H	Cl	Cl	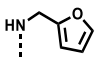	CN	56
53.	**4h/GMP-72**	H	Cl	Cl	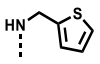	CN	28
54.	**4l/GMP-96**	H	Cl	Cl	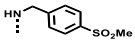	CN	58

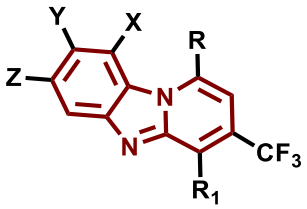

Compound Number/Code		X	Y	Z	R	R_1	[a]Yield (%)
55.	**4m/GMP-97**	H	Cl	Cl	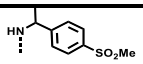	CN	6
56.	**4n/GMP-98**	H	Cl	Cl	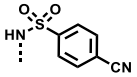	CN	26
57.	**4o/GMP-99**	H	Cl	Cl	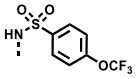	CN	21
58.	**4p/GMP-100**	H	Cl	Cl	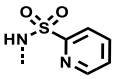	CN	10
59.	**5a/GMP-120**	H	H	H	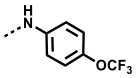	H	8
60.	**5e/GMP-120E**	H	H	H	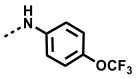	COOMe	19
61.	**1k/GMP-121**	H	H	H	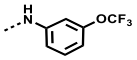	CN	10
62.	**1l/GMP-122**	H	H	H	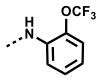	CN	33
63.	**5b/GMP-128**	H	H	H	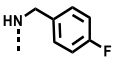	$CONH_2$	35
64.	**5c/GMP-129**	H	H	H	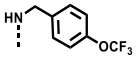	$CONH_2$	20
65.	**5d/GMP-130**	H	H	H	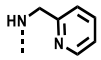	$CONH_2$	76

[a]Yield after isolation and purification of compound.

2.9 Chapter Summary

In this chapter, an account of previously reported antimalarial and antischistosomal activities of PBIs have been described. Initial SAR work on these title compounds and identified liabilities which contribute to the hypothesis, justification and aims of the study, have also been detailed. A rational approach to the medicinal chemistry design, the research program detailing the work flow, have been provided. Using representative intermediates and target compounds, the synthesis and characterisation of the compound library generated have been articulated as were the approaches to circumvent challenges encountered in the synthesis of some of the compounds. Detailed compound-specific synthesis and characterisation have been provided in the experimental information section, **Chapter 7**. The target compounds were then evaluated for pharmacological and physicochemical properties as presented in the subsequent chapters.

2.10 References

(1) Takeshita, H.; Watanabe, J.; Kimura, Y.; Kawakami, K.; Takahashi, H.; Takemura, M.; Kitamura, A.; Someya, K.; Nakajima, R. Novel Pyridobenzimidazole Derivatives Exhibiting Antifungal Activity by the Inhibition of β-1,6-Glucan Synthesis. *Bioorganic Med. Chem. Lett.* **2010**, *20* (13), 3893–3896.

(2) Ramachandran, G. S.; Hameed P. S.; Srivastava, A.; Shanbhag, G.; Morayya, S.; Rautela, N.; Awasthy, D.; Kavanagh, S.; Bharath, S.; Panduga, J. R. V.; Prabhakar, K. R.; Saralaya, R.; Nanduri, R.; Raichurkar, A.; Menasinakai, S.; Achar, V.; Jiménez-Díaz, M. B.; Martínez, M. S.; Angulo-Barturen, I.; Ferrer, S.; Sanz, L. M; Gamo, F.J.; Duffy, S.; Avery, V.M.; Waterson, D.; Lee, M.C.; Coburn-Flynn, O.; Fidock, D. A.; Iyer, P.S.; Narayanan, S.; Hosagrahara, V.; Sambandamurthy, V. K. N - Aryl-2-Aminobenzimidazoles: Novel, Efficacious, Antimalarial Lead Compounds. *J. Med. Chem.* **2014**, *57*, 6642–6652.

(3) Keurulainen, L.; Vahermo, M.; Puente-Felipe, M.; Sandoval-Izquierdo, E.; Crespo-Fernández, B.; Guijarro-López, L.; Huertas-Valentín, L.; de las Heras-Dueña, L.; Leino, T. O.; Siiskonen, A.; Ballell-Pages, L.; Sanz, L. M.; Castañeda-Casado, P.; Jiménez-Díaz, M. B.; Martínez-Martínez, M. S.; Viera, S.; Kiuru, P.; Calderón, F.; Yli-Kauhaluoma, J. A Developability-Focused Optimization Approach Allows Identification of *in vivo* Fast-Acting Antimalarials: N -[3-[(Benzimidazol-2-yl)Amino]Propyl]Amides. *J. Med. Chem.* **2015**, *58* (11), 4573–4580.

(4) Rida, S. M.; El-Hawash, S. A. M.; Fahmy, H. T. Y.; Hazzaa, A. A.; El-Meligy, M. M. M. Synthesis of Novel Benzofuran and Related Benzimidazole Derivatives for Evaluation Of *in vitro* Anti-HIV-1, Anticancer and Antimicrobial Activities. *Arch. Pharm. Res.* **2006**, *29* (10), 826–833.

(5) Camacho, J.; Barazarte, A.; Gamboa, N.; Rodrigues, J.; Rojas, R.; Vaisberg, A.; Gilman, R.; Charris, J. Synthesis and Biological Evaluation of Benzimidazole-5-Carbohydrazide Derivatives as Antimalarial, Cytotoxic and Antitubercular Agents. *Bioorganic Med. Chem.* **2011**, *19*, 2023–2029.

(6) Enumula, S.; Pangal, A.; Gazge, M.; Shaikh, J. A.; Ahmed, K. Diverse Pharmacological

Aspects of Benzimidazole Derivatives : A Review. *Res. J. Chem. Sci.* **2014**, *4* (4), 78–88.

(7) Shaharyar, M.; Mazumder, A.; Garg, R.; Pandey, R. D. Synthesis, Characterization and Pharmacological Screening of Novel Benzimidazole Derivatives. *Arab. J. Chem.* **2011**.

(8) Rida, S. M.; Soliman, F. S. G.; Badawey, E.-S. A. M.; El-Ghazzawi, E.; Kader, O.; Kappe, T. Benzimidazole Condensed Ring Systems. 1 . Syntheses and Biological Investigations of Some Substituted Pyrido[1,2-a]Benzimidazoles. *J. Heterocycl. Chem.* **1988**, *25* (4), 1087–1093.

(9) Kotovskaya, S. K.; Baskakova, Z. M.; Charushin, V. N.; Chupakhin, O. N.; Belanov, E. F.; Bormotov, N. I.; Balakhnin, S. M.; Serova, O. A. Synthesis and Antiviral Activity of Fluorinated Pyrido[1,2-a]Benzimidazoles. *Pharm. Chem. J.* **2005**, *39* (11), 574–578.

(10) Warrier, T.; Kapilashrami, K.; Argyrou, A.; Ioerger, T. R.; Little, D.; Murphy, K. C.; Nandakumar, M.; Park, S.; Gold, B.; Mi, J.; Zhang, T.; Meiler, E.; Rees, M.; Somersan-Karakaya, S.; Porras-De Francisco, E.; Martinez-Hoyos, M.; Burns-Huang, K.; Roberts, J.; Ling, Y.; Rhee, K. Y.; Mendoza-Losana, A.; Luo, M.; Nathan, C. F. N-Methylation of a Bactericidal Compound as a Resistance Mechanism in Mycobacterium Tuberculosis. *Proc. Natl. Acad. Sci.* **2016**, *113* (31), E4523 LP-E4530.

(11) Roemer, T.; Krysan, D. J. Antifungal Drug Development: Challenges, Unmet Clinical Needs, and New Approaches. *Cold Spring Harb. Perspect. Med.* **2014**, *4* (5), a019703–a019703.

(12) Lyons, D. M.; Huttunen, K. M.; Browne, K. A.; Ciccone, A.; Trapani, J. A.; Denny, W. A.; Spicer, J. A. Inhibition of the Cellular Function of Perforin by 1-Amino-2,4-Dicyanopyrido[1,2-a]Benzimidazoles. *Bioorg. Med. Chem.* **2011**, *19* (13), 4091–4100.

(13) Ndakala, A. J.; Gessner, R. K.; Gitari, P. W.; October, N.; White, K. L.; Hudson, A.; Fakorede, F.; Shackleford, D. M.; Kaiser, M.; Yeates, C.; Charman, S. A.; Chibale, K. Antimalarial Pyrido[1,2-a]Benzimidazoles. *J. Med. Chem.* **2011**, *54* (13), 4581–4589.

(14) Singh, K.; Okombo, J.; Brunschwig, C.; Ndubi, F.; Barnard, L.; Wilkinson, C.; Njogu, P. M.; Njoroge, M.; Laing, L.; Machado, M.; Prudêncio, M.; Reader, J.; Botha, M.; Nondaba, S.; Birkholtz, L. -M.; Lauterbach, S.; Churchyard, A.; Coetzer, T. L.; Burrows, J. N.; Yeates,

C.; Denti, P.; Wiesner, L.; Egan, T. J.; Wittlin, S.; Chibale, K. Antimalarial Pyrido[1,2- a]Benzimidazoles: Lead Optimization, Parasite Life Cycle Stage Profile, Mechanistic Evaluation, Killing Kinetics, and *in vivo* Oral Efficacy in a Mouse Model. *J. Med. Chem.* **2017**, *60* (4), 1432–1448.

(15) Okombo, J.; Singh, K.; Mayoka, G.; Ndubi, F.; Barnard, L.; Njogu, P. M.; Njoroge, M.; Gibhard, L.; Brunschwig, C.; Vargas, M.; Keiser, J.; Egan, T. J.; Chibale, K. Antischistosomal Activity of Pyrido[1,2- a]Benzimidazole Derivatives and Correlation with Inhibition of β-Hematin Formation. *ACS Infect. Dis.* **2017**, *3* (6), 411–420.

(16) Ndubi, F. W. Synthesis, Pharmacological and Solubility Evaluation of Antiplasmodial Pyrido[1,2-a]Benzimidazoles with Cyclic and Functionalized Amine Side Chain Substituents., Msc Dissertation; University of Cape Town, 2016.

(17) Urgaonkar, S.; Xu, J. H.; Verkade, J. G. Application of a New Bicyclic Triaminophosphine Ligand in Pd-Catalyzed Buchwald-Hartwig Amination Reactions of Aryl Chlorides, Bromides, and Iodides. *J. Org. Chem.* **2003**, *68* (22), 8416–8423.

(18) Muci, A. R.; Buchwald, S. L. *Practical Palladium Catalysts for C-N and C-O Bond Formation*; 2002.

(19) Hartwig, J. F. Approaches to Catalyst Discovery. New Carbon–heteroatom and Carbon–carbon Bond Formation. *Pure Appl. Chem.* **1999**, *71* (8), 1417–1423.

(20) Driver, M. S.; Hartwig, J. F. A Second-Generation Catalyst for Aryl Halide Amination: Mixed Secondary Amines from Aryl Halides and Primary Amines Catalyzed by (DPPF)PdCl 2. *J. Am. Chem. Soc.* **1996**, *118* (30), 7217–7218.

(21) Rickborn, B.; Jensen, F. R. A-Carbon Isomerization in Amide Dehydrations. *J. Org. Chem.* **1962**, *27*, 4608–4610.

(22) Katritzky, A.; Cai, C.; Meher, N. Efficient Synthesis of 1,5-Disubstituted Tetrazoles. *Synthesis (Stuttg).* **2007**, *2007* (8), 1204–1208.

Chapter 3

Antimalarial Profiling of Pyrido [1,2-*a*] benzimidazoles

3.1 Chapter overview

This chapter will address one of the specific aims of the thesis, which was to evaluate the biological activity of the target compounds with respect to their antimalarial effects. In addition to assessing the potency against the asexual blood stage parasites that are responsible for clinical symptoms, activities against the dormant liver and the transmissible gametocyte stage parasites, will also be presented. Furthermore, the potential for the target compounds to display cross-resistance with standard antimalarials will be evaluated by comparing their potency against both the drug-sensitive (*Pf*NF54) and multidrug-resistant (*Pf*K1) strains of *Plasmodium falciparum*. Towards investigating probable mechanisms of antimalarial action, the ability of the compounds to interfere with the haemoglobin degradation pathway will be discussed. Thereafter, the chapter will also detail the observed *in vitro* ADME profiles of the compounds especially in view of their microsomal metabolic stability and cytotoxicity, including the potential to interact with the myocardial potassium ion channel, hERG. Finally, results from the *in vivo* proof-of-concept antimalarial efficacy, in addition to *in vivo* pharmacokinetics following experimentation in mouse models will be presented.

3.2 *In vitro* asexual blood stage activity against the drug-sensitive *Pf*NF54 strain

Consistent with our outlined workflow, target compounds were first tested for their *in vitro* antiplasmodial activity against the asexual erythrocytic stage parasites responsible for the clinical manifestations of malaria. Initially, the experiments were carried out on the drug sensitive *Pf*NF54 strain either at the Division of Clinical Pharmacology, Department of Medicine, University of Cape Town (UCT) or at the Swiss Tropical and Public Health Institute (STPH), University of Basel, Switzerland, following established procedures.

In summary, at UCT, parasites were incubated with compounds reconstituted to varying concentrations in dimethyl sulfoxide (DMSO) and activity measured by monitoring the activity of the parasites' lactate dehydrogenase (pLDH). LDH is a redox enzyme involved in the last step of anaerobic respiration during glycolysis in which lactate is converted to pyruvate and NAD^+ reduced to NADH.[1,2] When parasite growth is inhibited, the accompanying decrease in metabolic activities, including glycolysis, is reflected in diminished LDH function. Experimentally, the NADH produced in this redox reaction can react with a probe substrate, producing a colour that is detected and quantified spectrophotometrically.[3–5] The readouts are then converted to logarithmic values and plotted against compound concentrations to generate dose-response curves from which compound concentrations resulting in half the maximum inhibition (IC_{50}) are determined.

In the case of *in vitro* antiplasmodial studies carried out at Swiss TPH, the modified [^{3}H]-Hypoxanthine incorporation assay was employed as a measure of parasite viability.[6–8] This assay exploits the fact that *Plasmodium* parasites do not have the capacity for de novo DNA synthesis. Therefore, they obtain bases from external sources in what is referred to as the salvage pathway of DNA synthesis.[9–11] For proliferating parasites, when such purine base precursors such as hypoxanthine are added to the parasite culture, viable cells will utilise them for DNA synthesis. In the hypoxanthine incorporation assay, radiolabelled hypoxanthine is used as the purine source. Consequently, proliferating parasites take up the hypoxanthine, and hence the radioactivity, which is detected and quantified by means of a scintillation counter. This assay is regarded as the gold-standard for measuring the proliferation and inhibition of *Plasmodium* parasites *in vitro*.[5]

As previously described in **Chapter 2**, the medicinal chemistry plan focussed on introducing diversity around the appendages to the PBI core as re-depicted in **Figure 3.1** below. The antiplasmodial data emanating from this work are presented in the subsequent **Tables 3.1-3.3**, stratified into the different SAR modification sites from which prevailing trends were extracted.

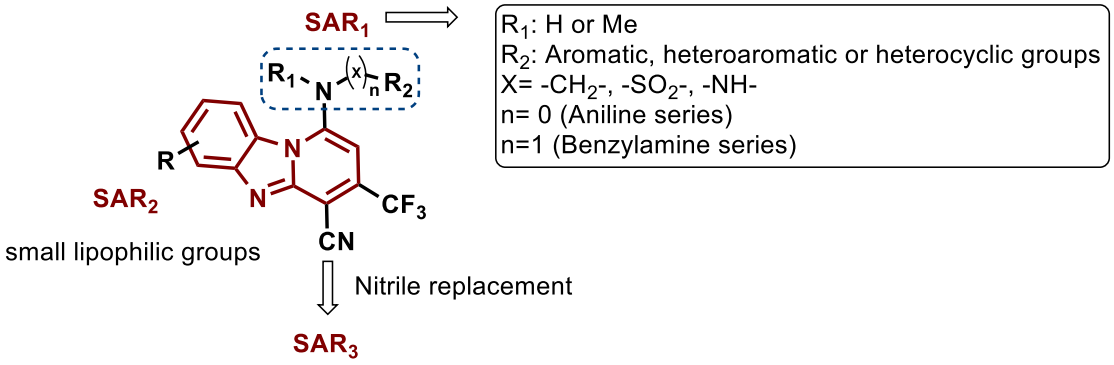

Figure 3.1: *SAR strategy followed in this research.*

3.2.1 SAR_1 Targets

Structural modifications at this site produced compounds that may be classified broadly into either N-linked (n=0; aniline-type) or N-methylene-linked (n=1; benzylamine-type) series (**Figure 3.1**). In the first series, the side group moiety comprises a phenyl ring directly linked to the PBI central core by a nitrogen. The electronic and lipophilic features of substitutions around the aromatic ring influenced the observed antiplasmodial activity. Unlike hydrophilic substituents, lipophilic groups on the aromatic side chains favoured antiplasmodial activity. Active analogues in the low [**1c/GMP-10** (IC_{50}=1.16 µM), **1d/GMP-11** (IC_{50}=1.01 µM), **1j/GMP-19** (IC_{50}=0.17 µM) and **1m/GMP-20** (IC_{50}=1.59 µM)] to moderate [**1a/GMP-06** (IC_{50}=2.14 µM) and **1e/GMP-12** (IC_{50}=2.26 µM)] micromolar range were identified (**Table 3.1**). The most active derivative in the series is **1j/GMP-19** (IC_{50}=0.17 µM) which has a trifluoromethoxy substituent that combines both lipophilic and electron-withdrawing properties.

Table 3.1: *Antiplasmodial (PfNF54) and β-hematin inhibition potency of* ***SAR₁*** *Targets.*

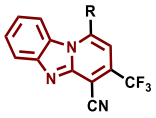

Compound Number/Code	R	[a]*In vitro* activity IC_{50} (µM)	
		PfNF54[b]	BHI
1a/GMP-06	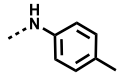	2.14	>100
1b/GMP-09	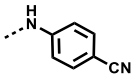	2.36	>100
1c/GMP-10	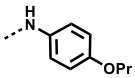	1.16	>100
1d/GMP-11	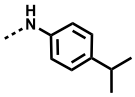	1.01	>100
1e/GMP-12	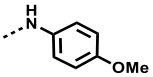	2.26	>100
1f/GMP-13	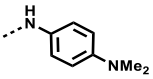	5.62	>100
1g/GMP-15	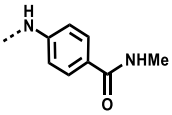	>10	>100
1h/GMP-17	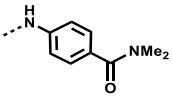	>2.36	>100
1i/GMP-18	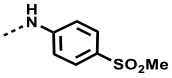	>2.32	>100
1j/GMP-19	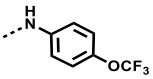	0.17	>100
1k/GMP-121	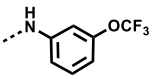	0.39	-

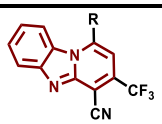

Compound Number/Code	R	[a]*In vitro* activity IC$_{50}$ (µM)	
		PfNF54[b]	BHI
1l/GMP-122	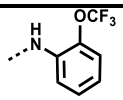	0.87	-
1m/GMP-20	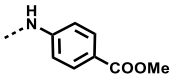	1.59	>100
1n/GMP-32		>2.83	>100
1o/GMP-37	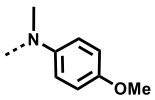	>5	>100
1p/GMP-46	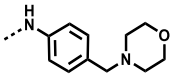	>2.21	50
2a/GMP-23	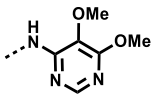	>2.82	>100
2b/GMP-30	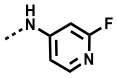	>2.52	>100
2c/GMP-31		>2.82	>100
2d/GMP-57		>2.69	>100
2e/GMP-58		4.42	>100
3a/GMP-24	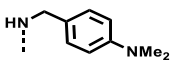	2.98	>100

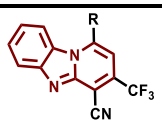

Compound Number/Code	R	[a]*In vitro* activity IC$_{50}$ (µM)	
		PfNF54[b]	BHI
3b/GMP-28	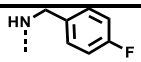	1.27	>100
3c/GMP-29	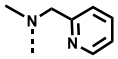	>2.72	>100
3d/GMP-33	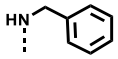	6.11	>100
3e/GMP-34	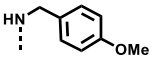	3.18	>100
3f/GMP-35	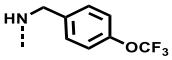	0.92	>100
3g/GMP-36	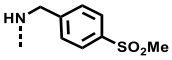	12.58	>100
3h/GMP-38	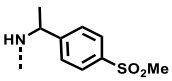	>2.68	>100
3i/GMP-45	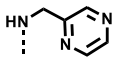	2.60	>100
3j/GMP-25	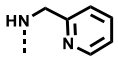	1.16	>100
3k/GMP-43	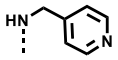	>2.72	>100
3l/GMP-44	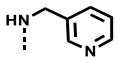	>2.72	>100
3m/GMP-47	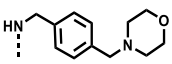	>5	>100
3n/GMP-48	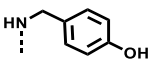	8.74	>100
3o/GMP-50	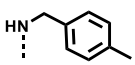	1.49	>100

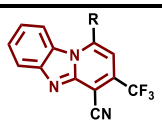

Compound Number/Code	R	[a]*In vitro* activity IC_{50} (µM)	
		PfNF54[b]	BHI
3p/GMP-52	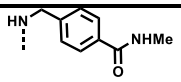	>2.36	>100
3q/GMP-53	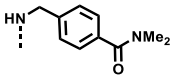	>2.28	>100
3r/GMP-54	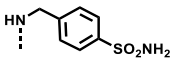	10.20	>100
3s/GMP-55	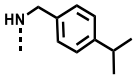	2.40	>100
3t/GMP-56		4.80	>100
3u/GMP-77		10.03	>100

[a]Values are a mean of n≥3 determinations. [b] Chloroquine and artesunate were used as controls whose established standard IC_{50} values from n≥10 determinations in our lab are 0.016 µM and 0.004 µM, respectively.

When a methylene linker (n=1; **Figure 3.1**) was introduced into the side group to extend the **SAR** from aniline-type to benzylamine-type series, some potent analogues were produced, achieving antiplasmodial activity in the low micromolar range: **3b/GMP-28** (IC_{50}=1.28 µM), **3f/GMP-35** (IC_{50}=0.917 µM) and **3o/GMP-50** (IC_{50}=1.49 µM) [**Table 3.1**]. As observed with the aniline-type series, the nature of the substituent on the aromatic ring was crucial with respect to antiplasmodial activity whereby, equally, lipophilic electron-withdrawing groups were favoured**.**

Isosteric replacement of the phenyl ring with various heteroaromatic groups produced diverse compounds including pyridyl (**2b/GMP-30**, **3j/GMP-25**, **3k/GMP-43**, **3l/GMP-44**), pyrimidyl (**2a/GMP-23**, **2d/GMP-57**, **3t/GMP-56**), pyrazinyl (**3i/GMP-45** and **2e/GMP-58**), and thiazolyl (**2c/GMP-31**) [**Table 3.1**]. Among them, only the pyridyl ring in the benzylamine series produced an active compound **3j/GMP-25** (IC_{50}=1.16 µM). Interestingly, there seems to be a stringent requirement with regards to the positioning of the nitrogen on the pyridyl moiety with only the 2 (ortho)-position (**3j/GMP-25**; IC_{50}=1.16 µM) entertained for potent activity while the 3 (*meta*)- and 4 (*para*)- positions produced compounds with lower activities as expressed with compounds **3l/GMP-44** and **3k/GMP-43**, respectively (**Table 3.1**).

The retention of activity upon isosteric replacement of the aromatic side chain provided new chemical space and enhanced the structural diversity in expanding the **SAR** profile of the series. This manipulation was also beneficial to the exploration of structure-property trends arising from analysis of physicochemical profiles of the generated analogues as discussed later in **Chapter 5**. Replacement of the bulky aromatic side groups with the more polar, heterocyclic groups like piperazine was detrimental to activity as seen with **3u/GMP-77** (IC_{50}= 10.03 µM).

When a methyl substituent was introduced on the nitrogen bridging the PBI core and the aromatic appendage (**R_1**, **Figure 3.1**), activity diminished as evident with **3c/GMP-29** (IC_{50} >2.72 µM) that bears a tertiary nitrogen compared to the analogue **3j/GMP-25** (IC_{50} =1.16 µM) in which this nitrogen is secondary. This observation may indicate unfavourable steric orientation in the case of a tertiary nitrogen or that the presence of a hydrogen-bonding centre, in the case of a secondary nitrogen, as in **3j/GMP-25,** are important for suitable interactions with the target leading to the observed biological activity.

3.2.2 SAR_2: Left Hand-side modified targets

Targets arising from structural changes on this portion of the PBI core are as exemplified in **Table 3.2**. Rewardingly, following this modification, there was a general trend towards retention or improvement in potency. For instance, **4d/GMP-68** (IC_{50}= 1.42 µM) is about equipotent to **3j/GMP-25** (IC_{50}= 1.16 µM) while **4c/GMP-67** (IC_{50}= 0.44 µM) and **4e/GMP-69** (IC_{50}= 0.40 µM) are about 2-4-fold as potent as their corresponding analogues, **3f/GMP-35** (IC_{50}= 0.84 µM) and **3o/GMP-50** (IC_{50}= 1.49 µM), respectively, which lack the dichloro modification (**Table 3.2**). Similarly, close to a 5-fold improvement in potency was observed with **4b/GMP-66** (IC_{50}= 0.26 µM), the dichloro substituted analogue of **3b/GMP-28** (IC_{50}= 1.28 µM) [**Table 3.2**].

Table 3.2: *Antiplasmodial (PfNF54) and β-hematin inhibition potency of* ***SAR₂*** *Targets.*

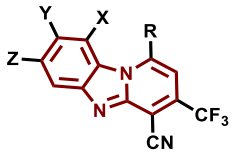

Compound Number/Code	X	Y	Z	R	[a]*In vitro* activity IC$_{50}$ (µM)	
					PfNF54[b]	BHI
4a/GMP-62	Cl	H	Cl	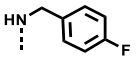	0.31	>100
4b/GMP-66	H	Cl	Cl	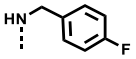	0.44	>100
4c/GMP-67	H	Cl	Cl	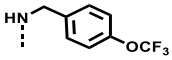	0.44	>100
4d/GMP-68	H	Cl	Cl	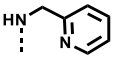	1.42	59
4e/GMP-69	H	Cl	Cl	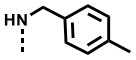	0.40	>100
4f/GMP-70	H	Cl	Cl	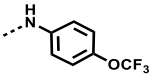	>1.97	32
4g/GMP-71	H	Cl	Cl		0.44	>100
4h/GMP-72	H	Cl	Cl		0.31	>100
4i/GMP-75	H	Cl	Cl	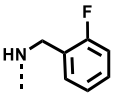	0.17	139
4j/GMP-76	H	Cl	Cl	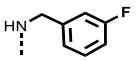	0.19	>100
4k/GMP-81	H	Cl	Cl		8.11	>100
4l/GMP-96	H	Cl	Cl	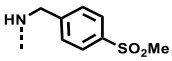	5.34	>100
4m/GMP-97	H	Cl	Cl	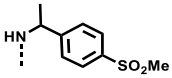	4.97	32
4n/GMP-98	H	Cl	Cl	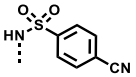	5.64	>100
4o/GMP-99	H	Cl	Cl	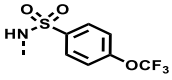	6.73	78

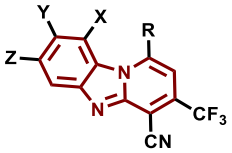

Compound Number/Code	X	Y	Z	R	[a]*In vitro* activity IC_{50} (µM)	
					PfNF54[b]	BHI
4p/GMP-100	H	Cl	Cl	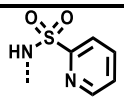	>6	>100

[a]Values are a mean of n≥3 determinations. [b] Chloroquine and artesunate were used as controls whose established standard *PfNF54* IC_{50} values from n≥10 determinations in our lab are 0.016 µM and 0.004 µM, respectively.

Further SAR iterations within this series revealed that the phenyl ring at **SAR_1** (**Figure 3.1**) could be replaced with smaller heteroaromatic systems such as furanyl **4g/GMP-71** (IC_{50}= 0.44 µM) and thiofuranyl **4h/GMP-72** (IC_{50}= 0.31 µM) with retention of activity when accompanied by changes on the LHS. However, replacement of the bulky aromatic side groups with the more polar, heterocyclic groups like piperazine, resulted in diminished activity as seen with **4k/GMP-81** (IC_{50}= 8.11 µM). Among analogues in which the methylene linker (n=1, **SAR_1**, **Figure 3.1**) is substituted by the more polar sulfonyl group (-SO_2-), poor antiplasmodial activity was observed as with **4o/GMP-99** (IC_{50}= 6.73 µM) vs **3f/GMP-35** (IC_{50}= 0.92 µM), respectively (**Table 3.2**).

When comparing the position of the chloro groups on the LHS of the scaffold, the 3,5- dichloro analogue **4a/GMP-62** (IC_{50}= 0.21 µM) and the 4,5-dichloro compound **4b/GMP-66** (IC_{50}= 0.26 µM) were equipotent indicating the negligible impact of regio-isomerism on this portion of the scaffold. On the contrary, regio-isomerism appears to be more crucial in the side groups at **SAR_1**. For example, moving the position of the substituents on the aromatic side group between *ortho*, *meta* and *para* positions resulted in **4j/GMP-76** (*meta*, IC_{50}= 0.19 µM) and **4i/GMP-75** (*ortho*, IC_{50}= 0.17 µM) being equipotent and about twice as potent as analogue **4b/GMP-66** (*para*, IC_{50}= 0.44 µM) [**Table 3.2**].

3.2.3 SAR_3 Targets

To explore effects on antiplasmodial activity by initiating structural changes around **SAR_3** (**Figure 3.1**), analogues of previously active targets were prepared in which the nitrile at this position was replaced with other small groups. Effectively, this modification resulted in compounds **5a/GMP-120** (H; IC_{50}= 4.24 µM), **5b/GMP-128**, ($CONH_2$; IC_{50} > 6 µM), **5c/GMP-129** ($CONH_2$, IC_{50}= 5.16 µM), **5d/GMP-130** ($CONH_2$, IC_{50} >10 µM) and **5e/GMP-120E** (COOMe, IC_{50}= 5.52 µM) [**Table 3.3**]. Realising a drastic drop in antiplasmodial potency, it was conjectured that a nitrile group at this site provides optimal activity.

Table 3.3: *Antiplasmodium (PfNF54) potency of* ***SAR₃*** *Targets.*

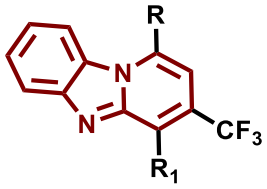

Compound Number/Code	R_1	R	[a,b]*In vitro* activity IC_{50} (µM) *PfNF54*
5a/GMP-120	H	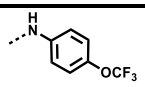	4.24
5b/GMP-128		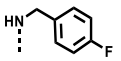	>6
5c/GMP-129		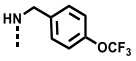	5.16
5d/GMP-130			>10
5e/GMP-120E	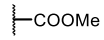	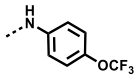	5.52

[a]Values are a mean of n≥3 determinations. [b] Chloroquine and artesunate were used as controls whose established standard *PfNF54* IC_{50} values from n≥10 determinations in our lab are 0.016 µM and 0.004 µM, respectively.

3.3 *In vitro* asexual blood stage activity against the multidrug-resistant *PfK1* strain

Antimalarial drug discovery projects aim to identify compounds with not only good potency against the sensitive strains of *Plasmodium* but also possessing activity against drug-resistant parasite strains. The preference is towards advancing a new antimalarial lead possessing chemical novelty and which is differentiated in its mechanism of action and that is not cross-resistant with current drugs.

Consequently, compounds with potent activity in the chloroquine sensitive (CQS) *Pf*NF54 strain ($IC_{50} \leq 1\mu M$), were also tested against the multi-drug resistant (CQR) *Pf*K1 strain. An assessment for the potential to manifest cross-resistance with chloroquine was performed by determining the fold change in the IC_{50} between drug-sensitive and drug-resistant strains, expressed as the resistance index (RI), calculated as the ratio of IC_{50}*Pf*K1 to IC_{50}*Pf*NF54. This assay was carried out at the Swiss TPH, using the modified [^{3}H]-Hypoxanthine incorporation assay described earlier.

Generally, activity trends were maintained across the strains whereby potent compounds retained their potency while inactive compounds in the CQS *Pf*NF54 strain also showed inactivity in the CQR *Pf*K1 strain (**Table 3.4**). These results, therefore, suggest that these compounds are unlikely to demonstrate cross-resistance with chloroquine as indicated by a less than 2-fold IC_{50} potency shift between the CQS and CQR parasite strains.

Table 3.4: *In vitro activities of frontrunner compounds against drug sensitive (PfNF54) and resistant (PfK1) asexual blood stage parasites.*

Compound number/code	Chemical structure	[a]Asexual blood stage IC_{50} (µM)		Resistance Index
		PfNF54	*PfK1*	*PfK1*IC_{50}: *PfNF54*IC_{50}
1j/GMP-19	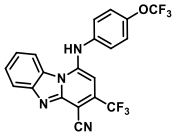	0.17	0.15	0.88
1k/GMP-121	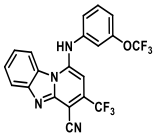	0.40	0.23	0.58
1l/GMP-122	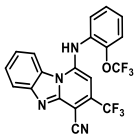	0.87	0.62	0.71
3b/GMP-28	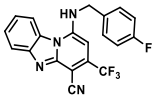	1.28	1.70	1.33
3f/GMP-35	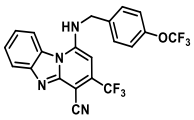	0.92	0.84	0.91
3j/GMP-25	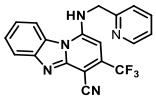	1.16	1.64	1.41
4a/GMP-62	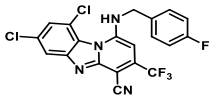	0.31	0.21	0.68
4b/GMP-66	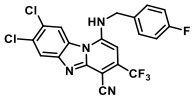	0.44	0.28	0.64
4c/GMP-67	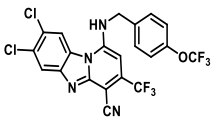	0.44	-	-
4d/GMP-68	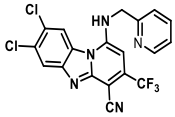	1.42	-	-

Compound number/code	Chemical structure	[a]Asexual blood stage IC_{50} (µM)		Resistance Index
		PfNF54	*PfK1*	*PfK1*IC_{50}: *PfNF54*IC_{50}
4e/GMP-69	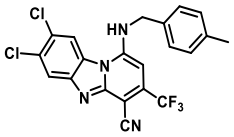	0.4	-	-
4g/GMP-71	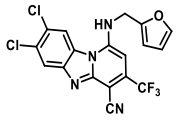	0.44	0.23	0.52
4h/GMP-72	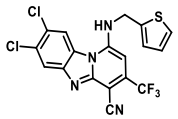	0.31	0.19	0.61
4i/GMP-75	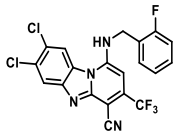	0.17	0.14	0.82
4j/GMP-76	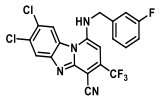	0.19	0.15	0.79
4l/GMP-96	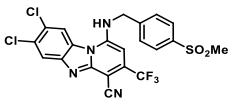	5.34	5.61	1.05
4o/GMP-99	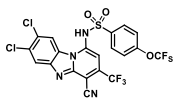	6.73	5.85	0.87
5a/GMP-120	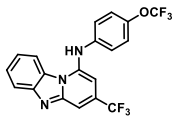	4.24	3.36	0.79
5c/GMP-129	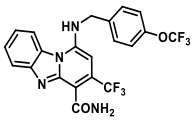	5.16	7.59	1.47
5d/GMP-130	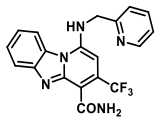	>10	>10	-
	Chloroquine	0.016	0.194	12
	Artesunate	0.004	0.003	0.75

[a]Activity determined using the [^{3}H]-Hypoxanthine incorporation assay and values are a mean of n≥3 determinations.

The resistance to chloroquine arises due to a mutation in the parasite membrane protein referred to as *Plasmodium falciparum* chloroquine resistance transporter, *Pf*CRT, responsible for the influx of chloroquine into the food vacuole of the parasite.[12–14] Subsequently, this mutation results in decreased intracellular accumulation of the drug hence reducing access to the site of action. From the observed activity against *Pf*K1 strain, PBIs obtained in this study may therefore not be substrates for the *Pf*CRT protein. Effectively, the demonstrated antiplasmodial activity may be presumed to arise through the ability of the compounds to gain access to the parasite and inflicting parasiticidal effects via different and, possibly, novel mechanisms.

3.4 Probing the mechanism of action

The library of compounds generated, being endowed with features present in standard antimalarial drugs like the quinolines which target the haemoglobin degradation process, were evaluated for their ability to inhibit beta hematin (BH) formation, an *in vitro* mimic of the *in vivo* hemozoin formation process.[15–17] The conversion of free soluble toxic heme *in vivo* to the insoluble inert hemozoin is promoted by several factors, including neutral lipids. Heme can be chemically synthesised and the formation of hemozoin mimicked *in vitro*.[18–21] The potential for small molecules to inhibit hemozoin formation can therefore be examined *in vitro* by measuring the inhibition of the formation of beta-hematin (the surrogate of hemozoin) from hematin (the *in vitro* analogue of heme), under optimised experimental conditions that mirror physiological conditions.

Besides possessing a planar architecture imparted by the PBI central core, the studied compounds have a rich electron density and protonatable centres. Planarity is a key feature facilitating interactions between heme molecules and the inhibitors of the hemozoin formation process. Moreover, the high electron density further augments binding of inhibitors to heme via by π-π hydrophobic interactions.[22] On the other hand, the existence of protonatable sites makes it feasible for compounds to accumulate in the acidic digestive food vacuole of the parasite due to a pH gradient.[23]

The protonated compound within the acidic food vacuole of the parasite has reduced permeability compared to the neutral, uncharged compound in the physiological pH outside the digestive vacuole and hence will not readily diffuse out of the parasite lysosome. Additional coordinate interactions between inhibitor molecules and heme are feasible via oppositely charged centres.[24,25]

The BH inhibition evaluation for target compounds was, therefore, conducted using established procedures in our lab.[15] Briefly, compounds were reconstituted in DMSO to yield a 20mM stock concentration from which serial dilutions were prepared. Next, the NP40 detergent was used to mediate BH formation in a preparation mix containing predetermined compound concentrations, hematin solution, buffer and pyridine solution. The inhibition of the formation of the beta-hematin was evaluated spectrophotometrically by observing the optical density of the complex formed between hematin and pyridine which observes the beer-lambert's law.[26,27] Hematin converted to BH is optically inactive. Consequently, a higher absorbance reading reflects greater inhibition of the BH formation process and hence greater compound potency. Control experiments using chloroquine, an established inhibitor of this pathway and the non-inhibitor drug pyrimethamine, were performed in addition to a blank in which no test compound was included. Concentrations resulting in 50% inhibitory effects were subsequently determined from constructed concentration-response curves. Resulting from this assay, compounds with an IC_{50} above 100 µM were classified as poor BH formation inhibitors.

Most of the compounds had weak BHI activity (IC_{50} > 100 µM) **Tables 3.1 and 3.2**. Only six compounds: **1p/GMP-46** (IC_{50}=50 µM); **4d/GMP-68** (IC_{50}=59 µM); **4f/GMP-70** (IC_{50}=32 µM); **4i/GMP-75** (IC_{50}=139 µM); **4m/GMP-97** (IC_{50}=32 µM) and **4o/GMP-99** (IC_{50}=78 µM) demonstrated BHI activity in the desired range (IC50 < 100 µM), with **4f/GMP-70** and **4m/GMP-97** displaying greatest potencies (IC_{50}=32 µM).

The dichloro substitution on the LHS improved the BHI potency **4m/GMP-97** (IC_{50}=32 µM) of the previously inactive **3h/GMP-38** (IC_{50}>100 µM) analogue, a pattern observed with **4d/GMP-68** (IC_{50}=59 µM) vs **3j/GMP-25** (IC_{50}>100 µM). A sulfonyl linker (X= -SO_2-, **Figure 3.1**, **SAR_1**) between the nitrogen attached to the PBI core and the aromatic portion of the side chain in the stead of a methylene group was detrimental to the potential to disrupt BH formation as in the case of **4p/GMP-100** (IC_{50}>100 µM) vs **4d/GMP-68** (IC_{50}=59 µM). Interestingly, the chiral compound **4m/GMP-97** (IC_{50}=32 µM) was more potent than its achiral analogue **4l/GMP-96** (IC_{50}>100 µM). Noteworthy, there is no obvious correlation between antiplasmodial activity and the ability of these compounds to inhibit BH formation (**Figure 3.2**).

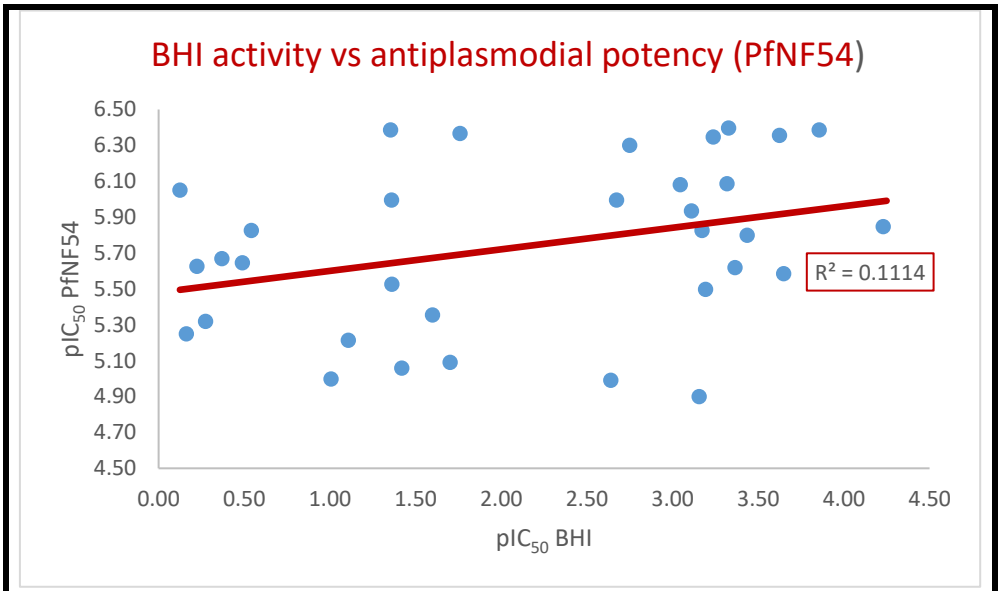

Figure 3.2: *Relationship between BHI and antiplasmodial potency; both are plotted as -log IC_{50} (pIC_{50}), µM.*

Several compounds weakly active in the BHI assay showed potent antiplasmodial activity (for example, **1j/GMP-19**: *Pf*NF54IC_{50}=0.17µM; BHIAIC_{50} >100 µM, **Table 3.1**) whereas some with good BHI activity also displayed good antiplasmodial potency (as with **4d/GMP-68:** *Pf*NF54IC_{50}=1.42 µM; BHIAIC_{50}=59 µM, **Table 3.2**). Whereas the planar architecture of these compounds would be expected to impart BHI capabilities as observed with analogous targets[15,28], it appears that the structural diversity pursued in this study introduced features that distorted the ability for appropriate binding to heme, hence the low BHI activities for most of the compounds. Nonetheless, owing to the presence of protonatable centres on these molecules, it is imaginable that intracellular uptake might occur to sufficient concentrations that may achieve meaningful inhibition of the haemoglobin degradation process which occurs largely in the digestive food vacuole of the parasite. This possibility is not recapitulated in the *in vitro* conditions of the assay.

Overall, with reference to the foregoing observations, it is conceivable that these compounds elicit antiplasmodial potency via a hemozoin independent mechanism of action or that other mechanisms, in addition to hemozoin formation inhibition, may be involved. To confidently establish the role of BHI as a contributing mechanism, the BH fractionation assay will be necessary.[28] In this evaluation, a decrease in the amount of BH accompanied by an increase in the fraction of hematin with increased compound concentrations is diagnostic for a true BH formation inhibitor.

3.5 Evaluation of liver and gametocyte stage activity

3.5.1 Introduction

In pursuing the specific aim of evaluating the stage-specificity and multi-stage antiplasmodial activity of derived compounds, selected compounds having good asexual blood stage activity ($IC_{50} \leq 1\mu M$) were tested against gametocytes and liver forms of *Plasmodium* parasites. The liver stage assays were performed at the *Instituto de Medicina Molecular, Faculdade de Medicina, Universidade de Lisboa, in Lisboa, Portugal*. On the other hand, the gametocyte assays were performed jointly at the Wits Research Institute for Malaria, University of the Witswatersrand (Wits) and the Department of Biochemistry, Institute of Sustainable Malaria Control, University of Pretoria (UP), South Africa. Two independent assay methods were applied for these gametocyte assays with the ATP-based and Luciferase line reporter-based platforms performed at Wits and UP, respectively.

Regarding the liver stage assay, a luciferase-expressing *Plasmodium berghei* line, *Pb*GFP-Luccon, was used to infect a human hepatoma cell line (HuH 7) and parasite viability, after incubation with test compounds, determined by luminescence readings using a luciferase assay kit.[29] Accordingly, lower luminescence reflect fewer number of viable parasites and hence greater potency of the test compound.

Concerning the assessment of the gametocytocidal activity of the selected compounds, the gametocytes were produced using the approach adopted from Carter[30] whereby nutritional restrictions and reduction of haematocrit were used to induce gametocytogenesis of the asexual *PfNF54* parasites. As mentioned earlier, and to facilitate accurate, sensitive and quantitative measurements of the gametocytocidal effects of test compounds, both the luciferase reporter and ATP-based assays were employed. Using these dual platforms, which target different metabolic processes, increases the chances of identifying active compounds in a chemically diverse data set.[2]

Briefly, the luciferase assay depends on the observations and recording of luminescence when a luciferin substrate is added to a parasite containing or expressing the luciferase enzyme. In this case, the *PfNF54* engineered to express the enzyme GFP-Luciferase according to the work by Lucantoni and co-workers was used.[31]

For specific early gametocyte stage detection, NF54-PfS16-GFP-Luc was used whereas NF54-Mal8p1.16-GFP-Luc was utilised for the late gametocyte stage.

In the ATP-based assay, the ability of the compounds to inhibit gametocyte growth was detected by monitoring changes in energy production by measuring ATP levels in a bioluminescent-based detection assay.[32] Since gametocytes display differential susceptibilities to drugs in the early vs. late stages of development,[33,34] the compounds were evaluated against these two stages. Stage specific action was determined by testing compounds against the parasite load established to be predominantly (>90%) early or late stage. Stage specificity towards either early or late gametocytes was determined by comparing the fold-change in the IC_{50} between the two stages whereby a ratio higher than 2 was interpreted to imply differential susceptibility.

All the compounds tested were active in both the liver and gametocyte stages of the *Plasmodium* parasite, in addition to the earlier observed blood stage activity (**Table 3.5**).

Table 3.5: *Liver and gametocyte stage activity of selected compounds.*[a]

Compound	*Pb* Liver stage IC_{50}	Luciferase reporter assay						ATP-based assay		Final Late Stage IC_{50}	IC_{50} Fold Change [b](EG:LG/ LG:EG)
		% mortality Early stage		IC_{50} Early stage	%mortality Late stage		IC_{50} Late stage	%mortality Late stage			
Assay conc.(µM)		1	5		1	5		1	5		
1j/GMP-19	0.11									3.32	
3b/GMP-28	0.89										
3f/GMP-35	0.48	7	18		1	0		0	0		
4a/GMP-62	1-10[c]	11	55	5.51	28	76	1.87	44	89	0.74	3.0/0.3
4b/GMP-66		15	46		81	91	5.73	44	89	0.69	
4c/GMP-67	0.19	15	64	11.91	13	22		88	89	0.21	
4d/GMP-68		3	17		22	64	6.80	5	61	2.48	
4e/GMP-69		23	54	1.06	12	54	6.32	61	89	0.60	0.2/6.0
4g/GMP-71	0.06	1	44		15	9		19	79	2	
4h/GMP-72	0.14	26	49		0	0		21	80	1.67	
4i/GMP-75	0.05	0	20		0	65	2.21	71	89	0.37	
4j/GMP-76	0.07	0	51	2.49	0	80	1.21	80	89	0.27	1.2/0.5
Primaquine	6.25										
Methylene blue				0.195			*0.143			[#]0.9	
DHA				0.043			*0.011			14	
MMV390048				0.214			0.14				

[a]Values are the average of n≥3 determinations. [b]EG: Early stage gametocyte; LG: Late stage gametocytes. [c]Estimated IC_{50} range based on primary activity screening. Value based on *luciferase and [#]ATP assay.

3.5.2 Liver stage activity

The complete set of compounds tested (**Table 3.5**) demonstrated *in vitro* sub-micromolar liver stage activity with potency greater than that observed for primaquine (IC_{50}=6.25 µM), the control drug used in this assay. With tafenoquine having received US FDA approval only recently, primaquine is presently the only clinical compound widely used for radical cure of *Plasmodium vivax* and *ovale*-induced malaria.[19] Despite the low *in vitro* activity observed with primaquine, the drug displays potent *in vivo* activity alluded to its biotransformation to the active metabolite.[37] An accurate extrapolation of the *in vivo* potency of these compounds is therefore not possible based on direct comparisons with primaquine but will, rather, require animal experimentation in a model recapitulating the liver stage infection. The bioactivation of primaquine has been demonstrated to be dependent on the CYP 2D6 enzyme which is polymorphic with up to half of the population being intermediate to poor metabolisers, a scenario that attracts caution in the use of primaquine in mass drug administration during malaria elimination campaigns.[37,38]

3.5.3 Gametocyte activity

Using the luciferase reporter assay at an initial compound screening concentration of 5 µM against early stage gametocytes, four compounds (**4a/GMP-62**, **4c**/**GMP-67**, **4e/GMP-69** and **4j/GMP-76**) achieved parasite mortality greater than 50%. At the lower concentration of 1 µM, only two compounds (**4e/GMP-69** and **4h/GMP-72**) resulted in ≥ 20% parasite death (**Table 3.5**). On examining the potency against the late stage gametocyte based on the luciferase reporter assay, six compounds induced a mortality of ≥50% at 5 µM while three compounds showed ≥20% mortality at 1 µM. In contrast, the ATP-based assay generally showed higher compound activity against the late stage gametocytes in comparison to the luciferase-based platform, with the exceptions of **4b/GMP-66** and **4d/GMP-68** at 1 µM for which the luciferase platform gave higher potency (**Table 3.5**).

The two assays employed to test for gametocytocidal activities of target molecules allow for the interrogation of different biochemical and metabolic pathways in the parasite and is a likely contributing reason for the discordant results observed between the assays. Notably, considering effects on late stage gametocytes, compound **4b/GMP-66** showed good activity only on the luciferase platform whereas **4c/GMP-67**, **4e/GMP-69**, **4i/GMP-75** and **4j/GMP-76** demonstrated good activity only on the ATP-based platform. Regardless of the platform, **4a/GMP-62**, **4d/GMP-68**, **4g/GMP-71** and **4h/GMP-72** produced moderate activity.

For compounds predicted, based on the initial screening at 1 and 5 µM to have IC_{50} values below 1 µM, full IC_{50} determinations were performed using three biological replicates, each carried out as technical triplicates. Conversely, those compounds estimated to be moderately potent (IC_{50} between 1-5 µM), were progressed for a single IC_{50} determination performed as a single biological assay in technical triplicates.

From these studies, two compounds, **4b/GMP-66** and **4j/GMP-76** achieved higher activity in the late gametocyte stage compared to the early forms of gametocytes. On the contrary, **4e/GMP-69** displayed greater potency towards the early gametocytes compared to the late gametocyte stage. The early and late gametocyte stages are distinct from morphological and biochemical perspectives. It is therefore possible for certain cellular and molecular pathways to be targeted by drugs in one stage and yet be either absent or incompletely developed in the other stage leading to the observed differential susceptibility.

With regards to transmission-blocking antimalarial properties, primaquine and the artemisinin-derived drugs artemether and artesunate, are the only clinically useful antimalarial drugs with demonstrable gametocytocidal activity and the WHO recommends use of Primaquine at a dose of 0.25mg/kg for targeting gametocytes.[39–41] Unfortunately, resistance towards artemisinins and the deficiency of the enzyme Glucose-6-phosphate dehydrogenase (G6PDH) important in primaquine metabolism, whose deficiency predisposes to potentially fatal haemolysis, raise concerns in the use of these agents and agitate for the discovery of novel, safe and efficacious antimalarial agents capable of targeting these sexual forms of *Plasmodium*.[2]

Taken together, in view of the sub-micromolar potency of these compounds across the life cycle stages, these PBI derivatives are promising leads towards the identification of pan-active agents capable of preventing transmission and enabling chemoprevention. From the current antimalarial arsenal, over 90% of the drugs do not show potent activity towards late stage gametocytes and only primaquine and atovaquone have liver stage activities.[42]

3.6 Profiling for *in vitro* cytotoxicity and microsomal metabolic stability

3.6.1 Cytotoxicity against CHO cell line

To guide selection of compounds for *in vivo* assays, compounds with the most potent *in vitro* antiplasmodial activity were prioritised to be evaluated for their cytotoxicity profile in the Chinese Hamster Ovarian cell line. Based on these studies, structure-cytotoxicity trends were delineated (**Table 3.6**). Cytotoxicity assessment allows for the determination of the risk for cellular toxicity by comparing the concentration required to elicit the desired biological activity to that which induces toxic effects to the normal, healthy cells.

The cytotoxicity assay was performed at UCT using the colorimetric 3-(4,5-dimethylthiazol-2-yl)-2,5-diphenyltetrazolium bromide (MTT) assay.[43] Briefly, the MTT assay works based on the conversion of the water-soluble tetrazolium dye (MTT) to the insoluble coloured product (formazan) by redox enzymes present in living, respiring cells. The resulting formazan is then solubilised, and its amount detected spectrophotometrically. Accordingly, viable cells are capable of respiration, thus have more redox activity, producing more formazan which is reflected in greater colour intensity and higher optical density readings.

As with the antiplasmodial assay, the IC_{50} values were calculated from which selectivity indices were derived. The selectivity index represents the ratio of the IC_{50} of the compound in *Plasmodium* parasites to that in the CHO cells. A higher ratio, which is a desirable profile, denotes that the compound is more selective for the parasite being targeted, in this case *Plasmodium*, than the healthy cells. To progress compounds according to the predetermined screening cascade, a SI of 10 was selected as the cut-off.

Generally, in both the aniline-type and benzylamine-type series without manipulations on the LHS, good selectivity indices (SI) were obtained. In this series, all the compounds had a SI above 30 except for **3o/GMP-50**, having a methyl substituent, that showed lower selectivity (SI=17). Compounds **1j/GMP-19**, **3j/GMP-25** and **3f/GMP-35** displayed the best safety profiles (SI>100). Interestingly, it appears that introducing a methylene bridge in the aromatic side chain of **1j/GMP-19** (SI=103) to give **3f/GMP-35** (SI>241) is beneficial to selectivity as the safety profile increases more than two-fold. Within the benzylamine series, better selectivity was achieved with **3f/GMP-35** (SI>241) that has the more lipophilic trifluoromethoxy substituent compared to **3b/GMP-28** (SI=35) bearing a fluoro substituent. On the other hand, the methyl substituted analogue **3o/GMP-50** had the least attractive safety profile (SI=17) [**Table 3.6**].

Notably, the LHS modification whereby dichloro substitutions were performed, although this improved the potency of many of the compounds, it also increased the potential for inducing cytotoxicity. Consequently, **3b/GMP-28** (SI=35) without this modification has a better safety profile than both **4a/GMP-62** (SI=5) and **4b/GMP-66** (SI=30) which have diminished selectivity whereas **3o/GMP-50** (SI=17) and **4e/GMP-69** (SI=15) have about the same selectivity profiles. Similarly, **3j/GMP-25** with an excellent safety profile (SI>234) completely lost selectivity when dichloro groups were introduced on the LHS to give **4d/GMP-68** (SI=0.5). Regio-isomerism of the LHS seems to impact on the selectivity profiles of these compounds since **4a/GMP-62** (SI=5) with a 3,5 dichloro substitution pattern is less selective compared to its 4, 5 dichloro substituted analogue **4b/GMP-66** (SI=30). In contrast, regio-isomerism with regards to the position of substituents on the aromatic side group appears inconsequential to selectivity as **4b/GMP-66** (*para*-F, SI=30), **4i/GMP-75** (*ortho*-F, SI=25) and **4j/GMP-76** (*meta*-F, SI-37) have comparable selectivity indices.

Overall, this series shows that the cytotoxicity profile of the compounds is amenable to modulation with subtle changes resulting in significant changes in SI. Ultimately, two out of the 14 compounds, **4a/GMP-62** and **4d/GMP-68**, failed to meet our defined criteria for compounds with good selectivity (SI>10).

Table 3.6: *In vitro microsomal metabolic stability and cytotoxicity profile of frontrunner analogues.*

Compound Number/Code	Structure	% rem. after 30min ($t_{1/2min}$)		*in vitro* IC_{50} (µM)		Selectivity Index
		MLM	HLM	CHO	NF54	
1j/GMP-19	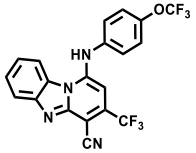	110 (>150)	105 (>150)	17.58	0.17	103
2e/GMP-58	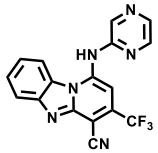	38 (22)	56 (36)	181.34	4.42	41
3b/GMP-28	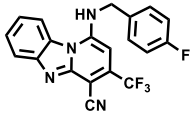	-	-	45	1.28	35
3f/GMP-35	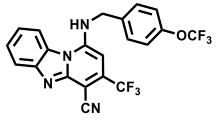	-	-	>222	0.92	>241
3j/GMP-25	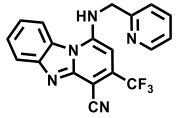	-	-	>272	1.16	>234

Compound Number/Code	Structure	% rem. after 30min ($t_{1/2min}$)		*in vitro* IC_{50} (µM)		Selectivity Index
		MLM	HLM	CHO	NF54	
3o/GMP-50	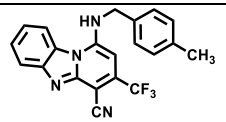	-	-	25	1.49	17
4a/GMP-62	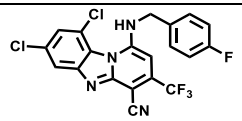	76 (75)	82 (105)	1.66	0.31	5
4b/GMP-66	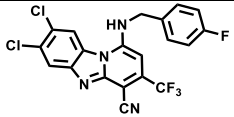	72 (63)	102 (>150)	13	0.44	30
4c/GMP-67	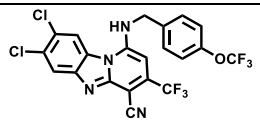	82 (105)	109 (>150)	5.02	0.44	11
4d/GMP-68	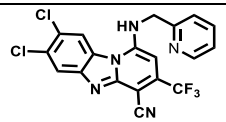	31 (18)	72 (63)	0.75	1.42	0.5
4e/GMP-69	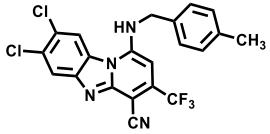	69 (56)	91 (>150)	6.06	0.4	15

Compound Number/Code	Structure	% rem. after 30min ($t_{1/2min}$)		*in vitro* IC_{50} (µM)		Selectivity Index
		MLM	HLM	CHO	NF54	
4g/GMP-71	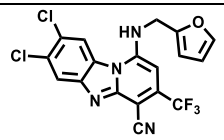	66 (50)	100 (>150)	4.84	0.44	10
4h/GMP-72	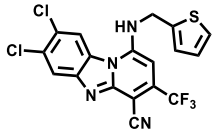	-	-	8.48	0.31	27
4i/GMP-75	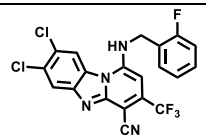	84 (119)	97 (>150)	4.30	0.17	25
4j/GMP-76	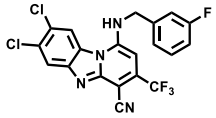	84 (119)	100 (>150)	7.03	0.19	37

MLM: Mouse Liver Microsomes; **HLM:** Human Liver Microsomes; **CHO**: Chinese Hamster Ovarian Cell lines; **%rem**: Percent compound remaining after 30 minutes incubation using the one-point assay; **$t_{1/2min}$**: Projected half-life in minutes; **SI**: selectivity index is the ratio of CHO IC_{50}: *PfNF54*IC_{50} All data represents the mean of n≥3 determinations.

3.6.2 *In vitro* hepatic microsomal metabolic stability

In vitro metabolic stability data enables the rational prediction of drug exposure in subsequent *in vivo* studies. For equally *in vitro* active compounds, highly metabolically labile analogues are expected to achieve low systemic levels which might compromise pharmacological outcomes in comparison to metabolically stable analogues. Accordingly, unlike the metabolically unstable molecules, their stable counterparts would ordinarily be considered for further *in vivo* investigations.

For this study, the single-point metabolic stability assay was employed[44] whereby prioritised compounds were incubated with mouse and human liver microsomes, (MLM) and (HLM), respectively, for 30 minutes and the incubation mixture investigated for changes consistent with metabolic transformations. Microsomes are hepatic sub-cellular fractions containing drug metabolising enzymes, chiefly CYP450, which are involved in Phase I drug metabolism of many clinically marketed drugs.[45,46]

Accordingly, compounds were incubated in microsomes with the requisite co-factors including NADPH and optimised conditions of temperature. After half-an hour, the amount of compound remaining unchanged was determined using LC-MS. The percentage of compound remaining was calculated and metabolic stability assigned according to the criteria in **Table 3.7**.

Table 3.7: *Metabolic stability criteria applied in this study*

% Compound remaining	Metabolic stability status
>75%	Highly Stable
50-74%	Moderately stable
<50%	Unstable

Based on the preceding analysis, the compounds, generally, showed moderate to high metabolic stability as tested in the mouse and human liver microsomes. Compounds incorporating heteroaromatic moieties tended to be more labile as exemplified by **2e/GMP-58** and **4d/GMP-68** (**Table 3.6**) which had less than 75% of compound remaining after 30 minutes incubation period in both HLM and MLM. Moreover, the compounds seem to be more efficiently metabolised in mouse than human microsomes except for **1j/GMP-19** which proved equally stable in both species. Overall, molecules with the greatest microsomal stability in both species, with over 75% remaining after an incubation period of 30 minutes were **1j/GMP-19**, **4i/GMP-75** and **4j/GMP-76** (**Table 3.6**).

Evaluation of species variation in drug metabolism is crucial in guiding follow-up experimental models. For instance, a compound that displays good microsomal metabolic stability in HLM but poor stability in MLM would require judicious choice of animal species for the *in vivo* proof-of-concept studies. Working with an *in vivo* mouse model for a compound showing low metabolic stability in MLM would likely result in poor exposure and potentially low efficacy leading to the termination of a series which would otherwise be promising and worthy of pursuit in view of its good microsomal metabolic stability in the HLM.

3.6.3 hERG interaction risk assessment

To understand the potential risk arising from interactions with the hERG potassium ion channel whose inhibition can cause fatal cardiac arrhythmias, representative compounds **1b/GMP-09**, **2a/GMP-23**, **4g/GMP-71**, **4h/GMP-72**, **4i/GMP-75** and **4j/GMP-76** were profiled. This experiment was carried out by Metrion Biosciences, Cambridge, United Kingdom. In summary, compounds were prepared as 10mM stock solutions in DMSO from which four- point concentrations (0.3, 1, 3 and 10 µM) were subsequently prepared by serial dilution in such a way that the final DMSO content was 0.1%. The CHO cell lines were used to express the hERG ion channel cells, which were accordingly validated biophysically and pharmacologically, using in-house procedures.

To test for the inhibition of the electrical performance of this ion channel, the electrophysiology pattern was observed in the presence of the test compounds at the pre-determined concentrations. In parallel, a blank, compound-free set-up containing the vehicle as well as a positive control containing verapamil hydrochloride were prepared. Each test concentration was performed in triplicate using three separate cells and electrophysiological readings used to examine the effects of the compounds on the hERG tail current amplitude in comparison to the positive control and the blank.

Concentration-response curves were then constructed based on the percent inhibition from each cell and 50% inhibitory concentrations determined. If the highest tested concentration (10 µM) failed to induce ≥ 40% inhibition, an arbitrary IC_{50} value of 30 µM (0.5 log units above 10 µM) was assigned and the compound considered to be inactive. Data for the tested compounds is summarised in **Table 3.8**.

Table 3.8: *hERG inhibition activity of selected compounds.*

Compound number/code	Chemical structure	% inhibition (SD) at 0.3 µM	[a]IC_{50}, µM
1b/GMP-09	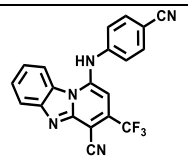	8.36 (2.82)	30
1j/GMP-19	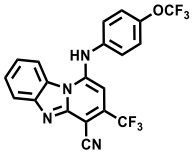	7.51 (2.85)	30
2a/GMP-23	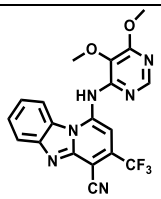	8.45 (6.40)	30
4g/GMP-71	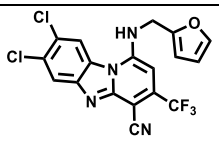	6.82 (2.81)	30
4h/GMP-72	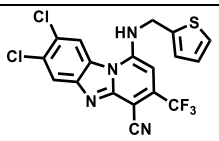	6.13 (5.14)	30
4i/GMP-75	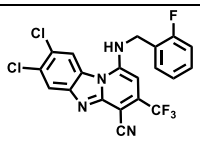	5.49 (3.90)	30
4j/GMP-76	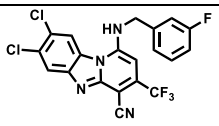	6.53 (4.15)	30

[a]Compounds showed less than 40% inhibition at the highest tested concentration of 10 µM and hence an arbitrary IC_{50} value 0.5 log units above 10 µM was assigned as the IC_{50} for these compounds. All values represent the mean of 3 results obtained from experiments performed as biological and technical triplicates.

This series showed no potential to cause cardiotoxicity arising from interactions with the hERG ion channel as depicted by the high IC_{50} values (>30 µM) [**Table 3.8**]. The positive control drug used in the experiment, verapamil hydrochloride, inhibited the target potently with IC_{50} between 0.2-0.8 µM which was consistent with the acceptable established value for this assay. Even though the assigned IC_{50} values for the compounds are imprecise, it nonetheless offers confidence in progressing active leads from the series.

3.7 *In vivo* antiplasmodium efficacy

Animal studies to provide proof-of-concept on the antimalarial potential of these series were conducted at the Swiss TPH on the most promising leads that fulfilled the progression criteria of *in vitro* potency and ADME, with acceptable cytotoxicity profiles. Based on these filters, compounds **1j/GMP-19** and **4i/GMP-75**, representing leads from the aniline and benzylamine series were selected. Accordingly, mice infected with the rodent species *P. berghei* were treated with **1j/GMP-19** and **4i/GMP-75** on four consecutive days at an oral dose of 50mg/kg (4X50mg/kg). The *in vivo* antimalarial efficacy was determined by comparing the parasitaemia in the infected untreated control and the treated animals. Animals were pronounced to have been cured if no parasitaemia was detected 30 days after treatment.

Table 3.9: *In vivo efficacy of lead targets and chloroquine.*

	1j/GMP-19	**4i/GMP-75**	**Chloroquine**
	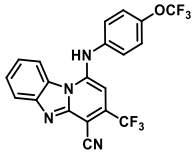	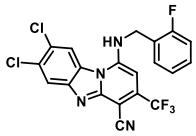	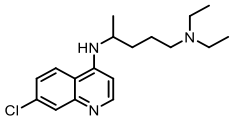
Dose (mg/kg)	4x50	4x50	4x30
Reduction in parasitaemia (%)	98	99.9	99.9
Mean survival days	12	14	21

Following *in vivo* experimentation in a murine model of malaria, it was gratifying to record an impressive 98% and 99.9% reduction in parasitaemia in mice treated with **1j/GMP-19** and **4i/GMP-75**, respectively (**Table 3.9**). This observation provided the vital proof-of-concept that, indeed, the test compounds achieved systemic exposure following oral administration and elicited antimalarial activity in the experimental animal model. Furthermore, the treated animals survived much longer compared to the control (MSD, 6 days), untreated group, with mean survival times of 12 and 14 days for **1j/GMP-19** and **4i/GMP-75**, respectively. In comparison, the reference drug used in the experiment, chloroquine, at a daily oral dose of 30mg/kg for four consecutive days (4X30mg/kg) achieved 99.9% reduction in parasitaemia and resulted in a mean survival time of 21 days.

The two compounds having achieved high *in vivo* activity, it was expected that this would translate into a longer survival span. However, this is not totally surprising as has been reported previously for related series of compounds[28,47] with solubility-limited absorption postulated to result in decreased bioavailability. For poorly soluble compounds, the absorption is largely driven by lipophilicity. Consequently, the absorption at a low dose may be about the same as that of a moderate dose since, at higher doses, the compound could precipitate in the gastro intestinal tract of the animal and is therefore not available for absorption. The presumed low exposure in the systemic circulation could result in sub-optimal levels of the compound *in vivo*. Several factors relating to drug disposition including binding to proteins or tissues and clearance could modify *in vivo* outcomes. To investigate some of these possible scenarios, we performed pharmacokinetic (PK) analysis on the two lead compounds-**1j/GMP-19** and **4i/GMP-75**- to understand the *in vivo* disposition of the series.

3.8 *In vivo* pharmacokinetic profile

The oral disposition of representative compounds **1j/GMP-19** and **4i/GMP-75** was studied in mice to enable investigation of the PK profile of this series. The PK studies were conducted at the Division of Clinical Pharmacology, Department of Medicine, University of Cape Town. In this regard, C57B1/6 mice (n=3) were dosed orally at 20mg/kg for each of the compounds while in another set, the animals (n=2 mice) were dosed intra-venously at 2mg/kg. Blood was sampled between 0-24 hours at the intervals shown in **Figure 3.3**. Corresponding PK parameters were calculated using non-compartmental analysis and are presented in **Table 3.10**.

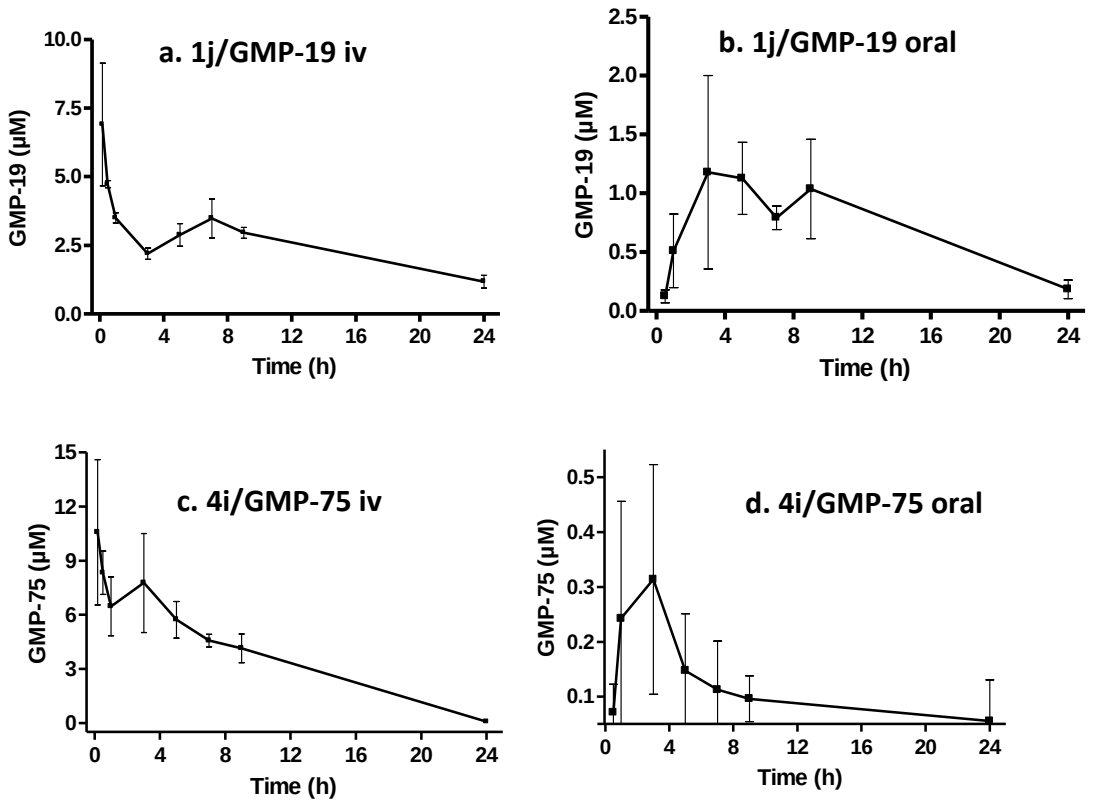

Figure 3.3: *Pharmacokinetics profile for a)* ***1j/GMP-19****, iv; b)* ***1j/GMP-19****, oral; c)* ***4i/GMP-75****, iv and d)* ***4i/GMP-75****, oral. Each data point represents the mean from 2 (iv) and 3 (oral) mice with error bars indicating the standard deviation.*

Compound **1j/GMP-19** displayed a delayed absorption profile as can be inferred from the time taken to reach the maximum concentration (T_{max}=5h) post oral administration. At the oral dose of 20mg/kg, the maximum concentration reached (C_{max}=1.1 µM) is six-fold above the *in vitro* IC_{50} value (0.17 µM) for this compound which, in conjunction with its good metabolic stability, corroborates the observed oral efficacy. Furthermore, **1j/GMP-19** maintains plasma levels above *in vitro* IC_{50} for over 20 hours in both the oral and iv routes of administration (**Figure 3.3**) and displays a low volume of distribution (Vd=0.9L/kg) and a very low plasma clearance (CL=0.97ml/min/kg) [**Table 3.10**].

Table 3.10: *Pharmacokinetics parameters for **1j/GMP-19** and **4i/GMP-75** in mice.*

	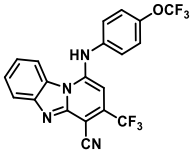		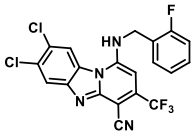	
	1j/GMP-19		**4i/GMP-75**	
Parameter	i.v. (2mg/kg) [a]	p.o. (20mg/kg) [b]	i.v. (2mg/kg) [a]	p.o. (20mg/kg) [b]
C_{max} (µM)	-	1.1	-	0.3
T_{max} (h)	-	5	-	3
$t_{1/2}$ (h)	11.4	7.86	2.6	0.3
V_d (L/kg)	0.90	-	0.18	-
CL (mL/min/kg)	0.97	-	0.81	-
$AUC_{0-\infty}$ (µM/L.min)	4774	1167	5426	138
Oral bioavailability (%)	-	2	-	<1%

[a]For intravenous dosing (n=2 mice), compounds were formulated in a solution of dimethylacetamide, polyethylene glycol and propylene glycol/ethanol mixture 4:1 at a ratio 1:3:6.[b] For oral dosing (n=3 mice), compounds were formulated as suspension in 100% HPMC.

In contrast to **1j/GMP-19**, **4i/GMP-75** attained peak plasma concentrations slightly earlier (Tmax= 3h). The C_{max} (0.3 µM), however, was much lower than that reached by **1j/GMP-19** and was less than 2-fold the *in vitro* IC_{50} (0.17 µM) for the compound. Similarly, **4i/GMP-75** had a shorter half-life ($t_{1/2}$=0.3h) than **1j/GMP-19**, a profile consistent with the previously observed *in vitro* microsomal metabolic stability whereby **4i/GMP-75** had 84% compound remaining after 30 minutes while **1j/GMP-19** remained unchanged after the same period, when evaluated in mouse liver microsomes. Just like **1j/GMP-19**, **4i/GMP-75** showed slow clearance (CL=0.81 mL/min/kg) but had a much lower volume of distribution (Vd=0.18 L/kg). Notably, both compounds had very low bioavailability: **1j/GMP-19** (F=2%) and **4i/GMP-75** (F < 1%).

Taken together, the pharmacokinetics analysis of these compounds reveal that they have delayed absorption, low volume of distribution and low *in vivo* clearance. The meagre bioavailability and variability in absorption, a frequent profile amongst compounds with poor solubility, indicates the need for optimising this parameter towards improved PK and, potentially, oral efficacy. Further investigations are required into understanding the tissue localisation and distribution of these compounds. Based on the high *in vitro* metabolic stability, low *in vivo* clearance and time above *in vitro* IC_{50} concentrations, these compounds are promising towards achieving long-duration of antimalarial action.

3.9 Chapter summary

In this chapter, the antimalarial activities of the PBI derivatives synthesised in this project have been described. Based on the medicinal chemistry iterations undertaken, tractable structure-activity relationship trends have been delineated. Arising from testing in both chloroquine sensitive and multidrug-resistant strains of *Plasmodium falciparum*, the series was found to have low cross-resistance potential relative to the quinoline antimalarial drugs. Besides possessing blood-stage activity, these analogues display potent activity towards the liver and gametocyte stages. Moreover, in probing the mechanism of antimalarial action, the molecules were evaluated for their potential to interfere with the formation of BH, an *in vitro* analogue of hemozoin. Only few compounds displayed good inhibitory activity which was nonetheless not always correlated to antiplasmodial activity. Additionally, the chapter has discussed metabolic stability and cytotoxicity in mammalian cells, along with the assessment of hERG interaction potential from which structure-property relationship trends were delineated. Finally, both the *in vivo* pharmacokinetics and efficacy of the frontrunner leads have been detailed, providing a basis for, and explanations of the observed antimalarial activity.

3.10 References

(1) Hinrichs, D. J.; Makler, M. T. Measurement of the Lactate Dehydrogenase Activity of *Plasmodium falciparum* as an Assessment of Parasitemia. *Am. J. Trop. Med. Hyg.* **1993**, *48* (2), 205–210.

(2) Reader, J.; Botha, M.; Theron, A.; Lauterbach, S. B.; Rossouw, C.; Engelbrecht, D.; Wepener, M.; Smit, A.; Leroy, D.; Mancama, D.; Coetzer, T. L.; Birkholtz, L. -M. Nowhere to Hide: Interrogating Different Metabolic Parameters of *Plasmodium falciparum* Gametocytes in a Transmission Blocking Drug Discovery Pipeline towards Malaria Elimination. *Malar. J.* **2015**, *14* (1), 213.

(3) Flannery, E. L.; Chatterjee, A. K.; Winzeler, E. A. Antimalarial Drug Discovery — Approaches and Progress towards New Medicines. *Nat. Rev. Microbiol.* **2013**, *11* (12), 849–862.

(4) Murphy, S. C.; Shott, J. P.; Parikh, S.; Etter, P.; Prescott, W. R.; Stewart, V. A. Review Article: Malaria Diagnostics in Clinical Trials. *Am. J. Trop. Med. Hyg.* **2013**, *89* (5), 824–839.

(5) de Cózar, C.; Caballero, I.; Colmenarejo, G.; Sanz, L. M.; Álvarez-Ruiz, E.; Gamo, F.-J.; Cid, C. Development of a Novel High-Density [^{3}H]Hypoxanthine Scintillation Proximity Assay To Assess *Plasmodium falciparum* Growth. *Antimicrob. Agents Chemother.* **2016**, *60* (10), 5949–5956.

(6) Chulay, J. D.; Haynes, J. D.; Diggs, C. L. *Plasmodium falciparum*: Assessment of *in vitro* Growth by [3H]Hypoxanthine Incorporation. *Exp. Parasitol.* **1983**, *55* (1), 138–146.

(7) Arnold, M. S. J.; Engel, J. A.; Chua, M. J.; Fisher, G. M.; Skinner-Adams, T. S.; Andrews, K. T. Adaptation of the [3 H]Hypoxanthine Uptake Assay for *In vitro* -Cultured Plasmodium Knowlesi Malaria Parasites. *Antimicrob. Agents Chemother.* **2016**, *60* (7), 4361–4363.

(8) Singh, S.; Srivastava, R. K.; Srivastava, M.; Puri, S. K.; Srivastava, K. In-Vitro Culture of *Plasmodium falciparum*: Utility of Modified (RPNI) Medium for Drug-Sensitivity Studies

Using SYBR Green I Assay. *Exp. Parasitol.* **2011**, *127* (1), 318–321.

(9) Downie, M. J.; Kirk, K.; Mamoun, C. B. Purine Salvage Pathways in the Intraerythrocytic Malaria Parasite *Plasmodium falciparum*. *Eukaryot. Cell* **2008**, *7* (8), 1231–1237.

(10) Hyde, J. E. Exploring the Folate Pathway in *Plasmodium falciparum*. *Acta Trop.* **2005**, *94* (3), 191–206.

(11) Ting, L.-M.; Shi, W.; Lewandowicz, A.; Singh, V.; Mwakingwe, A.; Birck, M. R.; Ringia, E. A. T.; Bench, G.; Madrid, D. C.; Tyler, P. C.; Evans, G. B.; Furneaux, R. H.; Schramm, V. L.; Kim, K. Targeting a Novel *Plasmodium falciparum* Purine Recycling Pathway with Specific Immucillins. *J. Biol. Chem.* **2005**, *280* (10), 9547–9554.

(12) Zhang, H.; Paguio, M.; Roepe, P. D. The Antimalarial Drug Resistance Protein *Plasmodium falciparum* Chloroquine Resistance Transporter Binds Chloroquine. *Biochemistry* **2004**, *43* (26), 8290–8296.

(13) Martin, R. E. The Malaria Parasite's Chloroquine Resistance Transporter Is a Member of the Drug/Metabolite Transporter Superfamily. *Mol. Biol. Evol.* **2004**, *21* (10), 1938–1949.

(14) Waller, K. L.; Muhle, R. A.; Ursos, L. M.; Horrocks, P.; Verdier-Pinard, D.; Sidhu, A. B. S.; Fujioka, H.; Roepe, P. D.; Fidock, D. A. Chloroquine Resistance Modulated *in vitro* by Expression Levels of the *Plasmodium falciparum* Chloroquine Resistance Transporter. *J. Biol. Chem.* **2003**, *278* (35), 33593–33601.

(15) Okombo, J.; Singh, K.; Mayoka, G.; Ndubi, F.; Barnard, L.; Njogu, P. M.; Njoroge, M.; Gibhard, L.; Brunschwig, C.; Vargas, M.; Keiser, J.; Egan, T. J.; Chibale, K. Antischistosomal Activity of Pyrido[1,2- a]Benzimidazole Derivatives and Correlation with Inhibition of β-Hematin Formation. *ACS Infect. Dis.* **2017**, *3* (6), 411–420.

(16) Kumar, S.; Guha, M.; Choubey, V.; Maity, P.; Bandyopadhyay, U. Antimalarial Drugs Inhibiting Hemozoin (Beta-Hematin) Formation: A Mechanistic Update. *Life Sci.* **2007**, *80* (9), 813–828.

(17) Burrows, J. N.; Chibale, K.; Wells, T. N. C. The State of the Art in Anti-Malarial Drug

Discovery and Development. *Curr. Top. Med. Chem.* **2011**, *11*, 1226–1254.

(18) Parapini, S.; Basilico, N.; Pasini, E.; Egan, T. J.; Olliaro, P.; Taramelli, D.; Monti, D. Standardization of the Physicochemical Parameters to Assess *in vitro* the β-Hematin Inhibitory Activity of Antimalarial Drugs. *Exp. Parasitol.* **2000**, *96* (4), 249–256.

(19) Pandey, A. V; Babbarwal, V. K.; Okoyeh, J. N.; Joshi, R. M.; Puri, S. K.; Singh, R. L.; Chauhan, V. S. Hemozoin Formation in Malaria: A Two-Step Process Involving Histidine-Rich Proteins and Lipids. *Biochem. Biophys. Res. Commun.* **2003**, *308* (4), 736–743.

(20) Egan, T. J. Recent Advances in Understanding the Mechanism of Hemozoin (Malaria Pigment) Formation. *J. Inorg. Biochem.* **2008**, *102* (5–6), 1288–1299.

(21) Egan, T. J.; Mavuso, W. W.; Ncokazi, K. K. The Mechanism of β-Hematin Formation in Acetate Solution. Parallels between Hemozoin Formation and Biomineralization Processes †. *Biochemistry* **2001**, *40* (1), 204–213.

(22) Kumar, S.; Guha, M.; Choubey, V.; Maity, P.; Bandyopadhyay, U. Antimalarial Drugs Inhibiting Hemozoin (β-Hematin) Formation: A Mechanistic Update. *Life Sci.* **2007**, *80* (9), 813–828.

(23) Egan, T. J.; Hunter, R.; Kaschula, C. H.; Marques, H. M.; Misplon, A.; Walden, J. Structure−Function Relationships in Aminoquinolines: Effect of Amino and Chloro Groups on Quinoline−Hematin Complex Formation, Inhibition of β-Hematin Formation, and Antiplasmodial Activity. *J. Med. Chem.* **2000**, *43* (2), 283–291.

(24) de Villiers, K. A.; Marques, H. M.; Egan, T. J. The Crystal Structure of Halofantrine–ferriprotoporphyrin IX and the Mechanism of Action of Arylmethanol Antimalarials. *J. Inorg. Biochem.* **2008**, *102* (8), 1660–1667.

(25) Ziegler, J.; Linck, R.; Wright, D. Heme Aggregation Inhibitors: Antimalarial Drugs Targeting an Essential Biomineralization Process. *Curr. Med. Chem.* **2001**, *8* (2), 171–189.

(26) Warhurst, D. C.; Craig, J. C.; Adagu, I. S.; Guy, R. K.; Madrid, P. B.; Fivelman, Q. L. Activity of Piperaquine and Other 4-Aminoquinoline Antiplasmodial Drugs against Chloroquine-

Sensitive and Resistant Blood-Stages of *Plasmodium falciparum*. *Biochem. Pharmacol.* **2007**, *73* (12), 1910–1926.

(27) Ketchum, M. A.; Lee, A. M.; Vekilov, P. G.; Rimer, J. D. Biomimetic Assay for Hematin Crystallization Inhibitors: A New Platform To Screen Antimalarial Drugs. *Cryst. Growth Des.* **2017**, *17* (1), 197–206.

(28) Singh, K.; Okombo, J.; Brunschwig, C.; Ndubi, F.; Barnard, L.; Wilkinson, C.; Njogu, P. M.; Njoroge, M.; Laing, L.; Machado, M.; Prudêncio, M.; Reader, J.; Botha, M.; Nondaba, S.; Birkholtz, L. -M.; Lauterbach, S.; Churchyard, A.; Coetzer, T. L.; Burrows, J. N.; Yeates, C.; Denti, P.; Wiesner, L.; Egan, T. J.; Wittlin, S.; Chibale, K. Antimalarial Pyrido[1,2- a]Benzimidazoles: Lead Optimization, Parasite Life Cycle Stage Profile, Mechanistic Evaluation, Killing Kinetics, and *in vivo* Oral Efficacy in a Mouse Model. *J. Med. Chem.* **2017**, *60* (4), 1432–1448.

(29) Machado, M.; Sanches-Vaz, M.; Cruz, J. P.; Mendes, A. M.; Prudêncio, M. Inhibition of Plasmodium Hepatic Infection by Antiretroviral Compounds. *Front. Cell. Infect. Microbiol.* **2017**, *7 (329), 1-9*.

(30) Carter, R.; Ranford-Cartwright, L.; Alano, P. The Culture and Preparation of Gametocytes of *Plasmodium falciparum* for Immunochemical, Molecular, and Mosquito Infectivity Studies. In *Protocols in Molecular Parasitology*; Hyde, J. E., Ed.; Humana Press: Totowa, NJ, 1993; pp 67–88.

(31) Lucantoni, L.; Duffy, S.; Adjalley, S. H.; Fidock, D. A.; Avery, V. M. Identification of MMV Malaria Box Inhibitors of *Plasmodium falciparum* Early-Stage Gametocytes Using a Luciferase-Based High-Throughput Assay. *Antimicrob. Agents Chemother.* **2013**, *57* (12), 6050–6062.

(32) Peatey, C. L.; Spicer, T. P.; Hodder, P. S.; Trenholme, K. R.; Gardiner, D. L. A High-Throughput Assay for the Identification of Drugs against Late-Stage *Plasmodium falciparum* Gametocytes. *Mol. Biochem. Parasitol.* **2011**, *180* (2), 127–131.

(33) Delves, M. J.; Ruecker, A.; Straschil, U.; Lelièvre, J.; Marques, S.; López-Barragán, M. J.; Herreros, E.; Sinden, R. E. Male and Female *Plasmodium falciparum* Mature

Gametocytes Show Different Responses to Antimalarial Drugs. *Antimicrob. Agents Chemother.* **2013**, *57* (7), 3268–3274.

(34) Buchholz, K.; Burke, T. A.; Williamson, K. C.; Wiegand, R. C.; Wirth, D. F.; Marti, M. A High-Throughput Screen Targeting Malaria Transmission Stages Opens New Avenues for Drug Development. *J. Infect. Dis.* **2011**, *203* (10), 1445–1453.

(35) Baird, J. K.; Surjadjaja, C. Consideration of Ethics in Primaquine Therapy against Malaria Transmission. *Trends Parasitol.* **2011**, *27* (1), 11–16.

(36) Njoroge, M.; Njuguna, N. M.; Mutai, P.; Ongarora, D. S. B.; Smith, P. W.; Chibale, K. Recent Approaches to Chemical Discovery and Development Against Malaria and the Neglected Tropical Diseases Human African Trypanosomiasis and Schistosomiasis. *Chem. Rev.* **2014**, *114* (22), 11138–11163.

(37) Pybus, B. S.; Marcsisin, S. R.; Jin, X.; Deye, G.; Sousa, J. C.; Li, Q.; Caridha, D.; Zeng, Q.; Reichard, G. A.; Ockenhouse, C.; Bennett, J.; Walker, L. A.; Ohrt, C.; Melendez, V. The Metabolism of Primaquine to Its Active Metabolite Is Dependent on CYP 2D6. *Malar. J.* **2013**, *12* (1), 212.

(38) Potter, B. M. J.; Xie, L. H.; Vuong, C.; Zhang, J.; Zhang, P.; Duan, D.; Luong, T.-L. T.; Bandara Herath, H. M. T.; Dhammika Nanayakkara, N. P.; Tekwani, B. L.; Walker, L. A.; Nolan, C. K.; Sciotti, R. J.; Zottig, V. E.; Smith, P. L.; Paris, R. M.; Read, L. T.; Li, Q.; Pybus, B. S.; Sousa, J. C.; Reichard, G. A.; Marcsisin, S. R. Differential CYP 2D6 Metabolism Alters Primaquine Pharmacokinetics. *Antimicrob. Agents Chemother.* **2015**, *59* (4), 2380–2387.

(39) Shekalaghe, S.; Drakeley, C.; Gosling, R.; Ndaro, A.; van Meegeren, M.; Enevold, A.; Alifrangis, M.; Mosha, F.; Sauerwein, R.; Bousema, T. Primaquine Clears Submicroscopic *Plasmodium falciparum* Gametocytes That Persist after Treatment with Sulphadoxine-Pyrimethamine and Artesunate. *PLoS One* **2007**, *2* (10), e1023.

(40) Bousema, T.; Okell, L.; Shekalaghe, S.; Griffin, J. T.; Omar, S.; Sawa, P.; Sutherland, C.; Sauerwein, R.; Ghani, A. C.; Drakeley, C. Revisiting the Circulation Time of *Plasmodium falciparum* Gametocytes: Molecular Detection Methods to Estimate the Duration of

Gametocyte Carriage and the Effect of Gametocytocidal Drugs. *Malar. J.* **2010**, *9* (1), 136.

(41) Delves, M.; Plouffe, D.; Scheurer, C.; Meister, S.; Wittlin, S.; Winzeler, E. A.; Sinden, R. E.; Leroy, D. The Activities of Current Antimalarial Drugs on the Life Cycle Stages of *Plasmodium*: A Comparative Study with Human and Rodent Parasites. *PLoS Med.* **2012**, *9* (2), e1001169.

(42) Plouffe, D. M.; Wree, M.; Du, A. Y.; Meister, S.; Li, F.; Patra, K.; Lubar, A.; Okitsu, S. L.; Flannery, E. L.; Kato, N.; Tanaseichuk, O.; Comer, E.; Zhou, B.; Kuhen, K.; Zhou, Y.; Leroy, D.; Schreiber, S. L.; Scherer, C. A.; Vinetz, J.; Winzeler, E. A. High-Throughput Assay and Discovery of Small Molecules That Interrupt Malaria Transmission. *Cell Host Microbe* **2016**, *19* (1), 114–126.

(43) Sumantran, V. N. Cellular Chemosensitivity Assays: An Overview. In *Cancer Cell Culture: Methods and Protocols*; Cree, I. A., Ed.; Humana Press: Totowa, NJ, 2011; pp 219–236.

(44) Manach, C. Le; Paquet, T.; Gonza, D.; Younis, Y.; Taylor, D.; Wiesner, L.; Lawrence, N.; Schwager, S.; Waterson, D.; Witty, M. J.; Wittlin, S.; Street, L. J.; Chibale, K. Medicinal Chemistry Optimization of Antiplasmodial Imidazopyridazine Hits from High Throughput Screening of a SoftFocus Kinase Library: Part 2. **2014,** 57 (21), 8839-8848.

(45) Rogers, J. F.; Nafziger, A. N.; Bertino, J. S. Pharmacogenetics Affects Dosing, Efficacy, and Toxicity of Cytochrome P450–metabolized Drugs. *Am. J. Med.* **2002**, *113* (9), 746–750.

(46) Guengerich, F. P. Cytochrome P450s and Other Enzymes in Drug Metabolism and Toxicity. *AAPS J.* **2006**, *8* (1), E101--E111.

(47) Ndakala, A. J.; Gessner, R. K.; Gitari, P. W.; October, N.; White, K. L.; Hudson, A.; Fakorede, F.; Shackleford, D. M.; Kaiser, M.; Yeates, C.; Charman, S. A.; Chibale, K. Antimalarial Pyrido[1,2-a]Benzimidazoles. *J. Med. Chem.* **2011**, *54* (13), 4581–4589.

Chapter 4

Antischistosomal Profiling of Pyrido [1,2-*a*] benzimidazoles

4.1 Chapter overview

In this chapter, the activity of target compounds towards adult and immature *Schistosomes* will be presented. Emanating from observed antischistosomal activities, structure-activity relationship trends will be extracted. As with the preceding chapter, the *in vitro* drug metabolism, pharmacokinetics and cytotoxicity profiles of selected compounds will be discussed. Based on *in vitro* microsomal metabolic stability profiles, metabolite identification studies will be discussed for selected compounds. Finally, using the frontrunner compounds, results of *in vivo* efficacy and pharmacokinetics will also be discussed.

4.2 *In vitro* antischistosomal activities

The chemical architecture and antiplasmodial potency of the synthesised PBI derivatives prompted their antischistosomal evaluation, following a drug repositioning approach. In so doing, the presence of common druggable biological pathways between *Plasmodium* parasites and schistosomes, such as the heme detoxification process, was presumed.[1] In line with current antischistosomal drug discovery programs[2,3] and with the intention of identifying leads that are active across multiple stages of the parasite, *in vitro* antischistosomal activities of target compounds was performed against adult worms and immature larva referred to as newly transformed schistosomula (NTS). As discussed before, the standard of care therapy in schistosomiasis, praziquantel, weakly targets immature forms of schistosomes which proceed to mature into adult worms and perpetuate the infection. Finding a multi-stage active antischistosomal lead that can eradicate both adult worms and the larval forms is therefore a key priority and target candidate profile for antischistosomal drug discovery and development.[4–6]

The antischistosomal assays were conducted at the Swiss TPH under the supervision of Prof. Jennifer Keiser. Briefly, infected snails were mechanically stimulated to shed *S. mansoni* cercariae which were transformed into schistosomula by removal of cercarial tail.[7] For assays against mature *Schistosomes*, the adult worms were harvested after 7-8 weeks from the hepatic portal and mesenteric veins of mice previously infected with cercariae.[7,8]

With the aim of prioritising compounds capable of targeting NTS, test compounds were first screened for activity at an initial concentration of 10 µM against juvenile *S. mansoni* worms. Thereafter, compounds that displayed significant inhibition (≥70%) of the NTS were subsequently exposed to adult schistosomes at a similar concentration. Compounds with significant activity in the adult worms at 10 µM were progressed for further dose-response experiments from which IC_{50} values were determined. Ensuing SAR trends were analysed based on the observed activities as presented in the following **Tables 4.1- 4.3**, stratified according to the SAR manipulations carried out in this project.

4.2.1 SAR_1 Targets

In the first series, where the side chain has the phenyl ring directly linked to the PBI core by a nitrogen (compounds **1a/GMP-06 - 2e/GMP-58**), 10 compounds were identified having activity in the low micromolar range (<10 µM). Out of these, **1b/GMP-09** (IC_{50}=0.21 µM), **1i/GMP-18** (IC_{50}=0.97 µM) and **1j/GMP-19** (IC_{50}=0.21 µM) all displayed sub-micromolar potency, while the unsubstituted analogue **1n/GMP-32** (IC_{50}=2.81 µM) had lower potency, suggesting that activity was favoured in compounds incorporating substituents with electron-withdrawing effects. On the contrary, hydrophilic groups on the aromatic side group (**R**, **Table 4.1**) abrogated activity as seen, for example, with **1g/GMP-15** and **1h/GMP-17**.

Table 4.1: *In vitro antischistosomal activity of* ***SAR₁*** *Targets in NTS and adult S. mansoni worms.*[a]

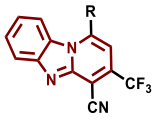

Compound Number/Code	R	% *S. mansoni* mortality at 10 µM		Adult IC_{50} (µM)
		NTS	Adult	
1a/GMP-06	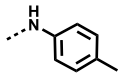	73.9	33.3	-
1b/GMP-09	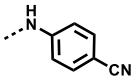	100	100	0.21
1c/GMP-10	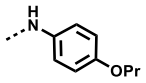	100	50	-
1e/GMP-12	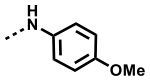	95.7	63.3	6.40
1f/GMP-13	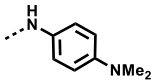	43.5	-	-
1g/GMP-15	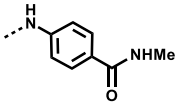	30.4	-	-
1h/GMP-17	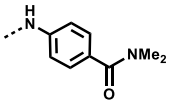	30.4	-	-
1i/GMP-18	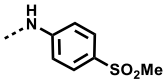	100	91.7	0.97
1j/GMP-19	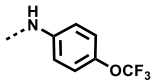	100	100	0.21
1k/GMP-121	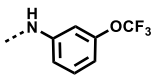	-	100	1.05
1l/GMP-122	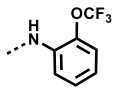	-	100	1.65
1n/GMP-32	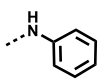	100	79.2	2.81

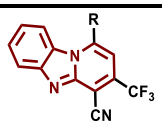

Compound Number/Code	R	% *S. mansoni* mortality at 10 µM		Adult IC_{50} (µM)
		NTS	Adult	
1o/GMP-37	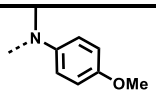	26.1	-	-
1p/GMP-46	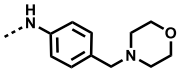	100	83.3	3.14
2a/GMP-23	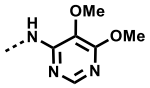	100	100	1.38
2b/GMP-30	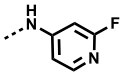	100	97.9	0.75
2c/GMP-31		100	100	0.4
2d/GMP-57	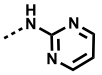	30.4	-	-
2e/GMP-58	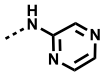	91.3	91.7	2.01
3a/GMP-24	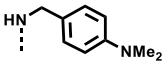	17.4	-	-
3b/GMP-28	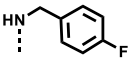	4.4	-	-
3c/GMP-29	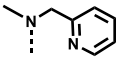	8.7	11.1	-
3d/GMP-33	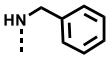	0	0	-
3e/GMP-34	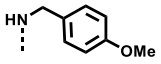	4.4	-	-
3f/GMP-35	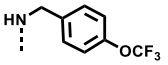	8.7	-	-
3g/GMP-36	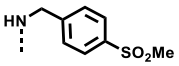	13	-	-

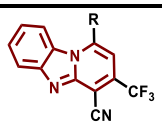

Compound Number/Code	R	% *S. mansoni* mortality at 10 µM		Adult IC_{50} (µM)
		NTS	Adult	
3h/GMP-38	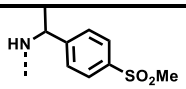	47.8	-	-
3i/GMP-45	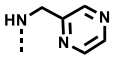	30.4	-	-
3j/GMP-25	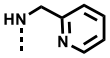	21.7	-	-
3k/GMP-43	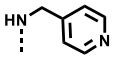	30.4	-	-
3l/GMP-44	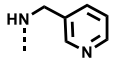	4.4	-	-
3m/GMP-47	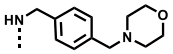	8.7	-	-
3n/GMP-48	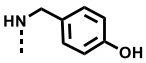	4.4	-	-
3o/GMP-50	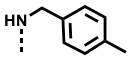	0	0	-
3p/GMP-52	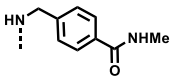	17.4	-	-
3q/GMP-53	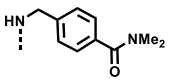	26.1	-	-
3r/GMP-54	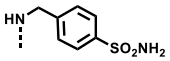	21.7	-	-
3s/GMP-55	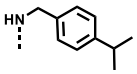	26.1	-	-
3t/GMP-56	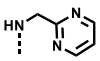	26.1	-	-
3u/GMP-77		9	-	-
3v/GMP-87	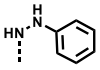	89	29	-

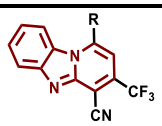

Compound Number/Code	R	% *S. mansoni* mortality at 10 µM		Adult IC_{50} (µM)
		NTS	Adult	
3w/GMP-88	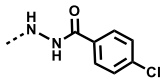	9	-	-
Praziquantel				0.1

[a]Values are a mean of n≥3 determinations.

Additional compounds with good antischistosomal activity were identified among compounds incorporating heteroaromatic side groups exemplified by pyrimidyl, pyridyl, thiazolyl and pyrazinyl groups as in **2a/GMP-23** (IC_{50}=1.38 µM), **2b/GMP-30** (IC_{50}=0.75 µM), **2c/GMP-31** (IC_{50}=0.4 µM) and **2e/GMP-58** (IC_{50}=2.01 µM), respectively. The retention of activity of these heteroaromatic analogues not only allowed for the exploration of new chemical spaces, but also had the attendant advantage of incorporating solubility-enhancing features.

The morpholino-containing analogue **1p/GMP-46** also displayed modest antischistosomal activity in both young and adult worms with a mortality of 100% and 83%, respectively, at 10 µM and an IC_{50} value of 3.14 µM against the adult worms. The positioning of the nitrogen atoms in the phenyl side chain seem crucial for antischistosomal activity since **2d/GMP-57**, in which the nitrogen atoms have a 2,6 relationship, showed poor activity compared to its regio-isomer **2e/GMP-58** (IC_{50}=2.01 µM) where the nitrogen atoms occur in a 2,5 relationship.

The next SAR analysis concerns a series of analogues comprising the aromatic side group attached to the PBI core via a methylamine bridge (**3a/GMP-24- 3t/GMP-56; Table 4.1**). In the absence of modifications elsewhere in the scaffold, these compounds displayed poor antischistosomal activity. Most of these compounds were weakly active against NTS at the screening concentration of 10 µM rendering them ineligible for additional screening in adult worms according to the workflow adopted in the assay. For example, in comparing **1j/GMP-19** (IC_{50} = 0.21 µM) vs **3f/GMP-35** (IC_{50} >10 µM); **1i/GMP-18** (IC_{50} = 0.97 µM) vs **3g/GMP-36** (IC_{50} >10 µM), the analogues with a methylene linker in each case, are all inactive. A similar pattern of inactivity was maintained with the heteroaromatic analogues of previously active aniline-type series compounds as in **2e/GMP-58** (IC_{50} = 2.01 µM) vs **3i/GMP-45** (IC_{50} >10 µM).

The capacity for the nitrogen connecting the PBI core and the aromatic appendage to act as a hydrogen-bond donor appears important for antischistosomal activity. In comparing **1e/GMP-12** vs **1o/GMP-37** and **3j/GMP-25** vs **3c/GMP-29**, there was a decrease in the mortality induced at 10 µM in both NTS and adult worms for **1o/GMP-37** and **3c/GMP-29** which contain a methyl substitution on this nitrogen.

Furthermore, when the methylene linker in **3d/GMP-33** (0% NTS and adult; 10 µM) was substituted by an amino group to produce **3v/GMP-87**, better activity in both the immature and adult worms was observed. Other side groups such as the more polar piperazine and hydrazide found in **3u/GMP-77** and **3w/GMP-88**, respectively, were detrimental to activity (9% NTS, 10 µM).

4.2.2. SAR_2 Targets

This SAR involved introducing changes on the LHS of the PBI core through installation of chloro- substitutions. Interestingly, for target compounds in the benzylamine series which were previously inactive, this modification seemed to restore their activity. For example, **3b/GMP-28** has poor activity (**Table 4.1**; IC_{50} >10 µM), with less than 10% reduction in juvenile worms and no effect against adult worms at 10 µM. In contrast, the analogues **4a/GMP-62** and **4b/GMP-66** (**Table 4.2**) with dichloro substitution on the phenyl portion of the PBI scaffold have potent activity at 10 µM against both juvenile and adult worms (98-100% mortality). Consistent observations are seen with **3o/GMP-50** vs **4e/GMP-69**; **3f/GMP-35** vs **4c/GMP-67** and **3j/GMP-25** vs **4d/GMP-68** in which enhanced mortality is observed with the di-chlorinated analogues, in both NTS and adult worms at 10 µM.

Regio-isomerism in the aromatic side group appears inconsequential to antischistosomal activity: shifting the position of the fluoro substituent from the *para* position in **4b/GMP-66** (100% NTS, 98% adult; 10 µM) to the *ortho*- [**4i/GMP-75** (IC_{50} = 0.38 µM)] and *meta*- [**4j/GMP-76** (IC_{50} = 0.40 µM)] analogues maintained good antischistosomal activity.

The relevance of chirality with regards to antischistosomal activity was evaluated by comparing the achiral compound **4l/GMP-96** (23% NTS), which has poor activity, to that of analogous racemic **4m/GMP-97** (100%, NTS and adult), which portrays good potency against both the immature and adult worms at 10µM. This observation may indicate the possible existence of a chiral target with which the compounds interact to elicit antischistosomal activity. This hypothesis will need to be tested through the synthesis and evaluation of the respective enantiomers.

Table 4.2: *In vitro antischistosomal activity of* ***SAR₂*** *Targets in NTS and adult worms.*[a]

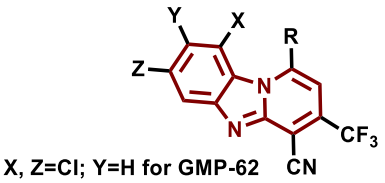

X, Z=Cl; Y=H for GMP-62
Others: X=H; Y, Z=Cl

Compound Number/ Code	R	% *S. mansoni* mortality at 10 µM		Adult IC_{50} (µM)
		NTS	Adult	
4a/GMP-62	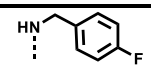	100	100	0.77
4b/GMP-66	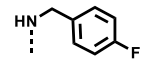	100	98	*-
4c/GMP-67	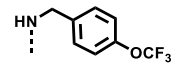	100	100	*-
4d/GMP-68	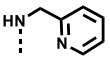	100	99	*-
4e/GMP-69	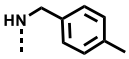	100	100	*-
4f/GMP-70	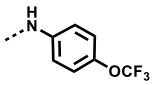	100	100	*-
4g/GMP-71	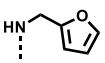	100	100	0.47
4h/GMP-72	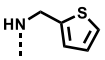	100	100	0.43
4i/GMP-75	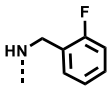	100	100	0.38
4j/GMP-76	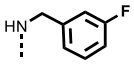	100	100	0.40
4l/GMP-96	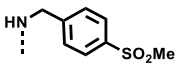	23	-	-
4m/GMP-97	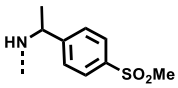	100	100	*-
4n/GMP-98	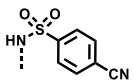	44	84	*-
4o/GMP-99	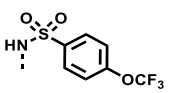	93	87	*-

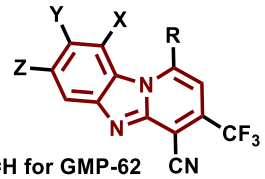

X, Z=Cl; Y=H for GMP-62
Others: X=H; Y, Z=Cl

Compound Number/ Code	R	% *S. mansoni* mortality at 10 µM		Adult IC_{50} (µM)
		NTS	Adult	
4p/GMP-100	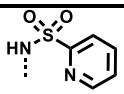	9	-	-
Praziquantel				0.1

[a]Values are a mean of n≥3 determinations. *Not determined as compound failed potency criteria at 1µM.

When the methylene linker in the side group **R** was replaced with a sulfonyl group, there were mixed observations: activity was lost with **4p/GMP-100** (9% NTS, 10 µM), an analogue of **4d/GMP-68** (100% NTS, 99% adult; 10 µM) whereas similar changes only diminished slightly the activity of **4o/GMP-99** (93% NTS, 87% adult; 10 µM), the analogue of **4c/GMP-67** (100% NTS and adult; 10 µM).

4.2.3 SAR_3 Targets

Towards interrogating the relevance of the nitrile substitution on the pyridyl portion of the PBI scaffold, some compounds were synthesised wherein this group was replaced by other small groups. It was discovered that this modification led to a decrease in antischistosomal activity as seen in **Table 4.3**. Taken together, these results suggest that the nitrile at this position is important or optimal for antischistosomal activity.

Table 4.3: *In vitro antischistosomal activity of* ***SAR_3*** *Targets in NTS and adult worms.*[a]

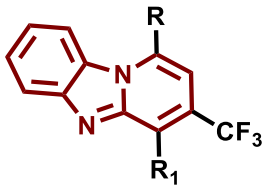

Compound Number/Code	R_1	R	% *S. mansoni* mortality at 10 µM		Adult IC_{50} (µM)
			NTS	Adult	
5a/GMP-120	H	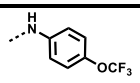	-	77	3.37
5b/GMP-128		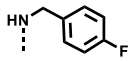	4	34	-
5c/GMP-129		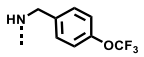	21	53	-
5d/GMP-130		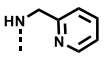	8	15	-
5e/GMP-120E		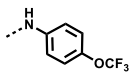	67	57	-
Praziquantel					0.1

[a]Values are a mean of n≥3 determinations.

4.3 Correlation between antischistosomal and BHI activity

Target compounds were evaluated against the BHI process as a putative mechanism of antischistosomal activity. As discussed previously in **Chapter 1**, this process is observed to occur in *Schistosoma* as in *Plasmodium* parasites. The potencies of the compounds in this assay is as recorded in **Chapter 3** alongside their antiplasmodial potency. In this section, an analysis for correlation between BHI activity and antischistosomal action of these compounds, is examined.

As observed with the antimalarial actions of these series, there was a lack of correlation between the ability to interfere with the formation of hemozoin and the observed antischistosomal potency (**Figure 4.1**). This inference is drawn from recorded good *in vitro* antischistosomal activities of compounds such as **1b/GMP-09**, **1j/GMP-19** and **4i/GMP-75** which displayed poor BHI action (IC_{50} >100 µM) while **1p/GMP-46**, **4f/GMP-70** and **4m/GMP-97** despite having potent BHI activity, were only weakly active against adult schistosomes at 1 µM.

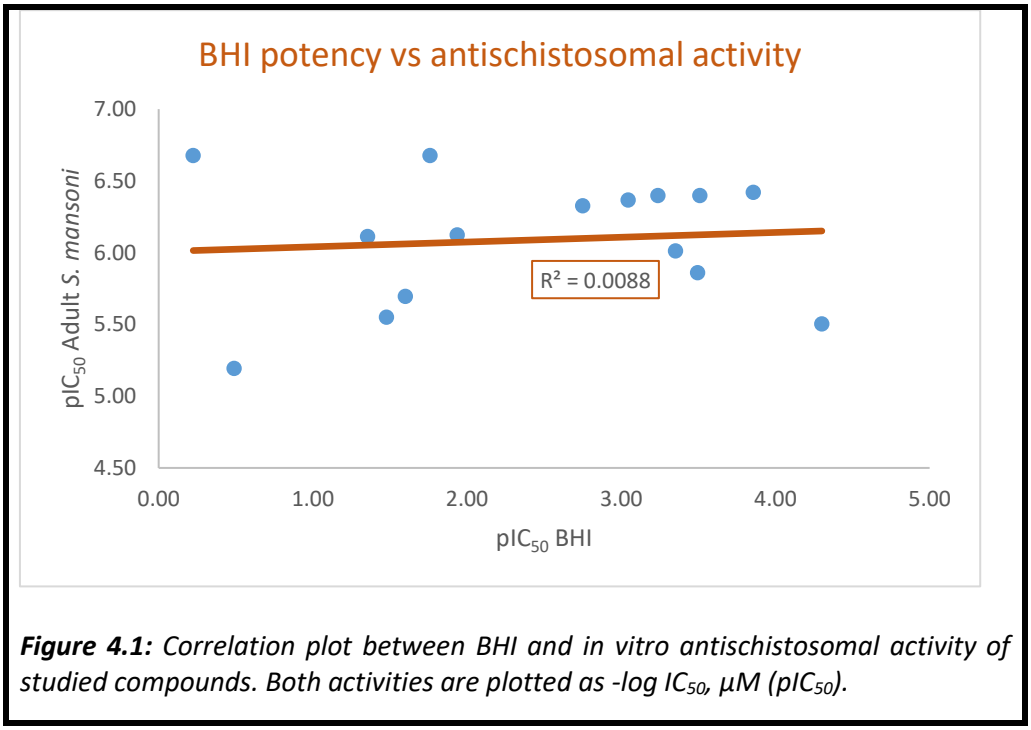

Figure 4.1: *Correlation plot between BHI and in vitro antischistosomal activity of studied compounds. Both activities are plotted as -log IC_{50}, µM (pIC_{50}).*

These results point to the likelihood of divergent or additional mechanisms of action besides inhibition of BH formation, through which these compounds may act to achieve the observed antischistosomal activities.

4.4 ADME and cytotoxicity profiling of frontrunner compounds

To gain insight into the anticipated pharmacokinetic behaviour, selective toxicity and to prioritise compounds for *in vivo* efficacy studies, *in vitro* metabolic stability and cytotoxicity experiments were conducted as explained in **Chapter 3.** Metabolic stability was carried out using mouse and human liver microsomes whereas cytotoxicity was evaluated using the Chinese Hamster Ovarian cell lines. The percentage of compound remaining after 30 minutes incubation was determined and the projected half-life calculated as previously described.[9] The data from these assays is as presented in **Table 4.4**.

Table 4.4: *In vitro metabolic stability and cytotoxicity profile of frontrunner analogues.[a]*

Compound Number/code	Chemical Structure	% rem. after 30min ($t_{1/2min}$)		*In vitro* IC_{50} (μM)		Selectivity Index
		MLM	HLM	CHO	Adult worms	
1b/GMP-09	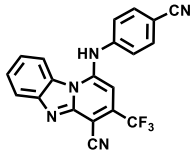	97 (>150)	92 (>150)	7.27	0.21	35
1i/GMP-18	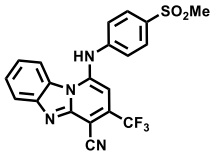	105 (>150)	77 (80)	148	0.97	153
1j/GMP-19	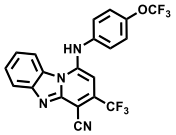	110 (>150)	105 (>150)	17.58	0.21	84
2a/GMP-23	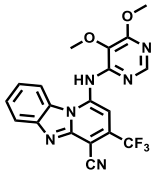	28 (17)	69 (57)	23.99	1.38	17

Compound Number/code	Chemical Structure	% rem. after 30min ($t_{1/2min}$)		*In vitro* IC_{50} (µM)		Selectivity Index
		MLM	HLM	CHO	Adult worms	
2b/GMP-30	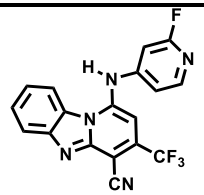	56 (36)	29 (17)	111.15	0.75	148
2c/GMP-31	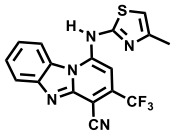	73 (66)	64 (47)	33.37	0.4O	83
2e/GMP-58	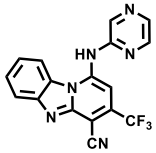	38 (22)	56 (36)	181.34	2.01	90
4a/GMP-62	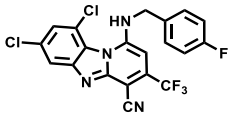	76 (75)	82 (105)	1.66	0.77	2
4b/GMP-66	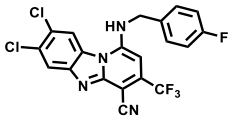	72 (63)	102 (>150)	13	1-10	

Compound Number/code	Chemical Structure	% rem. after 30min ($t_{1/2min}$)		*In vitro* IC_{50} (µM)		Selectivity Index
		MLM	HLM	CHO	Adult worms	
4c/GMP-67	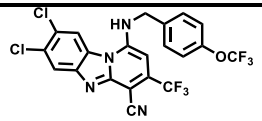	82 (105)	109 (>150)	5.02	1-10	
4d/GMP-68	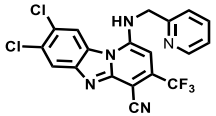	31 (18)	72 (63)	0.75	1-10	
4e/GMP-69	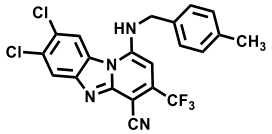	69 (56)	91 (>150)	6.06	1-10	
4g/GMP-71	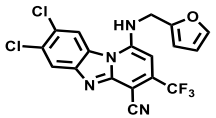	66 (50)	100 (>150)	4.84	0.47	10
4h/GMP-72	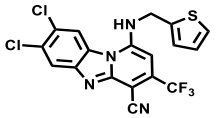			8.48	0.43	20
4i/GMP-75	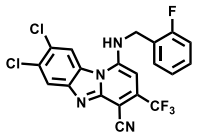	84 (119)	97 (>150)	4.30	0.38	11

Compound Number/code	Chemical Structure	% rem. after 30min ($t_{1/2min}$)		*In vitro* IC_{50} (µM)		Selectivity Index
		MLM	HLM	CHO	Adult worms	
4j/GMP-76	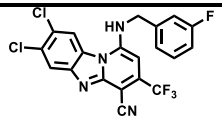	84 (119)	100 (>150)	7.03	0.40	18
4n/GMP-98	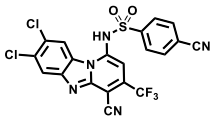	9 (9)	16 (11)	>50	1-10	
4o/GMP-99	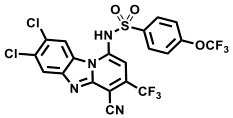	38 (21)	83 (112)	>50	1-10	

[a]Values are the mean of n≥3 determinations. **MLM**-mouse liver microsomes; **HLM**-human liver microsomes; **CHO**-Chinese Hamster ovarian cell line**. %rem**. Is the percent compound remaining; **$t_{1/2}$**: estimated half-life in minutes.

Overall, the most stable compounds were **1b/GMP-09**, **1j/GMP-19**, **4c/GMP-67, 4i/GMP-75** and **4j/GMP-76** in which over 80% of the compound was remaining after incubating for 30 minutes with an estimated half-life of over 100 minutes in both MLM and HLM. The lipophilic electron-withdrawing property of groups attached to the aromatic side chain (as in **1j/GMP-19** and **4c/GMP-67**) imparted better metabolic stability as opposed to hydrophilic, electron-rich substituents (as found in **1a/GMP-06**, **1i/GMP-18** and **4e/GMP-69**).

Introducing heteroatoms in the side chain decreased metabolic stability as evident with, **2a/GMP-23**, **2b/GMP-30, 2c/GMP-31, 2e/GMP-58,** and **4d/GMP-68** which had less than 75% of compound remaining in both MLM and HLM species. Similarly, when a sulfonyl group was used in the stead of a methylene linker, metabolic stability was greatly diminished with **4n/GMP-98** being the least metabolically stable compound in the sub-series with this modification.

Species variation in the metabolic stability of this series was evident. Metabolism was more efficient in mouse liver microsomes for ten of the tested compounds: **2a/GMP-23**, **2e/GMP-58**, **4b/GMP-66**, **4c/GMP-67, 4d/GMP-68, 4e/GMP-69, 4g/GMP-71, 4i/GMP-75, 4j/GMP-76, 4n/GMP-98** and **4o/GMP-99**. Only three compounds (**1i/GMP-18**, **2b/GMP-30** and **2c/GMP-31**) showed enhanced susceptibility to HLM compared to MLM whereas two compounds (**1b/GMP-09** and **1j/GMP-19**) were equally stable in both species.

Most of the compounds had a good cytotoxicity profile (SI>10) with only **4a/GMP-62**, with a selectivity index of 2, showing high potential for causing cytotoxicity. Evidently, as seen with the antimalarial evaluation of these compounds, although the introduction of chloro substitutions on the LHS of the molecules improved their antischistosomal potency, this also increased their risk for inducing cytotoxicity as reflected in their reduced selectivity indices (**Table 4.4**).

4.5 Metabolite identification studies for 2a/GMP-23 and 2e/GMP-58

For selected compounds (**2a/GMP-23** and **2e/GMP-58**) that portrayed good *in vitro* antischistosomal activity but were beset by enhanced susceptibility to drug metabolising enzymes, metabolite identification studies were conducted with the three-fold purposes of: **i)** Identifying the metabolic hotspot in the compounds, **ii)** understanding the nature of biotransformation and **iii)** establishing the putative metabolites. These studies were performed at the Division of Clinical pharmacology, Department of Medicine, UCT.

In summary, compounds were incubated separately in MLM and HLM in the presence of requisite co-factors and conditions such as NADPH, magnesium chloride and potassium phosphate buffer at pH 7.4 to mimic the physiological milieu. After shaking for 60 minutes at 37 ℃, chilled acetonitrile was added to the incubation mix which was then centrifuged and filtered prior to LC-MS analysis. Control experiments in which NADPH, microsomes or test compounds were individually excluded were prepared as described for the test compounds. The set up in which NADPH was excluded served to facilitate the evaluation of any non-CYP450-dependent metabolism. Moreover, the experiments where microsomes and test compounds were not included helped to assess any background instability, potentially due to chemical degradation of the compound in the experimental medium and instrumental instability, respectively. The LC-MS peaks resulting from the respective incubations were used to assign putative metabolic biotransformation and metabolites while referring to the parent structure and considering the mass difference pattern.

Regarding **2a/GMP-23**, incubation in HLM in the presence of NADPH showed two additional LC-MS peaks with [M+H] = 401, a mass difference of 14Da relative to the parent compound (**Figure 4.2b**). This pattern, consistent with the loss of a methyl group, was not discernible neither at the start of the incubation nor in the incubation lacking NADPH; a clear indication that it is most likely a metabolic transformation that required CYPP450 catalysis. Background and instrumental instability were ruled out based on the absence of similar profiles in the incubations in which microsomes and test compounds were excluded.

LC-MS analysis of the incubation of **2a/GMP-23** in MLM, interestingly, displayed only one additional peak and not two as seen with the HLM incubation. This peak maintained the 14Da mass difference pattern, suggesting, again, a mono-dealkylation process (**Figure 4.2c**). Examining the retention times of the peaks, both HLM and MLM produce the same metabolite that shows a peak at 2.5 minutes. This is most probably one of the de-alkylation metabolites arising from the removal of one of the methyl groups in the pyrimidyl side group. The other metabolite, which elutes at 3.2 minutes and is observed only in HLM, is likely the other de-alkylation product caused by removal of the other methyl group (**Figure 4.2**). It appears that MLM are not capable of performing this transformation at the tested conditions. These observations further support the disparity in metabolism between species as reflected in the overall metabolic stability between HLM and MLM as discussed earlier.

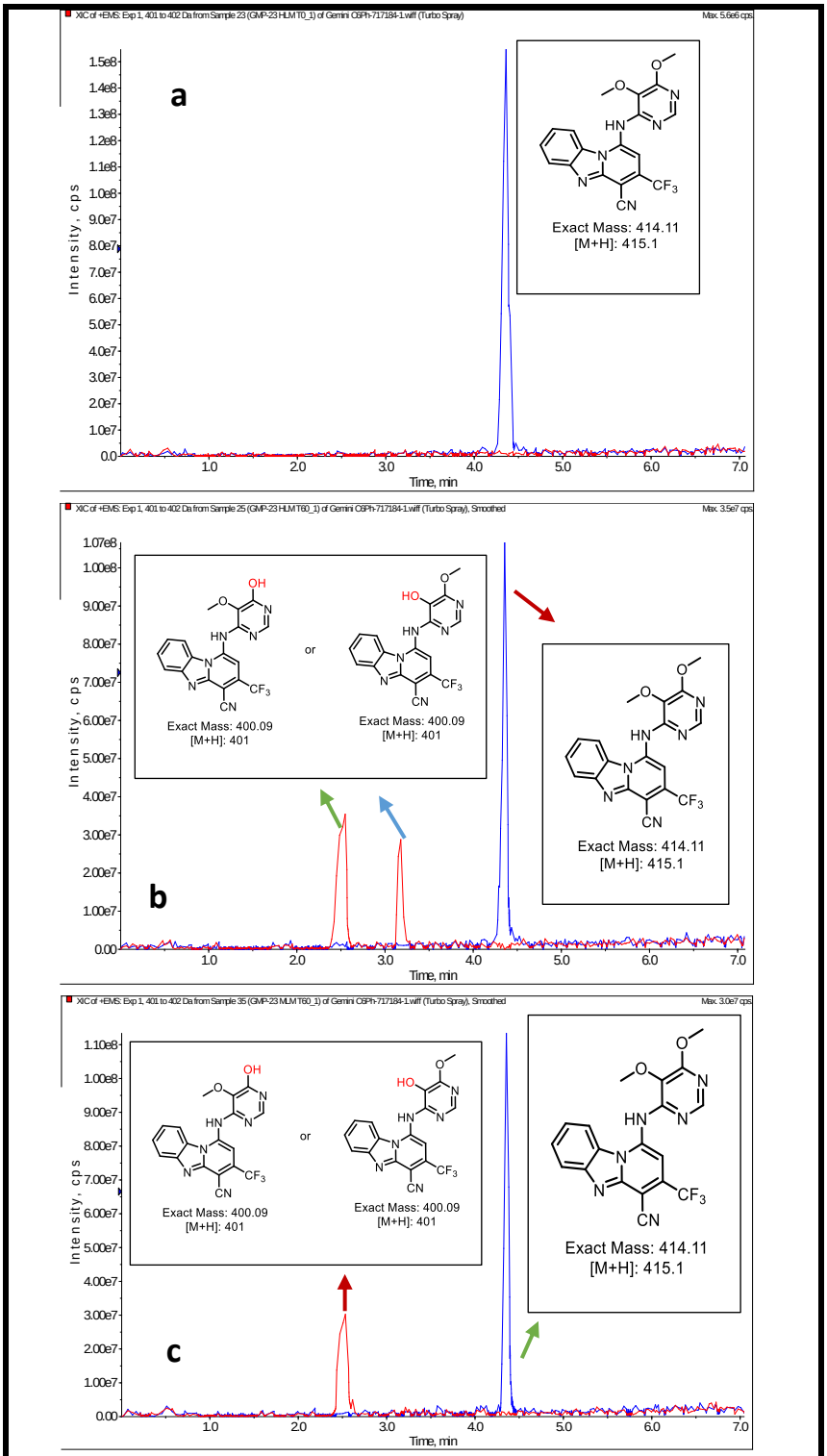

***Figure 4.2**: Extracted ion chromatogram for a) **2a/GMP-23** [M+H]=415 at T0 before incubation with HLM and b) **2a/GMP-23** [M+H]=415 and its two mono-dealkylation metabolites, each with [M+H]=401, at T60 and c) **2a/GMP-23** and its one mono-delakylation metabolite after incubation with MLM for 60 minutes.*

On the other hand, metabolite identification studies of **2e/GMP-58** revealed the major metabolite peak, in HLM, with a positive mass difference pattern of 17Da relative to the parent compound; indicative of a hydroxylation transformation (**Figure 4.3b**). Other minor peaks which were more polar compared to the parent compound, based on the retention times, could not be rationalised as their concentrations were insufficient for detection. The peaks could possibly be due to additional hydroxylation metabolites arising from changes to the PBI core or the pyrazinyl side group (**Figure 4.3b**).

In contrast to HLM, the peak corresponding to an additional mass of 17Da was the only visible signal with no additional minor peaks in MLM (**Figure 4.3c**). The observed metabolite peaks, including the minor ones in MLM, were not present in the incubations that lacked NADPH, test compound or microsomes, further attesting to the fact that they must be CYP450-mediated. Differences in observed profile of metabolites for **2e/GMP-58** between HLM and MLM, again, points to the probability of species differences in the metabolism of these compounds.

To better understand their potential antiparasitic potency, the putative metabolites of **2a/GMP-23** and **2e/GMP-58** described herein would need to be synthesized and tested *in vitro* for their antischistosomal activities.

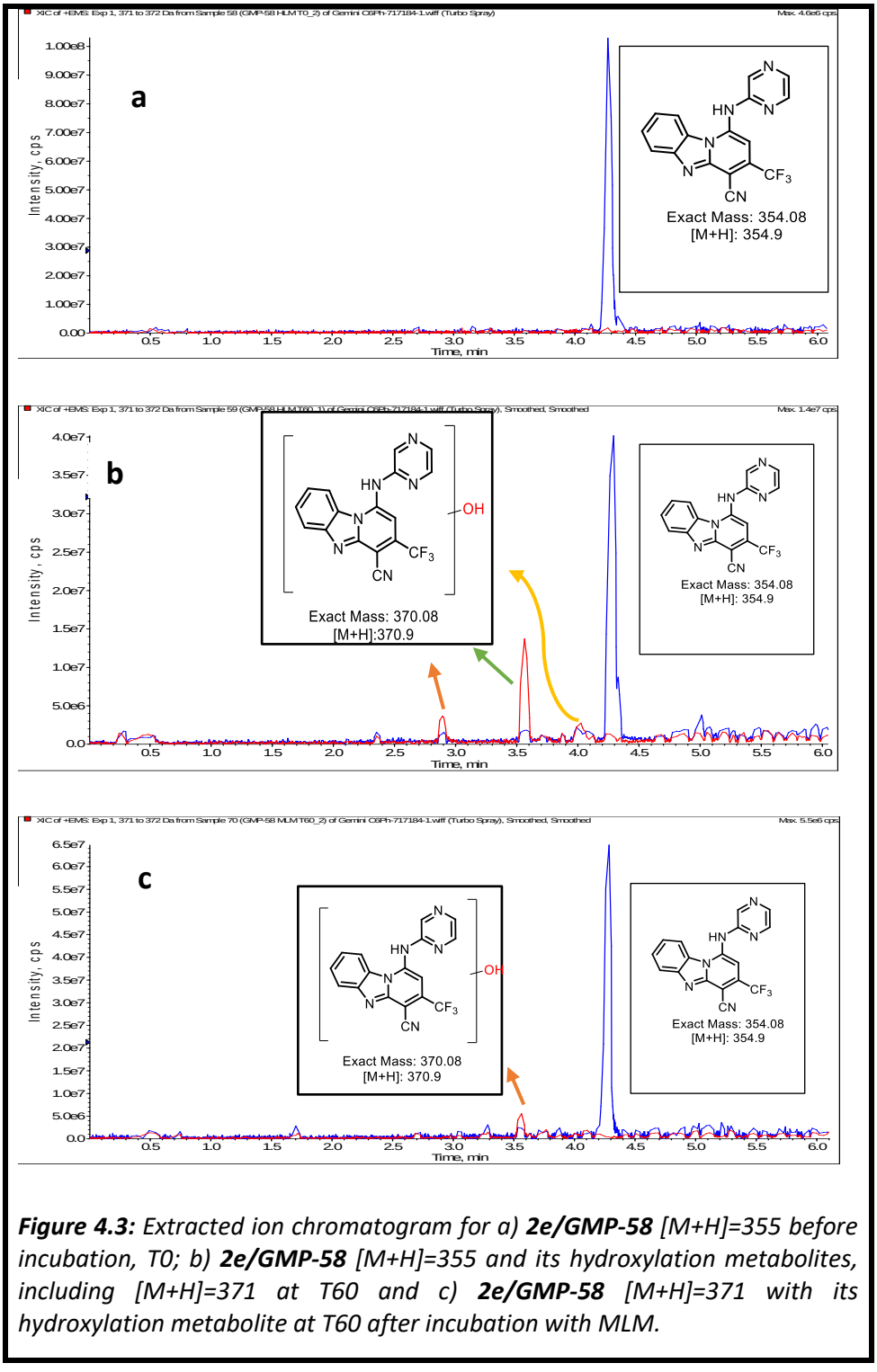

Figure 4.3: *Extracted ion chromatogram for a)* ***2e/GMP-58*** *[M+H]=355 before incubation, T0; b)* ***2e/GMP-58*** *[M+H]=355 and its hydroxylation metabolites, including [M+H]=371 at T60 and c)* ***2e/GMP-58*** *[M+H]=371 with its hydroxylation metabolite at T60 after incubation with MLM.*

4.6 *In vivo* efficacy and pharmacokinetics of lead compounds

Compounds were selected for *in vivo* proof-of-concept studies in a mouse model of schistosomiasis based on their *in vitro* potency and acceptable cytotoxicity profile. These experiments were carried out at the Swiss TPH under Prof. Jennifer Keiser. *In vivo* potency was measured based on the degree of worm reduction achieved in infected and treated mice relative to the initial cercarial infection load and comparing with infected but untreated mice, serving as controls. Accordingly, mice were dosed orally 49 days post-infection, with compounds dissolved or suspended in 7% tween 80 and 3% ethanol in water (v/v/v) at 400mg/kg. The dosing schedule coincided with the period at which the juvenile worms used in the infection phase would have matured into adults.[10] Twenty-one days after dosing, mice were sacrificed, dissected and adult worms retrieved from the mesenteric and hepatic portal blood vessels. The harvested worms were sexed, examined for lethal effects and the percent worm reduction for tested compounds determined. The results are as presented in **Table 4.5**.

Table 4.5: *In vivo efficacy of lead compounds.*

Compound Number/Code	Structure	Female Worm Reduction (%)	Total Worm Reduction (%)
1b/GMP-09	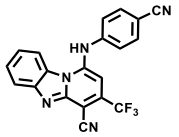	54	55
1i/GMP-18	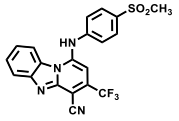	40	38
1j/GMP-19	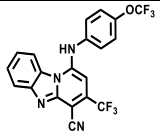	66	62
2a/GMP-23	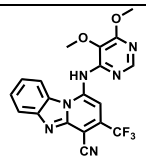	0	0
2b/GMP-30	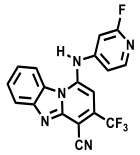	40	38
2c/GMP-31	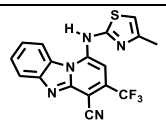	42	41
2e/GMP-58	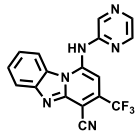	36	38
4g/GMP-71	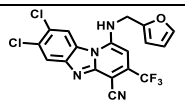	nd	30
4h/GMP-72	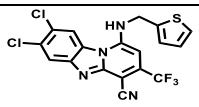	nd	41
4i/GMP-75	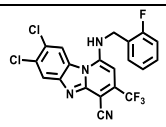	nd	69
4j/GMP-76	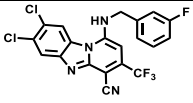	nd	60
nd: not determined			

Of the eleven compounds tested, **2a/GMP-23** failed to induce any *in vivo* effect, **1i/GMP-18**, **2b/GMP-30**, **2c/GMP-31, 2e/GMP-58**, **4g/GMP-71** and **4h/GMP-72** all produced slight (30-42%) reduction in worm burden while significant (>50%) reduction in worms was realised with **1b/GMP-09**, **1j/GMP-19**, **4i/GMP-75** and **4j/GMP-76**. Overall, the best efficacy was obtained with **1j/GMP-19, 4i/GMP-75** and **4j/GMP-76** that resulted in total worm reduction between 60-70%. It is notable that compounds bearing heteroaromatic side chains (**2a/GMP-23**, **2b/GMP-30**, **2c/GMP-31, 2e/GMP-58**, **4g/GMP-71**, and **4h/GMP-72**) generally produced low *in vivo* efficacy.

Expectedly, there was a trend towards poor activity for compounds that had shown low metabolic stability and higher activity for those with better metabolic stability. Although praziquantel has a short half-life, the drug displays potent activity due to active metabolites.[11] It is likely the metabolically unstable compounds encountered in this study are transformed to metabolites with decreased or no antischistosomal activity.

Furthermore, it is also probable that physicochemical hurdles are responsible, at least in part, for the low or lack of *in vivo* activity of some compounds such as **2a/GMP-23**. Compound **2a/GMP-23** is likely poorly absorbed, a hypothesis supported by a negative human intestinal absorption (HIA) index score predicted by Stardrop™ software; all other compounds were predicted to have a positive HIA score. Moreover, suboptimal bioavailability may be the reason for the lower efficacy of otherwise *in vitro* potent compounds with outstanding metabolic stability, such as **1j/GMP-19, 4i/GMP-75 and 4j/GMP-76**.

Pharmacokinetics experiments carried out on two representative compounds, **1j/GMP-19** and **4i/GMP-75**, as described previously in **Chapter 3**, confirmed that there was limited systemic exposure of these compounds following oral administration. Despite the low bioavailability of 1-2% at the oral dose of 20mg/kg used in the PK studies, the systemic exposure attained concentrations (0.3-1.1 µM) that match the *in vitro* IC_{50} values of the two compounds (0.21-0.38 µM). At the higher dosing schedule of 400mg/kg adopted for the efficacy studies, it is conceivable that systemic exposure did not increase proportionately with the dose.

Solubility-limited absorption, as further suggested by the delayed peaking of plasma compound concentrations, is a potential phenomenon contributing to the suboptimal efficacy of these compounds. Based on the low *in vivo* clearance and length of time above *in vitro* IC_{50} concentration for these compounds, improved bioavailability through modulation of solubility could potentially translate into enhanced efficacy of this series.

4.7 Conclusion

In conclusion, this chapter has described the antischistosomal properties of the target compounds generated in this study. Based on *in vitro* potency against the newly transformed schistosomula and adult worms, analysis of SAR trends has identified features compatible with good activity. Generally, electron-withdrawing groups as substituents on the aromatic appendage were favourable for potent activity. The aniline series generally provided more active compounds in the absence of changes on the LHS, compared to the benzylamine series. It was notable that changes on the LHS of the PBI scaffold restored the activity of previously inactive benzylamine series analogues.

As observed for the antimalarial properties of these compounds, there was no correlation between the ability of these compounds to interfere with the BHI process and their antischistosomal potency, and that introducing changes on the LHS diminished the selectivity of these compounds. Similarly, attempts to change the nitrile on the pyridyl portion of the PBI core was detrimental to antischistosomal activity. *In vitro* ADME evaluation indicated that heteroatoms in the structures of target compounds rendered them more susceptible to metabolism.

Arising from *in vivo* efficacy studies on selected compounds, good antischistosomal activities were displayed by **1j/GMP-19**, **4i/GMP-75** and **4j/GMP-76** which produced 60-70% worm burden reduction. Pharmacokinetics hurdles, especially solubility-limited absorption was identified as a likely contributing factor for the sub-optimal potency achieved by the lead compounds as was microsomal metabolic instability.

4.8 References

(1) Tchoubrieva, E. B.; Ong, P. C.; Pike, R. N.; Brindley, P. J.; Kalinna, B. H. Vector-Based RNA Interference of Cathepsin B1 in *Schistosoma mansoni*. *Cell. Mol. Life Sci.* **2010**, *67* (21), 3739–3748.

(2) Neves, B. J.; Dantas, R. F.; Senger, M. R.; Melo-Filho, C. C.; Valente, W. C. G.; de Almeida, A. C. M.; Rezende-Neto, J. M.; Lima, E. F. C.; Paveley, R.; Furnham, N.; Muratov, E.; Kamentsky, L.; Carpenter, A. E.; Braga, R. C.; Silva-Junior, F. P.; Andrade, C. H. Discovery of New Anti-Schistosomal Hits by Integration of QSAR-Based Virtual Screening and High Content Screening. *J. Med. Chem.* **2016**, *59* (15), 7075–7088.

(3) Panic, G.; Vargas, M.; Scandale, I.; Keiser, J. Activity Profile of an FDA-Approved Compound Library against *Schistosoma mansoni*. *PLoS Negl. Trop. Dis.* **2015**, *9* (7), e0003962.

(4) Neves, B. J.; Braga, R. C.; Bezerra, J. C. B.; Cravo, P. V. L.; Andrade, C. H. *In silico* Repositioning-Chemogenomics Strategy Identifies New Drugs with Potential Activity against Multiple Life Stages of *Schistosoma mansoni*. *PLoS Negl. Trop. Dis.* **2015**, *9* (1), e3435.

(5) Wang, W.; Wang, L.; Liang, Y.-S. Susceptibility or Resistance of Praziquantel in Human Schistosomiasis: A Review. *Parasitol. Res.* **2012**, *111* (5), 1871–1877.

(6) Rollinson, D.; Knopp, S.; Levitz, S.; Stothard, J. R.; Tchuem Tchuenté, L.-A.; Garba, A.; Mohammed, K. A.; Schur, N.; Person, B.; Colley, D. G.; Utzinger, J. Time to Set the Agenda for Schistosomiasis Elimination. *Acta Trop.* **2013**, *128* (2), 423–440.

(7) Manneck, T.; Haggenmüller, Y.; Keiser, J. Morphological Effects and Tegumental Alterations Induced by Mefloquine on Schistosomula and Adult Flukes of *Schistosoma mansoni*. *Parasitology* **2010**, *137*, 85–98.

(8) Keiser, J.; Vargas, M.; Rubbiani, R.; Gasser, G.; Biot, C. *In vitro* and *in vivo* Antischistosomal Activity of Ferroquine Derivatives. *Parasit. Vectors* **2014**, *7*, 424.

(9) González Cabrera, D.; Douelle, F.; Younis, Y.; Feng, T. S.; Le Manach, C.; Nchinda, A. T.; Street, L. J.; Scheurer, C.; Kamber, J.; White, K. L.; Montagnat, O. D.; Ryan, E.; Katneni, K.; Zabiulla, K. M.; Joseph, J. T.; Bashyam, S.; Waterson, D.; Witty, M. J.; Charman, S. A.;

Wittlin, S.; Chibale, K. Structure-Activity Relationship Studies of Orally Active Antimalarial 3,5-Substituted 2-Aminopyridines. *J. Med. Chem.* **2012**, *55*, 11022–11030.

(10) Siqueira, L. da P.; Fontes, D. A. F.; Aguilera, C. S. B.; Timóteo, T. R. R.; Ângelos, M. A.; Silva, L. C. P. B. B.; de Melo, C. G.; Rolim, L. A.; da Silva, R. M. F.; Neto, P. J. R. Schistosomiasis: Drugs Used and Treatment Strategies. *Acta Trop.* **2017**, *176*, 179–187.

(11) da Silva, V. B. R.; Campos, B. R. K. L.; de Oliveira, J. F.; Decout, J.-L.; do Carmo Alves de Lima, M. Medicinal Chemistry of Antischistosomal Drugs: Praziquantel and Oxamniquine. *Bioorg. Med. Chem.* **2017**, *25* (13), 3259–3277.

Chapter 5

Physicochemical Profiling of Pyrido [1,2-*a*] benzimidazoles

5.1 Chapter overview

This chapter will describe the physicochemical profile of the target compounds produced in this thesis. Consequently, structure-property correlations will be investigated towards establishing effects of structural changes on various physicochemical attributes. At the onset, the chapter will present solubility of the compounds based on an array of experimental and *in silico* methods. Subsequently, other physicochemical properties including lipophilicity and melting point will be described and interrelationships between the various physical and chemical characteristics for the project compounds investigated. Moreover, the profiled attributes will be compared to recommended classical medicinal chemistry references for leads projected to possess good drug metabolism and pharmacokinetics properties.

The chapter will also discuss the relationships between the physicochemical parameters of these compounds and their corresponding biological activities previously described in **Chapters 3** and **4**. At the end, the chapter will compare the physicochemical profile of the study compounds with that of marketed drugs and leads in antimalarial and antischistosomal drug discovery and development to identify any overlapping or diverging chemical spaces.

5.2 Solubility

5.2.1 Introduction

As alluded to previously, solubility is a key physicochemical property with pivotal significance in drug discovery and as such, its determination and optimisation of leads for this property early in the drug discovery continuum is paramount.[1,2] There are various methods used to measure solubility whose choice depends on factors such as turn-around time, throughput, cost and the stage reached in drug discovery and development. Generally, the two categories are thermodynamic and kinetic solubility.[1,3]

Thermodynamic solubility refers to the solubility of a compound in an aqueous media and is devoid of co-solvent effects. As such, the compound is directly dissolved in the aqueous solution and an equilibrium established between the dissolved and undissolved compound. Expectedly, this method provides more accurate evaluation of the solubility of a compound considering that an aqueous medium, simulating *in vivo* physiological conditions, is used. A downside of this method, however, is that it is time- consuming and is not amenable to high throughput.[3]

Conversely, in kinetic solubility, the compound is first pre-dissolved in an organic solvent, commonly DMSO, in which the compound is completely soluble. Subsequent dilutions are then prepared from the stock using an aqueous buffer.

In the initial phases of drug discovery projects, kinetic solubility is usually applied due to its higher throughput and lower costs compared to thermodynamic solubility assay. With a faster turn-around time, kinetic solubility generates data that can be used to interrogate biological data from *in vitro* bio-assays and allow for structure-solubility trends to be extracted.[4,5] Thermodynamic solubility, however, is considered superior and more meaningful further down the drug discovery pipeline when the crystalline nature of the compound is expected to have been characterised and its impact on solubility and other PK parameters established.

The thermodynamic solubility of a lead is critical in guiding *in vivo* experiments and formulation strategies including filing of regulatory applications for late discovery and early stage drug development.[6]

Based on molecular characteristics of compounds such as melting point and lipophilicity, equations and algorithms have also been developed to enable calculation or *in silico* prediction of solubility.[7–9] Application of these computational tools can be time saving and enable quicker ranking and selection of compounds deemed to possess favourable physicochemical properties.

In this research, solubility of the target compounds was evaluated using multiple methods comprising kinetic solubility based on the turbidimetric and HPLC-based methods as well as through *in silico* prediction tools and by employing general solubility equations initially proposed by Yalkowsky.[1]

5.2.2 Turbidimetric-based kinetic solubility determination

The turbidimetric assay is a kinetic solubility-based approach in which spectrophotometry is employed to determine solubility due to the turbidity that arises when the solubility limit of a compound is exceeded.[10] Accordingly, compounds were first dissolved in an organic solvent, DMSO, and diluted using potassium phosphate buffer, adjusted to pH 7.4, to yield a range of concentrations (0-200 µM). After equilibrating for two hours at ambient temperature, the optical density readings were recorded from which concentration-absorbance graphs were constructed using Microsoft® excel. From the plotted graphs, the concentration at which the curve deflected above the baseline was considered as the upper limit of solubility for the compound.

As part of a quality control check for the assay, two compounds representing a highly soluble drug (hydrocortisone) and a poorly soluble drug (reserpine) were used as controls (**Figure 5.1**). The hydrocortisone graph shows the lines remaining at baseline throughout the concentration range, implying the high solubility of the compound.

On the contrary, in the case of reserpine, whereas the line corresponding to the DMSO incubation remains at baseline, the corresponding aqueous buffer incubation line deflects from the baseline at barely 5 µM, reflecting the poor solubility of the compound (**Figure 5.1**).

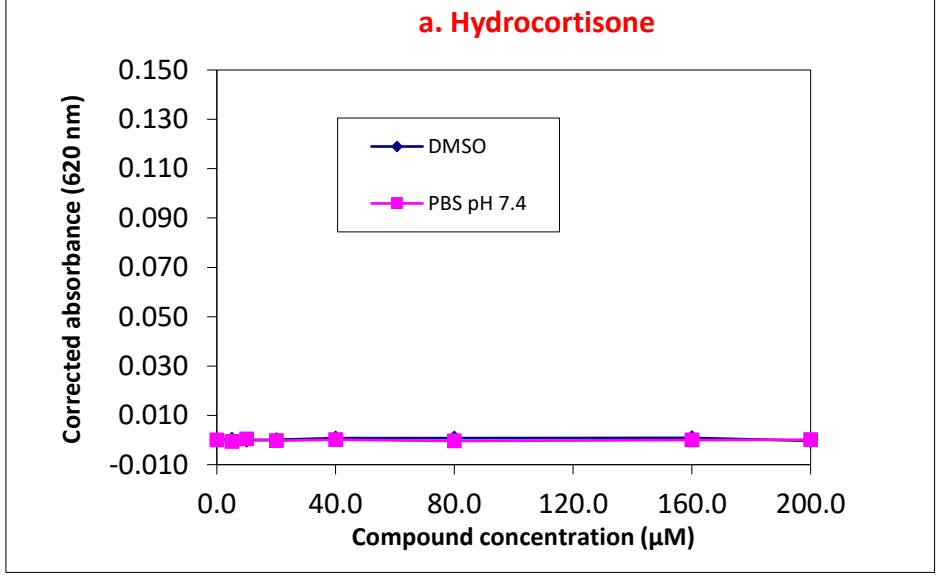

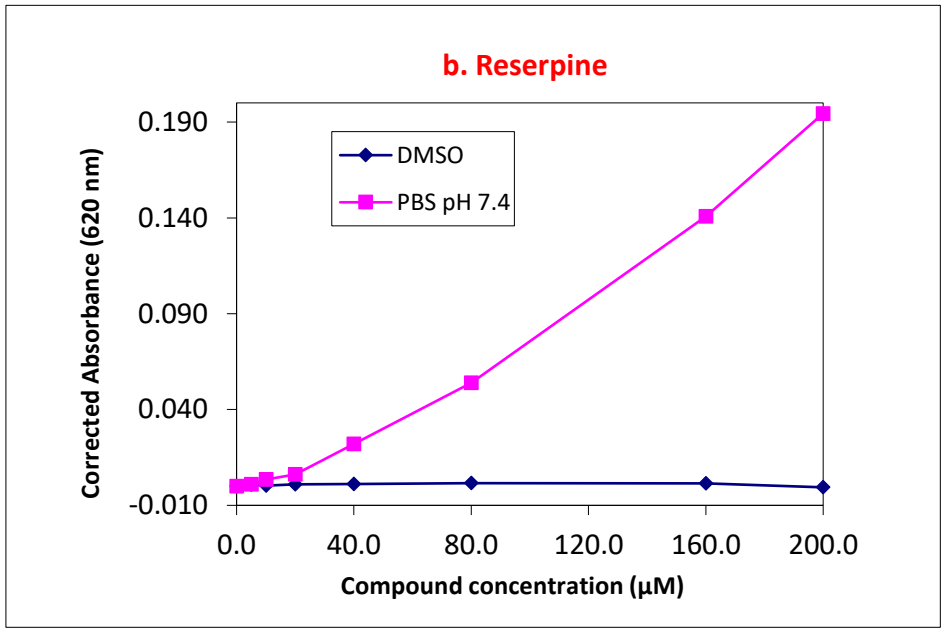

Figure 5.1: *Solubility graphs for (a) hydrocortisone and (b) reserpine in DMSO (blue line) and aqueous buffer pH 7.4 (purple line) using the turbidimetric-based kinetic solubility method.*

The solubility of test compounds was therefore determined as described above and the point of deviation from the baseline in the aqueous buffer incubation taken to represent the limit of solubility (**Table 5.1**).

5.2.3 HPLC-based kinetic solubility determination

Even though turbidimetric-based assays are relatively fast and less laborious to perform, with generally higher throughput, the presence of DMSO in the test samples modify their solubility.[11] To mitigate these solvent effects, a modified version of the turbidimetric solubility, incorporating a HPLC-based approach to determining the amount of compound dissolved, was pursued.

In this approach, first, a standard curve is constructed using low, medium and high concentrations of each test compound. Subsequently, assay samples are prepared as in the turbidimetric assay; however, a key difference is in drying off the DMSO followed by reconstitution of the ensuing solid sample material in aqueous buffer, a step which eliminates the enhancement of solubility due to DMSO. Re-dissolved samples were thereafter incubated at 37 ℃ with shaking for 30 minutes, after which the supernatant was filtered off and the concentration of dissolved sample determined by HPLC, with UV detection, against the previously constructed standard curve.

5.2.5 Solubility using General Solubility Equations (GSE)

The melting point and lipophilicity of a compound can be used to calculate the solubility of the compound according to general solubility equations, the first of which was proposed by Yalkowsky.[8]

$$\text{Log S} = 0.5 - \text{logP} - 0.01\,(\text{Tm} - 25) \quad \textbf{1}$$

$$\text{Log S} = 3.513 - 0.010\text{Tm} - 1.112\text{logP} \quad \textbf{2}$$

$$\text{Log S} = 0.16 - 0.63\text{clogP} - 0.0062\text{Mwt} + 0.066\text{nRB} - 0.74\text{AP} \quad \textbf{3}$$

Figure 5.2: *Solubility equations as proposed by (**1**) Yalkowsky[8], (**2**) Wang et al.,[1] and (**3**) Delaney.[9] LogP is the lipophilicity; Tm is the melting point in °C; Mwt. Is molecular weight; nRB is the number of rotatable bonds and AP is the aromatic proportion defined as the number of aromatic atoms ÷ total number of atoms in a molecule, excluding hydrogen atoms.*

The melting point reflects the strength of intermolecular forces, hence a measure of crystallinity within the compound, that would need to be broken prior to the solvation and dissolving of a compound by solvent molecules. Consequently, higher melting point compounds are generally predicted to have lower solubility. On the other hand, the lipophilicity of a compound is indicative of the likelihood for the compound to associate with an organic phase as opposed to an aqueous phase. Appropriately, compounds with higher lipophilicity (high clogP values) are generally less soluble.

The Yalkowsky equation (**Equation 1, Figure 5.2**) and some subsequent variations to it, such as those proposed by Wang and colleagues (**Equation 2, Figure 5.2**) were sampled to calculate the solubility of compounds generated in this project and the data obtained recorded in **Table 5.1**. In another modified solubility equation advanced by Delaney (**Equation 3**, **Figure 5.2**), molecular weight, clogP, number of rotatable bonds and aromatic proportion, have been explored to estimate the solubility of small molecules. This approach is particularly appealing to drug discovery scientists as it allows for quick solubility prediction without recourse to measuring any of the molecule descriptors employed in the equation as these can be readily

generated by various accessible software. Using this method, the solubility of compounds in this project were also calculated (**Table 5.1**).

Table 5.1: *Solubility of project compounds using assorted solubility methods.*[a]

Compound structure and Number/Code			Experimental		*In silico*			Calculated		
			T. sol	HPLC Sol.	ChemDraw®	StarDrop®	ChemAxon®	Yalkowsky	Delaney	Wang
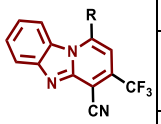	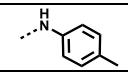	**1a/GMP-06**	<5	<5	1.07	4.61	0.17	0.03	2.84	4.67
	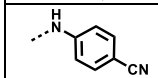	**1b/GMP-09**	5	<5	1.88	2.83	0.30	0.02	6.61	5.05
	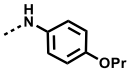	**1c/GMP-10**	10	<5	0.52	3.49	0.13	0.12	1.99	17.63
	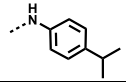	**1d/GMP-11**	5	<5	0.19	1.63	0.02	0.03	0.84	3.70
	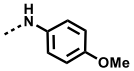	**1e/GMP-12**	20	<5	2.14	10.14	0.56	0.15	7.26	28.49
	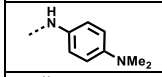	**1f/GMP-13**	5	<5	1.00	11.07	0.89	0.11	4.24	18.82
	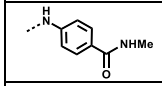	**1g/GMP-15**	<5	<5	1.86	7.09	0.45	0.54	16.30	126
	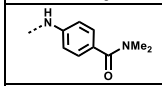	**1h/GMP-17**	10	<5	1.86	20.94	0.46	1.15	9.90	254
	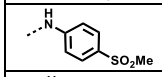	**1i/GMP-18**	5	<5	0.71	2.99	1.17	1.66	16.85	413
	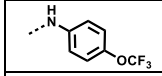	**1j/GMP-19**	20	<5	0.11	2.52	0.03	0.004	0.44	0.52
	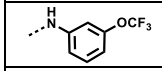	**1k/GMP-121**	20	5	0.11	2.52	0.03	7.76	0.44	992
	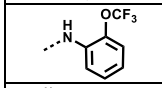	**1l/GMP-122**	20	<5	2.22	2.52	0.03	7.76	0.44	992
	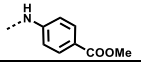	**1m/GMP-20**	10	-	1.18	3.42	0.36	-	4.86	-

Compound structure and Number/Code			Experimental		*In silico*			Calculated		
			T. sol	HPLC Sol.	ChemDraw®	StarDrop®	ChemAxon®	Yalkowsky	Delaney	Wang
	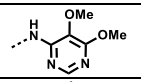	**2a/GMP-23**	80	6.4	13.15	9.59	0.62	8.13	21.04	1970
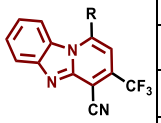	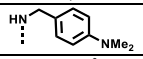	**3a/GMP-24**	20	<5	0.94	9.62	1.26	1.91	6.03	365
	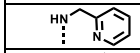	**3j/GMP-25**	20	<5	13.96	9.12	6.31	13.18	50.62	3479
	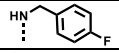	**3b/GMP-28**	20	<5	1.24	1.99	0.40	0.87	6.47	165
		**3c/GMP-29**	20	<5	4.99	6.96	7.08	12.30	18.11	2781
	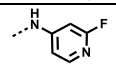	**2b/GMP-30**	20	<5	7.94	1.80	0.85	-	14.88	-
	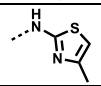	**2c/GMP-31**	20	17	7.96	15.74	1.00	0.74	11.85	157
		**1n/GMP-32**	20	<5	2.43	8.35	0.51	0.17	6.95	31
	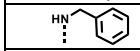	**3d/GMP-33**	20	<5	2.37	9.15	0.71	1.23	9.97	242
	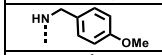	**3e/GMP-34**	20	<5	2.02	8.18	0.79	2.09	10.20	428
	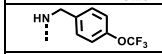	**3f/GMP-35**	20	<5	0.11	2.23	0.04	0.03	0.61	3.34
	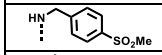	**3g/GMP-36**	10	<5	0.71	2.82	1.70	12.02	23.56	3189
	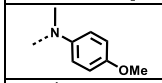	**1o/GMP-37**	20	<5	0.76	7.61	0.47	2.29	4.50	417
	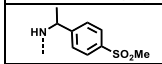	**3h/GMP-38**	10	<5	0.28	1.72	0.85	4.57	10.99	1090
	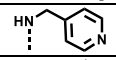	**3k/GMP-43**	20	<5	15.74	9.12	10.47	18.20	56.84	4901
	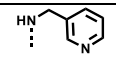	**3l/GMP-44**	20	<5	15.74	9.12	10.47	7.59	56.84	2043
	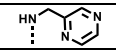	**3i/GMP-45**	20	<5	4.65	10.72	93.32	125.89	292.93	45503
	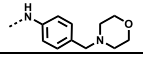	**1p/GMP-46**	20	<5	2.15	11.48	1.58	2.09	4.47	415

Compound structure and Number/Code			Experimental		*In silico*			Calculated		
			T. sol	HPLC Sol.	ChemDraw®	StarDrop®	ChemAxon®	Yalkowsky	Delaney	Wang
	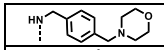	**3m/GMP-47**	20	<5	2.12	14.09	2.34	2.75	5.66	582
	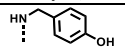	**3n/GMP-48**	20	<5	3.43	11.67	1.95	0.26	12.79	56.03
	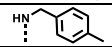	**3o/GMP-50**	10	<5	1.03	5.00	0.23	0.30	4.00	51
	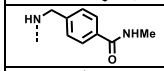	**3p/GMP-52**	20	<5	1.83	8.61	0.63	6.17	22.78	1541
	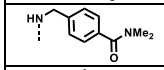	**3q/GMP-53**	20	<5	1.83	23.23	0.66	1.29	14.00	304
	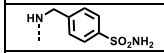	**3r/GMP-54**	20	<5	1.82	25.76	1.41	13.49	32.90	3806
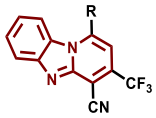	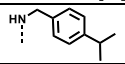	**3s/GMP-55**	10	<5	0.18	1.78	0.03	0.06	1.17	8.61
	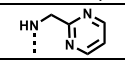	**3t/GMP-56**	20	-	76.38	10.72	18.20	-	57.70	-
	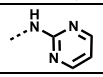	**2d/GMP-57**	20	21	29.79	8.17	2.00	3.63	41.42	926
		**2e/GMP-58**	20	<5	1.95	10.26	31.62	5.75	97.48	1709
		**3u/GMP-77**	160	27	63.39	345.14	26.92	56.23	142.35	16837
	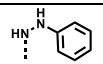	**3v/GMP-87**	5	-	0.50	-	0.54	93.33	-	15763
	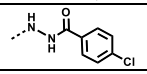	**3w/GMP-88**	10	-	0.12	-	0.06	162.18	-	29142
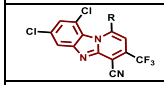	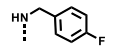	**4a/GMP-62**	5	<5	0.05	0.28	0.02	0.008	0.45	1.13
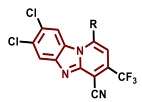	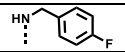	**4b/GMP-66**	5	<5	0.05	0.26	0.02	0.04	0.45	4.81
	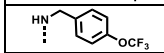	**4c/GMP-67**	<5	<5	0.004	0.49	0.002	0.85	0.04	84.95
		**4d/GMP-68**	5	<5	0.55	1.07	0.30	309	3.55	59687
	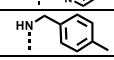	**4e/GMP-69**	5	<5	0.04	0.60	0.01	6.92	0.28	873

Compound structure and Number/Code			Experimental		*In silico*			Calculated		
			T. sol	HPLC Sol.	ChemDraw®	StarDrop®	ChemAxon®	Yalkowsky	Delaney	Wang
	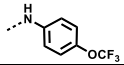	**4f/GMP-70**	<5	-	0.004	0.54	0.001	0.48	0.03	44.79
	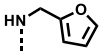	**4g/GMP-71**	5	<5	0.98	1.47	0.12	0.22	3.23	41.17
	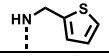	**4h/GMP-72**	5	<5	0.33	1.17	0.03	0.03	0.74	4.45
	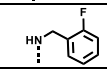	**4i/GMP-75**	10	<5	0.05	0.26	0.02	0.03	0.45	3.82
	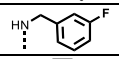	**4j/GMP-76**	5	5	0.05	0.26	0.02	0.03	0.45	4.10
	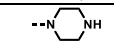	**4k/GMP-81**	40	-	2.51	49.20	1.23	-	9.83	-
	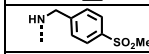	**4l/GMP-96**	80	<5	0.03	0.58	0.10	2.46	1.65	477
	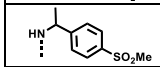	**4m/GMP-97**	40	<5	0.01	0.36	0.05	0.34	0.75	59.18
	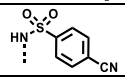	**4n/GMP-98**	20	<5	0.03	1.09	0.02	0.16	0.81	29.14
	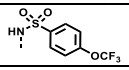	**4o/GMP-99**	10	<5	0.002	1.47	0.002	0.02	0.05	2.23
	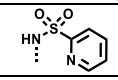	**4p/GMP-100**	20	<5	0.25	2.74	0.13	-	2.15	-
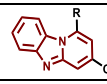	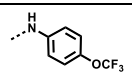	**5a/GMP-120**	5	<5	0.07	1.00	0.04	5.62	0.47	693
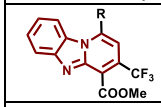	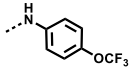	**5e/GMP-120E**	5	<5	0.11	1.87	0.03	5.50	0.32	675
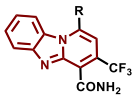	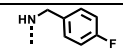	**5b/GMP-128**	40	<5	0.19	11.25	0.54	9.33	26.24	2297
	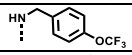	**5c/GMP-129**	40	<5	24.95	9.47	0.05	1.17	2.44	207
	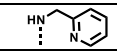	**5d/GMP-130**	80	5	1.07	23.78	8.32	338	205.82	116016

[a]All solubility values are in µM. T.sol: Turbidimetric solubility; HPLC Sol: solubility as determined by the HPLC-based DMSO "dry-down" method as described in the text.

5.2.4 *In silico* prediction of solubility

Structural features of a compound have a bearing on the overall solubility profile of the molecule. Based on this, solubility can be predicted by establishing the contribution of different portions of the molecule to solubility.[12] Utilising this information and by applying various algorithms, *in silico* solubility prediction can be performed. Several software have been developed in drug discovery for predicting physicochemical properties including solubility.[13] In this thesis, ChemDraw®[14], StarDrop™[15] and ChemAxon®[16] were utilised to predict solubility of the library set. All solubility values were converted into µM to allow for direct comparisons among the different solubility-determination approaches applied in this project (**Table 5.1**).

5.2.6 Comparisons of solubility from the different approaches

5.2.6.1 Experimental methods

As can be seen in **Table 5.1**, there were evident disparities in the solubility values of the compounds across the range of solubility methods employed. Within the experimentally determined solubility category, solubility readings from the turbidimetric method were generally either comparable to or higher than those obtained from the HPLC-based DMSO "dry-down" approach. This trend is not surprising given the expected solubility-enhancement effects in the turbidimetric assay due to the co-solvent effects of DMSO in which the test compounds were initially dissolved.[12] Nonetheless, turbidimetric solubility remained useful in providing estimated solubility and general overview of the ranking of compounds with respect to their solubility to facilitate analysis of structure-solubility relationships trends. Based on this method, most of the compounds displayed low solubility (≤20 µM).

The removal of DMSO in the HPLC-based method, hence annulling the possible solubility-enhancement effects of the organic solvent, allows for a more accurate recapitulation of the inherent solubility of compounds in aqueous media. Most of the compounds displayed low solubility (< 5 µM) with only **2a/GMP-23** (6 µM), **2c/GMP-31** (17 µM), **2d/GMP-57** (21 µM) and **3u/GMP-77** (27 µM) displaying solubility above 5 µM.

5.2.6.2 Computational methods

Computational models for predicting solubility depend of algorithms and compound training sets used to develop and validate them.[17,18] Consequently, variations are expected in the solubility values as predicted from different platforms consistent with the diversity in the chemical spaces occupied by compounds utilised in developing the respective models. Comparing the three computational platforms evaluated in this project, higher solubility values were generally obtained with StarDrop® whereas ChemAxon® returned the lowest predicted solubility for most of the compounds (**Figure 5.3**). Notably, the general solubility trend held across the three software wherein the compounds predicted to have high and low solubility values were largely the same with few exceptions.

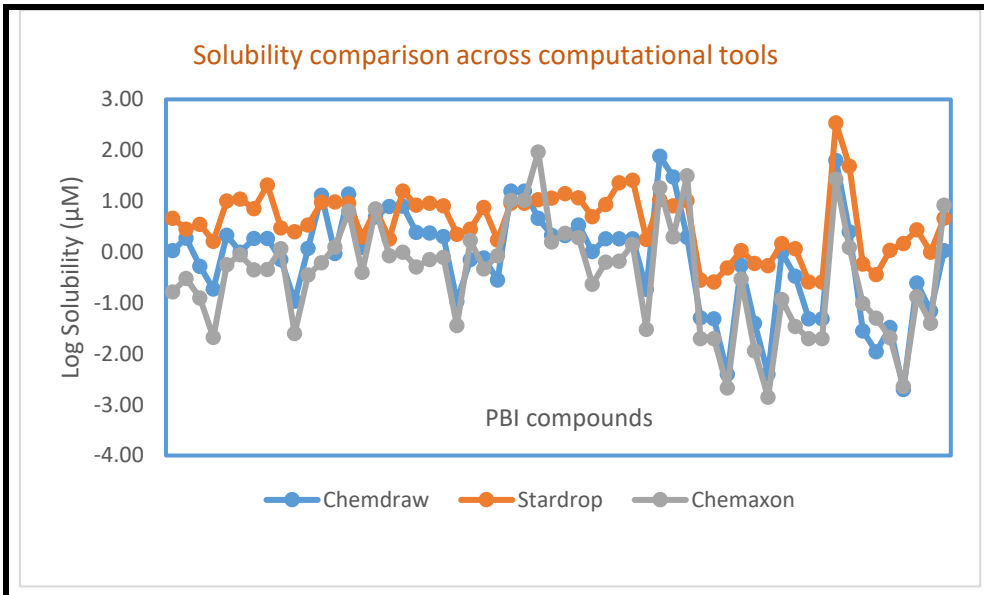

Figure 5.3: *In silico predicted solubility based on ChemDraw®, StarDrop® and ChemAxon® software.*

5.2.6.3 General solubility equations

As with computational tools, the solubility equations are based on algorithms such as linear regression models developed using variable compound data sets. Based on established relationships between various physicochemical properties and their influence on solubility, different parameters are accorded varying levels of significance in the algorithm. Thus, suitability of a solubility equation depends on the set of compounds used to develop, train and validate the model. Furthermore, the accuracy of the solubility values used in generating the models will also influence the performance of the solubility algorithms in predicting the solubility of a new data set of small molecules.[9]

In comparing the three solubility equations explored in calculating solubility of target compounds, the model by Wang and co-workers consistently predicted higher solubility. The Yalkowsky equation generally produced the least predicted solubility, often comparing more closely with the values from Delaney than those from Wang and colleagues (**Figure 5.4**).

In contrast to the other general solubility equations, the model proposed by Delaney obviates the need for experimental determination of physicochemical parameters. The descriptors included in the equation (Molecular weight, clogP, number of rotatable bonds and aromatic proportion) may be visualised as incorporating components that influence both the lipophilicity and melting point of a compound as contained in the other two solubility equations.

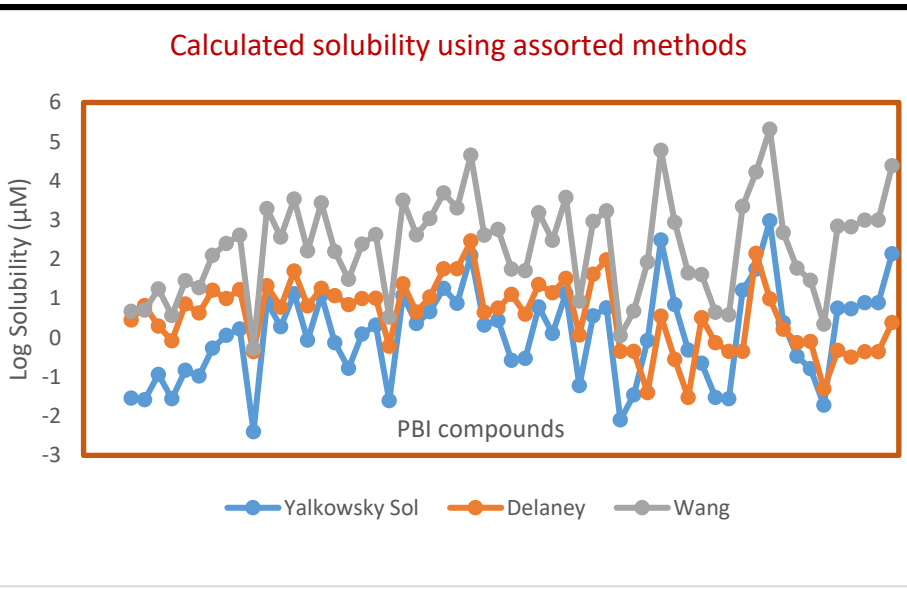

Figure 5.4: *Calculated solubility from different general solubility equations.*

In applying solubility equations to assess solubility, the ionizability of a compound is generally ignored to simplify the calculation. This, in effect, may lead to the under prediction of the true solubility of ionisable compounds. Overall, however, despite discrepancies in absolute solubility values, there was a general trend towards a uniform solubility pattern that would give the same ranking of compounds irrespective of the approach used.

5.3 Lipophilicity and Melting point of target compounds

5.3.1 Lipophilicity

As described previously, lipophilicity and melting point are primary characteristics useful in estimating other secondary characteristics such as solubility. Besides experimental determination of logP, computational tools are frequently applied to establish lipophilicity of compounds.[19–21] Furthermore, experimental parameters such as the retardation factor based on analytical Thin Layer Chromatography and the retention times on HPLC can be used as surrogates of hydrophobicity and polarity of compounds. For instance, using gradient HPLC, the lipophilicity of several compound sets has been determined.[5,22,23]

For this assessment, the clogP was computed using ChemAxon®. Additionally, HPLC-based retention times and the retardation factor profile based on analytical TLC on silica adsorbed on alumina and using a uniform mobile phase were used to compare the hydrophobicity of the compound series (**Table 5.2**).

The series demonstrated a wide range in their lipophilicity property (clogP=1.83 to 7.07) with most compounds having a clogP ≤ 5. Unsurprisingly, compounds incorporating heteroatoms in the side appendage (e.g., **3i/GMP-45**) had lowered clogP. Similarly, incorporating sulfonyl linkages (such as in **4o/GMP-99**) was observed to reduce lipophilicity over analogues that comprised methylene linkers (e.g. **4c/GMP-67**). Moreover, **SAR$_3$** targets (**5b/GMP-128**, **5c/GMP-129** and **5d/GMP-130**) that incorporated an amide moiety instead of a nitrile, had favourable clogP values.

5.3.2 Melting point

Other physicochemical properties were profiled for the compound series such as melting point. The melting point of molecules is dependent on the strength of intramolecular and intermolecular interactions with stronger forces requiring more energy to break up the solid lattice and thus higher melting points.[24] The compound data set displayed generally high melting points with most compounds melting above 200 °C.

Arising from the planar architecture imparted by the pyridobenzimidazole (PBI) core, these molecules can be envisaged as having potential for strong π-π interactions that would require more energy to break the crystal arrangement. Structural changes around the PBI appendages can be explored to disrupt this crystal packing and lower the melting point. For instance, introducing a methyl substitution on the nitrogen attached to the PBI core in **3j/GMP-25** (258 ℃) and **3e/GMP-34** (240℃) resulted in analogues **3c/GMP-29** (201℃) and **1o/GMP-37** (190℃), respectively, which have decreased melting points. The methyl substituents can potentially limit the stacking in the molecules by reducing the ability of these compounds to assume flat conformations (**Figure 5.5**).

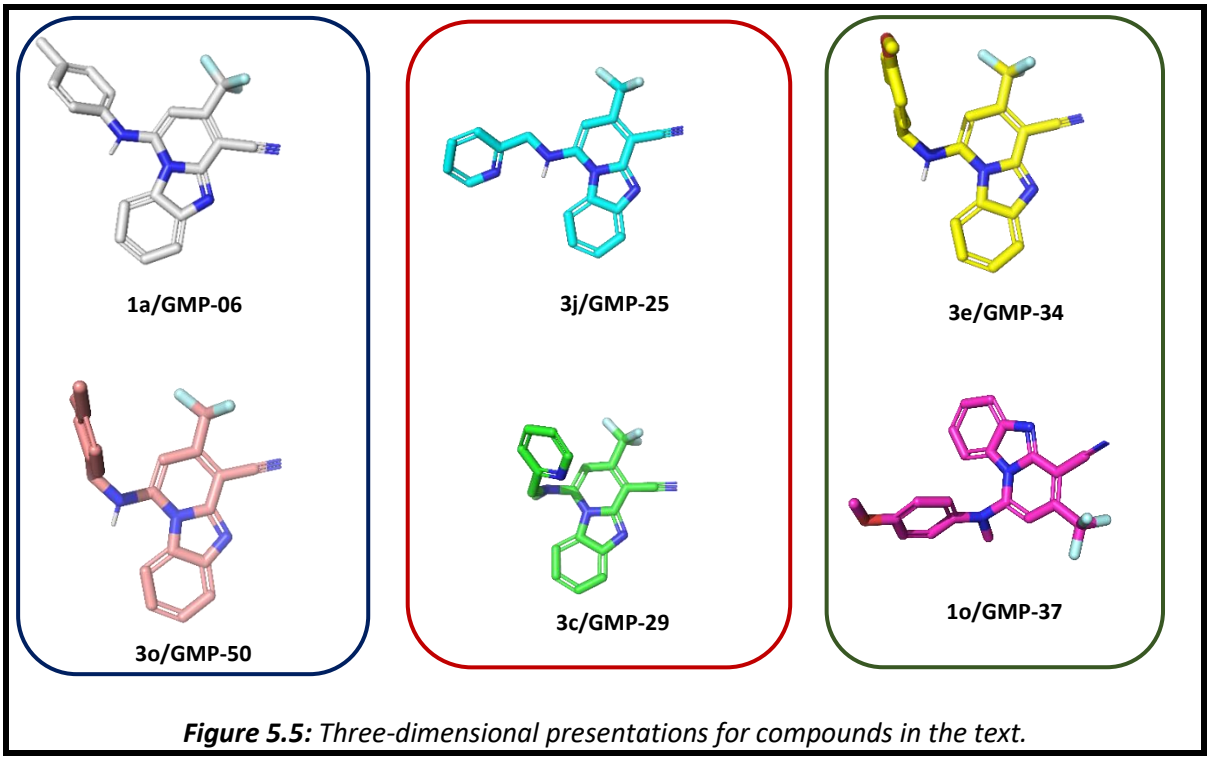

Figure 5.5: *Three-dimensional presentations for compounds in the text.*

Benzylamine analogues that differed from their aniline-type series counterparts only in having a methylene linker generally showed lower melting points. For example, in comparing the following pairs: **1a/GMP-06** (335 ℃) vs **3o/GMP-50** (258 ℃) ; **1e/GMP-12** (331 ℃) vs **3e/GMP-34** (240 ℃) ; **1f/GMP-13** (319 ℃) vs **3a/GMP-24** (218 ℃); **1g/GMP-15** (352 ℃) vs **3p/GMP-52** (270℃) and **1n/GMP-32** (310℃) vs **3d**/**GMP-33** (248℃), all the benzylamine series displayed reduced melting points over their aniline series analogues. The benzylamine series are expected to display greater molecular flexibility compared to the aniline series compounds as depicted by the three-dimensional structures of **1a/GMP-06** and **3o/GMP-50** in **Figure 5.5**. The methylene linker in benzylamine analogues, therefore, might contribute to disruption of planarity resulting in the observed decrease in melting point.

Hydrophilic substituents on the aromatic side group produced compounds with high melting points (for example **3n/GMP-48**, 345 ℃) most likely due to the potential for intermolecular hydrogen bonding, requiring more energy to break apart. Regio-isomerism on the side group appendage appeared to influence the melting points as seen with **1j/GMP-19** (328 °C), **1k/GMP-121** (287 °C) and **1l/GMP-122** (271°C). It may be hence conjectured that different regio-isomers assume varied crystal arrangements requiring different levels of energy to disrupt. Finally, **5a/GMP-120** and **5e/GMP-120E**, the cyano-replacement analogues of **1j/GMP-19** had much lower melting points possibly attributed to weaker intermolecular forces of attraction and reduced capacity for crystal packing.

5.4 Evaluation of target compounds for compliance with Lipinski's guideline

Physical and chemical characteristics of drugs can be used to estimate expected pharmacokinetic behaviour during *in vivo* studies. Primary physicochemical descriptors such as the size, topological polar surface area (tPSA), number of hydrogen-bond donors and acceptors and lipophilicity influence the overall physicochemistry and pharmacokinetics of a compound. Good oral absorption and bioavailability is expected for a compound that complies with Lipinski's guidelines, based on predefined descriptors, as previously discussed.[23,25,26]

Physicochemical attributes of compounds generated in this study were computed using ChemAxon® and output parameters compared with reference values advanced by Lipinski (**Table 5.2**). To follow is an assessment of compliance of the compound data set with the widely accepted medicinal chemistry criteria for good oral absorption.

Table 5.2: *Physicochemical profile and Lipinski compliance profile of target compounds.*

Compound structures		Compound Number/Code	Mw.	logP	HBD	HBA	HBA+HBD	TPSA	RB	Lipinski Compliance	MP (℃)	HPLC Retention time	TLC Rf
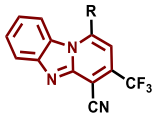	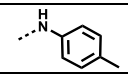	**1a/GMP-06**	366.35	4.94	1	3	4	53.12	3	Yes	335	3.223	0.53
	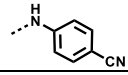	**1b/GMP-09**	377.33	4.28	1	4	5	76.91	3	Yes	>405	3.154	0.42
	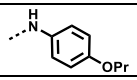	**1c/GMP-10**	410.40	5.15	1	4	5	62.35	6	No	254	3.297	0.47
	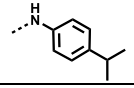	**1d/GMP-11**	394.40	5.67	1	3	4	53.12	4	No	264	3.338	0.58
	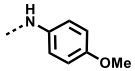	**1e/GMP-12**	382.35	4.27	1	4	5	62.35	4	Yes	331	3.112	0.42
	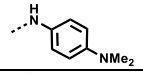	**1f/GMP-13**	395.39	4.54	1	4	5	56.36	4	Yes	319	3.086	0.42
	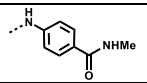	**1g/GMP-15**	409.37	3.50	2	4	6	82.22	4	Yes	352	3.045	0.08
	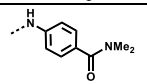	**1h/GMP-17**	423.40	3.73	1	4	5	73.43	4	Yes	296	2.950	0.08
	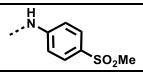	**1i/GMP-18**	430.41	3.27	1	5	6	87.26	4	Yes	326	3.025	0.13
	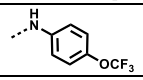	**1j/GMP-19**	436.32	5.86	1	4	5	62.35	5	No	328	3.461	0.42
	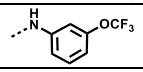	**1k/GMP-121**	436.32	5.86	1	4	5	62.35	5	No	287	3.540	0.33
	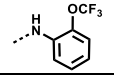	**1l/GMP-122**	436.32	5.86	1	4	5	62.35	5	No	271	3.463	0.40
	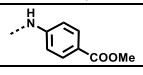	**1m/GMP-20**	410.36	4.43	1	4	5	79.42	5	Yes	-	3.267	0.34

Compound structures		Compound Number/Code	Mw.	logP	HBD	HBA	HBA+HBD	TPSA	RB	Lipinski Compliance	MP (℃)	HPLC Retention time	TLC Rf
	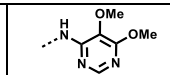	**2a/GMP-23**	414.35	3.38	1	7	8	97.36	5	Yes	246	3.011	0.256
	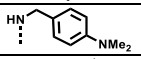	**3a/GMP-24**	409.42	4.29	1	4	5	56.36	5	Yes	218	3.202	0.42
		**3j/GMP-25**	367.34	3.05	1	4	5	66.01	4	Yes	258	3.062	0.42
	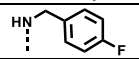	**3b/GMP-28**	384.34	4.33	1	3	4	53.12	4	Yes	248	3.040	0.36
	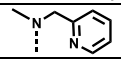	**3c/GMP-29**	381.36	3.65	0	4	4	57.22	4	Yes	201	2.879	0.31
	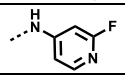	**2b/GMP-30**	371.30	3.75	1	4	5	66.01	3	Yes	ND	3.154	0.28
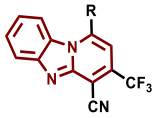	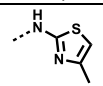	**2c/GMP-31**	373.36	3.90	1	4	5	66.01	3	Yes	298	3.114	0.11
	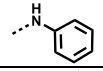	**1n/GMP-32**	352.32	4.43	1	3	4	53.12	3	Yes	310	3.249	0.28
	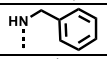	**3d/GMP-33**	366.35	4.18	1	3	4	53.12	4	Yes	248	3.070	0.28
	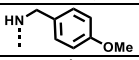	**3e/GMP-34**	396.37	4.03	1	4	5	62.35	5	Yes	240	3.052	0.50
	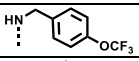	**3f/GMP-35**	450.34	5.62	1	4	5	62.35	6	No	274	3.241	0.44
	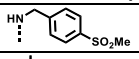	**3g/GMP-36**	444.43	3.03	1	5	6	87.26	5	Yes	264	2.751	0.14
	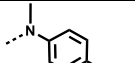	**1o/GMP-37**	396.37	4.49	0	4	4	53.56	4	Yes	190	3.032	0.64
	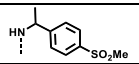	**3h/GMP-38**	458.46	3.44	1	5	6	87.26	5	Yes	265	2.795	0.19
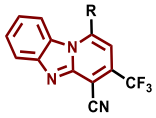	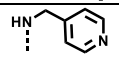	**3k/GMP-43**	367.34	2.97	1	4	5	66.01	4	Yes	252	2.774	0.03
	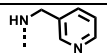	**3l/GMP-44**	367.34	2.97	1	4	5	66.01	4	Yes	290	2.898	0.06
	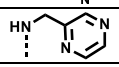	**3i/GMP-45**	368.32	1.83	1	5	6	78.90	4	Yes	282	2.871	0.22

Compound structures		Compound Number/Code	Mw.	logP	HBD	HBA	HBA+HBD	TPSA	RB	Lipinski Compliance	MP (℃)	HPLC Retention time	TLC Rf
	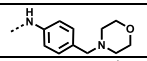	**1p/GMP-46**	451.45	4.15	1	5	6	65.59	5	Yes	228	2.927	0.06
	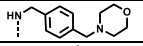	**3m/GMP-47**	465.48	3.91	1	5	6	65.59	6	Yes	240	2.867	0.06
	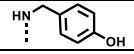	**3n/GMP-48**	382.35	3.88	2	4	6	73.35	4	Yes	345	2.996	
	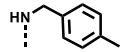	**3o/GMP-50**	380.37	4.70	1	3	4	53.12	4	Yes	258	3.266	0.42
	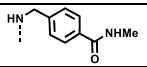	**3p/GMP-52**	423.40	3.26	2	4	6	82.22	5	Yes	270	2.684	0.06
	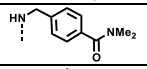	**3q/GMP-53**	437.43	3.48	1	4	5	73.43	5	Yes	316	2.989	0.08
	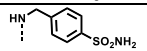	**3r/GMP-54**	445.42	2.79	2	5	7	113.28	5	Yes	283	2.621	0.06
	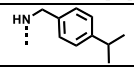	**3s/GMP-55**	408.43	5.43	1	3	4	53.12	5	No	254	3.396	0.44
	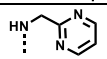	**3t/GMP-56**	368.32	2.95	1	5	6	78.90	4	Yes	-	3.089	0.32
	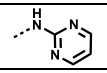	**2d/GMP-57**	354.30	3.18	1	5	6	78.90	3	Yes	301	3.050	0.22
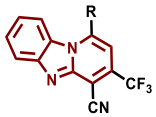		**2e/GMP-58**	354.30	2.59	1	5	6	78.90	3	Yes	340	3.187	0.22
	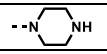	**3u/GMP-77**	345.33	2.56	1	4	5	56.36	2	Yes	244	2.576	0.07
	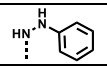	**3v/GMP-87**	367.34	4.78	2	4	6	65.15	4	Yes	264	3.379	0.79
	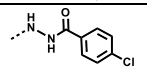	**3w/GMP-88**	429.79	4.54	2	4	6	82.22	4	Yes	273	3.141	0.20
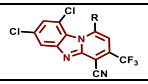	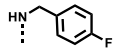	**4a/GMP-62**	453.22	5.54	1	3	4	53.12	4	No	330	3.107	0.66
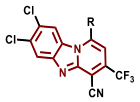	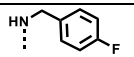	**4b/GMP-66**	453.22	5.54	1	3	4	53.12	4	No	267	3.389	0.59
	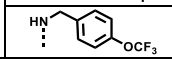	**4c/GMP-67**	519.23	6.82	1	4	5	62.35	6	No	270	3.569	0.52

Compound structures		Compound Number/Code	Mw.	logP	HBD	HBA	HBA+HBD	TPSA	RB	Lipinski Compliance	MP (℃)	HPLC Retention time	TLC Rf
	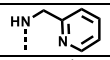	**4d/GMP-68**	436.22	4.26	1	4	5	66.01	4	Yes	-	2.940	0.55
	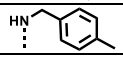	**4e/GMP-69**	449.26	5.91	1	3	4	53.12	4	No	-	3.153	0.55
	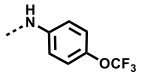	**4f/GMP-70**	505.20	7.07	1	4	5	62.35	5	No	-	3.730	0.54
	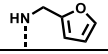	**4g/GMP-71**	425.19	4.45	1	3	4	66.26	4	Yes	295	2.954	0.52
	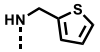	**4h/GMP-72**	441.25	5.31	1	3	4	53.12	4	No	296	3.597	0.52
	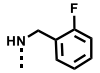	**4i/GMP-75**	453.22	5.54	1	3	4	53.12	4	No	277	3.168	0.52
	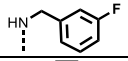	**4j/GMP-76**	453.22	5.54	1	3	4	53.12	4	No	275	3.095	0.52
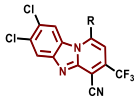	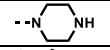	**4k/GMP-81**	414.21	3.77	1	4	5	56.36	2	Yes	-	2.925	0.79
	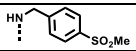	**4l/GMP-96**	513.32	4.23	1	5	6	87.26	5	No	213	3.036	0.27
	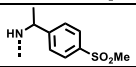	**4m/GMP-97**	527.34	4.65	1	5	6	87.26	5	No	257	3.046	0.40
	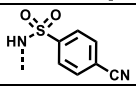	**4n/GMP-98**	510.27	4.54	1	5	6	111.05	3	No	>300	3.180	0.42
	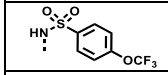	**4o/GMP-99**	569.26	6.11	1	5	6	96.49	5	No	237	3.347	0.47
	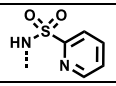	**4p/GMP-100**	486.25	4.06	1	5	6	100.15	3	Yes	-	3.098	0.38
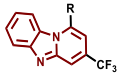	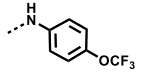	**5a/GMP-120**	411.31	6.00	1	3	4	38.56	5	No	266	3.254	0.33
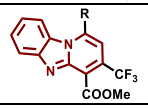	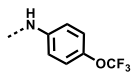	**5e/GMP-120E**	469.34	6.01	1	4	5	64.86	7	No	231	3.686	0.87

Compound structures		Compound Number/Code	Mw.	logP	HBD	HBA	HBA+HBD	TPSA	RB	Lipinski Compliance	MP (℃)	HPLC Retention time	TLC Rf
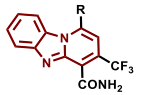	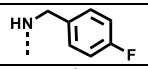	**5b/GMP-128**	402.35	3.32	2	3	5	72.42	5	Yes	246	2.942	0.24
	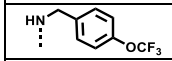	**5c/GMP-129**	468.36	4.61	2	4	6	81.65	7	Yes	225	3.013	0.26
	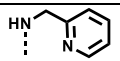	**5d/GMP-130**	385.35	2.04	2	4	6	85.31	5	Yes	218	2.640	0.21
Reference values			≤500	≤5	≤5	≤10	≤12	≤140	≤10				

Mw. Molecular weight (g/mol); **HBD**: Hydrogen bond donor (NH/OH) count; **HBA**: Hydrogen bond acceptor (N/O) count; **LogP**: log of the partition co-efficient between n-octanol and water; **tPSA**: topological polar surface area: all parameters were generated using ChemAxon® software. **MP**-melting point; **HPLC** retention times obtained according to the HPLC conditions described in the experimental section, Chapter 7; **TLC** retardation factor (R_f) as determined using 2%MeoH:DCM mobile phase.

Most compounds (68%) had all the considered physicochemical parameters agreeing with suggested guidelines for sufficient oral absorption and systemic exposure. Of the compounds with violations, 28% failed in only one parameter whereas 3% had two violations with no compound failing beyond two counts. Furthermore, the most violations were regarding lipophilicity (81%) and the remaining non-compliance attributed to molecular weight. Notably, there were more compounds that violated the Lipinski's guidelines arising from **SAR_2** modifications in which changes were performed on the LHS of the PBI scaffold by incorporating two halogen substitutions. This modification had the accompanying effect of increasing the overall molecular weight and lipophilicity of target compounds.

Number of rotatable bonds, which is a measure of the flexibility of a compound and hence impacts solubility and membrane permeation, was generally ≤5 for this series. With 7 rotatable bonds apiece, **5e/GMP-120E** and **5c/GMP-129**, both **SAR_3** targets incorporating an ester and amide groups, respectively had the highest number for this descriptor. It is generally agreed that compounds with less than 10 rotatable are likely to be well absorbed.[27]

The mean topological surface area, a measure of the total surfaces of polar atoms in a molecule, was 68.96±15.43Å^2 with **3r/GMP-54** (113.28Å^2), **4n/GMP-98** (111.05Å^2) and **4p/GMP-100** (100.15Å^2) possessing the highest tPSA (≥100Å^2) while **5a/GMP-120** (38.56Å^2) had the lowest value for this property. Higher tPSA correlates with increased tendency for hydrophilic interactions due to the higher count of heavy atoms (N/O) capable of hydrogen bonding. Very low tPSA is consistent with highly lipophilic molecules for which hydrophobic interactions are predominant. All the studied compounds were compliant with the recommended tPSA range of between 75-140 Å^2.[28,29]

When considering the number of hydrogen bond donors and hydrogen bond acceptors, all target compounds were compliant with the considered criteria. Moreover, the sum of the two properties, preferred not to exceed 12, was also met by all the compounds with no exception. Having the right balance of HBD and HBA atoms in a molecule ensures the correct degree of polarity to facilitate interaction with aqueous media while at the same time imparting appropriate hydrophobicity to membrane permeation towards systemic exposure.[30,31]

Interestingly, the two frontrunner compounds – **1j/GMP-19** and **4i/GMP-75** - which were characterised to possess potent *in vitro* antiplasmodial and antischistosomal activities as well as acceptable *in vitro* drug metabolism and pharmacokinetics profiles, failed to meet the lipophilicity criteria proposed by Lipinski. It is likely that had stringent adherence to the guideline been enforced, these target molecules, which also delivered the most promising *in vivo* efficacy outcomes, would have been filtered off and excluded from downstream assays. This observation affirms the caution with which the physicochemical characteristics should be treated in deciding compound progression in the discovery and development process since indiscriminate enforcement can cause de-prioritisation of otherwise promising target compounds.

Moreover, other pharmacokinetic factors such as *in vivo* biotransformation to active analogues or transporter-mediated absorption need to be considered in view of their impact on bioavailability.[32] There is a consensus that compounds beyond the rule of 5 are worth considering in drug development if they fulfil other critical criteria given the shift in protein targets against which small molecules are being developed. In the advent of the rule of 5, most pharmaceutical industry players focused on aminergic G-protein coupled receptors as drug targets for which the rule of 5 is largely applicable. Protein targets explored after the proposition of the rule of 5 have expanded and may necessitate revisiting the evaluation of physicochemical characteristics that are optimal, some of which may accommodate small molecules beyond the rule of 5.[27,33,34]

5.5 Correlation of physicochemical properties with biological activity

At a molecular level, biological activity is a consequence of the interaction between the ligand (chemical matter) and the protein target such as a receptor. The protein-ligand binding can be mediated by hydrophobic and polar forces, which are influenced by the physicochemical properties of the ligand. Additionally, access to the biological target by the ligand following oral administration (or during *in vitro* whole cell screening), requires the compound to cross biological membranes, a process that demands optimum physicochemical characteristics.

To evaluate the influence of the physicochemical properties of the target compounds on the observed biological activities, various correlations and comparisons were examined and ensuing trends noted as described in the following sections.

5.5.1 Lipophilicity vs antiplasmodial activity

Antiplasmodial activity was generally favoured when lipophilic electron-withdrawing groups were introduced into the appendages to the PBI core. Both lipophilic attributes at SAR_1 and SAR_2 correlated positively with improved antiplasmodial activity. It is plausible that lipophilic characteristics around these portions of the molecules offer beneficial interactions with putative targets in the parasite resulting in the observed antiparasitic activities. As can be seen in **Figure 5.6**, an increase in lipophilicity generally concurred with improved antiplasmodial potency.

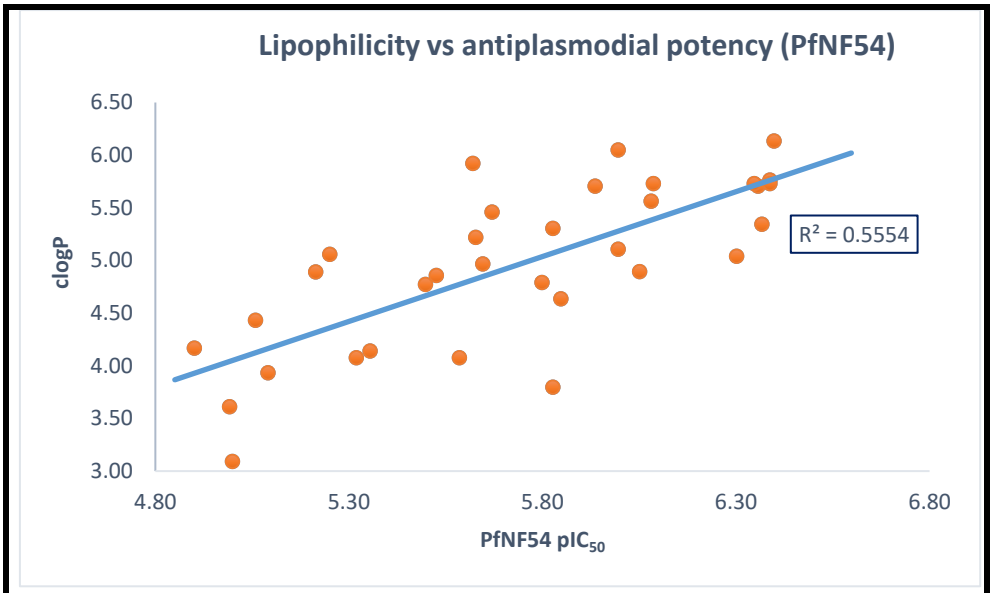

Figure 5.6: *Correlation plot of lipophilicity (clogP) vs PfNF54 potency expressed as -log IC_{50}, µM (pIC_{50}).*

5.5.2 Lipophilicity vs antischistosomal activity

In contrast to the trends observed with antiplasmodial potency of these compounds, there were mixed effects of lipophilicity on the antischistosomal activities of these analogues. On one hand, like compounds with potent antiplasmodial activity, **1j/GMP-19** and **4i/GMP-75** which have high lipophilicity, elicited potent antischistosomal activity. On the other hand, less lipophilic compounds such as **1b/GMP-09** and **1i/GMP-18** as well as those incorporating heteroaromatic groups such as **2a/GMP-23**, **2b/GMP-30**, **2c/GMP-31** and **2e/GMP-58** also maintained potent activity. Based on this observation, it may be presumed that there might be additional targets in *Schistosomes* with which the compounds may be interacting and for which a wider range of lipophilicity may be tolerated. As noted earlier in **Chapter 4**, an interesting observation is the restoration of activity among previously inactive analogues when lipophilic groups were introduced on the LHS of the PBI core**. Figure 5.7** is a correlation plot for lipophilicity vs antischistosomal activity for the analysed set of compounds which, evidently, reveals a lack of correlation between the two properties.

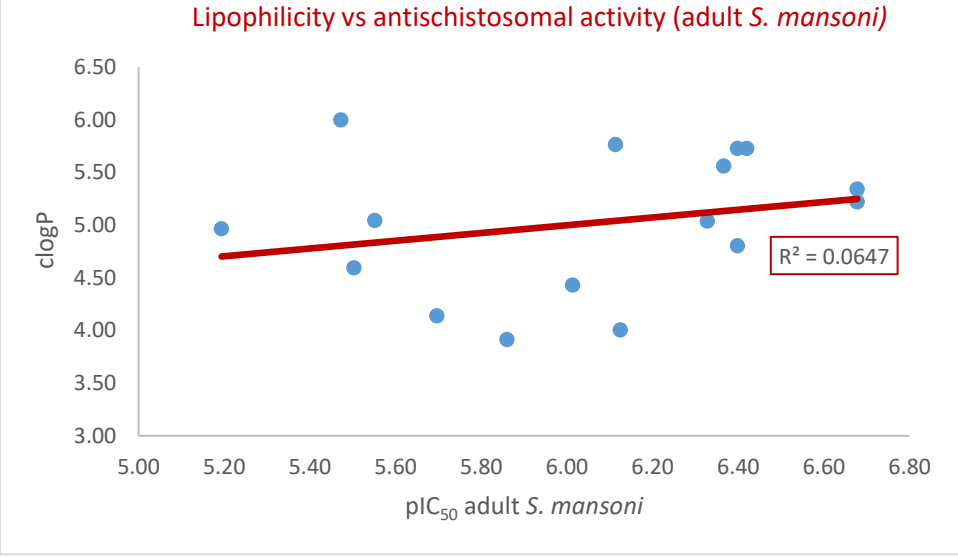

Figure 5.7: *Plot of lipophilicity (clogP) vs adult S. mansoni potency expressed as -logIC$_{50}$, µM (pIC$_{50}$).*

5.5.3 Lipophilicity vs BHI activity

The planar conformation and rigid tricyclic system present in the studied compounds offer favourable attributes for interaction with heme in the inhibition of the hemozoin formation process. Lipophilic π-π interactions between heme and recognized inhibitors of this biochemical pathway prompted the hypothesis that lipophilicity may be an important contributor to the observed BHI potency among some of the compounds.

Overall, there was a mixed profile regarding lipophilicity and BHI activity for these compounds (**Figure 5.8**). Whereas lipophilicity would have been expected to impart better BHI profile, other compound-specific factors, including the overall geometry, may have compromised potential compound-haematin binding interactions thus rendering them poor inhibitors. Additionally, other interactions comprising hydrogen-bonding and electrostatic forces are important contributors to BHI which may have been absent or minimal in the analysed molecules.

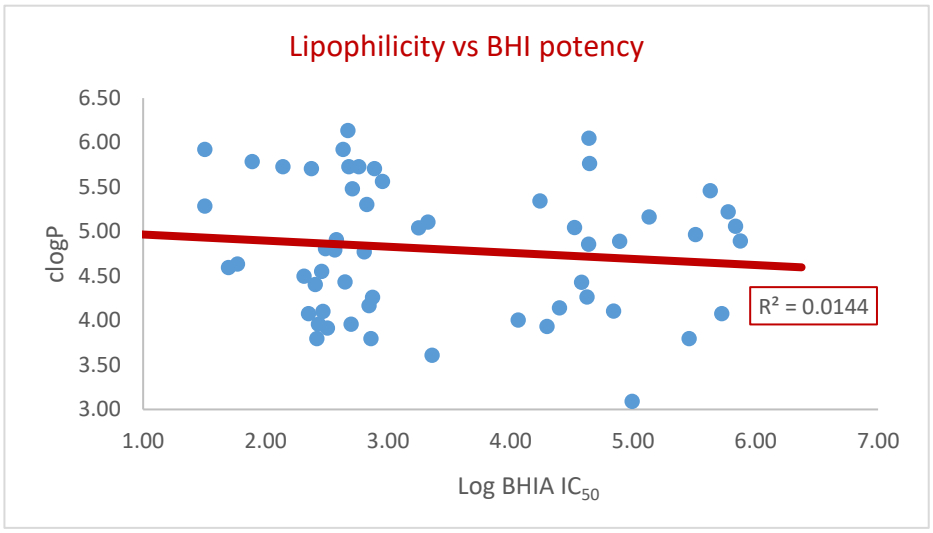

Figure 5.8: *Correlation plot of lipophilicity (clogP) vs BHI activity expressed as log IC_{50} (µM).*

5.5.4 Lipophilicity vs cytotoxicity

Introducing modifications on the LHS of the PBI scaffold, leading to the generation of **SAR_2** analogues, generally attenuated the selectivity of this series. This chemical change has an accompanying increase in lipophilicity due to the additional chlorine atoms in the molecule. High lipophilicity is generally associated with the propensity for indiscriminate binding to tissue proteins and other unintended targets, contributing to off-target toxicity.[35–37] Considering the analysed compounds, a weak correlation is portrayed between lipophilicity and cytotoxicity (**Figure 5.9**).

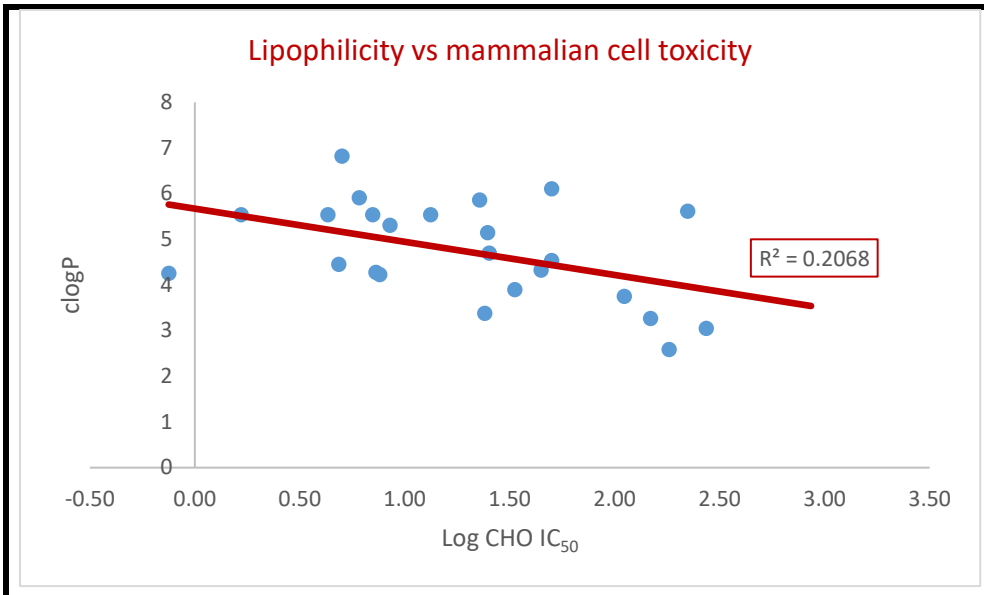

Figure 5.9: *Correlation plot of lipophilicity (clogP) vs mammalian cell toxicity (Log IC_{50}, µM) as examined in the CHO cell line.*

It remains to be investigated whether this toxicity profile is restricted to the nature of substituents (halogens in this case) or is generally driven by lipophilicity. To address this uncertainty, less lipophilic substitutes for the halogens should be evaluated at this position or hydrophilic electron-rich groups explored to reduce the lipophilicity. Resulting target compounds should then be assessed for their cytotoxicity profiles for comparison with the frontrunner compounds.

5.5.5 Lipophilicity vs metabolic stability and human intestinal absorption

5.5.5.1 Lipophilicity vs metabolic stability

In analysing the compounds data set, the more lipophilic drugs such as **1j/GMP-19** and **4i/GMP-75** displayed particularly high metabolic stability whereas the more hydrophilic molecules with lower lipophilicity (**2a/GMP-23**, **2b/GMP-30**, **2c/GMP-31**, **2e/GMP-58**, **4l/GMP-96** and **4m/GMP-97**) showed increased susceptibility to metabolism. This trend may be explained by the fact that the latter subset of compounds which showed decreased metabolic stability generally incorporate heteroatoms in their structures which increase the overall electron density in the molecules, a factor that has been implicated in enhanced metabolism by the CYP450 drug metabolising enzymes. Taken together, the data set displayed a positive correlation between lipophilicity and microsomal metabolic stability in HLM as depicted in **Figure 5.9**. Notably, this correlation is much weaker when considering MLM, probably highlighting species differences in metabolism of these compounds as mentioned previously.

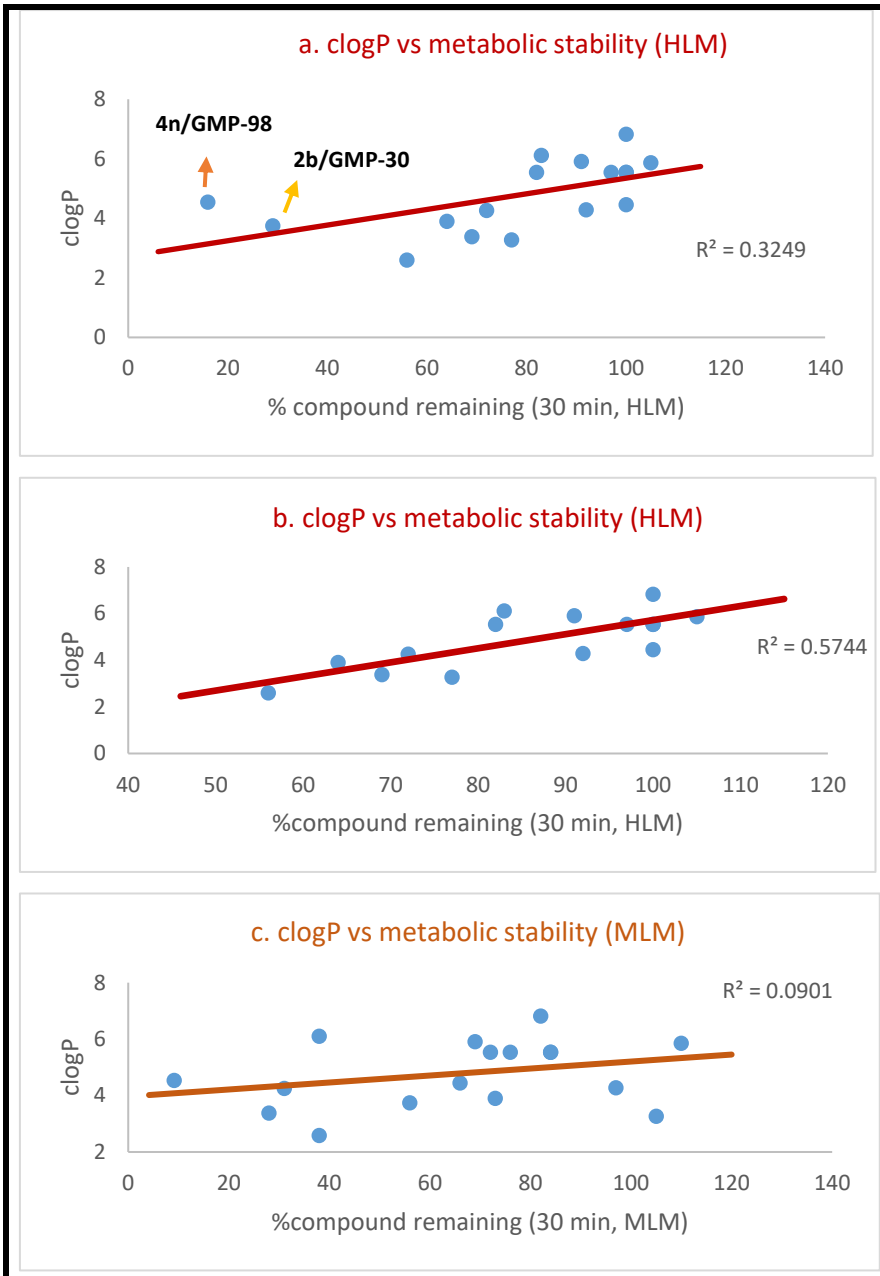

Figure 5.10: *Correlation plots of lipophilicity (clogP) vs metabolic stability expressed as percent compound after 30 minutes in: a) HLM, considering all compounds; b) HLM, with the exclusion of* ***2b/GMP-30*** *and* ***4n/GMP-98*** *and c) MLM, all compounds.*

5.5.5.2 Human intestinal absorption

Drug absorption is dependent on solubility and lipophilicity. Good solubility facilitates solubilisation of a drug prior to intestinal absorption, which is influenced by lipophilicity and size of the molecule. A poorly lipophilic drug will be unable to cross the lipid bilayer membrane whereas a highly lipophilic one may fail to efficiently traverse the hydrophilic interface. An optimal lipophilicity (clogP) of between 3 and 5 is generally deemed requisite for good oral absorption.

This series displayed lipophilicity largely compliant with recommended range with positively predicted human intestinal absorption (Stardrop®) for all compounds except **2a/GMP-23**. The pyrimidyl component of the side chain appendage, which contains two methoxy substituents likely contribute to this predicted poor intestinal absorption. Notably, **2a/GMP-23** failed to induce any *in vivo* efficacy when tested in the mouse model of schistosomiasis, despite having shown good *in vitro* potency; a fate likely attributable to poor absorption and systemic exposure following oral administration. A confirmatory investigation to this hypothesis would require performing pharmacokinetics studies on **2a/GMP-23** to establish its PK profile.

5.5.6 Ligand lipophilic efficiency of compound series

The impact of lipophilicity on biological activity may be further investigated by determining the ligand lipophilicity efficiency (LLE). This matrix evaluates the effect of increasing lipophilicity on the observed potency and is calculated according to **Equation 4** (**Figure 5.11**). The higher the LLE value, the better the compound interacts with the target protein over partitioning into an organic phase. A negative LLE is undesirable and generally implies the need for further potency and physicochemical optimisation to improve the profile of the compound. For leads intended for oral drug administration, a LLE of 5 to 7 is considered suitable.[38–40]

$$LLE = pIC_{50} - clogP \quad \text{.....} \mathbf{4}$$

Figure 5.11: *Ligand lipophilicity equation. LLE: ligand lipophilic efficiency; pIC_{50}: -log IC_{50} (Molar) (PfNF54 or adult S. Mansoni); clogP: calculated lipophilicity.*

This series generally produced compounds with low LLE, the best being **3j/GMP-25** with an LLE of only 2.03 in the antimalarial SAR and **2b/GMP-30** (LLE=2.12) in the antischistosomal SAR. For better pharmacokinetics outcomes, subsequent physicochemical optimisations focussed on reducing the lipophilicity and improving potency, are pertinent.

5.6 Interrelationships between physicochemical parameters

Physicochemical parameters are often interdependent such that modulating one parameter can effectively lead to changes in the other property. Assessing this interdependence can enable determination of the parameter that exerts greater influence towards modifying another property.

Based on the cassette of experimental and predicted physicochemical data of the studied compounds, correlations were analysed towards investigating which properties show interdependence and the nature of the correlation. Some of these relationships are presented in the following sections.

5.6.1 Melting point vs lipophilicity and solubility

Melting point values provide an indication of the strength of interactions within and between molecules of a compound. Molecules that experience strong hydrophobic forces, through for instance π-π stacking, are generally lipophilic. On the contrary, compounds capable of making hydrogen-bonding interactions, although may display high melting points, will have lower lipophilicity due to enhanced polarity.

Since melting points may be suggestive of the crystallinity of a molecule on which solubility depends, some relationship may be expected between melting point and solubility. Highly crystalline compounds require higher solvation energies resulting in lower solubility. However, if the high melting points is due to strong polar forces, the compounds will display high solubility.

In the library of compounds generated, there was neither a correlation between the melting point and lipophilicity nor between melting point and solubility (**Figure 5.12**). High melting points may arise from either an increase in the hydrophobic surface area or increased polarity in molecules, which facilitates hydrogen-bond interactions. This observation, therefore, implies that improvements in solubility or lipophilicity profile of molecules in this series cannot be realised by solely focussing on monitoring melting point patterns.

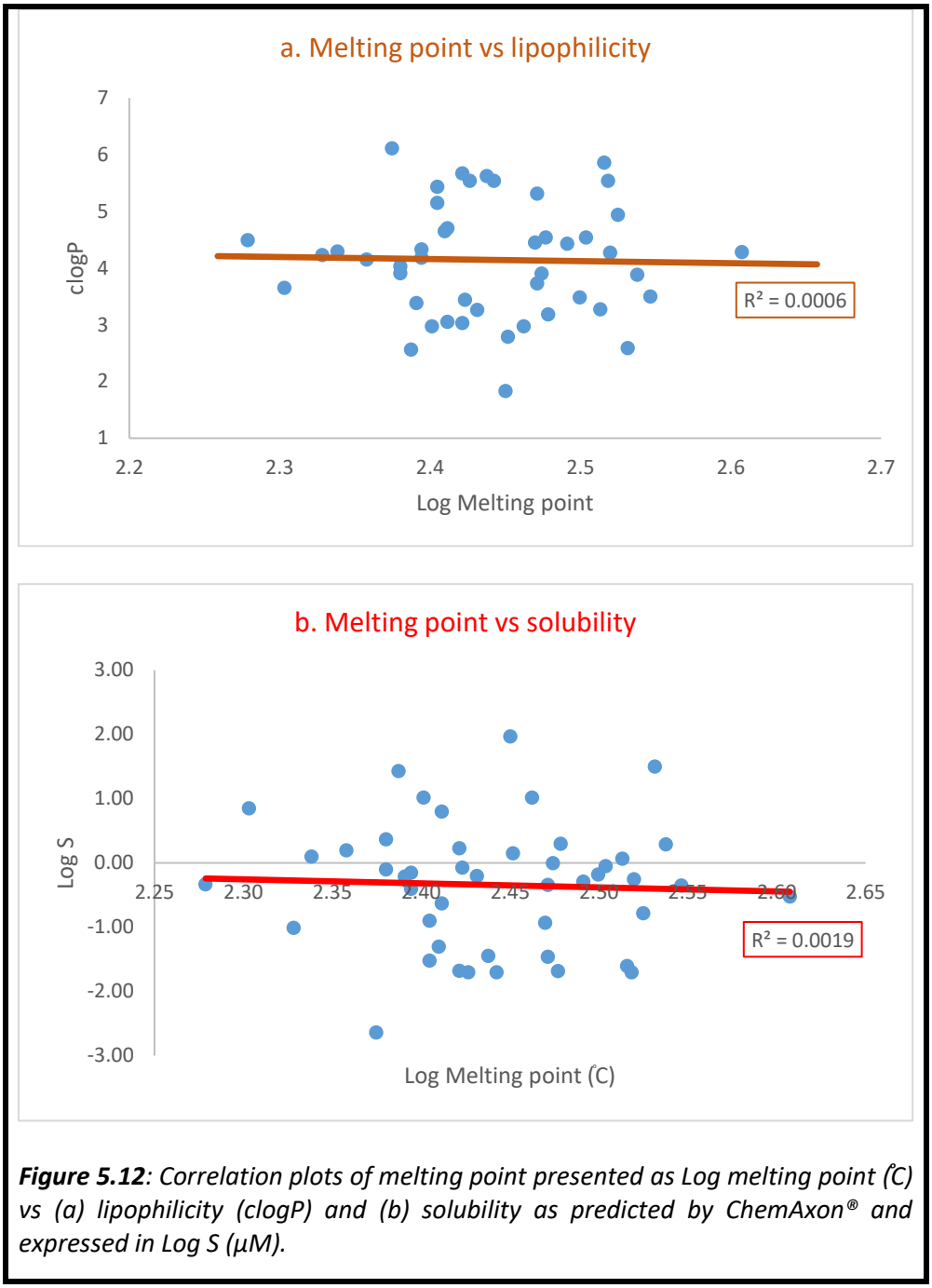

***Figure 5.12**: Correlation plots of melting point presented as Log melting point (°C) vs (a) lipophilicity (clogP) and (b) solubility as predicted by ChemAxon® and expressed in Log S (µM).*

5.6.2 Lipophilicity vs solubility

Whereas lipophilicity estimates the likelihood of a molecule to associate with an organic phase, solubility measures the amount of dissolved substance in aqueous media. In a given molecule, features that increase lipophilicity usually confer an opposing effect on solubility. Expectedly therefore, analysis of this compound set revealed an inverse correlation between the lipophilicity and solubility of the compounds (**Figure 5.13**). Thus, to achieve improved solubility among these compounds, medicinal chemistry strategies involving incorporation of water-solubilising features are vital. This approach is bound to decrease the lipophilicity of some of the compounds that flouted the Lipinski's guidelines on this property and can potentially improve oral absorption during *in vivo* studies.

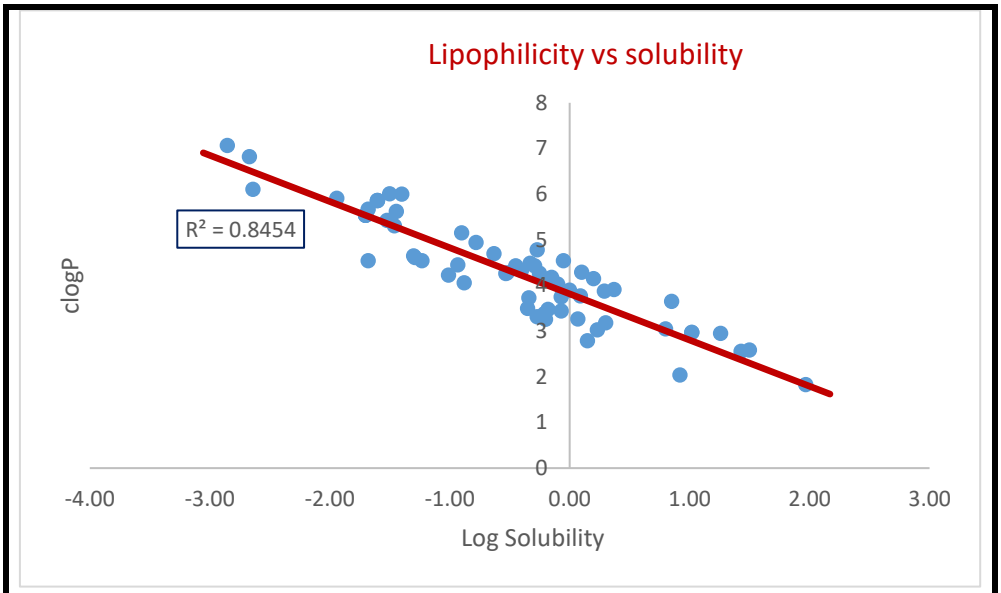

Figure 5.13: *Correlation plot between lipophilicity (clogP) and solubility as predicted by ChemAxon® and expressed as Log S (µM).*

5.6.3 Molecular weight vs solubility and lipophilicity

Molecular weight is a measure of molecular size and volume. In general, an increase in molecular weight corresponds to additional surfaces for interaction with solvent. Most lead-optimisation campaigns result in derivatives with higher molecular weight and accompanying increase in lipophilicity that decreases solubility of initial lead compounds.[41]

This general trend is reflected in the current data set whereby solubility was inversely correlated with molecular weight whereas lipophilicity increased with increasing molecular weight (**Figure 5.14**). Moreover, the inverse relationship between molecular weight and solubility (R^2=0.49) was stronger than the positive correlation between molecular weight and lipophilicity (R^2=0.28). Considering these findings, solubility improvements can be pursued by reducing the overall molecular weight of target molecules.

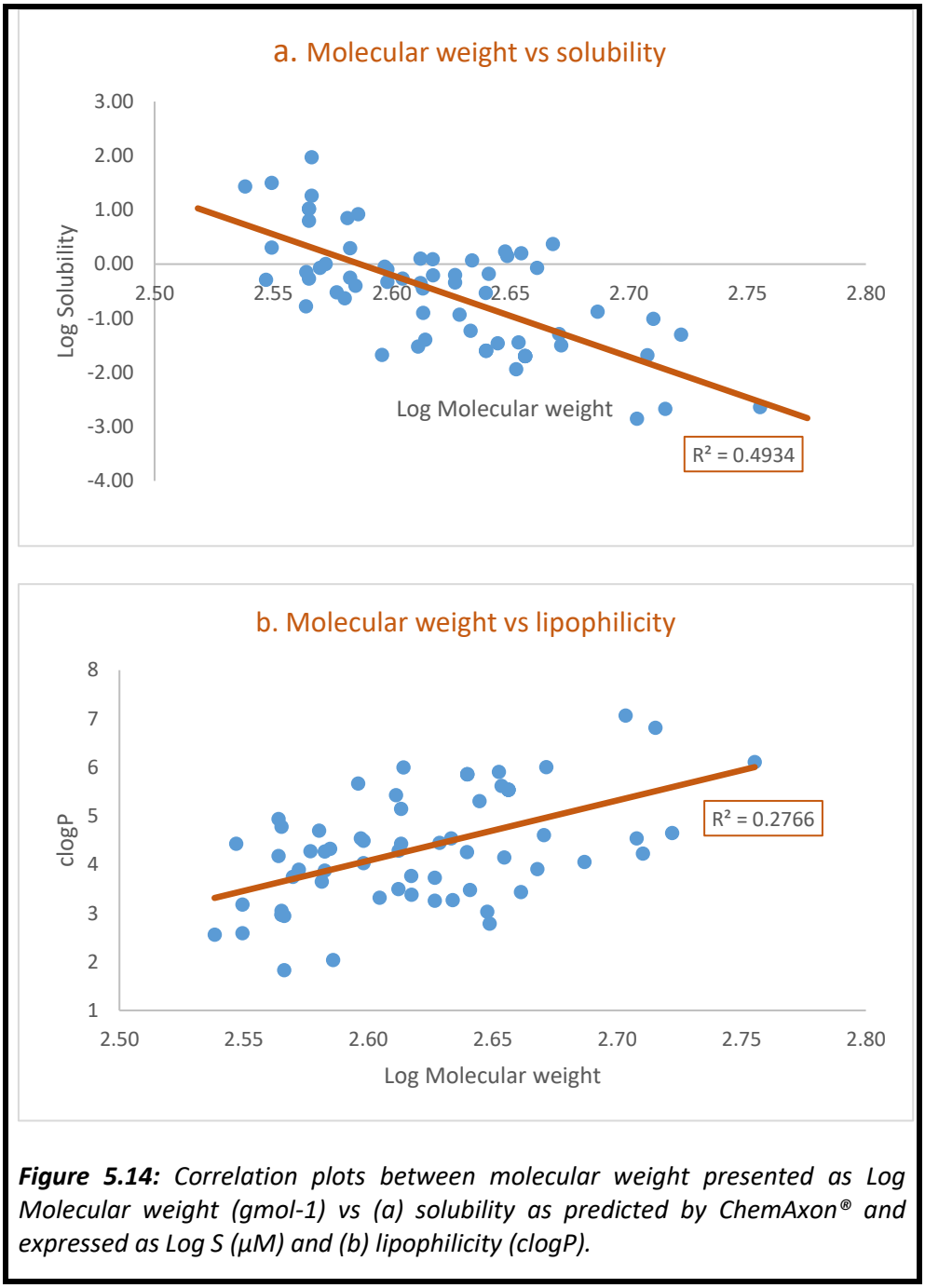

Figure 5.14: *Correlation plots between molecular weight presented as Log Molecular weight (gmol-1) vs (a) solubility as predicted by ChemAxon® and expressed as Log S (µM) and (b) lipophilicity (clogP).*

5.6.4. HPLC retention time and TLC retardation factor vs solubility and lipophilicity

Experimental data from analytical measurements such as retention time on HPLC and retardation factor from TLC analysis can give insights into the relative polarity or hydrophobicity of a series of compounds. In the absence of more elaborate solubility or lipophilicity measurements, these primary parameters can be used to rank compounds when compared to a known standard as explored in chromatographic hydrophobicity index measurements.[42–46]

The stationary phase employed in analytical TLC contains polar silanol groups which interact more strongly with polar compounds thus reducing the distance moved by such compounds when using a less polar mobile phase. The result is a lower retardation factor compared to that of a hydrophobic compound, which will partition better into the mobile phase than it does interact with the stationary phase.

In contrast, reversed phase HPLC, as used in this project, engages a non-polar stationary phase and a polar mobile phase. Accordingly, non-polar compounds associate more strongly with the stationary phase and remain retained in the column for longer leading to longer retention times.

There was an evident, albeit modest, direct relationship between TLC retardation factors and the HPLC retention times of the compounds as reflected in **Figure 5.15**. Furthermore, longer retention times were generally associated with lower solubility and higher lipophilicity while lower retardation factors were indicative of higher polarity within the compounds (**Figure 5.15**).

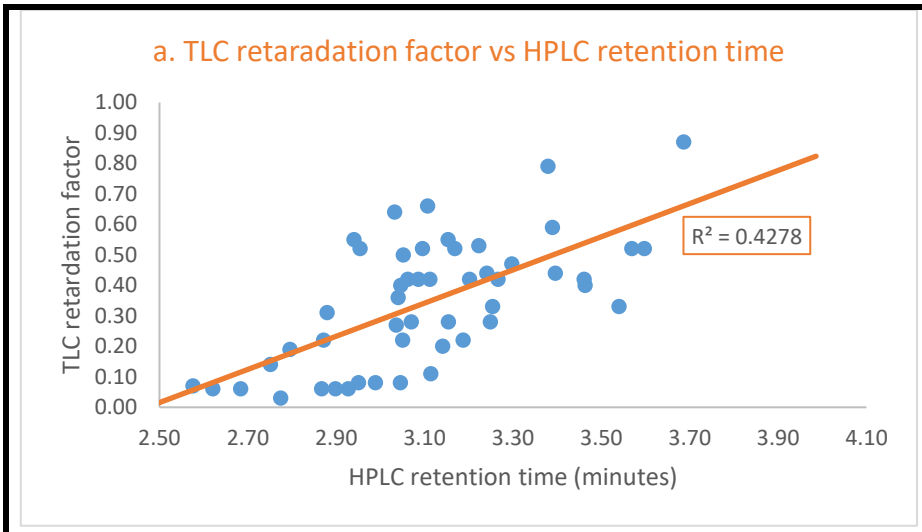

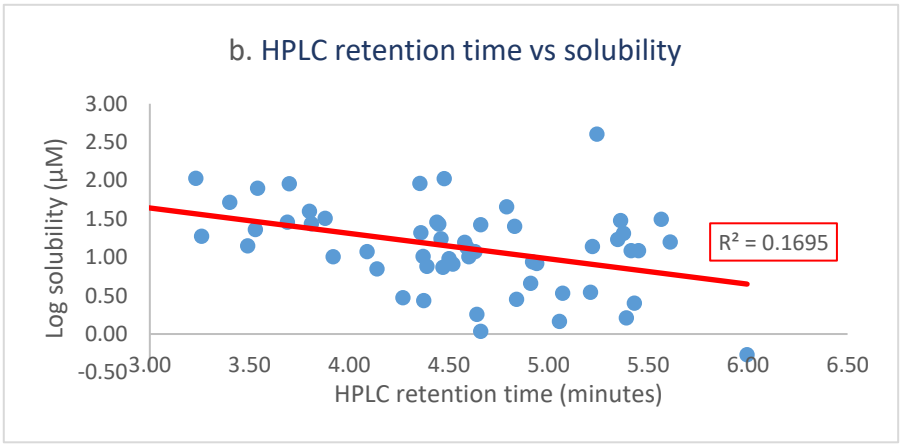

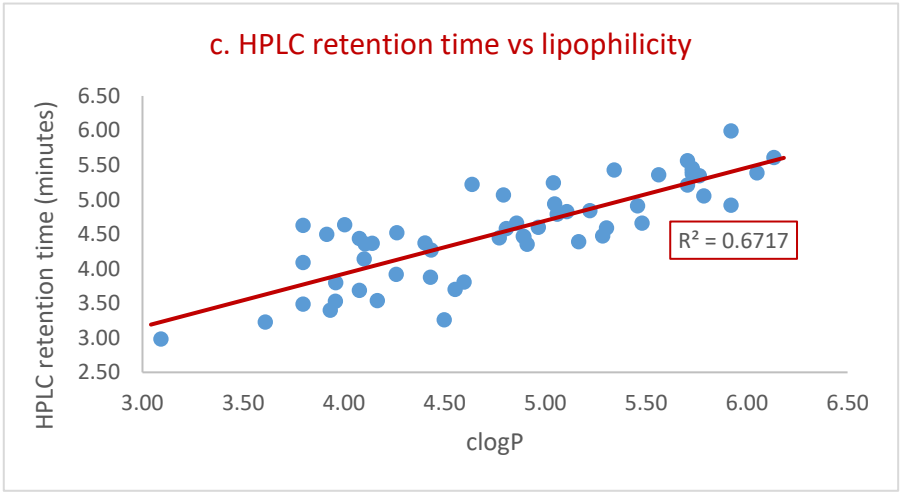

Figure 5.15: *Correlation plots between (a) TLC retardation factor vs HPLC retention time; (b) HPLC retention time vs solubility as predicted by ChemAxon® and expressed as Log S (µM) and (c) HPLC retention time vs lipophilicity (clogP).*

5.7 Comparisons of physicochemical properties of project compounds with marketed drugs and drug discovery leads

An analysis was performed with the aim of establishing similarities and differences in physicochemical profiles between the project compounds and clinically marketed drugs and leads in various stages of the drug discovery and development continuum. In this regard, the molecular descriptors: Molecular weight, clogP, HBD, HBA, tPSA and number of rotatable bonds were compared between the PBI project compounds and the approved drugs and discovery leads. For this assessment, a range of chemically diverse leads with reported sub-micromolar *in vitro* antiplasmodial potency or *in vivo* efficacy based on antimalarial animal studies, were considered. For the selected antischistosomal leads, a lower adult *S. mansoni in vitro* potency criterion of ≤10 µM, which is a generally accepted cut-off for antischistosomal drug discovery, was chosen.

When the PBIs (**1**) are compared against all the antischistosomal (**2**) and antimalarial agents (**3**) surveyed for this analysis, it was evident that the project compounds had a higher molecular weight and lipophilicity (**Table 5.3**). Besides, there were greater differences in the tPSA between the project compounds (**1**) and antischistosomal agents (**2**) than between project compounds (**1**) and antimalarial agents (**3**). Furthermore, the absolute mean values for hydrogen bond donors, hydrogen bond acceptors and number of rotatable bonds were largely comparable across the three categories of compounds.

In addition to the overall comparison of physicochemical properties between PBIs (**1**) and the antimalarial (**2**) and antischistosomal (**3**) agents grouped together, further analysis was performed wherein the antimalarial agents were sub-classified according their chemical class or mechanism of action (categories **4** to **8)** [**Table 5.3**]. This additional stratification of the compounds was intended to enable the determination of similarities or differences between the PBIs and those specific chemical classes. Based on the stratified comparison, PBIs (**1**) showed greater similarities in molecular weight with hemozoin inhibitors (**4**) and PI4K targeting agents (**8**). When considering lipophilicity, only the hemozoin inhibitors (**4**) approximated the average value observed for the PBIs (**1**) with much lower clogP values displayed by the other sub-classes [**Table 5.3**].

Table 5.3: *Physicochemical properties comparison between project compounds and drugs and leads in malaria and schistosomiasis drug discovery programs.* [a]

Category		n	Molecular weight	clogP	HBD	HBA	tPSA	nRB
(1)	PBIs	56	420 (50.5)	4.8 (0.74)	1.04 (0.33)	5.25 (0.96)	69.07 (15.72)	5.36 (0.96)
(2)	Antischistosomal agents	24	375.63 (105.78)	3.92 (1.34)	1.50 (0.83)	4.25 (1.48)	55.16 (22.84)	5.21 (2.26)
(3)	Antimalarial agents	47	378.79 (81.65)	3.34 (1.59)	1.57 (0.99)	5.17 (1.98)	65.45 (31.68)	5.23 (2.97)
Antimalarial leads and drugs stratified according to chemical class and mechanism of action								
(4)	Quinoline analogues and other Hemozoin inhibitors	26	400.41 (83.86)	4.14 (1.60)	1.58 (0.99)	4.62 (2.26)	55.82 (36.11)	6.81 (2.48)
(5)	Artemisinins and synthetic analogues	7	359 (71.81)	2.42 (0.57)	0.57 (0.79)	6.00 (1.15)	66.33 (20.14)	2.43 (2.44)
(6)	Folate synthesis Inhibitors	7	293.97 (58.49)	1.84 (1.12)	2.00 (0.58)	5.00 (1.38)	88.83 (20.26)	3.43 (1.51)
(7)	ATP4 targeting	3	391.80 (13.33)	3.21 (0.40)	2.67 (0.41)	4.67 (0.83)	63.34 (7.99)	1.67 (2.07)
(8)	PI4K targeting	4	411.55 (53.70)	2.46 (0.16)	1.75 (0.96)	6.75 (1.26)	87.20 (7.69)	5.75 (1.26)

[a]Parameters were determined using StarDrop® and values represent the mean (standard deviation) for each entry. n is the number of compounds in each category. Abbreviations**: clogP**-calculated partition co-efficient between n-octanol and water; **HBD**-hydrogen bond donor count; **HBA**-hydrogen bond acceptor count; **tPSA**-topological polar surface area and **nRB**-number of rotatable bonds. **ATP**-Adenosine triphosphate; **PI4K**-Phosphatidyl inositol-4-kinase.

To determine if the observed differences across the studied parameters were statistically significant, a Student's t-Test was performed using Microsoft® excel. The data for each set of pair being compared was treated as having unequal variance and the one-tailed distribution option applied.

As can be seen in **Table 5.4**, there were statistically significant differences in various physicochemical properties between PBIs and the categories of antimalarial and antischistosomal agents. Regarding molecular weight, PBIs did not show a significant difference only with hemozoin and PI4K targeting agents. Notably also, the discrepancy in lipophilicity was statistically significant across all the categories, when compared to the PBIs. Other attributes such as tPSA and number of rotatable bonds also showed significant differences to varying degrees across the categories. Arising from these analyses, it can be conjectured that the PBIs potentially occupy a different chemical space from that of most standard antimalarial and antischistosomal drugs and leads in discovery and development.

Table 5.4: *Statistical significance comparisons of physicochemical properties of project compounds, antischistosomal and antimalarial leads and drug.*

Category/Property	Mw	clogP	HBD	HBA	tPSA	nRB
A. PBIs vs antischistosomal drugs and leads	0.029*	0.003**	0.007**	0.002**	0.005**	0.379
B. PBIs vs antimalarial leads and drugs	0.002**	0.000***	0.000***	0.401	0.239	0.393
C. PBIs vs Hemozoin formation inhibitors	0.137	0.027*	0.005**	0.090	0.042*	0.004**
D. PBIs vs Artemisinin analogues	0.033*	0.000***	0.086	0.071	0.369	0.009**
E. PBIs vs Antifolates	0.000***	0.000***	0.002**	0.209	0.021*	0.007**
F. PBIs vs ATP targeting leads	0.047*	0.015*	0.019*	0.238	0.236	0.078
G. PBIs vs PI4K targeting leads	0.386	0.000***	0.116	0.047*	0.004**	0.290
[a]Difference is significant at *p<0.05; **p<0.01 and ***p<0.001. Abbreviations: **Mw**-molecular weight; **clogP**-calculated partition co-efficient between n-octanol and water; **HBD**-hydrogen bond donor count; **HBA**-hydrogen bond acceptor count; **tPSA**-topological polar surface area and **nRB**-number of rotatable bonds. **ATP**-Adenosine triphosphate; **PI4K**-Phosphatidyl inositol-4-kinase.						

5.8 Chapter summary

This chapter has described the physical and chemical profile of compounds generated in this thesis. Solubility values as determined by experimental and *in silico* methods although disparate, were consistent in their ability to guide structure-solubility relationship studies. Other structure-property relationships have been delineated as have the influence of physicochemical properties on biological activity.

Lipophilicity emerges as a key factor driving compound potency as well as increases in cellular toxicity risk. Optimisation of lipophilicity together with solubility have been highlighted as being vital in improving oral drug-likeness of lead compounds.

In comparison to widely recognised medicinal chemistry criteria predictive of good oral bioavailability, most of the compounds were found to be compliant. A further evaluation of physicochemical properties of project compounds in contrast to drugs and discovery leads or those under development reveal that there are potential divergent chemical spaces occupied by the PBIs. This observation makes the current series appealing as a new chemotype towards antimalarial and antischistosomal drug discovery and development.

5.9 References

(1) Wang, J.; Hou, T. Recent Advances on Aqueous Solubility Prediction. *Comb. Chem. High Throughput Screen.* **2011**, *14* (5), 328–338.

(2) Di, L.; Fish, P. V.; Mano, T. Bridging Solubility between Drug Discovery and Development. *Drug Discov. Today* **2012**, *17* (9–10), 486–495.

(3) Wang, J.; Wang, J.; Urban, L.; Urban, L. The Impact of Early ADME Profiling on Drug Discovery and Development Strategy. *Drug Discov. World* **2004**, 73–86.

(4) Alsenz, J.; Kansy, M. High Throughput Solubility Measurement in Drug Discovery and Development. *Adv. Drug Deliv. Rev.* **2007**, *59* (7), 546–567.

(5) Kerns, E. H. High Throughput Physicochemical Profiling for Drug Discovery. *J. Pharm. Sci.* **2001**, *90* (11), 1838–1858.

(6) Zhou, L.; Yang, L.; Tilton, S.; Wang, J. Development of a High Throughput Equilibrium Solubility Assay Using Miniaturized Shake-flask Method in Early Drug Discovery. *J. Pharm. Sci.* **2007**, *96* (11), 3052–3071.

(7) Ishikawa, M.; Hashimoto, Y. Improvement in Aqueous Solubility in Small Molecule Drug Discovery Programs by Disruption of Molecular Planarity and Symmetry. *J. Med. Chem.* **2011**, *54* (M), 1539–1554.

(8) Ran, Y.; Yalkowsky, S. H. Prediction of Drug Solubility by the General Solubility Equation (GSE). *J. Chem. Inf. Comput. Sci.* **2001**, *41* (2), 354–357.

(9) Delaney, J. S. ESOL: Estimating Aqueous Solubility Directly from Molecular Structure. *J. Chem. Inf. Comput. Sci.* **2004**, *44* (3), 1000–1005.

(10) Elder, D.; Holm, R. Aqueous Solubility: Simple Predictive Methods (*in silico*, *in vitro* and Bio-Relevant Approaches). *Int. J. Pharm.* **2013**, *453* (1), 3–11.

(11) Saal, C.; Petereit, A. C. Optimizing Solubility: Kinetic versus Thermodynamic Solubility Temptations and Risks. *Eur. J. Pharm. Sci.* **2012**, *47* (3), 589–595.

(12) Lipinski, C. A.; Lombardo, F.; Dominy, B. W.; Feeney, P. J. Experimental and Computational Approaches to Estimate Solubility and Permeability in Drug Discovery and Development Settings1PII of Original Article: S0169-409X(96)00423-1. The Article

Was Originally Published in Advanced Drug Delivery Reviews 23 (1997) 3. *Adv. Drug Deliv. Rev.* **2001**, *46* (1–3), 3–26.

(13) Hewitt, M.; Cronin, M. T. D.; Enoch, S. J.; Madden, J. C.; Roberts, D. W.; Dearden, J. C. *In silico* Prediction of Aqueous Solubility: The Solubility Challenge. *J. Chem. Inf. Model.* **2009**, *49* (11), 2572–2587.

(14) http://www.cambridgesoft.com/software/overview.aspx.

(15) https://www.optibrium.com/stardrop/.

(16) https://chemaxon.com/.

(17) Dearden, J. C. *In silico* Prediction of Aqueous Solubility. *Expert Opin. Drug Discov.* **2006**, *1* (1), 31–52.

(18) Bergström, C. A. S.; Wassvik, C. M.; Norinder, U.; Luthman, K.; Artursson, P. Global and Local Computational Models for Aqueous Solubility Prediction of Drug-Like Molecules. *J. Chem. Inf. Comput. Sci.* **2004**, *44* (4), 1477–1488.

(19) Mannhold, R.; Poda, G. I.; Ostermann, C.; Tetko, I. V. Calculation of Molecular Lipophilicity: State-of-the-Art and Comparison of LogP Methods on More than 96,000 Compounds. *J. Pharm. Sci.* **2009**, *98* (3), 861–893.

(20) Ghose, A. K.; Viswanadhan, V. N.; Wendoloski, J. J. Prediction of Hydrophobic (Lipophilic) Properties of Small Organic Molecules Using Fragmental Methods: An Analysis of ALOGP and CLOGP Methods. *J. Phys. Chem. A* **1998**, *102* (21), 3762–3772.

(21) Schroeter, T. S.; Schwaighofer, A.; Mika, S.; Ter Laak, A.; Suelzle, D.; Ganzer, U.; Heinrich, N.; Müller, K.-R. Predicting Lipophilicity of Drug-Discovery Molecules Using Gaussian Process Models. *ChemMedChem* **2007**, *2* (9), 1265–1267.

(22) Lombardo, F.; Shalaeva, M. Y.; Tupper, K. A.; Gao, F.; Abraham, M. H. ElogP Oct : A Tool for Lipophilicity Determination in Drug Discovery . *J. Med. Chem.* **2000**, *43* (15), 2922–2928.

(23) Leeson, P. D. Molecular Inflation, Attrition and the Rule of Five. *Adv. Drug Deliv. Rev.* **2016**, *101*, 22–33.

(24) Hughes, L. D.; Palmer, D. S.; Nigsch, F.; Mitchell, J. B. O. Why Are Some Properties More Difficult To Predict than Others? A Study of QSPR Models of Solubility, Melting Point,

and Log P. *J. Chem. Inf. Model.* **2008**, *48* (1), 220–232.

(25) Gleeson, M. P. Generation of a Set of Simple, Interpretable ADMET Rules of Thumb. *J. Med. Chem.* **2008**, *51* (4), 817–834.

(26) Ritchie, T. J.; Macdonald, S. J. F. How Drug-like Are 'Ugly' Drugs: Do Drug-Likeness Metrics Predict ADME Behaviour in Humans? *Drug Discov. Today* **2014**, *19* (4), 489–495.

(27) Alex, A.; Millan, D. S.; Perez, M.; Wakenhut, F.; Whitlock, G. A. Intramolecular Hydrogen Bonding to Improve Membrane Permeability and Absorption in beyond Rule of Five Chemical Space. *Medchemcomm* **2011**, *2* (7), 669.

(28) Fernandes, J.; Gattass, C. R. Topological Polar Surface Area Defines Substrate Transport by Multidrug Resistance Associated Protein 1 (MRP1/ABCC1). *J. Med. Chem.* **2009**, *52* (4), 1214–1218.

(29) Hughes, J. D.; Blagg, J.; Price, D. A.; Bailey, S.; DeCrescenzo, G. A.; Devraj, R. V.; Ellsworth, E.; Fobian, Y. M.; Gibbs, M. E.; Gilles, R. W.; Greene, N.; Huang, E.; Krieger-Burke, T.; Loesel, J.; Wager, T.; Whiteley, L.; Zhang, Y. Physiochemical Drug Properties Associated with *in vivo* Toxicological Outcomes. *Bioorg. Med. Chem. Lett.* **2008**, *18* (17), 4872–4875.

(30) Wu, P.; Nielsen, T. E.; Clausen, M. H. Small-Molecule Kinase Inhibitors: An Analysis of FDA-Approved Drugs. *Drug Discov. Today* **2016**, *21* (1), 5–10.

(31) Hou, T.; Wang, J.; Zhang, W.; Xu, X. ADME Evaluation in Drug Discovery. 6. Can Oral Bioavailability in Humans Be Effectively Predicted by Simple Molecular Property-Based Rules? *J. Chem. Inf. Model.* **2007**, *47* (2), 460–463.

(32) Zhang, M.-Q.; Wilkinson, B. Drug Discovery beyond the 'Rule-of-Five.' *Curr. Opin. Biotechnol.* **2007**, *18* (6), 478–488.

(33) Doak, B. C.; Over, B.; Giordanetto, F.; Kihlberg, J. Oral Druggable Space beyond the Rule of 5: Insights from Drugs and Clinical Candidates. *Chem. Biol.* **2014**, *21* (9), 1115–1142.

(34) Matsson, P.; Doak, B. C.; Over, B.; Kihlberg, J. Cell Permeability beyond the Rule of 5. *Adv. Drug Deliv. Rev.* **2016**, *101*, 42–61.

(35) Price, D. A.; Blagg, J.; Jones, L.; Greene, N.; Wager, T. Physicochemical Drug Properties

Associated with *in vivo* Toxicological Outcomes: A Review. *Expert Opin. Drug Metab. Toxicol.* **2009**, *5* (8), 921–931.

(36) Chen, M.; Borlak, J.; Tong, W. High Lipophilicity and High Daily Dose of Oral Medications Are Associated with Significant Risk for Drug-Induced Liver Injury. *Hepatology* **2013**, *58* (1), 388–396.

(37) Edwards, M. P.; Price, D. A. Role of Physicochemical Properties and Ligand Lipophilicity Efficiency in Addressing Drug Safety Risks; 2010; pp 380–391.

(38) Freeman-Cook, K. D.; Hoffman, R. L.; Johnson, T. W. Lipophilic Efficiency: The Most Important Efficiency Metric in Medicinal Chemistry. *Future Med. Chem.* **2013**, *5* (2), 113–115.

(39) Tarcsay, Á.; Nyíri, K.; Keserű, G. M. Impact of Lipophilic Efficiency on Compound Quality. *J. Med. Chem.* **2012**, *55* (3), 1252–1260.

(40) Hopkins, A. L.; Keserü, G. M.; Leeson, P. D.; Rees, D. C.; Reynolds, C. H. The Role of Ligand Efficiency Metrics in Drug Discovery. *Nat. Rev. Drug Discov.* **2014**, *13*, 105.

(41) Lipinski, C. A. Drug-like Properties and the Causes of Poor Solubility and Poor Permeability. *J. Pharmacol. Toxicol. Methods* **2000**, *44* (1), 235–249.

(42) Valkó, K.; Bevan, C.; Reynolds, D. Chromatographic Hydrophobicity Index by Fast-Gradient RP-HPLC: A High-Throughput Alternative to Log P/Log D. *Anal. Chem.* **1997**, *69* (11), 2022–2029.

(43) Valkó, K.; Plass, M.; Bevan, C.; Reynolds, D.; Abraham, M. . Relationships between the Chromatographic Hydrophobicity Indices and Solute Descriptors Obtained by Using Several Reversed-Phase, Diol, Nitrile, Cyclodextrin and Immobilised Artificial Membrane-Bonded High-Performance Liquid Chromatography Columns. *J. Chromatogr. A* **1998**, *797* (1–2), 41–55.

(44) Camurri, G.; Zaramella, A. High-Throughput Liquid Chromatography/Mass Spectrometry Method for the Determination of the Chromatographic Hydrophobicity Index. *Anal. Chem.* **2001**, *73* (15), 3716–3722.

(45) Valkó, K. Application of High-Performance Liquid Chromatography Based Measurements of Lipophilicity to Model Biological Distribution. *J. Chromatogr. A* **2004**,

1037 (1–2), 299–310.

(46) Young, R. J.; Green, D. V. S.; Luscombe, C. N.; Hill, A. P. Getting Physical in Drug Discovery II: The Impact of Chromatographic Hydrophobicity Measurements and Aromaticity. *Drug Discov. Today* **2011**, *16* (17–18), 822–830.

Chapter 6

Summary, Conclusion and Directions for Future Work

6.1 Summary

Previous phenotypic whole cell screening against the human malaria parasite *Plasmodium falciparum* identified active hits embodying a pyridobenzimidazole (PBI) core, thereby inspiring the exploration of this chemotype as a potential antimalarial drug discovery scaffold. Ensuing structure-activity relationship studies produced active compounds mainly incorporating alkyl amine side chains and for which physicochemical liabilities were implicated in downstream *in vivo* assays. Further medicinal chemistry iterations, the focus of this thesis work, were launched via introduction of various substituents around the PBI core, as depicted in **Figure 6.1**, to extend the chemical diversity in this scaffold in search of suitable antimalarial leads.

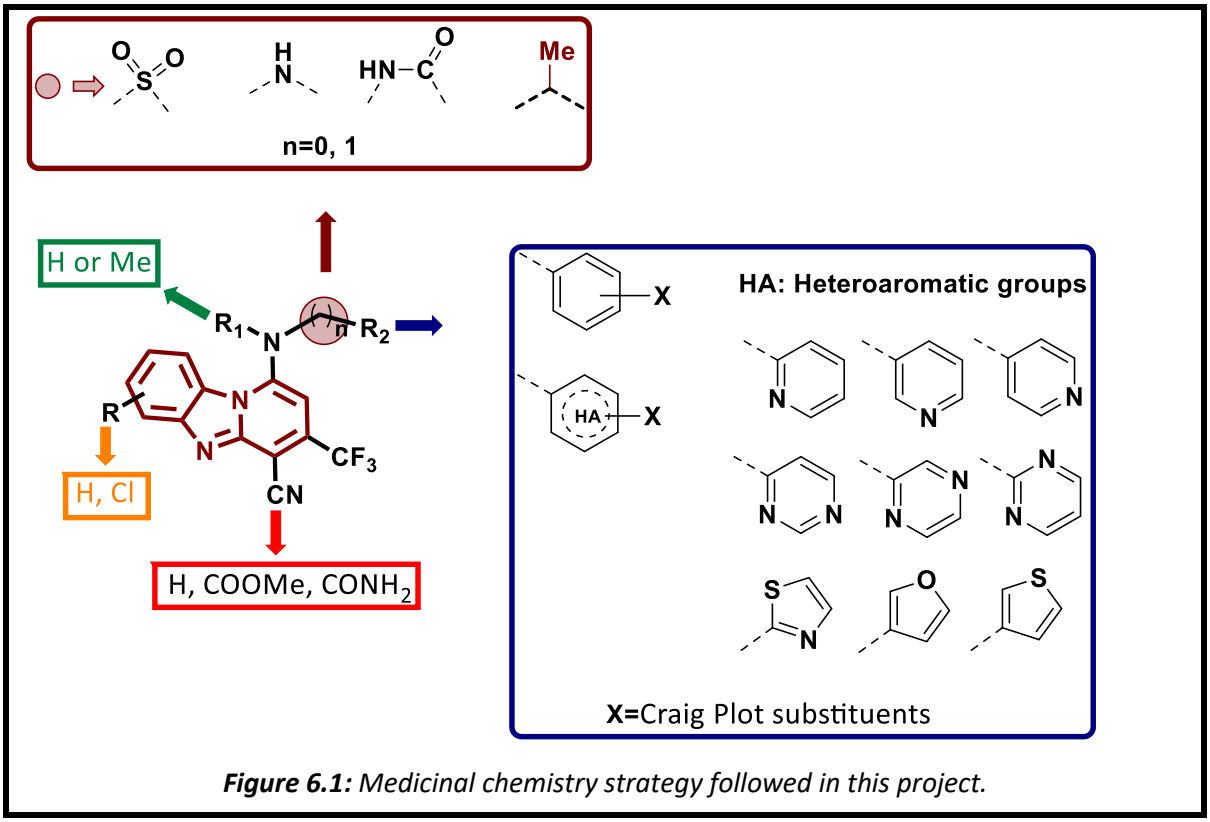

Figure 6.1: *Medicinal chemistry strategy followed in this project.*

Arising from this work, analogues with sub-micromolar potency against the asexual blood stage parasites of *Pf*NF54 were identified and structure-activity relationship trends observed as summarised in **Figure 6.2**. Generally, as opposed to hydrophilic electron-donating moieties, lipophilic electron- withdrawing Craig plot substituents on appended aromatic side group resulted in potent antiplasmodial activity. Manipulations on the left hand-side, by incorporating halogen groups, improved activity.

Additional assays revealed that these compounds retained activity against the multidrug-resistant *Pf*K1 strain, suggesting the unlikelihood of the compounds to show cross-resistance with drugs like chloroquine. Further evaluation against the liver and gametocyte stages of *Plasmodium* parasites revealed the multi-stage activity of these compounds and that most of the compounds displayed differential susceptibility to the late stage over early stage gametocytes.

Subsequent profiling of *in vitro* potent analogues for *in vitro* drug metabolism and pharmacokinetics allowed for the delineation of structure-property trends wherein the left hand-side modification was found to reduce the selectivity profile as examined in Chinese Hamster Ovarian cell lines (**Figure 6.2**). Notably, these compounds have low cardiotoxicity risk potential as evaluated in the hERG potassium ion channel inhibition assay whereby all the tested compounds were projected to interact weakly with this protein target.

Towards probing the mechanism of antiplasmodial action, prompted by the planar morphology, rich electron density and presence of protonatable sites, compounds were tested for their ability to inhibit the formation of beta haematin. Majority of the compounds were inactive in this assay with only few showing significant inhibition potency. Furthermore, there was no correlation between the beta haematin inhibition activity and the antiplasmodial activity of these compounds, suggesting different or additional antiparasitic mechanisms of action.

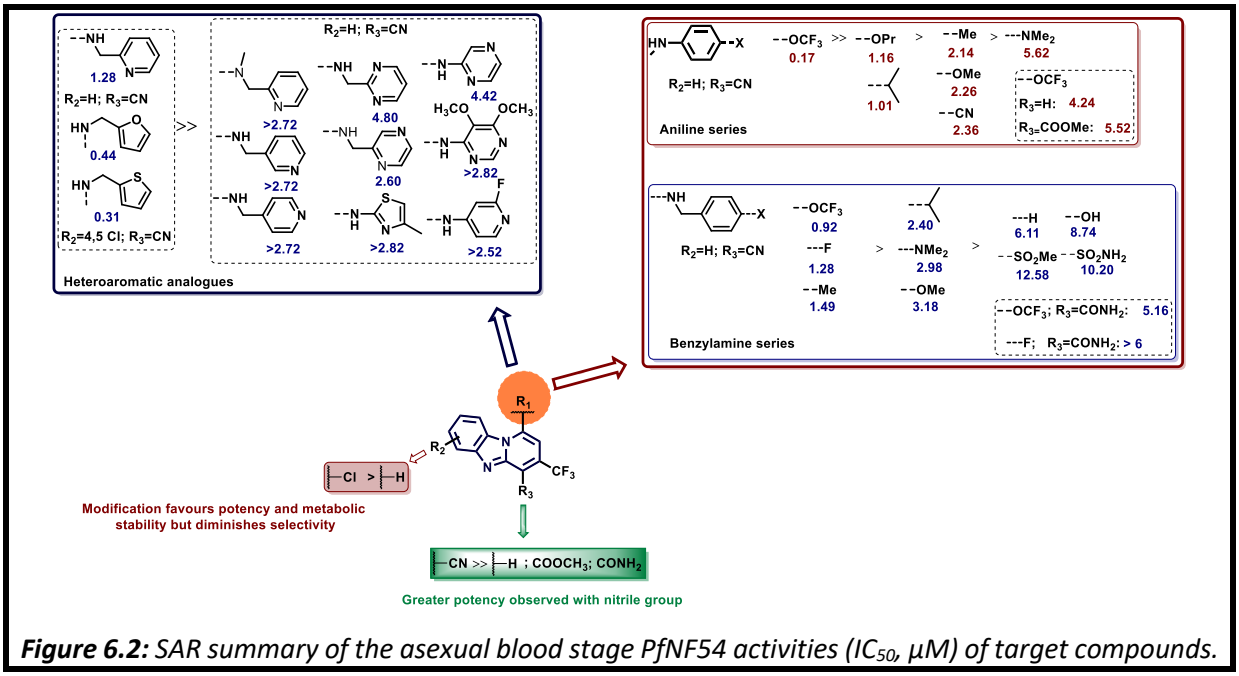

Figure 6.2: *SAR summary of the asexual blood stage PfNF54 activities (IC_{50}, µM) of target compounds.*

When subjected to *in vivo* antimalarial efficacy studies in a murine model of malaria, **1j/GMP-19** and **4i/GMP-75**, representing the two classes of compounds generated from the SAR iterations produced impressive 98% and 99.9% reduction in parasitaemia with mean survival times of 12 days and 14 days, respectively, compared to 6 days for the control, untreated animals. Pharmacokinetic studies revealed that systemic exposure was limited by the low solubility profiles of these compounds.

In the context of drug repositioning, the pyridobenzimidazole scaffold was evaluated for its potential application in antischistosomal drug discovery. The targets produced in the antimalarial program were therefore tested in adult and larva stages of *S. mansoni*. Several compounds with potent sub-micromolar activity against adult worms were identified (**Figure 6.3**). Additionally, these compounds also displayed good activity against the immature worms, a profile which is critical to the disruption of the *Schistosome* life cycle by preventing formation of more adult worms, a feature lacking with praziquantel, the current sole treatment for human schistosomiasis.

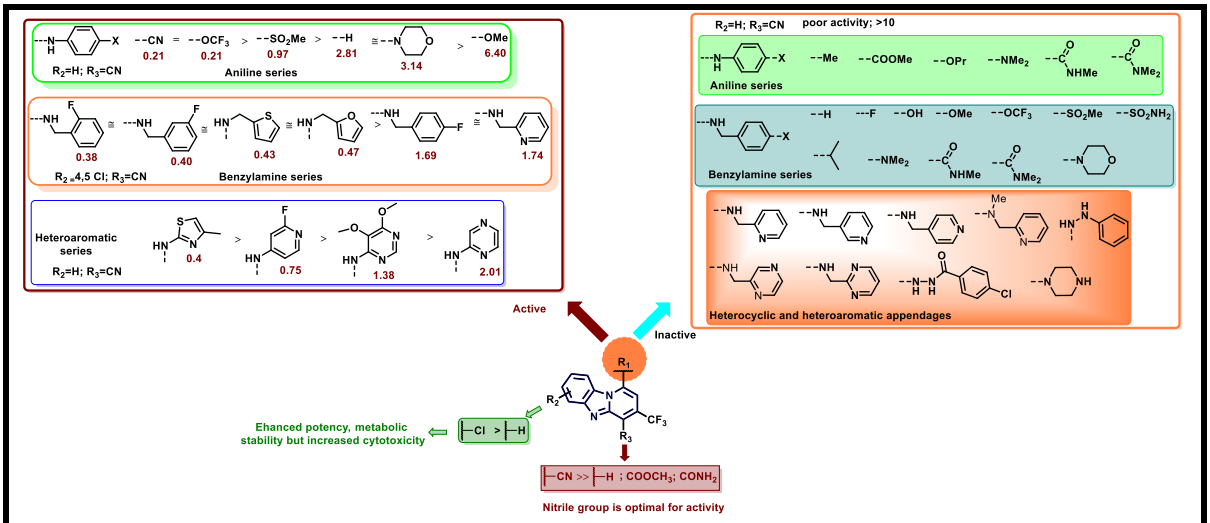

Figure 6.3: *SAR summary of the antischistosomal activities (IC_{50}, µM) of target compounds.*

Concerning *in vivo* antischistosomal efficacy of these series, the best activities were observed with **1j/GMP-19, 4i/GMP-75** and **4j/GMP-76** which produced between 60% and 70% total worm reductions. Other targets produced lesser *in vivo* efficacy probably due to the metabolically labile heteroaromatic side groups. Metabolite identification studies pointed to dealkylation and hydroxylation as the major metabolic pathways for **2a/GMP-23** and **2e/GMP-58**, the targets incorporating a substituted pyrimidyl and pyrazinyl side groups, respectively. It may thus be inferred that the metabolites of **2a/GMP-23** and **2e/GMP-58** are inactive, unlike those of praziquantel, the current standard antischistosomal drug which although having poor metabolic stability, maintains *in vivo* potency.

The observed overlap in the antimalarial and antischistosomal potency of these compounds as exemplified by **1j/GMP-19** and **4i/GMP-75** (**Table 6.1**) is interesting and lends support to the current practise of screening the database of antimalarial drugs or leads for antischistosomal activity. Besides the hemozoin formation pathway, there might be other unexplored molecular and biochemical pathways existent in the two parasites making drug repositioning a particularly appealing approach to expedite drug discovery for neglected tropical diseases such as schistosomiasis. The possibility of targeting two diseases with one single small molecule has the potential to reduce treatment costs and simplify treatment regimens.

Table 6.1: *In vitro and in vivo antimalarial and antischistosomal profile of frontrunner compounds.*

	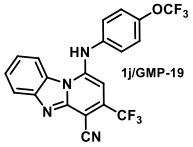 1j/GMP-19	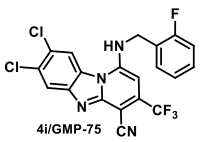 4i/GMP-75
P. falciparum NF54: IC_{50}, µM	0.17	0.17
P. falciparum K1: IC_{50}, µM	0.15	0.14
Adult *S. Mansoni:* IC_{50}, µM	0.21	0.38
CHO, IC_{50}, µM (SI)	17.58 (103)	4.31 (25)
% Plasmodium parasitaemia reduction at 4x50mg/kg oral dose	98.0	99.9
Mean Survival Days	12	14
Schistosome worm burden reduction (%) at a single oral dose of 400mg/kg	62	69

CHO: Chinese Hamster ovarian cell line.

Examination of physicochemical properties for the series showed compliance of most compounds with the widely accepted medicinal chemistry criteria for leads with predicted good oral absorption and bioavailability. Moreover, the series could be differentiated in a range of physicochemical parameters when compared to marketed drugs or leads in discovery and development for malaria and schistosomiasis. This observation shows the potential for novelty regarding the chemical space occupied by PBIs. Solubility, however, emerged as a critical property requiring further optimisation towards improving *in vivo* pharmacokinetics and oral efficacy.

Arising from analysis of structure-activity and structure-property trends, it is evident that the series displays an evolvable type of SAR with regards to both antimalarial and antischistosomal activities. Subtle changes to the compounds led to the generation of a library of compounds with a wide spectrum of differences in biological activity and a range in physicochemical attributes, an appealing characteristic for a drug discovery chemotype. For this scaffold, it is possible to modulate toxicity and other physicochemical attributes while retaining biological potency.

6.2 Conclusion

In conclusion, the work pursued in this thesis has contributed to the further understanding of the structural features compatible with antimalarial activities of 3-trifluoromethyl N-aryl-substituted pyrido [1,2-*a*] benzimidazoles. Moreover, in demonstrating the utility of drug repositioning as a drug discovery strategy, the antischistosomal potency of this series of compounds has been unravelled and accompanying SAR trends elucidated. The two lead compounds **1j/GMP-19** and **4i/GMP-75** identified from this research are worth of further investigations as promising antimalarial and antischistosomal leads possessing multi-stage antiparasitic activity. Given the spectrum of their activities, the two compounds, if adequately optimised, bear the potential to contribute to malaria chemoprevention and blocking transmission. Furthermore, the susceptibility of the larval stages of schistosomes further endears these compounds as suitable leads for schistosomiasis drug discovery.

6.3 Directions for future work

Arising from the structure-activity and structure-property relationship trends uncovered in this thesis, some directions for future work emerge. Based on diminished selectivity upon introduction of chloro atoms on the left-hand side of the PBI core, further medicinal chemistry iterations using chloro isosteric groups, such as the less lipophilic fluoro, should be explored. Towards improving solubility, incorporating substituents with hydrogen-bonding capacity or those with reduced lipophilicity compared to those used in the frontrunner compounds should be investigated as represented in **(Figure 6.4)**. Other solubility-enhancing approaches including formulation strategies and supramolecular derivation are also worth pursuing as they have the potential to improve the pharmacokinetic profile and oral efficacy of these compounds.

To ascertain the gametocytocidal potency of the compounds found active in this assay, the membrane feeding assay, considered to be the gold-standard of this investigation, should be explored. Moreover, a wider panel of *Plasmodium* parasite strains need to be tested to establish the spectrum of antiplasmodial activity of this series of compounds across various strains. Additional tests regarding resistance potential towards these compounds through, for example, mutant generation, will provide information on any similarities or differences in the mechanisms compared to that found with standard antimalarial drugs. Chemogenomic and proteomic analysis are also recommended to establish the potential targets and mechanism(s) of action for these compounds.

That the frontrunner compounds elicited impressive antimalarial efficacy in a mouse model despite low bioavailability inspire interest in studying their tissue distribution profile. Finally, given the potential novelty of the chemical space occupied by these compounds, drug hybrid strategies through chemically linking the PBIs with other antimalarial drugs comprising different scaffolds such as the quinolines, should be investigated. In combining with other recognised antimalarial chemotypes, synergy in antimalarial action and delayed emergence of resistance are potential benefits of this approach.

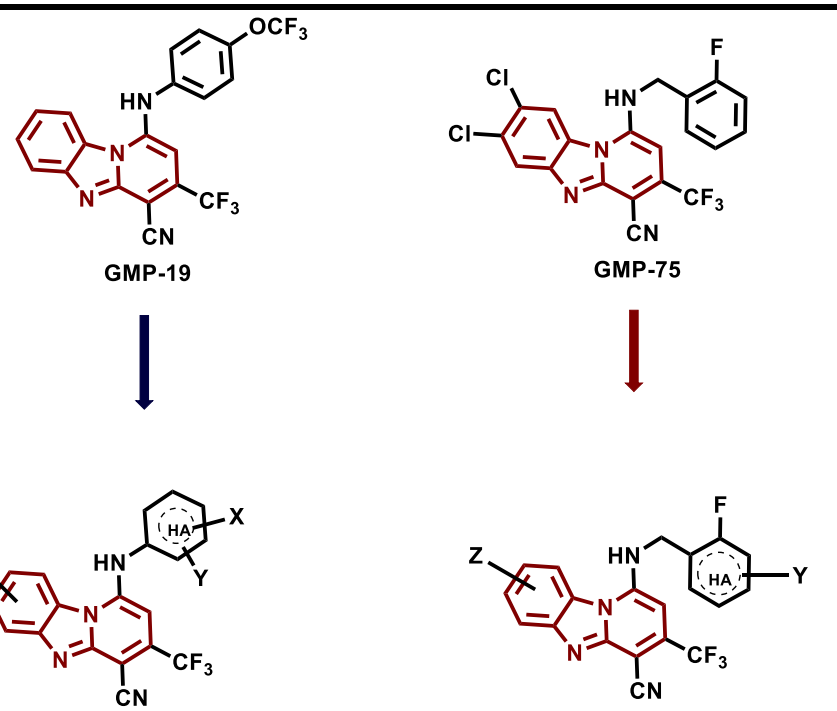

HA: Heteroaromatic groups
X: Lipophilic groups, bioisosteric to the OCF_3
Y: Additional substituent with hydrophilic character to improve solubility
Z: Bioisostere of the dichloro groups to reduce lipophilicity, improve selectivity and solubility

Figure 6.4: *SAR recommendations for future work based on* ***1j/GMP-19*** *and* ***4i/GMP-75****.*

Chapter 7

Experimental Information

7.1 Chapter overview

This chapter will provide additional information regarding the materials, methods and experimental procedures followed in this thesis. Firstly, the chemistry information will be described regarding general instrumentation and equipment used. This will then be followed by the synthesis and characterization of intermediate and target compounds. Thereafter, materials and methods used in the biological assays will be described together with *in vitro* ADME procedures and those for *in vivo* efficacy and pharmacokinetics studies. Finally, the procedure used to generate kinetic solubility data will also be described.

7.2 Chemistry

7.2.1 General information

Chemical reagents and analytical grade solvents used for reactions were purchased from either Sigma- Aldrich (South Africa) or Combi Blocks Limited (USA). Other solvents, such as methanol, dichloromethane, hexane and ethylacetate, were sourced from Kimix Chemicals (South Africa). Compounds were purified by either recrystallisation, trituration or by applying column chromatography. Column chromatography was performed on silica gel 60 (Fluka), particle size = 0.063−0.2 mm (70−230 mesh) as the stationary phase with appropriately optimised mobile phase. Identity and characterization of intermediates and target compounds was done by NMR and LC-MS, supplemented by TLC analysis using appropriate combinations of solvents as the mobile phase and silica adsorbed on alumina (Merck or Sigma-Aldrich) as the stationary phase.

NMR spectra were recorded on either a Varian Mercury-300 (^{1}H 300.1 MHz, ^{13}C 75.5 MHz) or a Bruker-400 (^{1}H 400.2 MHz, ^{13}C 100.6 MHz) instrument using DMSO-*d*6 or methanol-*d*4 as solvent. The multiplicity of ^{1}H NMR peaks is reported as either: s, singlet; bs, broad singlet; d, doublet; t, triplets; dd, doublet of doublets; dt, doublet of triplets; td, triplet of doublets; ddd, doublet of doublet of doublets or m, multiplets with the chemical shifts (in parts per million, ppm) and coupling constants (*J in Hertz, Hz)* recorded to three and two significant figures, respectively. Protons represented by the reported chemical shifts are indicated by a superscript integer corresponding to the numbering of protons in the chemical structure. Signals from ^{13}C NMR were obtained in the decoupled mode and chemical shifts are listed without assigning them to carbons in the structure as is conventional with most international medicinal chemistry journals.

The liquid chromatograph coupled to a mass spectrometer (LC-MS) system comprised an Agilent 1260 Infinity binary pump, an Agilent 1260 Infinity diode array detector, an Agilent 1290 Infinity column compartment, an Agilent 1260 Infinity standard autosampler and an Agilent 6120 quadrupole (single) mass spectrometer. The MS component was equipped with two ionisation techniques functioning via atmospheric pressure chemical ionisation (APCI) and electron-spray ionisation (ESI) of test compounds either in the positive or negative modes. In the positive ionisation mode, a pseudo-molecular ion corresponding to the (M+1) of the exact mass of the compound was obtained whereas a mass-to-charge (m/z) ratio peak corresponding to (M-1) was generated in the negative ionisation mode.

Sample purities were established by considering the peak area on LC corresponding to sample peak (as informed by the m/z ion on MS) relative to the total of all peak areas and expressed as a percentage. The column used for sample elution was a Kinetex Core C18 2.6 µm column (30 mm × 2.1 mm) with a gradient mobile phase consisting of two solvent systems employed (**Table 7.1**). Mobile phase A consisted of 0.4% acetic acid in 10 mM ammonium acetate in HPLC grade (type 1) water while mobile phase B contained 0.4% acetic acid, 10 mM ammonium acetate in a 9:1 ratio of HPLC grade methanol, and type 1 water. A flow rate of 0.7 mL/min and injection volume of 2 µL were applied and samples detected by means of a diode array detector using UV-absorbance over a 210-640 nm wavelength range.

Table 7.1: *HPLC gradient conditions for analysis of compounds.*

Time (min)	% A	% B
0.00	85	15
0.30	85	15
1.20	0.0	100
4.50	0.0	100

A: 10 mM NH_4OAc in buffer (0.4% acetic acid);

B: 10 mM NH_4OAc (0.4% acetic acid) in 90% HPLC grade MeOH in H_2O.

7.2.2 Synthesis and characterisation

7.2.2.1 SAR$_1$ intermediates

a) 1-hydroxy-3-(trifluoromethyl)benzo[4,5]imidazo[1,2-a]pyridine-4-carbonitrile: **IIIa**

2-(1H-benzo[d]imidazol-2-yl) acetonitrile **IIa** (1.0 equiv.), ethyl 4,4,4-trifluoro-3-oxobutanoate (1.2 equiv.) and ammonium acetate (2 equiv.) were stirred at 145°C for 2 hours. Reaction was monitored using TLC and LC-MS. Reaction mixture was cooled to 70°C, acetonitrile added while stirring for a further 10 minutes. After cooling to room temperature, the mixture was filtered, residue washed with acetonitrile and the product left to dry and used in subsequent step without further purification.

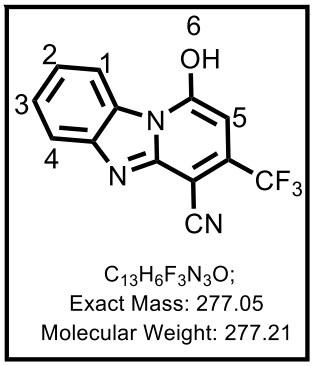

$C_{13}H_6F_3N_3O$;
Exact Mass: 277.05
Molecular Weight: 277.21

Obtained as a light yellow powder (66%); R_f (EtOAc:Hexane, 7:3) 0.8; ^{1}H NMR (400 MHz, DMSO) δ 14.10 (bs, 1H, H^6), 8.60 (d, J = 8.2 Hz, 1H, H^1), 7.71 – 7.56 (m, 2H, H^{3,4}), 7.46 (ddd, J = 8.6, 6.8, 1.8 Hz, 1H, H^2), 6.43 (s, 1H, H^5); ^{13}C NMR (101 MHz, DMSO) δ 158.05, 148.14, 138.59, 132.21, 127.46, 123.92, 123.48, 121.36, 116.71, 114.62, 112.24, 103.27, 64.56. MS (EI+) m/z calcd for $C_{13}H_6F_3N_3O$:277.05; found, 278.10 (M + 1).

b) 1-chloro-3-(trifluoromethyl)benzo[4,5]imidazo[1,2-a]pyridine-4-carbonitrile: **IVa**

Phosphoryl oxychloride ($POCl_3$; 20 equiv.) was added to 1-hydroxy-3-(trifluoromethyl) benzo[4,5]imidazo[1,2-a]pyridine-4-carbonitrile **IIIa** (1 equiv.) and stirred at 130°C for 3 hours. Excess $POCl_3$ was removed under reduced pressure. On cooling to room temperature, ice cold water was added with consistent stirring for 15 minutes. The mixture was neutralized using sodium carbonate, the crude product filtered off, washed with water, dried at ambient conditions and used subsequently without further purification.

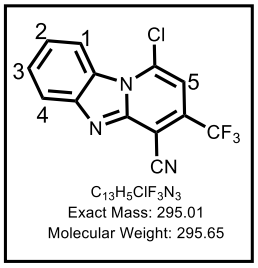

Obtained as tan brown (91%); R_f (EtoAc:Hexane, 3:7) 0.5; ^{1}H NMR (300 MHz, DMSO) δ 8.74 (d, *J* = 8.6 Hz, 1H, H^1), 8.08 (d, *J* = 8.3 Hz, 1H, H^4), 7.81 – 7.71 (m, 2H, $H^{3,5}$), 7.65 – 7.56 (m, 1H, H^2); ^{13}C NMR (101 MHz, DMSO) δ 158.10, 147.99, 138.63, 132.31, 127.83, 123.93, 123.57, 121.09, 116.77, 114.60, 112.19, 103.32, 64.50. MS (EI+) m/z calcd for $C_{13}H_5ClF_3N_3$:295.01; found, 296.00 (M + 1).

7.2.2.2 SAR_2 intermediates

a) General procedure for the synthesis of IIb and IIc

DMF (4 ml) was added to a mixture of the appropriately substituted diaminobenzene (1 equiv.) and ethyl cyanoacetate (3 equiv.). The reaction mixture was stirred and heated at 160 ˚C for 2 hours, cooled to room temperature and extracted using ethyl acetate. The organic layer was washed with 5% LiCl (5 x), distilled water (4 x), brine (5 x) and dried over $MgSO_4$. Organic solvent was removed in vacuo to obtain the product which was occasionally purified by column chromatography.

2-(5, 7-dichloro-1H-benzo[d]imidazol-2-yl) acetonitrile: IIb

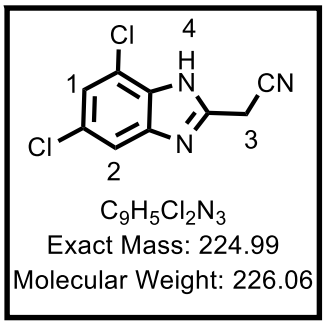

Obtained from 3,5-dichlorobenzene-1,2-diamine **Ia** and ethylcyano acetate as a brown solid (61%); R_f (EtOAc:Hexane, 1:1) 0.3; ^{1}H NMR (300 MHz, DMSO-d_6) δ 7.63 (d, J = 1.8 Hz, 1H, H^2), 7.39 (d, J = 1.8 Hz, 1H, H^1), 4.43 (s, 2H, H^3). ^{13}C NMR (101 MHz, DMSO) δ 147.89 (2C), 127.27, 122.11 (2C), 116.53, 113.57, 55.30, 18.84. MS (EI+) m/z calcd for $C_9H_5Cl_2N_3$:224.99; found, 226.60 (M + 1).

2-(5,6-dichloro-1H-benzo[d]imidazol-2-yl)acetonitrile: IIc

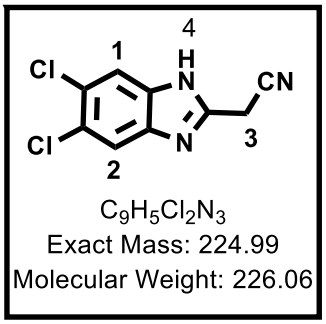

Obtained from 4,5-dichlorobenzene-1,2-diamine **Ib** and ethylcyano acetate as a brown solid (76%); R_f (EtOAc:Hexane, 1:1) 0.33; ^{1}H NMR (300 MHz, DMSO-d_6) δ 12.90 (s, 1H, H^4), 7.83 (s, 2H, $H^{1, 2}$), 4.41 (s, 2H, H^3). ^{13}C NMR (101 MHz, DMSO) δ 162.19, 148.31 (2C), 143.29, 127.18, 116.57 (2C), 116.13, 26.63. MS (EI+) m/z calcd for $C_9H_5Cl_2N_3$:224.99; found, 225.90 (M + 1).

b) General procedure for the synthesis of hydroxyl intermediates

The appropriately substituted benzimidazole acetonitrile (1 equiv.), ethyl 4,4,4-trifluoro-3-oxobutanoate (1.2 equiv.) and ammonium acetate (2 equiv.) were stirred at 145°C for 2 hours. Reaction was monitored using TLC and LCMS. Reaction mixture was cooled to 70°C, acetonitrile added while stirring for a further 10 minutes. After cooling to room temperature, the mixture was filtered, residue washed with acetonitrile and the product left to dry and used in subsequent step without further purification.

7,9-dichloro-1-hydroxy-3-(trifluoromethyl)benzo[4,5]imidazo[1,2-a]pyridine-4-carbonitrile: IIIb

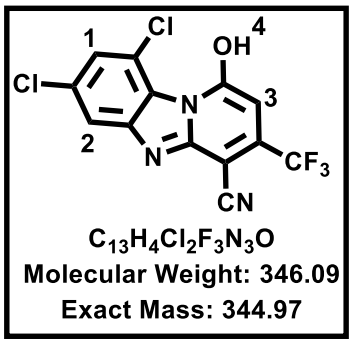

$C_{13}H_4Cl_2F_3N_3O$
Molecular Weight: 346.09
Exact Mass: 344.97

Obtained from **IIb** as a grey solid (28%); R_f (EtOAc:Hexane, 7:3) 0.18; ^{1}H NMR (300 MHz, DMSO-d_6) δ 8.48 (d, J = 2.0 Hz, 1H, H^2), 7.57 (d, J = 2.0 Hz, 1H, H^1), 5.93 (s, 1H, H^3). ^{13}C NMR (101 MHz, DMSO) δ 159.70, 153.00, 139.36, 131.27, 129.32, 127.54, 124.70, 123.47, 120.66, 117.43, 116.91, 114.45, 95.59. MS (EI-) m/z calcd for $C_{13}H_4Cl_2F_3N_3O$:344.97; found, 343.90 (M - 1).

7,8-dichloro-1-hydroxy-3-(trifluoromethyl)benzo[4,5]imidazo[1,2-a]pyridine-4-carbonitrile: IIIc

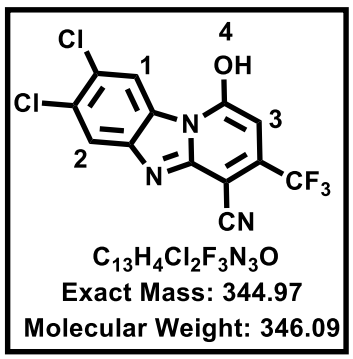

$C_{13}H_4Cl_2F_3N_3O$
Exact Mass: 344.97
Molecular Weight: 346.09

Obtained from **IIc** as a grey powder (49%); R_f (EtOAc:Hexane, 3:2) 0.31; ^{1}H NMR (300 MHz, DMSO-d_6) δ 8.64 (s, 1H, H^2), 7.83 (s, 1H, H^1), 5.85 (s, 1H, H^3). ^{13}C NMR (101 MHz, DMSO) δ 172.53, 169.51, 159.85, 154.00, 144.91, 129.71, 127.43, 124.22, 120.92, 117.79, 117.22, 116.56, 94.50. MS (EI-) m/z calcd for $C_{13}H_4Cl_2F_3N_3O$:344.97; found, 343.90 (M - 1).

c) General procedure for the synthesis of chloro intermediates

Phosphoryl oxychloride ($POCl_3$; 20 equiv.) was added to the appropriately substituted hydroxyl intermediate (1 equiv.) and stirred at 130°C for 3 hours. Excess $POCl_3$ was removed under reduced pressure. On cooling to room temperature, ice cold water was added with consistent stirring for 15 minutes. The mixture was neutralized using sodium carbonate, the crude product filtered off, washed with water and dried at ambient conditions and used without further purification.

1,7,9-trichloro-3-(trifluoromethyl)benzo[4,5]imidazo[1,2-a]pyridine-4-carbonitrile: IVb

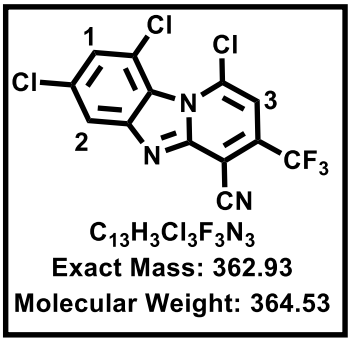

$C_{13}H_3Cl_3F_3N_3$
Exact Mass: 362.93
Molecular Weight: 364.53

Obtained from **IIIb** as a red-brown solid (63%); R_f (EtOAc:Hexane, 7:3) 0.56; ^{1}H NMR (300 MHz, DMSO-d_6) δ 8.77 (d, J = 1.7 Hz, 1H, H^2), 8.05 (d, J = 1.6 Hz, 1H, H^1), 7.94 (s, 1H, H^3); ^{13}C NMR (101 MHz, DMSO) δ 174.79, 158.66, 150.55, 144.16, 139.79, 133.58, 130.44, 126.23 (2C), 121.26, 115.13 (2C), 100.59. MS (EI+) m/z calcd for $C_{13}H_3Cl_3F_3N_3$:362.93; found, 363.90 (M +1).

1,7,8-trichloro-3-(trifluoromethyl)benzo[4,5]imidazo[1,2-a]pyridine-4-carbonitrile: IVc

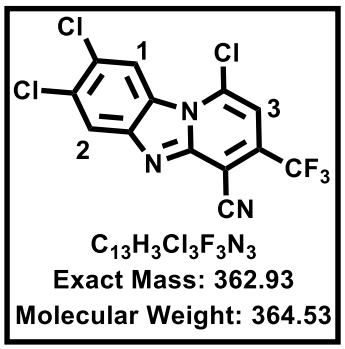

$C_{13}H_3Cl_3F_3N_3$
Exact Mass: 362.93
Molecular Weight: 364.53

Obtained from **IIIc** as a red solid (94%); R_f: (EtOAc:Hexane, 9:1) 0.53; ^{1}H NMR (300 MHz, DMSO-d_6) δ 8.86 (s, 1H, H^2), 8.36 (s, 1H, H^1), 7.86 (s, 1H,H^3); ^{13}C NMR (101 MHz, DMSO) δ 158.25, 150.17, 139.16, 132.68, 129.49, 127.76, 124.34, 120.29, 117.42 (2C), 114.55, 112.77, 101.70. MS (EI-) m/z calcd for $C_{13}H_3Cl_3F_3N_3$:362.93; found, 361.90 (M -1).

7.2.2.3 SAR$_3$ intermediates

a) Methyl 1-hydroxy-3-(trifluoromethyl)benzo[4,5]imidazo[1,2-a]pyridine-4-carboxylate:IIId

Synthesised using methyl 2-(1H-benzo[d]imidazol-2-yl)acetate **IId** according to the method described in **7.2.2.1a** and used subsequently without further purification.

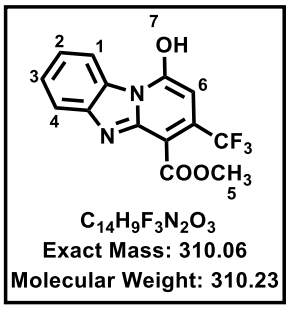

$C_{14}H_9F_3N_2O_3$
Exact Mass: 310.06
Molecular Weight: 310.23

Obtained as a light yellow powder (27%); R_f (EtOAc:Hexane, 2:3) 0.38; ^{1}H NMR (300 MHz, DMSO-d_6) δ 8.64 (d, *J* = 8.0 Hz, 1H, H^1), 7.77 (d, *J* = 8.1 Hz, 1H, H^4), 7.58 (td, *J* = 8.4, 7.9, 1.2 Hz, 1H, H^3), 7.41 (td, *J* = 7.9, 1.2 Hz, 1H, H^2), 6.40 (s, 1H, H^6), 3.90 (s, 3H, H^5). ^{13}C NMR (101 MHz, DMSO) δ 163.86, 158.49, 146.50, 137.93, 132.47, 127.51, 123.15, 121.81, 117.09, 116.75, 112.78, 111.53, 104.09, 52.35. MS (EI-) m/z calcd for $C_{14}H_9F_3N_2O_3$:310.06; found, 309.00(M-1).

b) Methyl 1-chloro-3-(trifluoromethyl)benzo[4,5]imidazo[1,2-a]pyridine-4-carboxylate:IVd

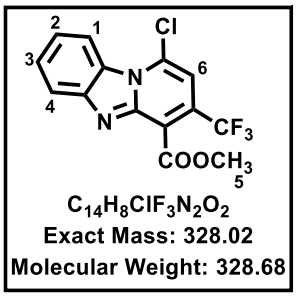

$C_{14}H_8ClF_3N_2O_2$
Exact Mass: 328.02
Molecular Weight: 328.68

Synthesised from **IIId** according to procedure described in **7.2.2.1b** and obtained as light yellow powder (90%); R_f (EtoAc:Hexane, 3:7) 0.63; ^{1}H NMR (400 MHz, DMSO-d_6) δ 8.65 (dt, J = 8.2, 1.0 Hz, 1H, H^1), 7.77 (dt, J = 8.1, 1.0 Hz, 1H, H^4), 7.62 – 7.55 (m, 1H, H^3), 7.42 (ddd, J = 8.4, 7.4, 1.1 Hz, 1H, H^2), 6.40 (s, 1H, H^6), 3.90 (s, 3H, H^5). ^{13}C NMR (101 MHz, DMSO) δ 164.01, 145.13, 133.01, 129.64, 127.55, 126.14, 125.80, 123.98, 123.60, 120.61, 116.45, 106.87, 106.83, 54.09. MS (EI+) m/z calcd for $C_{14}H_8ClF_3N_2O_2$:328.02; found, 328.80 (M+1).

c) 1-chloro-3-(trifluoromethyl)benzo[4,5]imidazo[1,2-a]pyridine-4-carboxamide: VI

Synthesised by reacting **IVa** with conc. Sulfuric acid (60 equiv.) at 85 °C with stirring for 2 hours. The reaction mixture was cooled and slowly added to ice-cold water while stirring. The precipitate that formed was filtered and dried at 50 °C in the oven and used without further purifications.

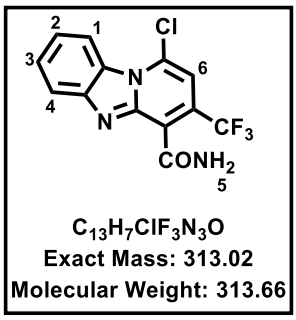

$C_{13}H_7ClF_3N_3O$
Exact Mass: 313.02
Molecular Weight: 313.66

Obtained as light grey powder (89%); R_f (2% MeoH/DCM) 0.14

^{1}H NMR (400 MHz, DMSO-d_6) δ 8.73 (d, J = 8.6 Hz, 1H, H^1), 8.14 (s, 1H, H^5), 8.03 (d, J = 8.2 Hz, 1H, H^4), 8.00 (s, 1H, H^5), 7.70 (ddd, J = 8.2, 7.1, 1.0 Hz, 1H, H^3), 7.56 (ddd, J = 8.4, 7.2, 1.1 Hz, 1H, H^2), 7.51 (s, 1H, H^6). ^{13}C NMR (101 MHz, DMSO) δ 164.27, 146.13, 145.05, 130.80, 129.50, 127.33, 126.10, 124.93, 124.30, 123.40, 120.62, 116.28, 107.19. MS (EI+) m/z calcd for $C_{13}H_7ClF_3N_3O$:313.02; found, 313.80 (M+1).

7.2.2.4 General procedures for the synthesis of target compounds

Target compounds were accessed via either of the two methods described hereafter. In the first instance, a nucleophilic substitution reaction, under microwave irradiation, was carried out using the elected amine and the appropriate chloro intermediate. In the second method, catalyst-mediated Buchwald-Hartwig reaction conditions were employed.

a) Nucleophilic substitution under microwave irradiation

The appropriate amine was added to a stirred mixture of the chloro intermediate (1.015mmol, 1 equiv.), triethylamine (2.03mmol, 2 equiv.) and tetrahydrofuran (THF) (4mL) and subjected to microwave irradiation at 150W, 80°C for 20-40 minutes. The cooled reaction mixture was transferred to a round bottom flask and concentrated. Minimum amount of either acetone or ethanol was added to precipitate the final product which was filtered off and dried. If further purification was needed, recrystallization in ethanol or column chromatography was performed.

1-(p-tolylamino)-3-(trifluoromethyl) benzo [4,5] imidazo [1,2-a]pyridine-4-carbonitrile: 1a/GMP-06.

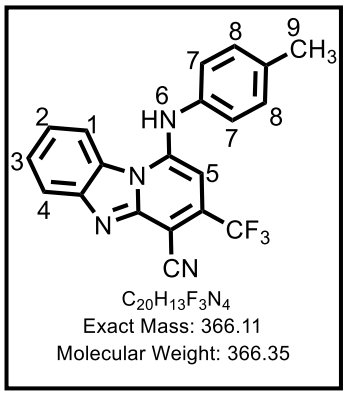

Obtained from **IVa** (0.3g, 1.015mmol, 1 equiv.) using *p*-toluidine (0.218g, 2.03mmol, 2 equiv.) as a yellow fluffy powder (38%). ^{1}H NMR (400 MHz, DMSO) δ 8.77 (d, *J* = 8.3 Hz, 1H, H^1), 7.74 (d, *J* = 7.9 Hz, 1H, H^4), 7.60 (t, *J* = 7.7 Hz, 1H, H^3), 7.49 – 7.34 (m, 1H, H^2), 7.26 (d, *J* = 8.0 Hz, 2H, H^7), 7.09 (d, *J* = 6.2 Hz, 2H, H^8), 6.25 (s, 1H, H^5), 2.35 (s, 3H, H^9). ^{13}C NMR (151 MHz, DMSO) δ 148.42, 147.89, 135.37, 134,52, 131.42, 128.71, 127.33, 125.04 (2C), 124.03, 123.13, 121.97 (2C), 121.30, 119.62, 117.83, 114.91, 112.47, 96.91, 20.94. MS (EI+) m/z calcd for $C_{20}H_{13}F_3N_4$:366.11; found, 367.10 (M + 1). HPLC purity: 99%.

1-((4-propoxyphenyl) amino)-3-(trifluoromethyl) benzo[4,5] imidazo[1,2-a]pyridine-4-carbonitrile 1c/GMP-10.

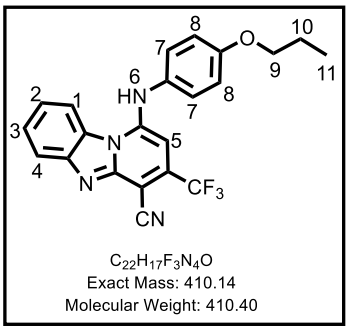

Obtained from **IVa** (0.3g, 1.015mmol, 1 equiv.) using 4-propoxyaniline (0.46g, 3.045mmol, 3 equiv.) as a light green powder (56%). ^{1}H NMR (400 MHz, DMSO) δ 8.77 (d, *J* = 8.3 Hz, 1H, H^1), 7.78 (d, *J* = 7.2 Hz, 1H, H^4), 7.61 (t, *J* = 7.7 Hz, 1H, H^3), 7.43 (t, *J* = 7.8 Hz, 1H, H^2), 7.18 (s, 2H, H^7), 7.04 (d, *J* = 8.7 Hz, 2H, H^8), 6.21 (s, 1H, H^5), 3.99 (t, *J* = 6.5 Hz, 2H, H^9), 1.85 – 1.70 (m, 2H, H^{10}), 1.02 (t, *J* = 7.4 Hz, 3H, H^{11}). ^{13}C NMR (151 MHz, DMSO) δ 148.38, 144.85, 142.84, 138.92, 132.78, 128.71, 126.86, 123.64, 122.56, 121.82 (2C), 119.92, 117.18, 116.21 (2C), 114.92, 112.36, 110.64, 94.78, 69.98, 22.57, 10.75. MS (EI+) m/z calcd for $C_{22}H_{17}F_3N_4O$:410.14; found, 411.10 (M + 1). HPLC purity: 99%.

1-((4-isopropylphenyl)amino)-3-(trifluoromethyl)benzo[4,5]imidazo[1,2-a]pyridine-4-carbonitrile 1d/GMP-11.

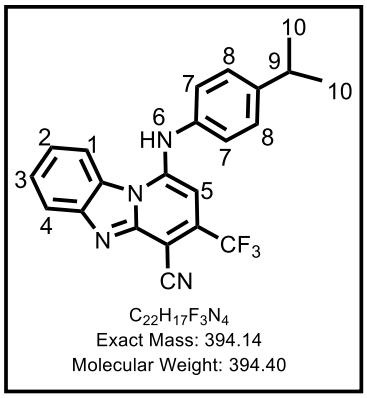

$C_{22}H_{17}F_3N_4$
Exact Mass: 394.14
Molecular Weight: 394.40

Obtained from **IVa** (0.3g, 1.015mmol, 1 equiv.) using 4-isopropylaniline (0.412g, 3.045mmol, 3 equiv.), triethylamine (0.205g (0.28ml); 2.03mmol, 2Eq) as a yellow powder (23%); m.p. 262-266 °C; R_f (MeOH: DCM, 0.5:9.5) 0.53; ^{1}H NMR (400 MHz, DMSO) δ 8.78 (d, *J* = 7.9 Hz, 1H, H^1), 7.75 (d, *J* = 11.3 Hz, 1H, H^4), 7.60 (t, *J* = 7.6 Hz, 1H, H^3), 7.42 (t, *J* = 7.8 Hz, 1H, H^2), 7.33 (d, *J* = 8.1 Hz, 2H, H^7), 7.13 (s, 2H, H^8), 6.28 (s, 1H, H^5), 3.01 – 2.89 (m, 1H, H^9), 1.27 (d, *J* = 6.9 Hz, 6H, H^{10}); ^{13}C NMR (151 MHz, DMSO) δ 148.60, 145.17, 137.56, 135.40, 134.84, 133.92, 131.78. 129.34, 128.77, 127.87, 127.13, 125.40, 123.65, 122.58 (2C), 121.78, 117.16 (2C), 114.98, 33.58, 24.41 (2C). MS (EI+) m/z calcd for $C_{22}H_{17}F_3N_4$:394.14; found, 395.10 (M + 1). HPLC purity: 99%.

1-((4-methoxyphenyl) amino)-3-(trifluoromethyl) benzo[4,5] imidazo[1,2-a]pyridine-4-carbonitrile 1e/GMP-12.

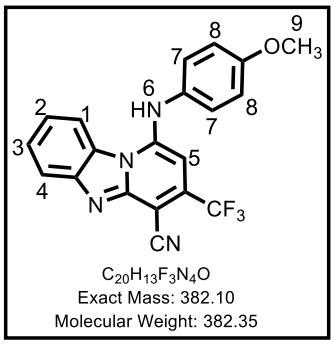

$C_{20}H_{13}F_3N_4O$
Exact Mass: 382.10
Molecular Weight: 382.35

Obtained from **IVa** (0.3g, 1.015mmol, 1 equiv.) using 4-isopropylaniline (0.375g, 3.045mmol, 3 equiv.) as a light green powder (51%). ^{1}H NMR (400 MHz, DMSO) δ 8.78 (d, *J* = 7.3 Hz, 1H, H^1), 8.35 (d, *J* = 8.4 Hz, 1H, H^4), 7.61 (t, *J* = 7.6 Hz, 1H, H^3), 7.44 (t, *J* = 7.9 Hz, 1H, H^2), 7.19 (d, *J* = 8.6 Hz, 2H, H^7), 7.05 (d, *J* = 8.4 Hz, 2H, H^8), 6.18 (s, 1H, H^5), 3.80 (s, 3H, H^9). ^{13}C NMR (101 MHz, DMSO) δ 157.43, 149.23, 148.60, 134.78, 128.72, 127.09, 126.83, 124.89 (2C), 124.10, 122.41, 121.38, 118.71, 117.17, 115.60 (2C), 114.89, 112.82, 88.74, 55.92. MS (EI+) m/z calcd for $C_{20}H_{13}F_3N_4O$:382.10; found, 383.10 (M + 1). HPLC purity: 96%.

1-((4-(dimethylamino)phenyl)amino)-3-(trifluoromethyl)benzo[4,5]imidazo[1,2-a]pyridine-4- carbonitrile 1f/GMP-13.

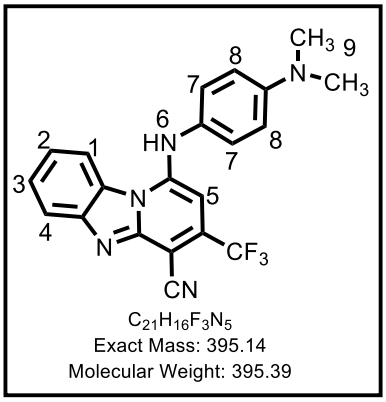

Obtained from **IVa** (0.3g, 1.015mmol, 1 equiv.) using N^1,N^1-dimethylbenzene-1,4-diamine (0.415g, 3.045mmol, 3 equiv.) as a dark green powder (51%). ^{1}H NMR (300 MHz, DMSO) δ 8.75 (d, *J* = 8.4 Hz, 1H, H^1), 7.82 (d, *J* = 7.4 Hz, 1H, H^4), 7.61 (t, *J* = 7.6 Hz, 1H, H^3), 7.43 (t, *J* = 7.9 Hz, 1H, H^2), 7.18 (d, *J* = 7.3 Hz, 2H, H^7), 6.84 (d, *J* = 8.6 Hz, 2H, H^8), 6.15 (s, 1H, H^5), 2.95 (s, 6H, H^9). ^{13}C NMR (101 MHz, DMSO) δ 150.01, 149.05, 148.88, 141.89, 135.92, 132.68, 128.73, 126.99 (2C), 125.91, 121.92, 121.35 (2C), 118.86, 117.94, 116.82, 115.32, 113.65, 96.72, 46.58 (2C). MS (EI+) m/z calcd for $C_{21}H_{16}F_3N_5$:395.14; found, 396.10 (M + 1). HPLC purity: 96%.

4-((4-cyano-3-(trifluoromethyl)benzo[4,5]imidazo[1,2-a]pyridin-1-yl)amino)-N-methylbenzamide 1g/GMP-15.

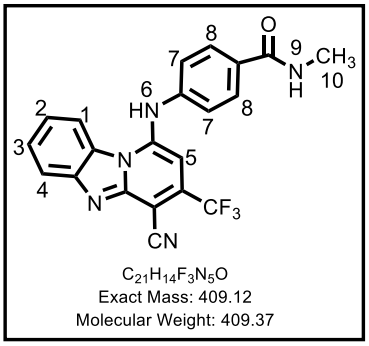

Obtained from **IVa** (0.3g, 1.015mmol, 1 equiv.) using 4-amino-N-methylbenzamide (0.458g, 3.045mmol, 3 equiv.), triethylamine (0.205g (0.28ml); 2.03mmol, 2 equiv.) as a light yellow fluffy powder (13%). ^{1}H NMR (400 MHz, DMSO) δ 8.81 (d, *J* = 8.2 Hz, 1H, H^1), 8.16 (d, *J* = 4.2 Hz, 1H, H^9), 7.90 (d, *J* = 8.6 Hz, 2H, H^7), 7.70 (d, *J* = 8.1 Hz, 1H, H^4), 7.63 – 7.57 (m, 1H, H^3), 7.46 – 7.40 (m, 1H, H^2), 7.15 (d, *J* = 8.0 Hz, 2H, H^8), 6.28 (s, 1H, H^5), 2.83 (d, *J* = 4.5 Hz, 3H, H^{10}). ^{13}C NMR (151 MHz, DMSO) δ 166.84, 148.54, 148.08, 138.26, 134.98, 130.36, 129.19 (2C), 128.77, 127.24, 125.44, 123.63, 122.97, 121.68 (2C), 117.61 (2C), 115.05, 113.39, 95.97, 26.35. MS (EI+) m/z calcd for $C_{21}H_{14}F_3N_5O$:409.12; found, 410.10 (M + 1). HPLC purity: 98%.

1-((4-(trifluoromethoxy)phenyl)amino)-3-(trifluoromethyl)benzo[4,5]imidazo[1,2-a]pyridine-4- carbonitrile 1j/GMP-19.

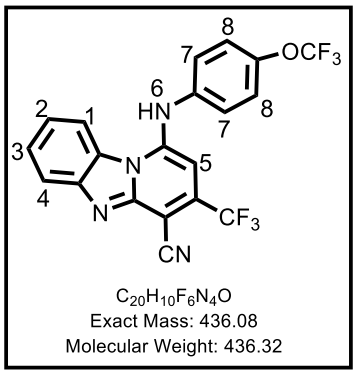

Obtained from **IVa** (0.3g, 1.015mmol, 1 equiv.) using 4-(trifluoromethoxy)aniline (0.36g, 2.03mmol, 2 equiv.) as a light green fluffy powder (16%). ^{1}H NMR (400 MHz, DMSO) δ 8.82 (d, *J* = 8.1 Hz, 1H, H^{1}), 7.69 (d, *J* = 8.0 Hz, 1H, H^{4}), 7.64 – 7.54 (m, 1H, H^{3}), 7.46 – 7.42 (m, 1H, H^{2}), 7.39 (d, *J* = 8.3 Hz, 2H, H^{7}), 7.20 (d, *J* = 8.4 Hz, 2H, H^{8}), 6.24 (s, 1H, H^{5}). ^{13}C NMR (151 MHz, DMSO) δ 148.53, 144.88, 135.23, 128.91, 127.21, 125.36, 123.71, 122.92, 122.71 (2C), 121.81, 121.58, 120.05, 119.68, 117.77 (2C), 115.20, 113.38, 95.93, 46.29. MS (EI+) m/z calcd for $C_{20}H_{10}F_6N_4O$:436.08; found, 437.10 (M + 1). HPLC purity: 99%.

Methyl 4-((4-cyano-3-(trifluoromethyl)benzo[4,5]imidazo[1,2-a]pyridin-1-yl)amino)benzoate: 1m/GMP-20.

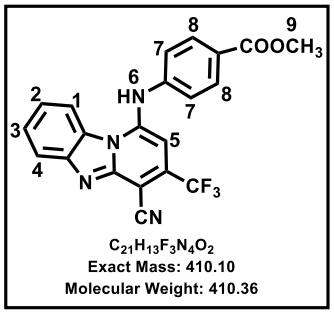

Obtained from **IVa** (0.3g, 1.015mmol, 1equiv.) using methyl 4-aminobenzoate (0.184g, 1.218mmol, 1.2 equiv.) as a light green fluffy powder (19%); R_f (MeOH: DCM, 0.5:9.5) 0.42; ^{1}H NMR (400 MHz, DMSO) δ 8.80 (d, *J* = 8.2 Hz, 1H, H^{1}), 8.00 (d, *J* = 8.4 Hz, 2H, H^{8}), 7.68 (d, *J* = 8.0 Hz, 1H, H^{4}), 7.60 (t, *J* = 7.6 Hz, 1H, H^{3}), 7.42 (t, *J* = 7.8 Hz, 1H, H^{2}), 7.18 (d, *J* = 8.2 Hz, 2H, H^{7}), 6.27 (s, 1H, H^{5}), 3.87 (s, 3H, H^{9}); ^{13}C NMR (101 MHz, DMSO) δ 166.47, 148.42, 147.89, 135.37, 131.42 (2C), 128.71, 127.33, 125.04 (2C), 124.03, 123.13, 121.97 (2C), 121.30, 117.83, 114.91, 114.03, 112.47, 96.91, 52.19. MS (EI+) m/z calcd for $C_{21}H_{13}F_3N_4O_2$:410.10; found, 411.10 (M + 1). HPLC purity: 95%.

1-((4-(dimethylamino)benzyl)amino)-3-(trifluoromethyl)benzo[4,5]imidazo[1,2-a]pyridine-4-carbonitrile 3a/GMP-24.

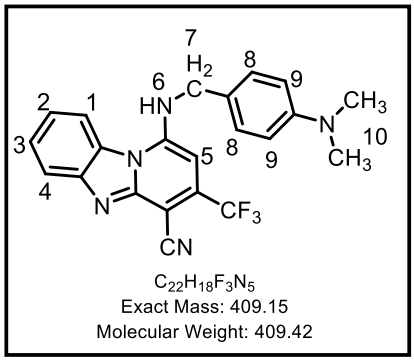

Obtained from **IVa** (0.3g, 1.015mmol, 1 equiv.) using 4-(aminomethyl)-N,N-dimethylaniline (0.183g, 1.218mmol, 1.2 equiv.) as a yellow powder (56%). ^{1}H NMR (300 MHz, DMSO) δ 8.69 (d, *J* = 8.4 Hz, 1H, H^{1}), 8.58 (bs, 1H, H^{6}), 7.92 (d, *J* = 7.8 Hz, 1H, H^{4}), 7.72 – 7.59 (m, 1H, H^{3}), 7.53 – 7.43 (m, 1H, H^{2}), 7.33 (d, *J* = 8.7 Hz, 2H, H^{8}), 6.72 (d, *J* = 8.8 Hz, 2H, H^{9}), 6.36 (s, 1H, H^{5}), 4.77 (s, 2H, H^{7}), 2.87 (s, 6H, H^{10}). ^{13}C NMR (101 MHz, DMSO) δ 150.34, 149.83, 148.46, 145.44, 137.25, 136.94, 128.60 (2C), 128.28, 127.07, 124.50, 124.11, 121.73, 121.38, 119.35, 115.54, 114.88, 112.88 (2C), 86.70, 46.58 (2C). MS (EI-) m/z calcd for $C_{22}H_{18}F_3N_5O$:409.15; found, 408.10 (M - 1). HPLC purity: 99%.

1-((pyridin-2-ylmethyl)amino)-3-(trifluoromethyl)benzo[4,5]imidazo[1,2-a]pyridine-4-carbonitrile 3j/GMP-25.

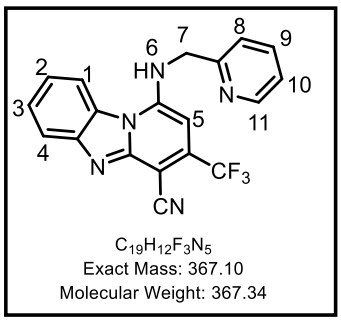

Obtained from **IVa** (0.3g, 1.015mmol, 1 equiv.) using pyridin-2-ylmethanamine (0.132g, 1.218mmol, 1.2 equiv.) as a light green fine powder (63%). 1H NMR (300 MHz, DMSO) δ 8.76 – 8.59 (m, 3H, $H^{1,6,11}$), 7.93 (d, *J* = 8.1 Hz, 1H, H^{4}), 7.85 (td, *J* = 7.7, 1.8 Hz, 1H, H^{9}), 7.65 (t, *J* = 7.7 Hz, 1H, H^{10}), 7.57 (d, *J* = 7.9 Hz, 1H, H^{8}), 7.54 – 7.47 (m, 1H, H^{3}), 7.42 – 7.33 (m, 1H, H^{2}), 6.40 (s, 1H, H^{5}), 4.99 (s, 2H, H^{7}). ^{13}C NMR (101 MHz, DMSO) δ 156.06, 149.87, 149.43, 148.30, 145.57, 137.68, 137.24, 128.33, 127.10, 124.14, 123.30, 122.38, 122.02, 121.32, 119.55, 115.22, 114.55, 86.72, 48.56. MS (EI+) m/z calcd for $C_{19}H_{12}F_3N_5$:367.10; found, 368.1 (M + 1). HPLC purity: 97%.

1-((4-fluorobenzyl)amino)-3-(trifluoromethyl)benzo[4,5]imidazo[1,2-a]pyridine-4-carbonitrile 3b/GMP-28.

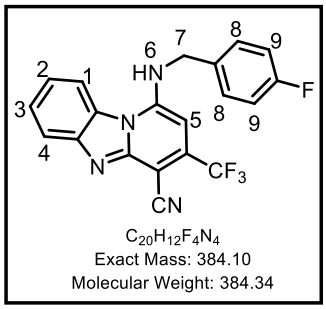

Obtained from **IVa** (0.3g, 1.015mmol, 1 equiv.) using (4-fluorophenyl)methanamine (0.152g, 1.218mmol, 1.2 equiv.) as a light green powder (59%). ^{1}H NMR (300 MHz, DMSO) δ 8.71 (d, *J* = 8.3 Hz, 1H, H^{1}), 8.63 (bs, 1H, H^{6}), 7.92 (d, *J* = 8.2 Hz, 1H, H^{4}), 7.71 – 7.61 (m, 1H, H^{3}), 7.61 – 7.53 (m, 2H, H^{8}), 7.53 – 7.45 (m, 1H, H^{2}), 7.25 – 7.16 (m, 2H, H^{9}), 6.30 (s, 1H, H^{5}), 4.90 (s, 2H, H^{7}). ^{13}C NMR (101 MHz, DMSO) δ 163.26, 160.84, 149.97, 148.43, 137.33, 134.34, 133.80, 129.70 (2C), 129.62, 128.48, 127.05, 121.80, 119.35, 115.92 (2C), 115.71, 114.59, 86.63, 46.56. MS (EI+) m/z calcd for $C_{20}H_{12}F_4N_4$:384.10; found, 385.1 (M + 1). HPLC purity: 96%.

1-(methyl(pyridin-2-ylmethyl)amino)-3-(trifluoromethyl)benzo[4,5]imidazo[1,2-a]pyridine-4- carbonitrile 3c/GMP-29.

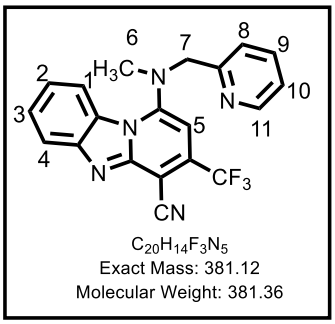

Obtained from **IVa** (0.3g, 1.015mmol, 1 equiv.) using N-methyl-1- (pyridin-2-yl)methanamine (0.148g, 1.218mmol, 1.2 equiv.) as a dark green solid (63%). ^{1}H NMR (300 MHz, DMSO) δ 8.52 (ddd, *J* = 4.9, 1.8, 0.9 Hz, 1H, H^{11}), 8.42 (d, *J* = 8.4 Hz, 1H, H^{1}), 8.01 (d, *J* = 8.1 Hz, 1H, H^{4}), 7.80 (td, *J* = 7.7, 1.8 Hz, 1H, H^{9}), 7.69 (ddd, *J* = 8.3, 7.3, 1.0 Hz, 1H, H^{3}), 7.53 (ddd, *J* = 8.4, 7.2, 1.2 Hz, 1H, H^{2}), 7.42 (d, *J* = 7.8 Hz, 1H, H^{8}), 7.32 (ddd, *J* = 7.5, 4.9, 1.1 Hz, 1H, H^{10}), 6.85 (s, 1H, H^{5}), 4.76 (s, 2H, H^{7}), 2.98 (s, 3H, H^{6}). ^{13}C NMR (101 MHz, DMSO) δ 155.73, 154.08, 149.70, 148.00, 145.57, 137.36, 136.33, 136.00, 129.15, 127.40, 123.91, 123.34, 122.74, 119.93, 117.18, 113.64, 96.69, 96.65, 90.06, 58.79. MS (EI+) m/z calcd for $C_{20}H_{14}F_3N_5$:381.12; found, 382.10 (M + 1). HPLC purity: 96%.

1-(phenylamino)-3-(trifluoromethyl)benzo[4,5]imidazo[1,2-a]pyridine-4-carbonitrile 1n/GMP-32.

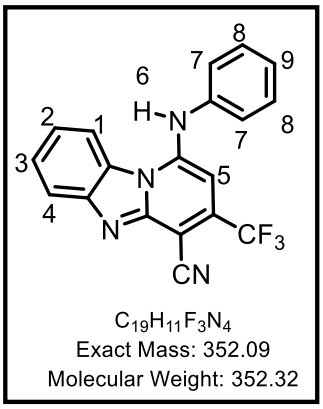

$C_{19}H_{11}F_3N_4$
Exact Mass: 352.09
Molecular Weight: 352.32

Obtained from **IVa** (0.3g, 1.015mmol, 1 equiv.) using aniline (0.113g, 1.218mmol, 1.2 equiv.), triethylamine (0.205g (0.28ml); 2.03mmol, 2 equiv) as a yellow powder (23%). ^{1}H NMR (300 MHz, DMSO) δ 8.80 (d, *J* = 8.2 Hz, 1H, H^1), 7.70 (d, *J* = 7.0 Hz, 1H, H^4), 7.59 (t, *J* = 7.3 Hz, 1H, H^3), 7.50 – 7.37 (m, 3H, $H^{2, 7}$), 7.27 – 7.00 (m, 3H, $H^{8, 9}$), 6.22 (s, 1H, H^5). ^{13}C NMR (101 MHz, DMSO) δ 148.59, 148.45, 148.29, 136.94, 134.74, 132.38, 130.10, 128.77, 127.17 (2C), 124.55, 124.09, 122.75 (2C), 122.59, 119.85, 117.54, 115.05, 114.40. MS (EI+) m/z calcd for $C_{19}H_{11}F_3N_4$:352.09; found, 353.10 (M + 1). HPLC purity: 99%.

1-(benzylamino)-3-(trifluoromethyl)benzo[4,5]imidazo[1,2-a]pyridine-4-carbonitrile 3d/GMP-33.

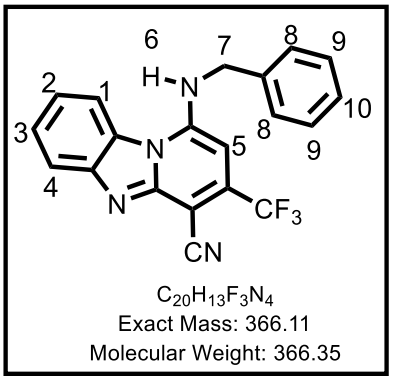

$C_{20}H_{13}F_3N_4$
Exact Mass: 366.11
Molecular Weight: 366.35

Obtained from **IVa** (0.3g, 1.015mmol, 1 equiv.) using phenylmethanamine (0.131g, 1.218mmol, 1.2 equiv.) as a dark yellow solid (50%). ^{1}H NMR (300 MHz, DMSO) δ 8.73 (d, *J* = 8.4 Hz, 1H, H^1), 7.91 (d, *J* = 7.6 Hz, 1H, H^4), 7.70 – 7.59 (m, 1H, H^3), 7.53 – 7.43 (m, 3H, $H^{2, 8}$), 7.41 – 7.33 (m, 2H, H^9), 7.34 – 7.24 (m, 1H, H^{10}), 6.29 (s, 1H, H^5), 4.91 (s, 2H, H^7). ^{13}C NMR (101 MHz, DMSO) δ 150.07, 148.58, 145.42, 137.83, 137.22, 129.07 (2C), 128.55, 127.81 (2C), 127.55 (2C), 126.92, 124.17, 121.67, 119.19, 115.70, 114.83, 86.79, 47.41. MS (EI+) m/z calcd for $C_{20}H_{13}F_3N_4$:366.11; found, 367.10 (M + 1). HPLC purity: 98%.

1-((4-methoxybenzyl)amino)-3-(trifluoromethyl)benzo[4,5]imidazo[1,2-a]pyridine-4-carbonitrile 3e/GMP-34.

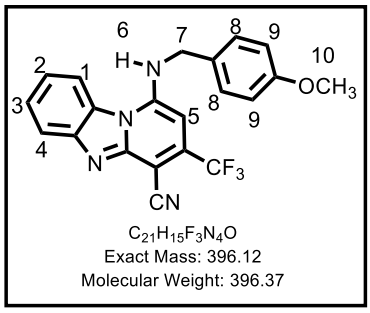

$C_{21}H_{15}F_3N_4O$
Exact Mass: 396.12
Molecular Weight: 396.37

Obtained from **IVa** (0.3g, 1.015mmol, 1 equiv.) using (4-methoxyphenyl)methanamine (0.167g, 1.218mmol, 1.2 equiv.) as a light green solid (43%). ^{1}H NMR (300 MHz, DMSO) δ 8.71 (d, *J* = 8.4 Hz, 1H, H^1), 7.91 (d, *J* = 8.1 Hz, 1H, H^4), 7.64 (t, *J* = 7.6 Hz, 1H, H^3), 7.52 – 7.41 (m, 3H, $H^{2,8}$), 6.98 – 6.89 (m, 2H, H^9), 6.31 (s, 1H, H^5), 4.82 (s, 2H, H^7), 3.74 (s, 3H, H^{10}). ^{13}C NMR (101 MHz, DMSO) δ 159.24, 149.98, 148.55, 145.43, 137.09, 129.58, 128.95 (2C), 128.49, 126.94, 124.02, 121.66, 121.44, 119.22, 115.66, 114.80, 114.65 (2C), 86.76, 55.64, 46.82. MS (EI+) m/z calcd for $C_{21}H_{15}F_3N_4O$:396.12; found, 397.10 (M + 1). HPLC purity: 99%.

1-((4-(trifluoromethoxy)benzyl)amino)-3-(trifluoromethyl)benzo[4,5]imidazo[1,2-a]pyridine-4- carbonitrile 3f/GMP-35.

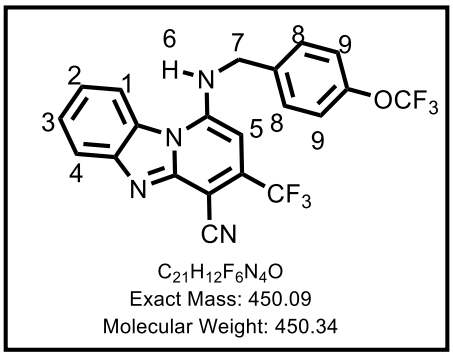

$C_{21}H_{12}F_6N_4O$
Exact Mass: 450.09
Molecular Weight: 450.34

Obtained from **IVa** (0.3g, 1.015mmol, 1 equiv.) using (4-(trifluoromethoxy)phenyl)methanamine (0.233g, 1.218mmol, 1.2 equiv.) as a yellow shiny solid (49%). ^{1}H NMR (300 MHz, DMSO) δ 8.71 (d, *J* = 8.4 Hz, 1H, H^1), 7.92 (d, *J* = 7.7 Hz, 1H, H^4), 7.72 – 7.60 (m, 3H, $H^{3,8}$), 7.49 (ddd, *J* = 8.4, 7.2, 1.2 Hz, 1H, H^2), 7.37 (dd, *J* = 8.8, 0.9 Hz, 2H, H^9), 6.31 (s, 1H, H^5), 4.95 (s, 2H, H^7). ^{13}C NMR (101 MHz, DMSO) δ 150.00, 148.48, 148.17, 137.28, 135.81, 133.84, 130.28, 129.51, 128.51, 127.00, 126.78, 124.13, 122.84, 121.48 (2C), 119.22, 115.75 (2C), 114.49, 86.73, 46.50. MS (EI+) m/z calcd for $C_{21}H_{12}F_6N_4O$:450.09; found, 451.10 (M + 1). HPLC purity: 99%.

1-((4-(methylsulfonyl)benzyl)amino)-3-(trifluoromethyl)benzo[4,5]imidazo[1,2-a]pyridine-4-carbonitrile 3g/GMP-36.

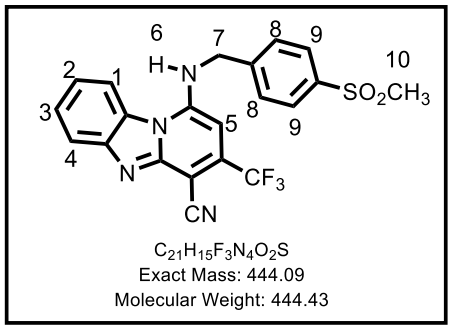

Obtained from **IVa** (0.3g, 1.015mmol, 1 equiv.) using (4-(methylsulfonyl)phenyl)methanamine (0.226g, 1.218mmol, 1.2 equiv.) as a tan solid (56%). ^{1}H NMR (300 MHz, DMSO) δ 8.74 (d, *J* = 8.3 Hz, 1H, H^1), 7.98-7.88 (m, 3H, $H^{4,9}$), 7.79 (d, *J* = 8.3 Hz, 2H, H^8), 7.65 (t, *J* = 7.6 Hz, 1H, H^3), 7.54 – 7.45 (m, 1H, H^2), 6.31 (s, 1H, H^5), 5.04 (s, 2H, H^7), 3.21 (s, 3H, H^{10}). ^{13}C NMR (101 MHz, DMSO) δ 150.04, 148.22, 144.13, 140.23, 136.98, 128.56, 128.23 (2C), 127.50 (2C), 126.99, 122.24, 121.78, 121.17, 119.38, 119.14, 115.83, 114.75, 86.83, 47.01, 44.10. MS (EI+) m/z calcd for $C_{21}H_{15}F_3N_4O_2S$:444.09; found, 445.10 (M + 1). HPLC purity: 99%.

1-((4-methoxyphenyl)(methyl)amino)-3-(trifluoromethyl)benzo[4,5]imidazo[1,2-a]pyridine-4- carbonitrile 1o/GMP-37.

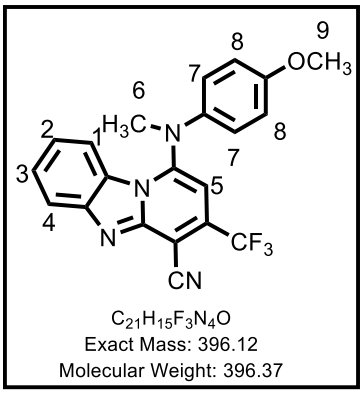

Obtained from **IVa** (0.3g, 1.015mmol, 1 equiv.) using 4-methoxy-N-methylaniline (0.167g, 1.218mmol, 1.2 equiv.) as a dark red solid (15%). ^{1}H NMR (400 MHz, DMSO) δ 7.95 (d, *J* = 8.2 Hz, 1H, H^1), 7.88 (dt, *J* = 8.5, 0.9 Hz, 1H, H^4), 7.57 (ddd, *J* = 8.3, 7.1, 1.1 Hz, 1H, H^3), 7.27 (ddd, *J* = 8.4, 7.1, 1.2 Hz, 1H, H^2), 7.10 – 7.03 (m, 3H, $H^{5,7}$), 6.87 – 6.80 (m, 2H, H^8), 3.69 (s, 3H, H^9), 3.59 (s, 3H, H^6). ^{13}C NMR (101 MHz, DMSO) δ 156.34, 150.85, 148.00, 145.37, 139.07, 136.28, 135.87, 128.40, 127.25, 122.52, 121.58 (2C), 119.70, 117.06, 115.33 (2C), 113.78, 100.06, 91.88, 55.75, 41.83. MS (EI+) m/z calcd for $C_{21}H_{15}F_3N_4O$:396.12; found, 397.10 (M + 1). HPLC purity: 98%.

1-((1-(4-(methylsulfonyl)phenyl)ethyl)amino)-3-(trifluoromethyl)benzo[4,5]imidazo[1,2-a]pyridine- 4-carbonitrile 3h/GMP-38.

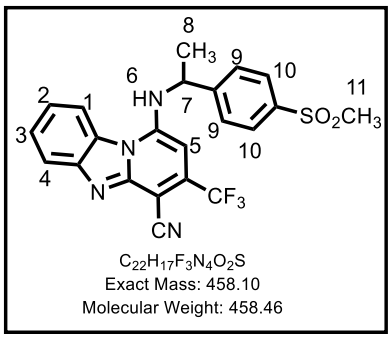

$C_{22}H_{17}F_3N_4O_2S$
Exact Mass: 458.10
Molecular Weight: 458.46

Obtained from **IVa** (0.3g, 1.015mmol, 1 equiv.) using 1-(4-(methylsulfonyl)phenyl)ethan-1-amine (0.248g, 1.218mmol, 1.2 equiv.) as a yellow fluffy powder (38%). ^{1}H NMR (400 MHz, DMSO) δ 8.65 (d, *J* = 7.74 Hz, 1H, H^1), 7.97 – 7.92 (m, 2H, H^{10}), 7.92 – 7.85 (m, 3H, $H^{4, 9}$), 7.65 (t, *J* = 7.7 Hz, 1H, H^3), 7.49 (t, *J* = 7.6 Hz, 1H, H^2), 6.23 (s, 1H, H^5), 5.30 (q, *J* = 6.8 Hz, 1H, H^7), 3.17 (s, 3H, H^{11}), 1.80 (d, *J* = 6.7 Hz, 3H, H^8). ^{13}C NMR (101 MHz, DMSO) δ 149.54, 139.86, 134.27, 127.70 (2C), 126.85, 126.45, 125.70, 125.37, 124.58, 124.22, 121.93, 121.81 (2C), 121.40, 116.78, 116.56, 116.35, 95.84, 54.25, 43.73, 23.00. MS (EI+) m/z calcd for $C_{22}H_{17}F_3N_4O_2S$:458.10; found, 459.10 (M + 1). HPLC purity: 99%.

1-((pyridin-3-ylmethyl)amino)-3-(trifluoromethyl)benzo[4,5]imidazo[1,2-a]pyridine-4-carbonitrile 3l/GMP-44.

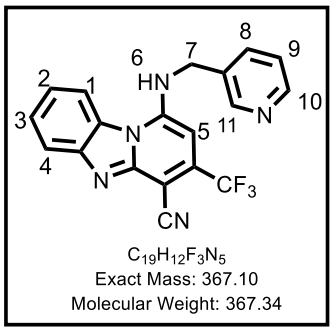

$C_{19}H_{12}F_3N_5$
Exact Mass: 367.10
Molecular Weight: 367.34

Obtained from **IVa** (0.3g, 1.015mmol, 1 equiv.) using pyridin-3-ylmethanamine (0.132g, 1.218mmol, 1.2 equiv.) as a yellow powder (62%). ^{1}H NMR (400 MHz, DMSO) δ 8.75 (d, *J* = 1.6 Hz, 1H, H^{11}), 8.70 (d, *J* = 8.4 Hz, 1H, H^1), 8.51 (dd, *J* = 4.8, 1.6 Hz, 1H, H^{10}), 7.98 – 7.86 (m, 2H, $H^{4, 8}$), 7.70 – 7.59 (m, 1H, H^3), 7.53 – 7.43 (m, 1H, H^2), 7.40 (ddd, *J* = 7.9, 4.8, 0.8 Hz, 1H, H^9), 6.34 (s, 1H, H^5), 4.96 (s, 2H, H^7). ^{13}C NMR (101 MHz, DMSO) δ 150.38 (2C), 148.16, 144.89, 143.36, 137.34, 136.34, 134.41, 133.80, 129.07, 124.63, 122.37, 119.81, 115.05 (2C), 106.72, 95.92, 85.77, 45.34. MS (EI+) m/z calcd for $C_{19}H_{12}F_3N_5$:367.10; found, 368.10 (M + 1). HPLC purity: 98%.

1-((pyrazin-2-ylmethyl)amino)-3-(trifluoromethyl)benzo[4,5]imidazo[1,2-a]pyridine-4-carbonitrile 3i/GMP-45.

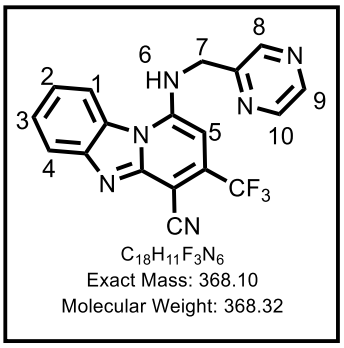

Obtained from **IVa** (0.3g, 1.015mmol, 1 equiv.) using pyrazin-2- ylmethanamine (0.133g, 1.218mmol, 1.2 equiv.) as a yellow powder (53%). ^{1}H NMR (400 MHz, DMSO) δ 8.88 (d, *J* = 1.4 Hz, 1H, H^8), 8.71 – 8.65 (m, 2H, $H^{1,9}$), 8.61 (d, *J* = 2.6 Hz, 1H, H^{10}), 7.91 (d, *J* = 8.1 Hz, 1H, H^4), 7.64 (t, *J* = 7.7 Hz, 1H, H^3), 7.53 – 7.42 (m, 1H, H^2), 6.47 (s, 1H, H^5), 5.09 (s, 2H, H^7). ^{13}C NMR (101 MHz, DMSO) δ 148.16 (3C), 144.89, 143.36, 137.34, 136.34, 134.41, 133.80, 129.07, 124.63, 122.37, 119.81, 115.05 (2C), 106.72, 85.77, 45.34. MS (EI+) m/z calcd for $C_{18}H_{11}F_3N_6$:368.10; found, 369.10 (M + 1). HPLC purity: 99%.

1-((4-(morpholinomethyl)phenyl)amino)-3-(trifluoromethyl) benzo[4,5] imidazo[1,2-a]pyridine-4- carbonitrile 1p/GMP-46.

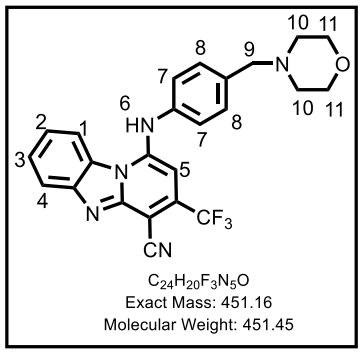

Obtained from **IVa** (0.3g, 1.015mmol, 1 equiv.) using 4-(morpholinomethyl)aniline (0.234g, 1.218mmol, 1.2 equiv.) and purified by column chromatography (1%MeOH:DCM) as an orange powder (25%). ^{1}H NMR (300 MHz, DMSO) δ 8.79 (d, *J* = 8.1 Hz, 1H, H^1), 7.61 (d, *J* = 8.1 Hz, 1H, H^4), 7.47 – 7.38 (m, 3H, $H^{3,7}$), 7.22 (t, *J* = 7.4 Hz, 1H, H^2), 7.07 (d, *J* = 8.2 Hz, 2H, H^8), 5.95 (s, 1H, H^5), 3.99 (s, 2H, H^9), 3.81-3.61 (m, 4H, H^{11}), 3.02-2.79 (m, 4H, H^{10}). ^{13}C NMR (101 MHz, DMSO) δ 149.61, 134.71, 132.13 (2C), 130.01, 127.23, 126.46, 125.70, 125.51 (2C), 124.88, 122.47, 121.41, 121.24, 120.48, 117.17 (2C), 115.34, 113.14, 64.99 (2C), 61.03, 52.24 (2C). MS (EI+) m/z calcd for $C_{24}H_{20}F_3N_5O$:451.16; found, 452.10 (M + 1). HPLC purity: 97%.

1-((4-(morpholinomethyl)benzyl)amino)-3-(trifluoromethyl)benzo[4,5]imidazo[1,2-a]pyridine-4- carbonitrile: 3m/GMP-47.

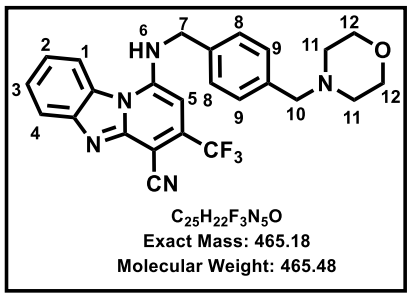

Obtained from **IVa** (0.3g, 1.015mmol, 1 equiv.) using (4-(morpholinomethyl)phenyl)methanamine (0.251g, 1.218mmol, 1.2 equiv.) as a yellow powder (48%). ^{1}H NMR (300 MHz, DMSO) δ 8.74 (d, *J* = 8.4 Hz, 1H, H^1), 8.63 (bs, 1H, H^6), 7.92 (d, *J* = 7.8 Hz, 1H, H^4), 7.65 (t, *J* = 7.6 Hz, 1H, H^3), 7.54 – 7.42 (m, 3H, $H^{2,8}$), 7.32 (d, *J* = 8.0 Hz, 2H, H^9), 6.29 (s, 1H, H^5), 4.90 (s, 2H, H^7), 3.65 – 3.52 (m, 4H, H^{12}), 3.49 (s, 2H, H^{10}), 2.46-2.26 (m, 4H, H^{11}). ^{13}C NMR (101 MHz, DMSO) δ 149.56, 148.26, 145.35, 136.70, 129.88(2C), 128.39, 127.44 (2C), 127.05, 125.92, 123.98, 122.62, 121.65, 119.26, 115.90, 115.55, 114.73, 86.76, 66.45(2C), 62.24, 53.45 (2C), 46.86. MS (EI+) m/z calcd for $C_{25}H_{22}F_3N_5O$:465.18; found, 466.10 (M + 1). HPLC purity: 99%.

1-((4-hydroxybenzyl)amino)-3-(trifluoromethyl)benzo[4,5]imidazo[1,2-a]pyridine-4-carbonitrile 3n/GMP-48.

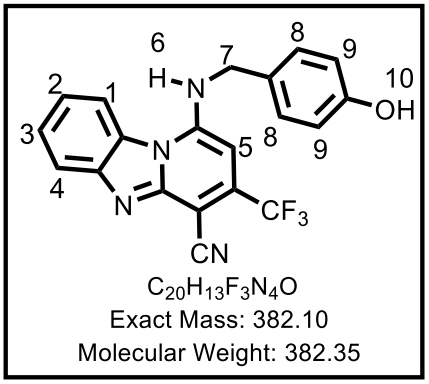

Obtained from **IVa** (0.3g, 1.015mmol, 1 equiv.) using 4-(aminomethyl)phenol (0.250g, 2.03mmol, 2 equiv) as a yellow fine powder (70%). ^{1}H NMR (400 MHz, DMSO) δ 8.70 (d, *J* = 8.4 Hz, 1H, H^1), 8.57 (bs, 1H,^{6}), 7.91 (d, *J* = 8.1 Hz, 1H, H^4), 7.65 (t, *J* = 7.6 Hz, 1H, H^3), 7.48 (t, *J* = 7.7 Hz, 1H, H^2), 7.32 (d, *J* = 8.3 Hz, 2H, H^8), 6.76 (d, *J* = 8.4 Hz, 2H, H^9), 6.31 (s, 1H, H^5), 4.78 (s, 2H, H^7). ^{13}C NMR (101 MHz, DMSO) δ 157.17, 149.90, 148.57, 146.13, 145.25, 136.71, 128.91(2C), 128.40, 127.71, 126.97, 121.54, 121.42, 119.21, 115.88(2C), 115.65, 115.02, 86.89, 46.74. MS (EI+) m/z calcd for $C_{20}H_{13}F_3N_4$:382.10; found, 383.10 (M + 1). HPLC purity: 99%.

1-((4-methylbenzyl)amino)-3-(trifluoromethyl)benzo[4,5]imidazo[1,2-a]pyridine-4-carbonitrile 3o/GMP-50.

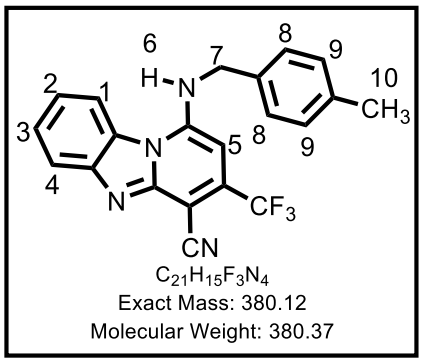

Obtained from **IVa** (0.3g, 1.015mmol, 1 equiv.) using p-tolylmethanamine (0.246g, 2.03mmol, 2 equiv.) as a yellow fluffy powder (35%). ^{1}H NMR (300 MHz, DMSO) δ 8.71 (d, *J* = 8.4 Hz, 1H, H^1), 8.64 (bs, 1H, H^6), 7.93 (d, *J* = 8.1 Hz, 1H, H^4), 7.66 (t, *J* = 7.3 Hz, 1H, H^3), 7.56 – 7.43 (m, 1H, H^2), 7.40 (d, *J* = 8.0 Hz, 2H, H^8), 7.18 (d, *J* = 7.8 Hz, 2H, H^9), 6.30 (s, 1H, H^5), 4.86 (s, 2H, H^7), 2.29 (s, 3H, H^{10}). ^{13}C NMR (101 MHz, DMSO) δ 149.81, 148.37, 145.37, 137.06, 135.43, 134.46, 131.64, 129.69, 128.23, 127.50, 127.03, 121.69 (2C), 119.39 (2C), 115.61, 114.83, 112,74, 86.41, 46.57, 21.14. MS (EI+) m/z calcd for $C_{21}H_{15}F_3N_4$:380.12; found, 381.10 (M + 1). HPLC purity: 99%.

4-(((4-cyano-3-(trifluoromethyl)benzo[4,5]imidazo[1,2-a]pyridin-1-yl)amino)methyl)-N-methylbenzamide 3p/GMP-52.

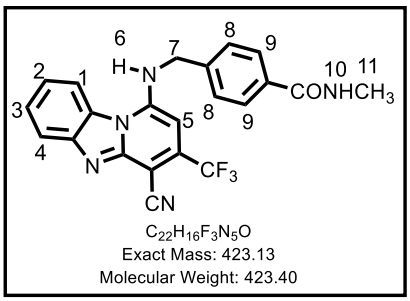

Obtained from **IVa** (0.3g, 1.015mmol, 1 equiv.) using 4-(aminomethyl)-N-methylbenzamide (0.333g, 2.03mmol, 2 equiv.) as a brown powder (30%). ^{1}H NMR (300 MHz, DMSO) δ 8.74 (d, *J* = 8.3 Hz, 1H, H^1), 8.39 (d, *J* = 4.8 Hz, 1H, H^{10}), 7.90 (d, *J* = 8.0 Hz, 1H, H^4), 7.83 (d, *J* = 8.1 Hz, 2H, H^9), 7.67-7.54 (m, 3H, $H^{3,8}$), 7.47 (t, *J* = 7.9 Hz, 1H, H^2), 6.24 (s, 1H, H^5), 4.95 (s, 2H, H^7), 2.78 (d, *J* = 4.5 Hz, 3H, H^{11}). ^{13}C NMR (101 MHz, DMSO) δ 166.81, 150.10, 148.65, 145.30, 141.15, 134.04, 132.94, 130.76, 128.63, 127.83, 127.32 (2C), 126.85, 121.56 (2C), 119.07, 118.54, 117.48, 115.81, 86.83, 47.17, 26.66. MS (EI+) m/z calcd for $C_{22}H_{16}F_3N_5O$:423.13; found, 424.10 (M + 1). HPLC purity: 99%.

4-(((4-cyano-3-(trifluoromethyl)benzo[4,5]imidazo[1,2-a]pyridin-1-yl)amino)methyl)-N,N-dimethylbenzamide 3q/GMP-53.

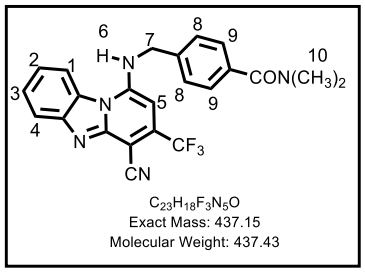

Obtained from **IVa** (0.3g, 1.015mmol, 1 equiv.) using 4-(aminomethyl)-N,N-dimethylbenzamide (0.362g, 2.03mmol, 2 equiv.) as a yellow shiny solid (67%). ^{1}H NMR (300 MHz, DMSO) δ 8.77 (d, *J* = 8.4 Hz, 1H, H^1), 7.90 (d, *J* = 7.8 Hz, 1H, H^4), 7.64 (t, *J* = 7.5 Hz, 1H, H^3), 7.57 (d, *J* = 8.2 Hz, 2H, H^9), 7.51 – 7.43 (m, 1H, H^2), 7.40 (d, *J* = 8.3 Hz, 2H, H^8), 6.28 (s, 1H, H^5), 4.95 (s, 2H, H^7), 2.93 (s, 6H, H^{10}). ^{13}C NMR (101 MHz, DMSO) δ 170.37, 150.01, 148.66, 145.36, 142.98, 139.28, 135.96, 128.56, 127.74, 127.36 (2C), 126.90, 121.63, 119.10, 118.32, 116.94, 115.82, 115.11(2C), 86.87, 47.05, 46.06 (2C). MS (EI+) m/z calcd for $C_{23}H_{18}F_3N_5O$:437.15; found, 438.10 (M + 1). HPLC purity: 99%.

4-(((4-cyano-3-(trifluoromethyl)benzo[4,5]imidazo[1,2-a]pyridin-1-yl)amino)methyl)-benzenesulfonamide 3r/GMP-54.

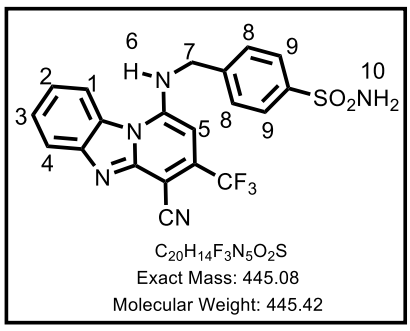

Obtained from **IVa** (0.3g, 1.015mmol, 1 equiv.) using 4-(aminomethyl)benzenesulfonamide (0.378g, 2.03mmol, 2 equiv.) as light brown shiny crystals (52%). ^{1}H NMR (300 MHz, DMSO) δ 8.73 (d, *J* = 8.4 Hz, 1H, H^1), 8.65 (bs, 1H, H^6), 7.93 (d, *J* = 7.7 Hz, 1H, H^4), 7.83 (d, *J* = 8.5 Hz, 2H, H^9), 7.70 (d, *J* = 8.5 Hz, 2H, H^8), 7.67 – 7.61 (m, 1H, H^3), 7.54 – 7.44 (m, 1H, H^2), 7.34 (bs, 2H, H^{10}), 6.28 (s, 1H, H^5), 5.00 (s, 2H, H^7). ^{13}C NMR (101 MHz, DMSO) δ 149.97, 148.52, 143.58, 141.90, 137.22, 128.48, 127.90 (2C), 127.03, 126.34 (2C), 124.11, 121.76, 121.32, 119.28, 115.78 (2C), 114.93, 86.42, 46.82. MS (EI+) m/z calcd for $C_{20}H_{14}F_3N_5O_2S$:445.08; found, 446.00 (M + 1). HPLC purity: 99%.

1-((4-isopropylbenzyl)amino)-3-(trifluoromethyl)benzo[4,5]imidazo[1,2-a]pyridine-4-carbonitrile 3s/GMP-55.

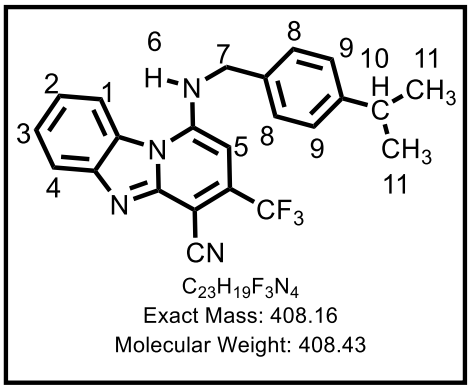

Obtained from **IVa** (0.3g, 1.015mmol, 1 equiv.) using (4-isopropylphenyl)methanamine (0.182g, 1.218mmol, 1.2 equiv.) as a yellow powder (65%). ^{1}H NMR (300 MHz, DMSO) δ 8.73 (d, *J* = 8.3 Hz, 1H, H^1), 7.88 (d, *J* = 7.9 Hz, 1H, H^4), 7.62 (t, *J* = 7.5 Hz, 1H, H^3), 7.44 (m, 3H, $H^{2,8}$), 7.24 (d, *J* = 8.1 Hz, 2H, H^9), 6.31 (s, 1H, H^5), 4.84 (s, 2H, H^7), 2.87 (m, 1H, H^{10}), 1.18 (d, *J* = 6.9 Hz, 6H, H^{11}). ^{13}C NMR (101 MHz, DMSO) δ 150.10, 148.82, 147.93, 145.37, 136.68, 135.53, 132.84, 128.64, 127.64, 126.95, 126.75, 124.71, 121.46 (2C), 118.99, 115.75 (2C), 115.30, 86.78, 47.29, 33.55, 24.31 (2C). MS (EI+) m/z calcd for $C_{23}H_{19}F_3N_4$:408.16; found, 409.10 (M + 1). HPLC purity: 99%.

1-(piperazin-1-yl)-3-(trifluoromethyl) benzo [4,5] imidazo[1,2-a]pyridine-4-carbonitrile 3u/GMP-77.

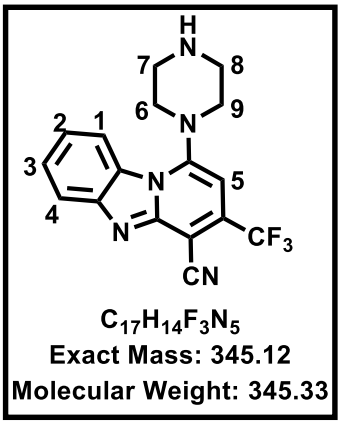

Obtained from **IVa** (0.1g, 0.338mmol, 1 equiv.) and piperazine (0.146g, 1.69mmol, 5 equiv.) as a yellow solid (38%). ^{1}H NMR (300 MHz, Methanol-d_4) δ 8.44 (d, *J* = 8.9 Hz, 1H, H^4), 7.96 (d, *J* = 8.4 Hz, 1H, H^1), 7.69 (t, *J* = 7.7 Hz, 1H, H^3), 7.57 (t, *J* = 7.7 Hz, 1H, H^2), 6.87 (s, 1H, H^5), 3.60 (d, *J* = 11.7 Hz, 2H, $H^{7e,8e}$), 3.30 – 2.96 (m, 6H, $H^{6,9,7a,8a}$). ^{13}C NMR (101 MHz, DMSO) δ 154.52, 147.89, 145.30, 136.31, 128.95, 127.37 (2C), 122.82, 119.98, 116.67 (2C), 113.72, 95.05, 51.46 (2C), 44.86 (2C). MS (EI+) m/z calcd for $C_{17}H_{14}F_3N_5$:345.12; found, 346.10 (M + 1). HPLC purity: 99%.

1-((3-(trifluoromethoxy)phenyl)amino)-3-(trifluoromethyl)benzo[4,5]imidazo[1,2-a]pyridine-4-carbonitrile: 1k/GMP-121.

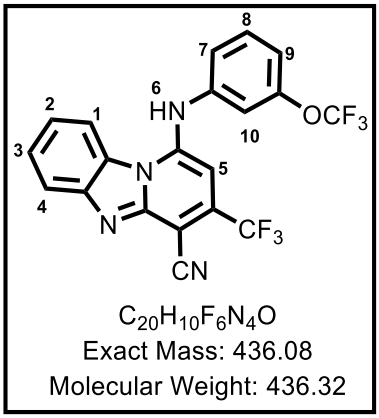

Obtained from **IVa** (0.1g, 0.338 mmol, 1 equiv.) using 3-(trifluoromethoxy) aniline (0.072g, 0.406 mmol, 1.2 equiv.) as a yellow solid (10%), m.p. 285-289 °C; R_f (EtoAc: Hex, 1:5) 0.26; ^{1}H NMR (300 MHz, DMSO-d_6) δ 8.81 (d, J = 8.3 Hz, 1H, H^1), 7.58 (m, 3H, $H^{2,4,9}$), 7.42 (t, J = 7.8 Hz, 1H, H^3), 7.19 – 6.96 (m, 3H, $H^{7,8,10}$), 6.23 (s, 1H, H^5). ^{13}C NMR (101 MHz, DMSO) δ 149.82, 148.61, 148.38, 135.72, 133.54, 131.74, 128.58, 127.31, 124.01, 123.11, 121.86, 121.27 (2C), 119.32, 117.88, 115.96, 115.17, 114.61, 112.64, 96.61. MS (EI+) m/z calcd for $C_{20}H_{10}F_6N_4O$:436.08; found, 437.10 (M + 1). HPLC purity: 98%.

1-((2-(trifluoromethoxy)phenyl)amino)-3-(trifluoromethyl)benzo[4,5]imidazo[1,2-a]pyridine-4-carbonitrile: 1l/GMP-122.

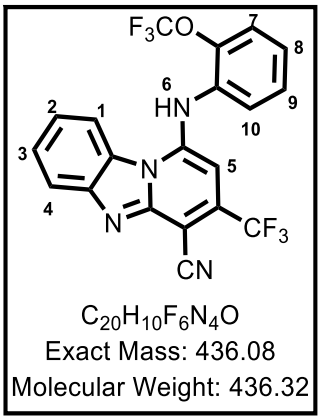

Obtained from **IVa** (0.1g, 0.338 mmol, 1 equiv.) using 2-(trifluoromethoxy) aniline (0.072g, 0.406 mmol, 1.2 equiv.) as a yellow solid (29%), m.p. 270-272°C; R_f (1% MeoH/DCM) 0.47; ^{1}H NMR (300 MHz, DMSO-d_6) δ 8.87 (d, J = 8.3 Hz, 1H, H^1), 7.75 – 7.52 (m, 2H,$H^{4,3}$), 7.52 – 7.34 (m, 3H,$H^{2,7,8}$), 7.22 (m, 2H,$H^{9,10}$), 6.10 (s, 1H,H^5). ^{13}C NMR (101 MHz, DMSO) δ 148.65, 141.74, 140.85, 135.03, 134.72, 133.29, 129.07, 128.59, 127.43, 124.84, 123.90, 123.24, 122.01, 121.27, 119.47, 117.73, 115.18, 112.16, 100.00, 97.15. MS (EI+) m/z calcd for $C_{20}H_{10}F_6N_4O$:436.08; found, 437.10 (M + 1). HPLC purity: >99%.

N-(4-(trifluoromethoxy) phenyl)-3-(trifluoromethyl)benzo[4,5]imidazo[1,2-a]pyridin-1-amine: 5a/GMP-120.

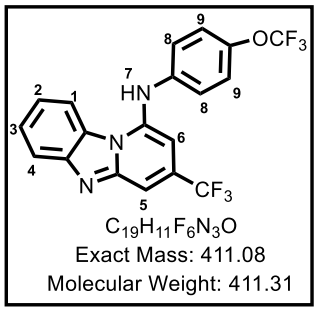

Obtained, serendipitously, from **IVd** (0.1g, 0.304mmol, 1 equiv.) using 4-(trifluoromethoxy)aniline (0.108g, 0.608 mmol, 2 equiv.). Yellow solid (19%), m.p. 266-268 °C; R_f (EtoAC: Hex, 1:4) 0.17; ^{1}H NMR (400 MHz, DMSO-d_6) δ 8.52 (d, J = 8.6 Hz, 1H, H^1), 7.99 (d, J = 8.3 Hz, 1H, H^4), 7.95 (s, 1H, H^5), 7.77 (t, J = 7.8 Hz, 1H, H^3), 7.55 (td, J = 7.9, 7.3, 1.0 Hz, 1H, H^2), 7.47 – 7.35 (m, 4H, $H^{8,9}$), 7.00 (s, 1H, H^6). ^{13}C NMR (101 MHz, DMSO) δ 145.99, 144.54, 140.66, 137.63, 135.40, 128.68, 127.43, 124.44, 123.35, 123.08 (2C), 121.72, 121.87 (2C), 119.36, 117.99, 116.00, 103.65, 97.79. MS (EI+) m/z calcd for $C_{19}H_{11}F_6N_3O$:411.08; found, 412.00 (M + 1). HPLC purity: 98%.

1-((4-fluorobenzyl)amino)-3-(trifluoromethyl)benzo[4,5]imidazo[1,2-a]pyridine-4-carboxamide: 5b/GMP-128.

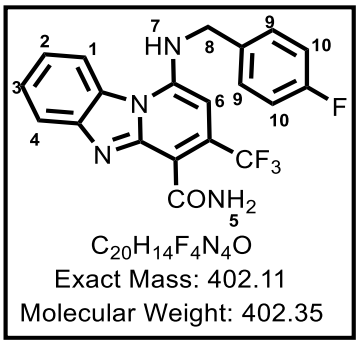

Obtained from **VI** (0.1g, 0.32mmol, 1 equiv.) using 4-fluorobenzylamine (0.048g, 0.385 mmol, 1.2 equiv.) as a light yellow powder (35%), m.p. 244-246 °C; R_f (2% MeoH/DCM) 0.21; ^{1}H NMR (600 MHz, DMSO-d_6) δ 8.66 (d, J = 8.4 Hz, 1H, H^1), 8.02 (s, 1H, H^5), 7.90 (d, J = 8.2 Hz, 1H, H^4), 7.81 (s, 1H, H^5), 7.65 (bs, 1H, H^7), 7.61 (t, J = 7.6 Hz, 1H, H^3), 7.57 (dd, J = 8.5, 5.6 Hz, 2H, H^{10}), 7.48 – 7.42 (m, 1H, H^2), 7.20 (t, J = 8.9 Hz, 2H, H^9), 6.03 (s, 1H, H^6), 4.74 (s, 2H, H^8). ^{13}C NMR (151 MHz, DMSO) δ 165.14, 162.09, 160.48, 146.64, 146.09, 144.77, 134.00, 129.11 (2C), 127.62, 125.77, 124.11 (2C), 122.29, 120.67, 118.81, 115.16, 113.47, 84.12, 45.53. MS (EI+) m/z calcd for $C_{20}H_{14}F_4N_4O$:402.11; found, 403.10 (M + 1). HPLC purity: >99%.

1-((4-(trifluoromethoxy)benzyl)amino)-3-(trifluoromethyl)benzo[4,5]imidazo[1,2-a]pyridine-4-carboxamide: 5c/GMP-129.

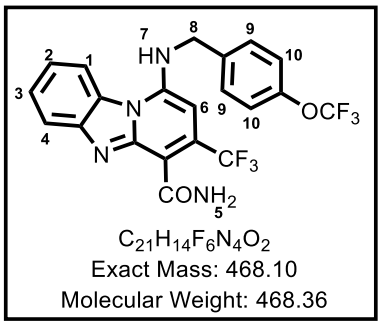

$C_{21}H_{14}F_6N_4O_2$
Exact Mass: 468.10
Molecular Weight: 468.36

Obtained from **VI** (0.1g, 0.32mmol, 1 equiv.) using 4-trifluorobenzylamine (0.075g, 0.385 mmol, 1.2 equiv.) as a light grey solid (20%), m.p. 206-208 °C; R_f (EtoAc: Hex 7:3) 0.21; ^{1}H NMR (300 MHz, DMSO-d_6) δ 8.67 (d, J = 8.2 Hz, 1H, H^1), 8.03 (s, 2H, H^5), 7.90 (d, J = 8.1 Hz, 1H, H^4), 7.62 – 7.52 (m, 1H, H^3), 7.45 – 7.38 (m, 1H, H^2), 7.48 (bs, 1H,H^7), 7.44 (d, J = 7.1 Hz, 2H, H^{10}), 7.37 (d, J = 7.7 Hz, 2H,H^9), 6.02 (s, 1H, H^6), 4.79 (s, 2H, H^8). ^{13}C NMR (151 MHz, DMSO) δ 165.14, 162.09, 160.48, 146.64, 146.09, 144.77, 134.00, 129.11 (2C), 127.62, 127.30, 125.77, 124.11, 122.29, 120.67, 118.81, 115.16 (2C), 113.47, 84.12, 45.53. MS (EI+) m/z calcd for $C_{21}H_{14}F_6N_4O_2$:468.10; found, 469.10 (M + 1). HPLC purity: 95%.

1-((pyridin-2-ylmethyl)amino)-3-(trifluoromethyl)benzo[4,5]imidazo[1,2-a]pyridine-4-carboxamide: 5d/GMP-130.

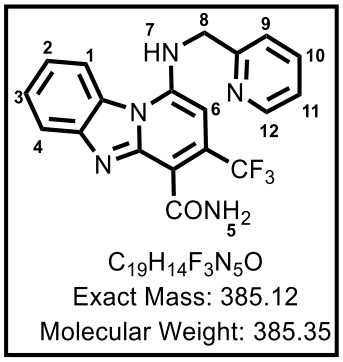

$C_{19}H_{14}F_3N_5O$
Exact Mass: 385.12
Molecular Weight: 385.35

Obtained from **VI** (0.15g, 0.48 mmol, 1 equiv.) using 2-picolylamine (63g/0.08mL, 0.58 mmol, 1.2 equiv.) as a light grey solid (66%), m.p.215-218°C; R_f(2% MeoH/DCM) 0.15; ^{1}H NMR (300 MHz, DMSO-d_6) δ 8.69 (d, J = 8.2 Hz, 1H, H^1), 8.63 (d, J = 4.2 Hz, 1H, H^{12}), 8.05 (s, 2H, H^5), 7.91 (d, J = 8.3 Hz, 1H, H^4), 7.82 (td, J = 7.7, 1.6 Hz, 1H, H^3), 7.66 (d, J = 4.2 Hz, 1H, H^{11}), 7.62 (s, 1H, H^6), 7.61 – 7.52 (m, 1H, H^9), 7.47 (t, J = 7.8 Hz, 1H, H^2), 7.40 – 7.29 (m, 1H, H^{10}), 6.10 (bs, 1H, H^7), 4.85 (s, 2H, H^8). ^{13}C NMR (101 MHz, DMSO) δ 165.65, 157.24, 149.41, 147.19, 146.70, 145.36, 137.55, 128.09, 126.32, 125.12, 123.10, 122.39, 122.14, 121.35, 119.44, 115.51, 113.73,

84.42, 48.57. MS (EI+) m/z calcd for $C_{19}H_{14}F_3N_5O$:385.12; found, 386.10 (M + 1). HPLC purity: >99%.

7,9-dichloro-1-((4-fluorobenzyl)amino)-3-(trifluoromethyl)benzo[4,5]imidazo[1,2-a]pyridine-4- carbonitrile 4a/GMP-62.

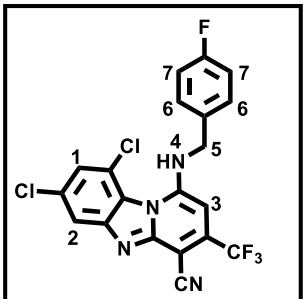

$C_{20}H_{10}Cl_2F_4N_4$
Exact Mass: 452.02
Molecular Weight: 453.22

Obtained from **IVb** (0.1g, 0.274mmol, 1 equiv.) and (4-fluorophenyl)methanamine (0.041g, 0.329mmol, 1.2 equiv.) as a yellow solid (86%). ^{1}H NMR (300 MHz, DMSO-d_6) δ 8.82 (d, *J* = 4.1 Hz, 1H, H^2), 8.70 (s, 1H, H^4), 7.81 (d, *J* = 6.8 Hz, 1H, H^1), 7.56 (dd, *J* = 8.5, 5.5 Hz, 2H, H^6), 7.20 (t, *J* = 8.9 Hz, 2H, H^7), 6.32 (s, 1H, H^3), 4.89 (s, 2H, H^5). ^{13}C NMR (101 MHz, DMSO) δ 163.13, 160.71, 150.15 (2C), 141.56, 137.93, 133.95, 129.83, 129.50 (2C), 126.22, 125.36, 123.06, 121.27, 115.87 (2C), 114.78, 112.78, 88.01, 46.85. MS (EI+) m/z calcd for $C_{20}H_{10}Cl_2F_4N_4$:452.02; found, 453.00 (M + 1). HPLC purity: 99%.

7,8-dichloro-1-((4-fluorobenzyl)amino)-3-(trifluoromethyl)benzo[4,5]imidazo[1,2-a]pyridine-4- carbonitrile 4b/GMP-66.

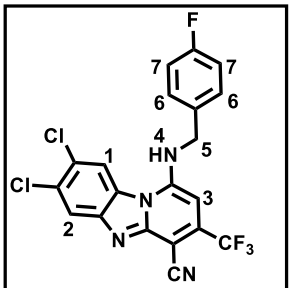

$C_{20}H_{10}Cl_2F_4N_4$
Exact Mass: 452.02
Molecular Weight: 453.22

Obtained from **IVc** (0.163g, 0.448mmol, 1 equiv.) and (4-fluorophenyl)methanamine (0.0618g, 0.493mmol, 1.2 equiv.) as a yellow solid (22%). ^{1}H NMR (300 MHz, DMSO-d6) δ 9.03 (s, 1H, H^2), 7.69 (s, 1H, H^1), 7.52 (dd, *J* = 8.6, 5.6 Hz, 2H, H^6), 7.43 (dd, *J* = 8.4, 5.6 Hz, 2H, H^7), 6.00 (s, 1H, H^3), 4.59 (s, 2H, H^5). ^{13}C NMR (101 MHz, DMSO) δ 162.97, 160.18, 154.24, 150.99, 145.67, 139.02, 135.82, 134.57, 130.64, 129.58, 125.88, 119.90, 117.50, 116.55, 115.63, 115.57, 115.18, 100.00, 88.62, 43.67. MS (EI+) m/z calcd for $C_{20}H_{10}Cl_2F_4N_4$:452.02; found, 453.00 (M + 1). HPLC purity: 97%.

7,8-dichloro-1-((4-(trifluoromethoxy)benzyl)amino)-3-(trifluoromethyl)benzo[4,5]imidazo[1,2- a]pyridine-4-carbonitrile 4c/GMP-67.

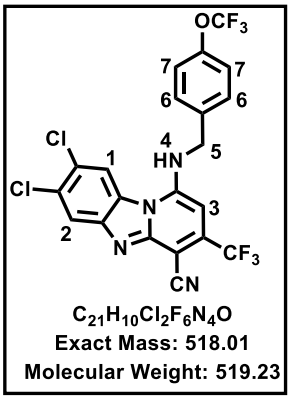

Obtained from **IVc** (0.15g, 0.411mmol, 1 equiv.) and (4-(trifluoromethoxy)phenyl)methanamine (0.094g, 0.493mmol, 1.2 equiv.) as a brown solid (25%). ^{1}H NMR (300 MHz, DMSO-d_6) δ 9.04 (s, 1H, H^{2}), 7.70 (s, 1H, H^{1}), 7.59 (dd, J = 14.0, 8.6 Hz, 2H, H^{7}), 7.38 (t, J = 8.8 Hz, 2H, H^{6}), 6.01 (s, 1H, H^{3}), 4.64 (s, 2H, H^{5}). ^{13}C NMR (101 MHz, DMSO) δ 151.42, 148.67, 148.48, 137.28, 134.58, 132.48, 130.43, 129.51, 128.51, 127.00 (2C), 124.13, 121.48 (2C), 119.22, 116.56, 115.75, 114.49, 112.94, 86.73, 51.67. MS (EI+) m/z calcd for $C_{21}H_{10}Cl_2F_6N_4O$:518.01; found, 519.00 (M + 1). HPLC purity: 99%.

7,8-dichloro-1-((pyridin-2-ylmethyl)amino)-3-(trifluoromethyl)benzo[4,5]imidazo[1,2-a]pyridine-4- carbonitrile 4d/GMP-68.

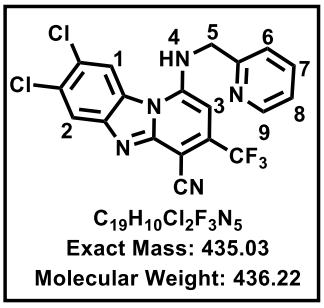

Obtained from **IVc** (0.15g, 0.411mmol, 1 equiv.) and (pyridin-2-ylmethanamine (0.0534g, 0.493mmol, 1.2 equiv.) as a brown solid (39%). ^{1}H NMR (300 MHz, DMSO-d_6) δ 9.01 (s, 1H, H^{2}), 8.66 – 8.52 (m, 1H, H^{9}), 8.10 (s, 1H, H^{1}), 7.83 (td, J = 7.6, 1.8 Hz, 1H, H^{7}), 7.58 (d, J = 7.9 Hz, 1H, H^{6}), 7.42 – 7.26 (m, 1H, H^{8}), 6.39 (s, 1H, H^{3}), 4.94 (s, 2H, H^{5}). ^{13}C NMR (101 MHz, DMSO) δ 150.22, 149.36 (2C), 145.21, 137.52 (2C), 129.15, 128.31, 127.64, 123.18, 122.26 (2C), 119.39, 118.56, 117.09, 116.96, 115.08, 88.03, 49.95. MS (EI+) m/z calcd for $C_{19}H_{10}Cl_2F_3N_5$:435.03; found, 436.00 (M + 1). HPLC purity: 97%.

7,8-dichloro-1-((4-methylbenzyl)amino)-3-(trifluoromethyl)benzo[4,5]imidazo[1,2-a]pyridine-4- carbonitrile 4e/GMP-69.

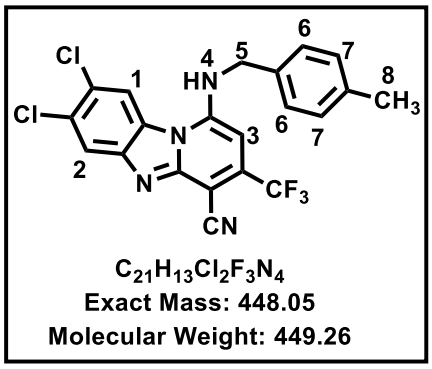

Obtained from **IVc** (0.15g, 0.411mmol, 1 equiv.) and *p*-tolylmethanamine (0.058g, 0.494mmol, 1.2 equiv.) as a brown powder (50%). ^{1}H NMR (300 MHz, DMSO-d_6) δ 9.06 (s, 1H, H^2), 7.74 (s, 1H, H^1), 7.35 (d, J = 8.1 Hz, 2H, H^6), 7.20 (d, J = 7.9 Hz, 2H, H^7), 6.03 (s, 1H, H^3), 4.59 (s, 2H, H^5), 2.31 (s, 3H, H^8). ^{13}C NMR (101 MHz, DMSO) δ 160.73, 159.00, 155.06, 146.31, 135.62, 134.93, 129.58, 129.21 (2C), 127.62 (2C), 126.38, 121.69, 119.39, 117.52, 116.80, 115.61, 114.83, 88.39, 42.88, 21.08. MS (EI+) m/z calcd for $C_{21}H_{13}Cl_2F_3N_4$:448.05; found, 449.00 (M + 1). HPLC purity: 99%.

7,8-dichloro-1-((4-(trifluoromethoxy)phenyl)amino)-3-(trifluoromethyl)benzo[4,5]imidazo[1,2- a]pyridine-4-carbonitrile 4f/GMP-70.

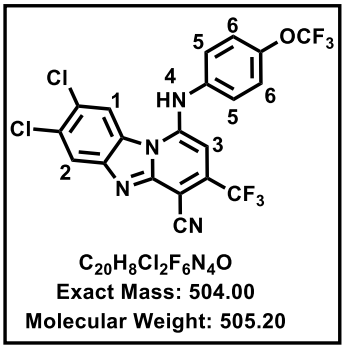

Obtained from **IVc** (0.15g, 0.411mmol, 1 equiv.) and 4-(trifluoromethoxy)aniline (0.088g, 0.494mmol, 1.2 equiv.) as dark (red-brown) crystals (9%). ^{1}H NMR (300 MHz, DMSO-d_6) δ 8.93 (s, 1H, H^2), 7.79 (s, 1H, H^1), 7.36 – 7.30 (m, 2H, H^5), 7.12 – 7.04 (m, 2H, H^6), 5.76 (s, 1H, H^3). ^{13}C NMR (101 MHz, DMSO) δ 163.05, 156.19, 148.53, 142.12, 137.62, 128.91, 127.21, 125.36, 123.75 (2C), 122.46 (2C), 120.35, 117.64 (2C), 115.20, 113.50, 102.34, 95.93, 46.29. MS (EI+) m/z calcd for $C_{20}H_8Cl_2F_6N_4$:504.00; found, 505.00 (M + 1). HPLC purity: 98%.

7,8-dichloro-1-((furan-2-ylmethyl)amino)-3-(trifluoromethyl)benzo[4,5]imidazo[1,2-a]pyridine-4- carbonitrile 4g/GMP-71.

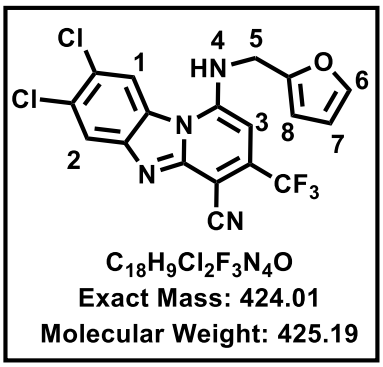

$C_{18}H_9Cl_2F_3N_4O$
Exact Mass: 424.01
Molecular Weight: 425.19

Obtained from **IVc** (0.15g, 0.411mmol, 1 equiv.) and furan-2-ylmethanamine (0.048g, 0.494mmol, 1.2 equiv.) as a brown solid (56%). ^{1}H NMR (300 MHz, DMSO-d_6) δ 9.00 (s, 1H, H^2), 7.90 (s, 1H, H^1), 7.63 (dd, J = 1.8, 0.9 Hz, 1H, H^6), 6.43 (m, 2H, $H^{7,8}$), 6.27 (s, 1H, H^3), 4.72 (s, 2H, H^5). ^{13}C NMR (101 MHz, DMSO) δ 155.27, 153.52, 150.99, 145.30, 142.96, 142.30, 134.97, 130.77, 128.78, 123.76, 117.67, 117.45, 114.20, 110.89, 107.15, 94.33, 93.02, 43.95. MS (EI+) m/z calcd for $C_{18}H_9Cl_2F_3N_4$:424.01; found, 425.00 (M + 1). HPLC purity: 99%.

7,8-dichloro-1-((thiophen-2-ylmethyl)amino)-3-(trifluoromethyl)benzo[4,5]imidazo[1,2-a]pyridine- 4-carbonitrile 4h/GMP-72.

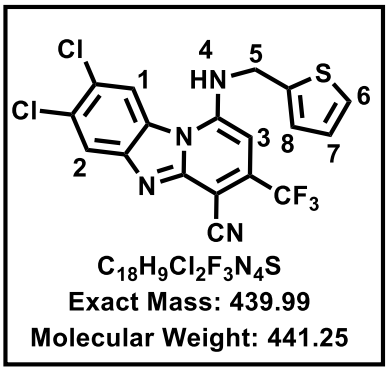

$C_{18}H_9Cl_2F_3N_4S$
Exact Mass: 439.99
Molecular Weight: 441.25

Obtained from **IVc** (0.15g, 0.411mmol, 1 equiv.) and thiophen-2- ylmethanamine (0.056g, 0.494mmol, 1.2 equiv.) as a brown solid (28%). ^{1}H NMR (300 MHz, DMSO-d_6) δ 9.16 (s, 1H, H^2), 7.77 (s, 1H, H^1), 7.42 (dd, J = 5.0, 1.3 Hz, 1H, H^6), 7.11 – 7.05 (m, 1H, H^8), 7.02 (dd, J = 5.0, 3.4 Hz, 1H, H^7), 6.05 (s, 1H, H^3), 4.80 (s, 2H,H^5). ^{13}C NMR (101 MHz, DMSO) δ 150.91, 145.53, 138.51, 130.23, 129.21, 128.19, 127.02 (2C), 124.34 (2C), 123.52, 123.23, 117.75 (2C), 116.95 (2C), 88.34, 47.38. MS (EI+) m/z calcd for $C_{18}H_9Cl_2F_3N_4S$:439.99; found, 441.00 (M + 1). HPLC purity: 98%.

7,8-dichloro-1-((2-fluorobenzyl)amino)-3-(trifluoromethyl)benzo[4,5]imidazo[1,2-a]pyridine-4- carbonitrile 4i/GMP-75.

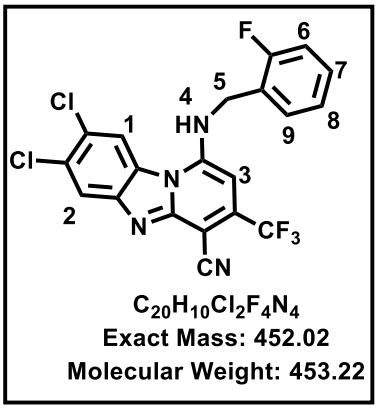

Obtained from **IVc** (0.1g, 0.274mmol, 1 equiv.) and (2-fluorophenyl)methanamine (0.069g, 0.548mmol, 2 equiv.) as an orange solid (58%). ^{1}H NMR (300 MHz, DMSO-d_6) δ 9.00 (s, 1H, H^{2}), 7.94 (s, 1H, H^{1}), 7.59 (t, J = 7.5 Hz, 1H, H^{8}), 7.40 – 7.12 (m, 3H, $H^{6, 7, 9}$), 6.22 (s, 1H, H^{3}), 4.79 (s, 2H, H^{5}). ^{13}C NMR (101 MHz, DMSO) δ 161.91, 159.49, 152.40, 150.75, 145.34, 136.58, 132.84, 131.42, 129.92, 129.22, 126.94, 127.87, 124.84, 121.78, 118.14, 117.37 (2C), 116.51, 115.46, 87.88. MS (EI+) m/z calcd for $C_{20}H_{10}Cl_2F_4N_4$:452.02; found, 453.00 (M + 1). HPLC purity: 98%.

7,8-dichloro-1-((3-fluorobenzyl)amino)-3-(trifluoromethyl)benzo[4,5]imidazo[1,2-a]pyridine-4- carbonitrile 4j/GMP-76.

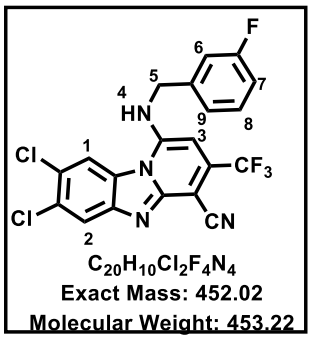

Obtained from **IVc** (0.1g, 0.274mmol, 1 equiv.) and (3-fluorophenyl)methanamine (0.069g, 0.548mmol, 2 equiv.) as a yellow solid (37%). ^{1}H NMR (300 MHz, DMSO-d_6) δ 9.05 (s, 1H, H^{2}), 8.69 (bs, 1H, H^{4}), 8.20 (s, 1H, H^{1}), 7.51 – 7.29 (m, 3H, $H^{7, 8, 9}$), 7.18 – 7.06 (m, 1H, H^{6}), 6.32 (s, 1H, H^{3}), 4.96 (s, 2H, H^{5}). ^{13}C NMR (101 MHz, DMSO) δ 161.91, 159.49, 152.40, 150.75, 145.34, 136.58, 131.42, 129.96, 129.22, 127.87, 125.10, 124.70, 121.78, 118.14, 117.37(2C), 116.51, 115.65, 115.46, 87.83. MS (EI+) m/z calcd for $C_{20}H_{10}Cl_2F_4N_4$:452.02; found, 453.00 (M + 1). HPLC purity: 97%.

7,8-dichloro-1-(piperazin-1-yl)-3-(trifluoromethyl)benzo[4,5]imidazo[1,2-a]pyridine-4-carbonitrile: 4k/GMP-81.

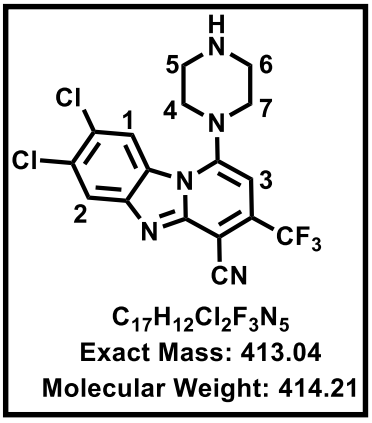

$C_{17}H_{12}Cl_2F_3N_5$
Exact Mass: 413.04
Molecular Weight: 414.21

Obtained from **IVc** (0.1g, 0.274mmol, 1 equiv.) and piperazine (0.118g, 1.372mmol, 5 equiv.) as a yellow solid (53%); R_f (5% MeoH: DCM); 0.33 ^{1}H NMR (300 MHz, Methanol-d_4) δ 8.56 (s, 1H, H^2), 8.08 (s, 1H, H^1), 6.96 (s, 1H, H^3), 3.61 (d, J = 11.9 Hz, 2H, $H^{5e,6e}$), 3.33 – 3.27 (m, 4H, $H^{5a,6a,4e,7e}$), 3.18 (dd, J = 12.7, 6.3 Hz, 2H, $H^{4a,7a}$). ^{13}C NMR (101 MHz, DMSO) δ 154.20 (2C), 149.71, 144.71, 130.07, 128.22, 124.71, 120.92 (2C), 117.68 (2C), 113.34, 96.37, 51.04 (2C), 44.64 (2C). MS (EI+) m/z calcd for $C_{17}H_{12}Cl_2F_3N_5$:413.04; found, 414.00 (M + 1). HPLC purity: 99%.

dichloro-1-((4-(methylsulfonyl)benzyl)amino)-3-(trifluoromethyl)benzo[4,5]imidazo[1,2-a]pyridine-4-carbonitrile 4l/GMP-96.

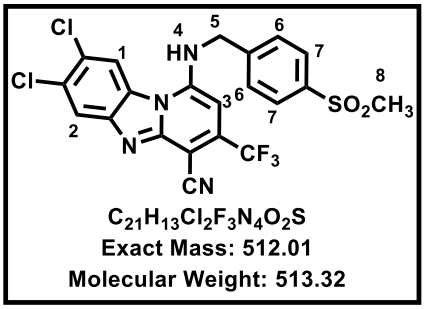

$C_{21}H_{13}Cl_2F_3N_4O_2S$
Exact Mass: 512.01
Molecular Weight: 513.32

Obtained from **IVc** (0.2g, 0.55mmol, 1 equiv.) and (4-(methylsulfonyl) phenyl)methanamine (0.138g, 1.357mmol, 0.746 equiv.) as a brown solid (58%). ^{1}H NMR (300 MHz, DMSO-d_6) δ 9.11 (bs, 1H, H^4), 8.17 (s, 1H, H^1), 8.05 (s, 1H, H^2), 7.91 (d, J = 8.5 Hz, 2H, H^7), 7.75 (d, J = 8.5 Hz, 2H, H^6), 6.24 (s, 1H, H^3), 5.00 (s, 2H, H^5), 3.21 (s, 3H, H^8). ^{13}C NMR (101 MHz, DMSO) δ 160.38, 150.68, 150.25, 149.66, 146.47, 144.95, 138.07, 135.72, 133.78, 130.50, 128.25, 127.96 (2C), 127.63 (2C), 121.12, 119.42, 117.22, 108.24, 46.22, 44.21. MS (EI-) m/z calcd for $C_{21}H_{13}Cl_2F_3N_4O_2S$:512.01; found, 511.00 (M - 1). HPLC purity: 97%.

7,8-dichloro-1-((1-(4-(methylsulfonyl)phenyl)ethyl)amino)-3-(trifluoromethyl)benzo[4,5] imidazo [1,2-a]pyridine-4-carbonitrile 4m/GMP-97.

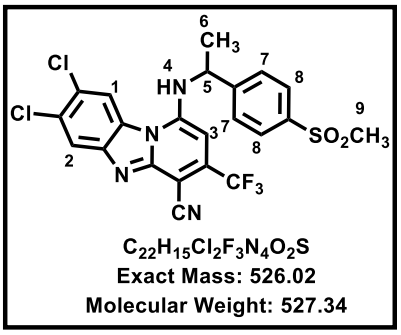

Obtained from **IVc** (0.2g, 0.55mmol, 1 equiv.) and 1-(4-(methylsulfonyl)phenyl)ethan-1-amine (0.189g, 0.95mmol, 1.73 equiv.) as a yellow solid (6%). ^{1}H NMR (300 MHz, DMSO-d6) δ 8.83 (s, 1H, H^{1}), 8.24 (s, 1H, H^{2}), 7.95 (d, *J* = 8.6 Hz, 2H, H^{8}), 7.88 (d, *J* = 8.4 Hz, 2H, H^{7}), 6.27 (s, 1H, H^{3}), 5.47 – 5.30 (m, 1H, H^{5}), 3.21 (s, 3H, H^{9}), 1.80 (d, *J* = 7.7 Hz, 3H, H^{6}). ^{13}C NMR (101 MHz, DMSO) δ 162.33, 162.10, 153.77, 148.58, 133.77, 133.21, 130.84, 128.76, 127.70 (2C), 126.87, 126.35, 124.58, 121.81 (2C), 117.96, 116.73, 114.52, 96.89, 63.59, 44.08, 22.97. MS (EI-) m/z calcd for $C_{22}H_{15}Cl_2F_3N_40_2S$:526.02; found, 525.00 (M - 1). HPLC purity: 97%.

b) Amination using Buchwald-Hartwig conditions

A mixture of the chloro intermediate, the appropriate amine (1.2 equiv.), Tris(dibenzylideneacetone) dipalladium(0), $Pd_2(dba)_3$ (0.1 equiv.), 2,2'-Bis(diphenylphosphino)-1,1'-binaphthyl (BINAP) (0.06 equiv.) or BrettPhos (0.04 equiv.) or RuPhos (0.1 equiv.), Potassium carbonate, K_2CO_3 or Caesium Carbonate, Cs_2CO_3 (3 equiv.) and toluene:tert-butanol (1:1; 5ml) or 1,4-dioxane (5mL) were stirred in a sealed tube at 100-120˚C for 4-17 hours. Reactions were monitored by TLC and LC-MS. The cooled reaction mixture was stirred in ethylacetate (50ml) and water (100ml) for 10-20 minutes. The separated organic layer was washed with water (2X50ml), followed by saturated NaCl (2X50ml), dried over magnesium sulphate and filtered over celite. The organic fraction was concentrated under reduced pressure and ethanol used to precipitate the crude product which was filtered to furnish the final product. In some cases, compounds were purified by recrystallization from ethanol or by column chromatography.

1-((4-cyanophenyl)amino)-3-(trifluoromethyl)benzo[4,5]imidazo[1,2-a]pyridine-4-carbonitrile 1b/GMP-09.

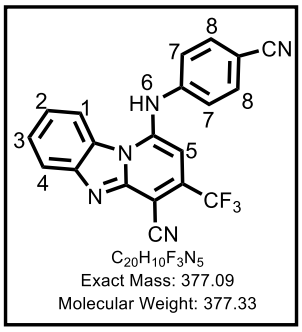

Obtained from **IVa** (0.3g, 1.015mmol, 1 equiv.) using 4-aminobenzonitrile (0.24g, 1.218mmol, 1.2 equiv.) as a pale-yellow powder (27%). ^{1}H NMR (300 MHz, DMSO) δ 8.80 (d, *J* = 7.9 Hz, 1H, H^1), 7.84 (d, *J* = 8.7 Hz, 2H, H^8), 7.66 (d, *J* = 7.3 Hz, 1H, H^4), 7.63 – 7.56 (m, 1H, H^3), 7.49 – 7.36 (m, 1H, H^2), 7.21 (d, *J* = 8.5 Hz, 2H, H^7), 6.22 (s, 1H, H^5). ^{13}C NMR (101 MHz, DMSO) δ 148.37, 148.11, 135.32, 135.00, 134.41, 132.48, 130.84, 128.61, 127.40, 123.17, 122.96 (2C), 119.80, 118.34, 117.93 (2C), 116.74, 115.21, 105.52, 96.60. MS (EI+) m/z calcd for $C_{20}H_{10}F_3N_5$:377.09; found, 378.10 (M + 1). HPLC purity: 99%.

4-((4-cyano-3-(trifluoromethyl)benzo[4,5]imidazo[1,2-a]pyridin-1-yl)amino)-N,N-dimethylbenzamide 1h/GMP-17.

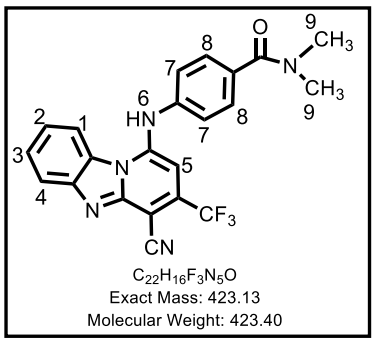

Obtained from **IVa** (0.3g, 1.015mmol, 1 equiv.) using 4-amino-N,N-dimethylbenzamide (0.2g, 1.218mmol, 1.2 equiv.) as a yellow powder (18%). ; ^{1}H NMR (300 MHz, DMSO) δ 8.81 (d, *J* = 8.3 Hz, 1H, H^{1}), 7.67 (d, *J* = 8.3 Hz, 1H, H^{4}), 7.59 (t, *J* = 7.4 Hz, 1H, H^{3}), 7.48 (d, *J* = 8.3 Hz, 2H, H^{7}), 7.42 (t, *J* = 8.2 Hz, 1H, H^{2}), 7.12 (d, *J* = 6.8 Hz, 2H, H^{8}), 6.27 (s, 1H, H^{5}), 3.00 (s, 6H, H^{9}). ^{13}C NMR (151 MHz, DMSO) δ 170.55, 148.55, 148.21, 135.01, 132.14, 129.21, 128.77, 127.22 (2C), 126.74, 125.37, 123.63, 122.92, 121.79, 120.00, 118.82, 117.72 (2C), 115.04, 96.35, 46.06 (2C). MS (EI+) m/z calcd for $C_{22}H_{16}F_3N_5O$:423.13; found, 424.10 (M + 1). HPLC purity: 98%.

1-((4-(methylsulfonyl) phenyl) amino)-3- (trifluoromethyl) benzo[4,5]imidazo [1,2-a]pyridine-4- carbonitrile 1i/GMP-18.

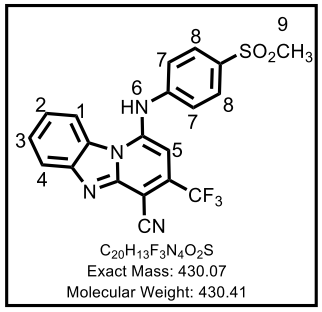

Obtained from **IVa** (0.3g, 1.015mmol, 1 equiv.) using 4-(methylsulfonyl)aniline (0.209g, 1.218mmol, 1.2 equiv.) as a yellow powder (40%). ^{1}H NMR (300 MHz, DMSO) δ 8.79 (d, *J* = 8.0 Hz, 1H, H^{1}), 7.88 (d, *J* = 8.6 Hz, 2H, H^{8}), 7.62 (d, *J* = 7.9 Hz, 1H, H^{4}), 7.51 – 7.41 (m, 1H, H^{3}), 7.29 – 7.20 (m, 3H, $H^{2,7}$), 6.00 (s, 1H, H^{5}), 3.21 (s, 3H, H^{9}). ^{13}C NMR (101 MHz, DMSO) δ 155.13, 149.37, 133.81, 132.83, 130.01, 129.64, 129.07, 127.68, 125.52, 122.74 (2C), 121.41, 120.45, 117.20 (2C), 115.04, 106.70, 91.45, 86.09, 44.03. MS (EI+) m/z calcd for $C_{20}H_{13}F_3N_4O_2S$:430.07; found, 431.00 (M + 1). HPLC purity: 99%.

1-((5,6-dimethoxypyrimidin-4-yl)amino)-3-(trifluoromethyl) benzo[4,5] imidazo[1,2-a]pyridine-4- carbonitrile 2a/GMP-23.

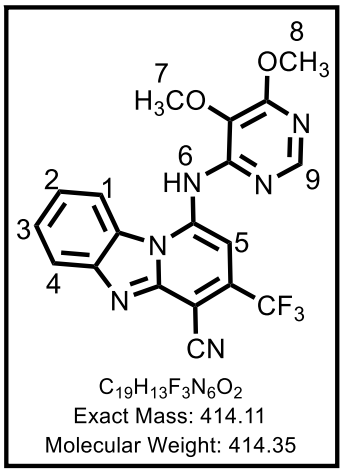

Obtained from **IVa** (0.3g, 1.015mmol, 1 equiv.) using 5,6-dimethoxypyrimidin-4-amine (0.189g, 1.218mmol, 1.2 equiv.) as a yellow fluffy powder (17%). ^{1}H NMR (300 MHz, DMSO) δ 9.08 (d, *J* = 10.1 Hz, 1H, H^{1}), 8.36 (s, 1H, H^{9}), 7.69 (d, *J* = 8.7 Hz, 1H, H^{4}), 7.67 – 7.59 (m, 1H, H^{3}), 7.52 – 7.43 (m, 1H, H^{2}), 7.40 (s, 1H, H^{5}), 4.00 (s, 3H, H^{8}), 3.80 (s, 3H, H^{7}). ^{13}C NMR (101 MHz, DMSO) δ 163.29, 162.70, 151.38, 147.54, 141.49, 135.42, 135.09, 128.73, 127.71(2C), 124.15, 123.12 (2C), 121.42, 118.52, 114.91, 100.05, 60.64, 54.00. MS (EI+) m/z calcd for $C_{19}H_{13}F_3N_6O_2$:414.11; found, 415.10 (M + 1). HPLC purity: 98%.

1-((2-fluoropyridin-4-yl)amino)-3-(trifluoromethyl)benzo[4,5]imidazo[1,2-a]pyridine-4-carbonitrile 2b/GMP-30.

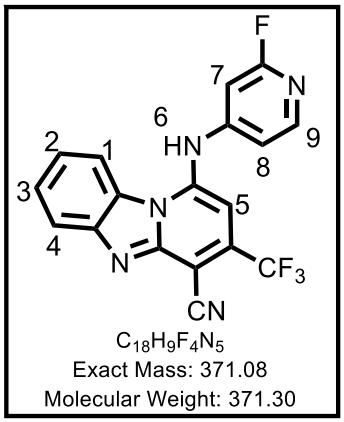

Obtained from **IVa** (0.3g, 1.015mmol, 1 equiv.) using 2-fluoropyridin-4- amine (0.137g, 1.218mmol, 1.2 equiv.) as a yellow powder (6%). ^{1}H NMR (400 MHz, DMSO) δ 8.78 (d, *J* = 8.3 Hz, 1H, H^{1}), 8.13 (d, *J* = 5.4 Hz, 1H, H^{9}), 7.68 (d, *J* = 8.1 Hz, 1H, H^{4}), 7.57 (t, *J* = 7.6 Hz, 1H, H^{3}), 7.38 (t, *J* = 7.9 Hz, 1H, H^{2}), 6.98 (dt, *J* = 5.4, 1.7 Hz, 1H, H^{8}), 6.72 (s, 1H, H^{7}), 6.23 (s, 1H, H^{5}). ^{13}C NMR (101 MHz, DMSO) δ 166.34, 164.04, 161.07, 148.68 (2C), 135.88, 128.78, 127.21, 124.13, 122.77, 121.40, 117.91, 116.13, 115.31, 113.38, 101.75, 101.36, 95.71. MS (EI+) m/z calcd for $C_{18}H_9F_4N_5$:371.08; found, 372.10 (M + 1). HPLC purity: 99%.

1-((4-methylthiazol-2-yl)amino)-3-(trifluoromethyl)benzo[4,5]imidazo[1,2-a]pyridine-4-carbonitrile 2c/GMP-31.

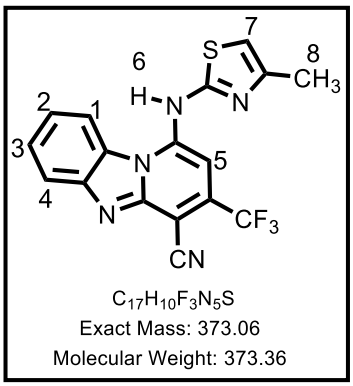

$C_{17}H_{10}F_3N_5S$
Exact Mass: 373.06
Molecular Weight: 373.36

Obtained from **IVa** (0.3g, 1.015mmol, 1 equiv.) using 4-methylthiazol- 2-amine (0.139g, 1.218mmol, 1.2 equiv.) as a brown powder (37%). ^{1}H NMR (400 MHz, DMSO) δ 9.04 (d, *J* = 8.0 Hz, 1H, H^1), 7.83 (d, *J* = 8.1 Hz, 1H, H^4), 7.59 (ddd, *J* = 8.3, 7.2, 1.2 Hz, 1H, H^3), 7.41 (ddd, *J* = 8.4, 7.2, 1.2 Hz, 1H, H^2), 6.97 (s, 1H, H^5), 6.84 (d, *J* = 1.2 Hz, 1H, H^7), 2.33 (d, *J* = 1.2 Hz, 3H, H^8). ^{13}C NMR (101 MHz, DMSO) δ 150.97, 148.06, 140.91, 137.55, 136.71, 136.39, 131.52, 129.88, 126.78, 121.87, 118.93, 118.18, 117.84, 114.97, 104.81, 100.04, 14.62. MS (EI+) m/z calcd for $C_{17}H_{10}F_3N_5S$:373.06; found, 374.10 (M + 1). HPLC purity: 99%.

1-((pyridin-4-ylmethyl)amino)-3-(trifluoromethyl)benzo[4,5]imidazo[1,2-a]pyridine-4-carbonitrile 3k/GMP-43.

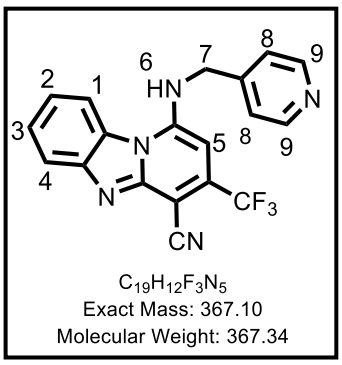

$C_{19}H_{12}F_3N_5$
Exact Mass: 367.10
Molecular Weight: 367.34

Obtained from **IVa** (0.15g, 0.51mmol, 1 equiv.) using pyridin-4- ylmethanamine (0.066g, 0.062ml; 0.609mmol, 1.2 equiv.) as a brown powder (20%). ^{1}H NMR (300 MHz, DMSO) δ 8.72 (d, *J* = 8.4 Hz, 1H, H^1), 8.62 (bs, 1H, H^6), 8.55 (d, *J* = 6.0 Hz, 2H, H^9), 7.94 (d, *J* = 8.2 Hz, 1H, H^4), 7.67 (t, *J* = 7.5 Hz, 1H, H^3), 7.58 – 7.39 (m, 3H, $H^{2,8}$), 6.26 (s, 1H, H^5), 4.98 (s, 2H, H^7). ^{13}C NMR (101 MHz, DMSO) δ 158.18, 150.26 (2C), 148.21, 147.06, 142.92, 133.29, 133.09, 131.24, 128.64, 128.33, 127.12, 122.49 (2C), 121.86, 119.30, 115.78, 114.84, 46.27. MS (EI+) m/z calcd for $C_{19}H_{12}F_3N_5$:367.10; found, 368.10 (M + 1). HPLC purity: 98%.

1-((pyrimidin-2-ylmethyl)amino)-3-(trifluoromethyl)benzo[4,5]imidazo[1,2-a]pyridine-4-carbonitrile 3t/GMP-56.

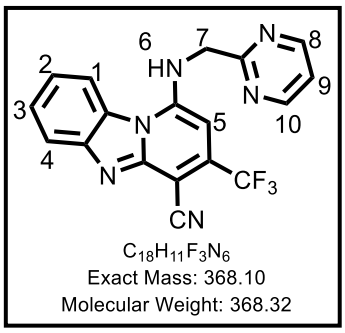

$C_{18}H_{11}F_3N_6$
Exact Mass: 368.10
Molecular Weight: 368.32

Obtained from **IVa** (0.15g, 0.51mmol, 1 equiv.) using pyrimidin-2- ylmethanamine (0.066g, 0.61mmol, 1.2 equiv.) as a red powder (6%). ^{1}H NMR (600 MHz, DMSO) δ 8.88 (d, *J* = 4.9 Hz, 2H, $H^{8,10}$), 8.70 (d, *J* = 8.4 Hz, 1H, H^1), 8.61 (bs, 1H, H^6), 7.95 (d, *J* = 8.1 Hz, 1H, H^4), 7.67 (t, *J* = 7.6 Hz, 1H, H^3), 7.55 – 7.47 (m, 2H, $H^{2,9}$), 6.48 (s, 1H, H^5), 5.13 (s, 2H, H^7). ^{13}C NMR (151 MHz, DMSO) δ 165.36, 158.23 (2C), 150.27, 148.36, 145.51, 137.33, 131.62, 128.19, 126.91, 123.75, 121.52, 120.30, 119.02, 115.22, 114.57, 86.83, 65.14. MS (EI+) m/z calcd for $C_{18}H_{11}F_3N_6$:368.10; found, 369.10 (M + 1). HPLC purity: 98%.

1-(pyrimidin-2-ylamino)-3-(trifluoromethyl)benzo[4,5]imidazo[1,2-a]pyridine-4-carbonitrile 2d/GMP-57.

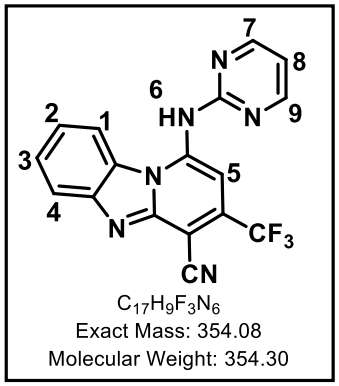

$C_{17}H_9F_3N_6$
Exact Mass: 354.08
Molecular Weight: 354.30

Obtained from **IVa** (0.15g, 0.51mmol, 1 equiv.) using pyrimidin-2-amine (0.058g, 0.61mmol, 1.2 equiv.) as an orange powder (25%). ^{1}H NMR (300 MHz, DMSO) δ 8.99 (d, *J* = 8.4 Hz, 1H, H^1), 8.77 (d, *J* = 5.1 Hz, 2H, $H^{7,9}$), 7.83 (d, *J* = 8.0 Hz, 1H, H^4), 7.71 (s, 1H, H^5), 7.66 – 7.46 (m, 1H,H^3), 7.46 – 7.29 (m, 1H, H^2), 7.11 (t, *J* = 5.1 Hz, 1H, H^8). ^{13}C NMR (151 MHz, DMSO) δ 158.43, 150.56, 148.30, 143.29, 135.63, 129.69, 126.91, 125.67, 123.86, 122.12, 121.73, 120.42, 118.97, 117.44, 115.05, 112.64, 96.36. MS (EI+) m/z calcd for $C_{17}H_9F_3N_6$:354.08; found, 355.10 (M + 1). HPLC purity: 98%.

1-(pyrazin-2-ylamino)-3-(trifluoromethyl)benzo[4,5]imidazo[1,2-a]pyridine-4-carbonitrile 2e/GMP-58.

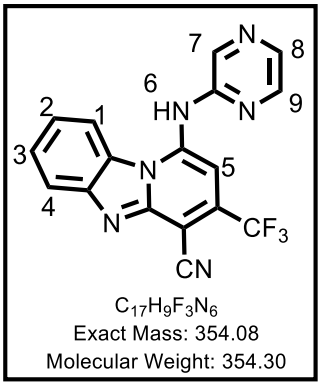

Obtained from **IVa** (0.15g, 0.51mmol, 1 equiv.) using pyrazin-2-amine (0.058g, 0.61mmol, 1.2 equiv.) as an orange powder (23%). ^{1}H NMR (400 MHz, DMSO) δ 9.08 (d, *J* = 8.4 Hz, 1H, H^1), 8.54 (d, *J* = 1.4 Hz, 1H, H^7), 8.41 (dd, *J* = 2.7, 1.4 Hz, 1H, H^8), 8.25 (d, *J* = 2.7 Hz, 1H, H^9), 7.69 (ddd, *J* = 8.1, 1.2, 0.7 Hz, 1H, H^4), 7.63 (ddd, *J* = 8.2, 7.3, 1.1 Hz, 1H, H^3), 7.57 (s, 1H, H^5), 7.47 (ddd, *J* = 8.5, 7.3, 1.3 Hz, 1H, H^2). ^{13}C NMR (101 MHz, DMSO) δ 161.20, 156.43, 149.86, 147.99, 147.30, 142.50 (2C), 138.59, 135.58, 128.83, 127.54, 123.16, 118.91, 118.58, 114.80, 112.86, 99.37. MS (EI+) m/z calcd for $C_{17}H_9F_3N_6$:354.08; found, 355.10 (M + 1). HPLC purity: 98%.

4-cyano-N-(7,8-dichloro-4-cyano-3-(trifluoromethyl)benzo[4,5]imidazo[1,2-a]pyridin-1-yl) benzene sulphonamide 4n/GMP-98.

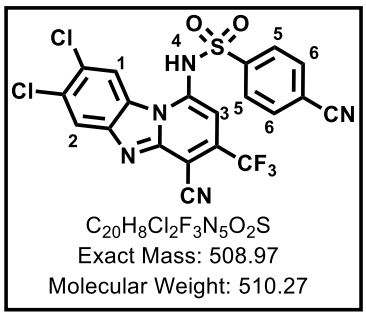

Obtained from **IVc** (0.1g, 0.274mmol, 1 equiv.) and 4-cyanobenzenesulfonamide (0.06g, 0.329mmol, 1.2 equiv.) as a yellow solid (26%). ^{1}H NMR (300 MHz, DMSO-d_6) δ 8.91 (s, 1H, H^1), 8.14 – 7.88 (m, 5H, H^{2,5,6}), 6.77 (s, 1H, H^3). ^{13}C NMR (101 MHz, DMSO) δ 160.90, 158.91, 153.29, 152.32, 150.28, 148.25, 145.11, 141.56, 136.66, 133.55 (2C), 127.19 (2C), 125.74, 122.09, 119.72, 115.15, 114.63, 108.93, 97.85. MS (EI-) m/z calcd for $C_{20}H_8Cl_2F_3N_5O_2S$:508.97; found, 507.90 (M - 1). HPLC purity: 97%.

N-(7,8-dichloro-4-cyano-3-(trifluoromethyl)benzo[4,5]imidazo[1,2-a]pyridin-1-yl)-4-(trifluoromethoxy)benzenesulfonamide 4o/GMP-99.

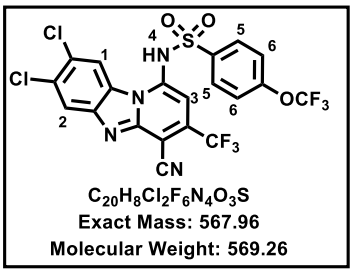

Obtained from the reaction between **IVc** (0.1g, 0.274mmol, 1 equiv.) and 4-(trifluoromethoxy)benzenesulfonamide (0.079g, 0.329mmol, 1.2 equiv.) as a brown powder (21%). ^{1}H NMR (300 MHz, DMSO-d_6) δ 8.90 (s, 1H, H^1), 8.04 (m, 3H, $H^{2,5}$), 7.54 (d, J = 8.0, 2H, H^6), 6.75 (s, 1H, H^3). ^{13}C NMR (101 MHz, DMSO) δ 152.29, 150.91, 150.78, 147.36, 145.13, 143.23, 140.19, 129.29 (2C), 128.88, 128.81, 122.36, 121.70, 121.57 (2C), 119.14, 118.91, 115.11, 107.89, 91.57. MS (EI-) m/z calcd for $C_{20}H_8Cl_2F_6N_4O_3S$:567.96; found, 566.90 (M-1). HPLC purity: 95%.

N-(7,8-dichloro-4-cyano-3-(trifluoromethyl)benzo[4,5]imidazo[1,2-a]pyridin-1-yl)pyridine-2-sulfonamide 4p/GMP-100.

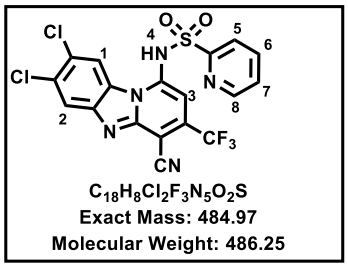

Obtained from **IVc** (0.1g, 0.274mmol, 1 equiv.) and pyridine-2-sulfonamide (0.052g, 0.329mmol, 1.2 equiv.) as a dark brown powder (10%). ^{1}H NMR (400 MHz, DMSO-d_6) δ 9.08 (s, 1H, H^1), 8.69 – 8.63 (m, 1H, H^8), 8.08 – 7.99 (m, 2H, $H^{5,6}$), 7.97 (s, 1H, H^2), 7.58 (ddd, J = 6.8, 4.7, 2.1 Hz, 1H, H^7), 7.04 (s, 1H, H^3). ^{13}C NMR (101 MHz, DMSO) δ 178.80, 164.26, 163.54, 160.73, 152.10, 150.98, 150.27, 148.67, 146.38, 142.05, 131.51, 126.66 (2C), 120.03 (2C), 106.09, 92.81, 89.35. MS (EI-) m/z calcd for $C_{18}H_8Cl_2F_3N_5O_2S$:484.97; found, 483.90 (M - 1). HPLC purity: 95%.

Methyl 1-((4-(trifluoromethoxy)phenyl)amino)-3-(trifluoromethyl)benzo[4,5]imidazo[1,2-a]pyridine-4-carboxylate: 5e/GMP-120E.

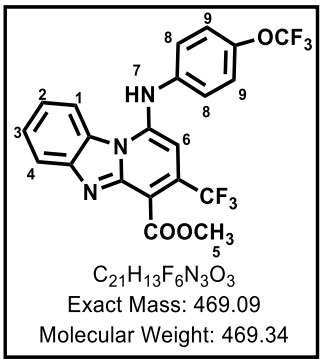

Obtained from **IVd** (0.2g, 0.608mmol, 1 equiv.) using 4-(trifluoromethoxy)aniline (0.22g, 1.22 mmol, 2 equiv.) as a yellow solid (48%), m.p. 230-233 °C; R_f (1% MeoH/DCM) 0.38; ^{1}H NMR (400 MHz, DMSO-d_6) δ 8.88 (d, J = 8.4 Hz, 1H, H^1), 7.81 (d, J = 8.1 Hz, 1H, H^4), 7.62 – 7.52 (m, 1H, H^3), 7.45 – 7.38 (m, 1H, H^2), 7.36 (d, J = 8.6 Hz, 2H, H^9), 7.13 (d, J = 8.7 Hz, 2H, H^8), 6.35 (s, 1H, H^6), 3.89 (s, 3H, H^5). ^{13}C NMR (101 MHz, DMSO) δ 164.08, 148.31, 147.91, 147.17, 144.47, 135.94, 128.01, 126.92, 124.71, 123.25 (2C), 122.85, 122.63 (2C), 121.98, 117.85, 113.40, 113.21, 112.99, 98.53, 52.03. MS (EI+) m/z calcd for $C_{21}H_{13}Cl_2F_6N_30_3$:469.09; found, 470.00 (M + 1). HPLC purity: 96%.

7.3 Biological assays

7.3.1 *In vitro* antiplasmodial assays

7.3.1.1 Asexual blood stage activity using the LDH assay at UCT

The chloroquine-sensitive NF54 strain of *Plasmodium falciparum* was used in testing the antiplasmodial asexual blood stage activity of test compounds. The parasites were cultured and maintained according to the approach by Trager and Jensen with slight variations.[1] The antiplasmodial activity was monitored by determining the activity of the parasite lactate dehydrogenase enzyme.

Stock solutions of samples were prepared at 20 mg/ml in 100% DMSO and kept at -20℃ prior to analysis. On the assay day, subsequent dilutions of the stock solutions were prepared in medium to give the highest starting concentration of 100 µg/ml. From these, serial dilutions in complete medium were performed to achieve ten concentrations with the concentration range being between 0.2-100 µg/ml. Using these concentrations, a dose response analysis was performed to establish the concentration resulting in inhibition of parasite growth by 50%. Chloroquine and artesunate were employed as controls for all the assays for which their initial testing concentrations was 1000 ng/ml. The dilution approach adopted for the samples and controls was similar. In each case, the final concentration of DMSO had no effects on parasite growth. Non-linear dose-response curves generated in GraphPad Prism v.4.0 software facilitated calculation of the IC_{50} values.

7.3.1.2. Asexual blood stage activity using the modified [^{3}H]-hypoxanthine incorporation assay at Swiss TPH

The modified [^{3}H]-hypoxanthine incorporation assay was used to test compounds against drug-sensitive (NF54) and resistant (K1) strains of *Plasmodium falciparum*. The parasites were cultivated in human erythrocytes as previously described[1,2] but with some variations to the medium which comprised RPMI 1640 supplemented with 0.5% ALBUMAX® II, 25 mM Hepes, 25 mM $NaHCO_3$ (pH 7.3), 0.36 mM hypoxanthine, and 100 µg/ml neomycin. Parasite cultures were maintained in an environment of 37 °C, 3% O_2, 4% CO_2, and 93% N_2 in humidified modular chambers.

Test compounds were dissolved in 100% DMSO, by sonication, to give 10 mg/ml stock solutions and diluted in culture medium devoid of hypoxanthine. Infected erythrocytes (100 microliter per well with 2.5% hematocrit and 0.3% parasitemia) were added to each compound titrated in 100 microliter duplicates over a 64-fold range and incubated for 48 h. After this period, 0.5 microCi of [^{3}H] hypoxanthine in 50 microliter media was added and the culture plates allowed to incubate for a further 24 h. From the parasites harvested on glass-fiber filters at the end of the total incubation period, radioactivity was determined using a Betaplate liquid scintillation counter (Wallac, Zurich). The radioactivity was recorded as counts per minute per well at each concentration of test compound and presented as percentage relative to the untreated controls. The concentrations resulting in 50% inhibition (IC_{50}) was determined by linear interpolation.[3]

7.3.1.3 *In vitro* activity against P. berghei liver stages.

Liver stage infection was initiated using *P. berghei* parasites with human hepatoma cell line, Huh-7 cells, as host cells. These were cultured in 1640 RPMI medium supplemented with 10% v/v fetal calf serum (FCS), 1% v/v non-essential amino acids, 1% v/v penicillin/streptomycin, 1% v/v glutamine and 10 mM HEPES. Additionally, an environment of pH 7, 37℃ and 5% CO_2 was maintained. Luminescence of Huh-7 cell lysates 48 hours after infection with a firefly luciferase-expressing *P. berghei* line, PbGFP-Luccon, was used to determine the degree of inhibition of the *P. berghei* liver stage infection as described previously.[4,5]

Briefly, cells (10×10^3/well) were seeded in 96-well plates the day before drug treatment and infection. Predetermined amounts of test compounds were weighed and dissolved in 100% DMSO to give 10 mM stock solutions. Dilutions of the stock solution with medium were then performed to provide the desired concentrations. One hour prior to infection with parasite, medium was replaced with fresh medium containing the appropriate concentration of each compound. After a further one hour, sporozoites (10,000 spz/well), freshly obtained through disruption of salivary glands of infected female *Anopheles stephensi* mosquitoes, were added to the wells and plates centrifuged at 1700 g for 5 minutes.

The Biotium's Firefly Luciferase Assay Kit was employed to establish the parasite load, 48 hours after infection whereas the AlamarBlue assay (Invitrogen, UK) was used to determine the effects of the compounds on the viability of Huh-7 cells. Results from dose-response curves were processed by nonlinear regression analysis and EC_{50} values determined using GraphPad software.

7.3.1.4 *In vitro* activity against gametocyte stage.

Two different platforms, ATP- and luciferase reporter line-based assays, were used to determine the gametocytocidal effects of test compounds. In the luciferase assays, two transgenic parasite lines, NF54-PfS16-GFP-Luc (early stage) and NF54-Mal8p1.16-GFP-Luc (late stage), which enable stage-specific assessment of gametocytocidal activity, were utilised. The bioluminescent ATP assay provided an additional independent evaluation of late stage gametocyte activity of test compounds.

Gametocytes were produced as per Reader and co-workers.[6] Experiments were performed on day 5 and 10 (representing >90% of either early stage I/II/III or mature stage IV/V gametocytes, respectively). In each case, assays were set up using a 2 to 3% gametocytaemia, 1.5% haematocrit culture and 48 h drug pressure in a gas chamber (90% N_2, 5% O_2, and 5% CO_2) and temperature maintained at 37 °C. Luciferase activity was determined in 20 µl parasite lysates by adding 50 µl luciferin substrate (Promega Luciferase Assay System) at room temperature and detection of resultant bioluminescence at an integration constant of 10 s with the GloMax®-Multi+ Detection System with Instinct® Software. For the ATP assay, gametocytes representing >90% of late stage IV/V gametocytes (predominantly stage V) were enriched using density gradient centrifugation and magnetic separation. Drug dilutions were placed in triplicate in 96-well plates. Approximately 50 000 gametocytes in glucose-rich complete medium were added to each well in a final volume of 100 µl and the plates incubated for 24 h in a humidified gas chamber (90% N_2, 5% O_2, and 5% CO_2) at 37 °C. ATP levels were determined using the BacTiter-Glo™ assay (Promega) in accordance with manufacturer's instructions, at room temperature in the dark with assay substrate incubated for 10 minutes. Bioluminescence was detected at an integration constant of 0.5 s with the GloMax®- Multi+ Detection System with Instinct® Software.

7.3.2 *In vitro* antischistosomal assays

7.3.2.1 Screening against Newly Transformed Schistosomula

Newly transformed schistosomula (NTS) were obtained from *Schistsosoma mansoni* cercaria according to previously described methods.[7,8] Briefly, light stimulation of snails was applied to produce cercaria whose tails were subsequently removed by washing the cercarial suspension three times with cold Hank's Basal Salt Solution (HBSS). The resultant NTS were incubated overnight in culture medium for use the following day. The culture Medium consisted of Medium 199 (Invitrogen, Carlsbad, CA) supplemented with 5% fetal calf serum (Lucerne, Switzerland) and 1% penicillin/ streptomycin mixture (Lucerne, Switzerland).

Test compounds and controls were prepared by dissolving in 100% DMSO (Fluka, Buchs, Switzerland) to make 10 mM stock concentrations. NTS (100) were transferred in each well of a 96-well plate containing culture medium and 10 µM test compound for a final well volume of 250 µL. The test set up was performed in triplicates while NTS incubated in <1% DMSO acted as control. The plate was incubated at 37 °C and 5% CO_2 for up to 72 hours after which NTS were microscopically examined for any lethality using the scale of 3 (normal activity and morphological alteration) to 0 (dead).

7.3.2.2 Adult S. mansoni Worms.

Adult *S. mansoni* worms were obtained from mice previously infected subcutaneously with ca. 80-100 cercariae. After 7-8 weeks, the mice were euthanized using CO_2 and the worms harvested from the hepatic portal and mesenteric veins. Male and female worms were paired, and two pairs incubated in each well in a 24-well plate with 2mL culture medium and the test compound (10 µM). The culture medium consisted of RPMI 1640 (Invitrogen, Carlsbad, CA) supplemented with 5% fetal calf serum (Lucerne, Switzerland) and 1% penicillin/streptomycin mixture (Lucerne, Switzerland). Incubations containing less than 1% DMSO were used as controls.

The plates were incubated at 37 °C and 5% CO_2 for up to 72 hours, after which the worms were examined microscopically, and effects scored using a scale from 3 (normal activity and no morphological alterations) to 0 (dead). Compound concentration causing 50% lethality (IC_{50}) in the adult worms was determined for compounds with >60% activity. All viability scores were averaged across replicates and normalized to the average viability scores of the control wells. Subsequently, IC_{50} values were calculated using CompuSyn2 (ComboSyn Inc., Paramus, NJ).

7.3.3 Beta haematin inhibition

Controls and test compounds were reconstituted to 20 mM in 100% DMSO (Fluka, Buchs, Switzerland). In a 96-well plate, columns 1-11 were filled with a solution constituting water/305.5 µM NP40/DMSO at a v/v ratio of 70%/20%/10%, respectively, while to column 12, 140 µLof water and 40 µL of 305.5 µM NP40 were introduced to mediate the formation of β-hematin. To column 12, 20 µL of 20 mM compound stock solution was added and 100 µL of this solution serially diluted to column 2. Column 1 was left as a blank with no compound present (0 µM). Some 100 µL of haematin suspension, prepared by suspending an aliquot (178.8 µL) of haematin stock solution in 20 mL of a 1 M acetate buffer, pH 4.9, was added into each well and the plates left to incubate for 5 hours at 37 °C. Thereafter, pyridine solution (32 µl) comprising 20% water, 20% acetone, 10% 2 M HEPES buffer (pH 7.4) and 50% pyridine was added followed by the addition of 60 µL of acetone to all wells. Optical readings of the plates were taken at 405 nm to give concentration-response values. The concentrations resulting in 50% inhibition of the process were determined using GraphPad Prism v.4.0 software (La Jolla, USA).

7.4 Pharmacokinetics and efficacy studies

7.4.1 *In vitro* metabolic stability

Metabolic stability was conducted using the one-time point assay.[9] Experiments were performed in triplicate in a 96-well microtiter plate using test compounds at a concentration of 0.1 µM, incubated individually in a solution containing 0.35 mg/mL mouse (male mouse BALB/c, Xenotech) or human (mixed gender, Xenotech) liver microsomes. NADPH (1 mM) in phosphate buffer (100 mM) and at pH 7.4 were added to the wells to initiate metabolic reactions and the plates incubated for 30 minutes. After this period, 300 µL of ice-cold acetonitrile containing internal standard (carbamazepine, 0.0236 µg/mL) was added to each well to quench the reactions. The supernatant was centrifuged and filtered after which LC-MS/MS (Agilent Rapid Resolution HPLC, AB SCIEX 4000 QTRAP MS) analysis was performed to determine concentration of test compounds. Differences in the amounts of compounds before and after incubation were therefore determined by LC-MS/MS and results recorded as per cent compound remaining after 30 minutes incubation. Search for products of metabolism was not performed during the metabolic stability assay.

7.4.2 Cytotoxicity

In vitro cytotoxicity was conducted on the Chinese Hamster ovarian cell lines using the 3-(4,5-dimethylthiazol-2-yl)-2,5-diphenyltetrazolium bromide (MTT) assay.[10] Test compounds were dissolved in 100% DMSO to yield a 20 mg/mL stock solution while the reference standard, emetine, was dissolved in distilled water to prepare a 2 mg/mL solution. From an initial test compound and control concentration of 100 µg/mL, serial 10-fold dilutions, in complete medium, were performed to achieve six concentrations with 0.001 µg/mL being the lowest concentration. The highest concentration of DMSO exposed to cells had no effects on cell viability. Plates were incubated for 48 h with 100 µL of drug and 100 µL of cell suspension in each well after which they were developed by the addition of 25 µL of sterile MTT (Thermo Fisher Scientific) to each well and a further incubation in the dark for 4 hours. Thereafter, the plates were centrifuged, the medium aspirated off and DMSO (100 µL) added to dissolve crystals and absorbance readings taken at 540 nM. Nonlinear dose-response curve fitting analysis conducted using GraphPad Prism v.4.0 software (La Jolla, USA), was applied to generate IC_{50} values. The assay was conducted in triplicate and conducted on two separate occasions.

7.4.3 hERG interaction

Inhibition potency for test compounds towards the hERG potassium ion channel was carried out using a four-point concentration-response format applying the QPatch hERG assay, Metrion biosciences, Cambridge, United Kingdom.[11,12] Test compounds were dissolved in 100% DMSO to give a 10mM stock solution and thereafter diluted further in DMSO using 0.5-log unit dilutions to achieve the screening concentrations of 0.3, 1, 3 and 10 µM.

Chinese hamster ovarian cell lines stably expressing hERG were used. Electrophysiological recordings of hERG currents were obtained according to in-house procedures and effects on hERG tail current measured. Concentration-response curves were constructed by cumulative double sample additions of each concentration to the same cell. Experiments were carried out in three separate cells and as technical replicates. Inhibition activity was calculated as the reduction in the mean peak current in the test compound relative to the peak current prior to exposure of the cells to the compounds. Percent inhibition values from each cell were used to construct concentration-response curves using the 4-parameter logistic fit with 0% and 100% inhibition levels fixed at very low and very high concentration, respectively and concentrations resulting in a 50% inhibition determined. Verapamil was used as a positive control and was treated in the same way as samples.

7.4.4 Metabolite identification studies

Metabolite identification studies were performed in male mouse (BALB/c, Xenotech) and human (mixed gender, Xenotech) liver microsomes. Microsomes (1 mg/mL) were suspended in a solution containing $MgCl_2$ (0.67 mg/mL) and phosphate buffer (100mM, pH 7.4). The test compound was spiked in a portion of this microsome mix, in a separate Eppendorf tube, to achieve a compound concentration of 10 µM. A buffer mixture was also prepared, containing only phosphate buffer and $MgCl_2$ (0.67 mg/mL) but not microsomes.

Two separate 96-well microtiter plates were used; one for T0 (0 minutes) and the other for T60 (60 minutes) incubations set up. Each plate was laid out to accommodate four sets of incubations in duplicates. In the first case, 90 µL of the microsomal mix containing the test compound (10 µM) was introduced into two separate sets of wells. In another set of wells, 90 µL from the pre-mix lacking microsomes (buffer mixture) was placed. To yet another set of wells, a control was prepared by placing an aliquot of 90 µL from the microsomal mix which did not have the test compound. Thereafter, NADPH (10µL, 1mM) was added to one of the two sets of wells containing microsomal mix that had been spiked with test compound. To the other sets of wells, 10 µL of buffer was added such that all the wells held a total volume of 100 µL of samples. The above procedures were performed for both T0 and T60 plates. To one of the plates (T0 plate), 300 µL of acetonitrile was added to all the wells and the plate immediately stored at -20 °C, pending analysis. The other plate (T60 plate) was incubated for 60 minutes at 37 °C with gentle shaking, prior to adding acetonitrile (300 µL) in all wells. Both T0 and T60 plates were centrifuged and the supernatant transferred to a clean microtiter plate for LC-MS/MS analysis following in-house procedures.

7.4.5 *In vivo* antimalarial efficacy

This work was carried out at the Swiss Tropical and Public Health Institute in accordance with Swiss national and cantonal regulations on animal welfare. *In vivo* antimalarial efficacy studies were conducted in mice harbouring *Plasmodium berghei* infection. A GFP-transfected *P. berghei* ANKA strain (donated by A. P. Waters and C. J. Janse, Glasgow and Leiden Universities respectively), was used to infect three mice and the level of parasitemia determined by flow cytometry, having a detection limit of 0.1% (that is, 1 parasite per 1,000 erythrocytes). A solution or suspension of test compounds in 90/10 Tween80/ethanol (v/v), diluted 10 times with water, was administered orally as four consecutive doses at 4, 24, 48 and 72 h post-infection. The control group of mice received only the vehicle which has no antimalarial activity. Activity was then determined by calculating the difference between the mean per cent parasitemia for the control and treated groups, presented as a per cent relative to the control group. Mice were cured if parasitemia was undetectable on day 30 after the infection, as examined by light microscopy.

7.4.6 *In vivo* antischistosomal efficacy

The *in vivo* antischistosomal efficacy of frontrunner compounds was carried out in compliance with the Swiss national and cantonal regulations on animal welfare at the Swiss Tropical and Public Health Institute, Switzerland. Groups of four NMRI mice, previously infected with *Schistosoma mansoni* cercariae and presently containing chronic *S. mansoni* infection were treated orally, at a dose of 400 mg/kg, with test compounds dissolved in 7% Tween 80 and 3% ethanol in water (v/v/v). Untreated control mice received only the vehicle, 7% Tween 80 and 3% ethanol in water, which lacks antischistosomal properties. Animals were euthanized on day 21 after treatment using the CO_2 method and dissected. Surviving worms were retrieved from the mesenteric veins and the liver, counted and sexed as previously described.[13] Activity of test compounds was determined by comparing the worm reduction in the treated animals relative to the worm burden in the infected but untreated control groups.

7.4.7 *In vivo* pharmacokinetics

The pharmacokinetic studies were conducted with prior approval of the Animal Ethics Committee of the University of Cape Town (approval number 017/026) in accordance with the South African National Standard (SANS 10386:008) for the Care and Use of Animals for Scientific Purposes,[14] and guidelines from the Department of Health.[15] The studies were performed in male (C57B1/6) mice housed in temperature-controlled rooms and fed a standard diet with free access to water. Test compounds were weighed and prepared freshly before dosing. For intravenous dosing, compounds were prepared in dimethylacetamide, poly- ethylene glycol, and propylene glycol/ethanol mixture 4:1 at a ratio of 1:3:6. An intravenous dose of 2 mg/kg contained in a volume of 50 µL was administered to two mice via the tail vein after anesthetizing the animals.

For oral administration, compounds were suspended in 2mL of 100% hydroxypropyl methylcellulose and given to three mice by gavage at a dose of 20 mg/kg. Blood samples were drawn from the tail of each animal at specified time intervals and collected into microcentrifuge tubes equipped with the anticoagulant lithium heparin S12. Samples were kept on ice and transferred to storage at −80 °C within 1 hour of collection, pending analysis. Samples were subsequently analysed by high-performance liquid chromatography and mass spectrometry (LC-MS/MS) following in-house procedures.

7.5 Physicochemical property profiling

7.5.1 Turbidimetric-based kinetic solubility

Target compounds and controls were dissolved in DMSO to make 10 mM stock solutions. From this, a predilution plate was prepared in Nunc™ 96-well fluorescence plates in triplicate by serial dilution in DMSO such that a concentration range of between 0.125 and 8 mM was achieved. Each predilution solution was then used to make secondary dilutions in DMSO and PBS (0.01 M; pH 7.4) in a second plate in triplicates such that each well contained 200µl of solvent and covering a concentration range of between 0 (solvent only, no compound) to 200 µM. After incubation at room temperature for 2 hours, absorbance was measured at 620nm using a SpectraMax 340PC microplate reader (Molecular Devices, Sunnydale, CA). Concentration-absorbance curves were then plotted in Microsoft Excel® and the point of deflection from baseline in the PBS incubation was considered the limit of solubility of a compound. Hydrocortisone and reserpine were treated similarly and used as controls for a highly and poorly soluble compound, respectively.

7.5.2 Solubility using HPLC-based DMSO "dry-down" method

This method of determining kinetic solubility of test compounds was employed to minimise the solvent-enhancement of solubility experienced in the turbidimetric method. Test compounds were dissolved in 100% DMSO to yield 10 mM stock solutions. HPLC analysis with UV-detection was used to construct calibration curves for each compound using low (11 µM), medium (100 µM) and high (220 µM) concentrations. The high and medium concentrations were prepared by placing 4.4 µL and 2 µL aliquots of the 10 mM stock solution into wells A and B of a 96-well microtiter plate and diluted by adding 195.6 µl and 198 µl of DMSO, respectively. On the other hand, the low concentration was prepared into well C by diluting 10 µL, obtained from well A, with 190 µL of DMSO to yield a 20-fold dilution of the 220 µM concentration.

Thereafter, each test sample (4 µL of 10mM stock), in triplicates, was placed in wells D, E and F and DMSO removed by freeze-drying under Genevac®. This step reduces solubility-enhancement due to DMSO. Phosphate buffer (200 µL) at pH 7.4 was added to the wells now containing the dry solid material of test samples. The plates were covered and placed on a shaker at 37 °C for 24 hours. After this period, the plates were centrifuged for 15 minutes at 3,500 rpm using a digitor 21R® centrifuge set at 23 °C and supernatant carefully transferred to an analytical 96-well microtiter plate for HPLC analysis fitted with UV-detection. Concentration of dissolved samples was determined by comparing the average peak areas produced by the samples (wells D, E, F) against the previously constructed standard curve using samples in wells A, B and C.

7.6 References

(1) Trager, W.; Jensen, J. Human Malaria Parasites in Continuous Culture. *Science* **1976**, *193* (4254), 673–675.

(2) Dorn, A.; Stoffel, R.; Matile, H.; Bubendorf, A.; Ridley, R. G. Malarial Hemozoin/β-Hematin Supports Heme Polymerization in the Absence of Protein. *Nature* **1995**, *374*, 269.

(3) Huber, W.; Koella, J. C. A Comparison of Three Methods of Estimating EC_{50} in Studies of Drug Resistance of Malaria Parasites. *Acta Trop.* **1993**, *55* (4), 257–261.

(4) Machado, M.; Sanches-Vaz, M.; Cruz, J. P.; Mendes, A. M.; Prudêncio, M. Inhibition of Plasmodium Hepatic Infection by Antiretroviral Compounds. *Front. Cell. Infect. Microbiol.* **2017**, *7* (329), 1–9.

(5) Ploemen, I. H. J.; Prudêncio, M.; Douradinha, B. G.; Ramesar, J.; Fonager, J.; van Gemert, G.-J.; Luty, A. J. F.; Hermsen, C. C.; Sauerwein, R. W.; Baptista, F. G.; Mota, M. M.; Waters, A. P.; Que, I.; Lowik, C. W. G. M.; Khan, S. M.; Janse, C. J.; Franke-Fayard, B. M. D. Visualisation and Quantitative Analysis of the Rodent Malaria Liver Stage by Real Time Imaging. *PLoS One* **2009**, *4* (11), e7881.

(6) Reader, J.; Botha, M.; Theron, A.; Lauterbach, S. B.; Rossouw, C.; Engelbrecht, D.; Wepener, M.; Smit, A.; Leroy, D.; Mancama, D.; Coetzer, T. L.; Birkholtz, L. -M. Nowhere to Hide: Interrogating Different Metabolic Parameters of *Plasmodium falciparum* Gametocytes in a Transmission Blocking Drug Discovery Pipeline towards Malaria Elimination. *Malar. J.* **2015**, *14* (1), 213.

(7) Manneck, T.; Haggenmüller, Y.; Keiser, J. Morphological Effects and Tegumental Alterations Induced by Mefloquine on Schistosomula and Adult Flukes of *Schistosoma mansoni*. *Parasitology* **2010**, *137*, 85–98.

(8) Ramalho-Pinto, F. J.; Gazzinelli, G.; Howells, R. E.; Mota-Santos, T. A.; Figueiredo, E. A.; Pellegrino, J. *Schistosoma mansoni*: Defined System for Stepwise Transformation of Cercaria to Schistosomule *in vitro*. *Exp. Parasitol.* **1974**, *36* (3), 360–372.

(9) Bertrand, M.; Jackson, P.; Walther, B. Rapid Assessment of Drug Metabolism in the

Drug Discovery Process. *Eur. J. Pharm. Sci.* **2000**, *11*, S61–S72.

(10) Liu, Y.; Peterson, D. A.; Kimura, H.; Schubert, D. Mechanism of Cellular 3-(4,5-Dimethylthiazol-2-Yl)-2,5-Diphenyltetrazolium Bromide (MTT) Reduction. *J. Neurochem.* **2002**, *69* (2), 581–593.

(11) Mathes, C. QPatch: The Past, Present and Future of Automated Patch Clamp. *Expert Opin. Ther. Targets* **2006**, *10* (2), 319–327.

(12) Kutchinsky, J.; Friis, S.; Asmild, M.; Taboryski, R.; Pedersen, S.; Vestergaard, R. K.; Jacobsen, R. B.; Krzywkowski, K.; Schrøder, R. L.; Ljungstrøm, T.; Hélix, N.; Sørensen, C. B.; Bech, M.; Willumsen, N. J. Characterization of Potassium Channel Modulators with QPatch™ Automated Patch-Clamp Technology: System Characteristics and Performance. *Assay Drug Dev. Technol.* **2003**, *1* (5), 685–693.

(13) Xiao, S. H.; Keiser, J.; Chollet, J.; Utzinger, J.; Dong, Y.; Endriss, Y.; Vennerstrom, J. L.; Tanner, M. *In vitro* and *in vivo* Activities of Synthetic Trioxolanes against Major Human Schistosome Species. *Antimicrob. Agents Chemother.* **2007**, *51* (4), 1440–1445.

(14) SABS Standards Division. *South African Bureau of Standards, South African National Standard: The Care and Use of Animals for Scientific Purposes (SANS 10386:2008) 1st Ed*; Groenkloof, Pretoria.

(15) Department of Health, Republic of South Africa. *Ethics in Health Research. Principles, Processes and Structures*; Pretoria, Republic of South Africa., 2015.